

DEVELOPMENTS IN PETROLEUM SCIENCE 48

APPLIED GEOTHERMICS FOR PETROLEUM ENGINEERS

I.M. Kutasov

ELSEVIER



DEVELOPMENTS IN PETROLEUM SCIENCE 48

APPLIED GEOTHERMICS FOR PETROLEUM ENGINEERS

www.engbookspdf.com



Volumes 1-5, 7, 10, 11, 13, 14, 16, 17, 21, 22, 23-27, 29, 31 are out of print.

6 *Fundamentals of Numerical Reservoir Simulation*
8 *Fundamentals of Reservoir Engineering*
9 *Compaction and Fluid Migration*
12 *Fundamentals of Fractured Reservoir Engineering*
15a *Fundamentals of Well-log Interpretation,* ***1.*** *The acquisition of logging data*
15b *Fundamentals of Well-log Interpretation,* ***2.*** *The interpretation of logging data*
18a *Production and Transport of Oil and Gas,* ***A.*** *Flow mechanics and production*
18b *Production and Transport of Oil and Gas,* ***B.*** *Gathering and Transport*
19a *Surface Operations in Petroleum Production, I*
19b *Surface Operations in Petroleum Production, II*
20 *Geology in Petroleum Production*
28 *Well Cementing*
30 *Carbonate Reservoir Characterization: A Geologic-Engineering Analysis, Part I*
32 *Fluid Mechanics for Petroleum Engineers*
33 *Petroleum Related Rock Mechanics*
34 *A Practical Companion to Reservoir Stimulation*
35 *Hydrocarbon Migration Systems Analysis*
36 *The Practice of Reservoir Engineering*
37 *Thermal Properties and Temperature related Behavior of Rock/fluid Systems*
38 *Studies in Abnormal Pressures*
39 *Microbial Enhancement of Oil Recovery – Recent Advances – Proceedings of the 1992 International Conference on Microbial Enhanced Oil Recovery*
40a *Asphaltenes and Asphalts, I*
41 *Subsidence due to Fluid Withdrawal*
42 *Casing Design – Theory and Practice*
43 *Tracers in the Oil Field*
44 *Carbonate Reservoir Characterization: A Geologic-Engineering Analysis, Part II*
45 *Thermal Modeling of Petroleum Generation: Theory and Applications*
46 *Hydrocarbon Exploration and Production*
47 *PVT and Phase Behaviour of Petroleum Reservoir Fluids*
48 *Applied Geothermics for Petroleum Engineers*



DEVELOPMENTS IN PETROLEUM SCIENCE 48

APPLIED GEOTHERMICS FOR PETROLEUM ENGINEERS

I.M. KUTASOV
Consultant
MultiSpectrum Technologies
Santa Monica, CA 90401, USA



1999
ELSEVIER
Amsterdam – Lausanne – New York – Oxford – Shannon – Singapore – Tokyo



ELSEVIER SCIENCE B.V.
Sara Burgerhartstraat 25
P.O. Box 211, 1000 AE Amsterdam, The Netherlands

© 1999 Elsevier Science B.V. All rights reserved.

This work is protected under copyright by Elsevier Science, and the following terms and conditions apply to its use:

Photocopying
Single photocopies of single chapters may be made for personal use as allowed by national copyright laws. Permission of the publisher and payment of a fee is required for all other photocopying, including multiple or systematic copying, copying for advertising or promotional purposes, resale, and all forms of document delivery. Special rates are available for educational institutions that wish to make photocopies for non-profit educational classroom use.

Permissions may be sought directly from Elsevier Science Rights & Permissions Department, PO Box 800, Oxford OX5 1DX, UK; phone: (+44) 1865 843830, fax: (+44) 1865 853333, e-mail: permissions@elsevier.co.uk. You may also contact Rights & Permissions directly through Elsevier's home page (http://www.elsevier.nl), selecting first 'Customer Support', then 'General Information', then 'Permissions Query Form'.

In the USA, users may clear permissions and make payments through the Copyright Clearance Center, Inc., 222 Rosewood Drive, Danvers, MA 01923, USA; phone: (978) 7508400, fax: (978) 7504744, and in the UK through the Copyright Licensing Agency Rapid Clearance Service (CLARCS), 90 Tottenham Court Road, London W1P 0LP, UK; phone: (+44) 171 631 5555; fax: (+44) 171 631 5500. Other countries may have a local reprographic rights agency for payments.

Derivative Works
Tables of contents may be reproduced for internal circulation, but permission of Elsevier Science is required for external resale or distribution of such material.
Permission of the publisher is required for all other derivative works, including compilations and translations.

Electronic Storage or Usage
Permission of the publisher is required to store or use electronically any material contained in this work, including any chapter or part of a chapter.

Except as outlined above, no part of this work may be reproduced, stored in a retrieval system or transmitted in any form or by any means, electronic, mechanical, photocopying, recording or otherwise, without prior written permission of the publisher.
Address permissions requests to: Elsevier Science Rights & Permissions Department, at the mail, fax and e-mail addresses noted above.

Notice
No responsibility is assumed by the Publisher for any injury and/or damage to persons or property as a matter of products liability, negligence or otherwise, or from any use or operation of any methods, products, instructions or ideas contained in the material herein. Because of rapid advances in the medical sciences, in particular, independent verification of diagnoses and drug dosages should be made.

First edition 1999

Library of Congress Cataloging in Publication Data
A catalog record from the Library of Congress has been applied for.

ISBN: 0 444 82887 7

♾ The paper used in this publication meets the requirements of ANSI/NISO Z39.48-1992 (Permanence of Paper).
Printed in The Netherlands.

DEDICATION

To my wife Z. Kutasov for moral support and encouragement

ACKNOWLEDGMENT

I thank my former colleagues and graduate students of the Petroleum Engineering and Geosciences Department at the Louisiana Tech University for their contributions and helpful discussions.
A preliminary draft of the manuscript was reviewed by
Dr. L. Eppelbaum (Dept. of Geophysics, Tel Aviv University) who made many helpful suggestions for improvement. His assistance is greatly appreciated.
On my request Dr. L. Eppelbaum wrote the Section 7.8:
"Interpretation of Temperature Surveys in Shallow Wells".
Lastly, I also appreciate the great effort provided by the staff of ELSEVIER in editing and handling the manuscript.

Contents

DEDICATION

ACKNOWLEDGMENT

1 INTRODUCTION 1

1.1 Scope of the Monograph 1

1.2 Objectives of Monograph 2

1.3 Potential Applications 2

1.4 Symbols and Units 3

2 TEMPERATURE FIELD OF RESERVOIRS 4

2.1 Thermal Properties of Formations 4

2.2 Heat Flow and Temperature 10

2.2.1 Geothermal Gradient and Heat Flow 10

2.2.2 Temperature and Lithological Profile 13

2.2.3 Regional Patterns of Heat Flow 15

2.2.4 Annual Temperature Variation 17

2.2.5 Mechanisms of Heat Transfer 18

2.3 Basic Heat Transfer Equations 20

2.3.1 The Differential Heat Conductivity Equation 20

2.3.2 Main Assumptions 21

2.3.3 Laplace Equation 23

2.3.4 Poisson Equation 23

2.3.5 Stefan Relationship 24

2.3.6 Initial and Boundary Conditions 24

2.3.7 Dimensionless Parameters 26

2.4 Thermal Regime of Permafrost 27

2.4.1 Temperature of Frozen Rocks 27
2.4.2 Thickness and Dynamics of Permafrost 30
2.4.3 Offshore Permafrost 34
2.4.4 Change of Mechanical Properties at Thawing 35
2.5 Temperature Anomalies due to Topographic and Geological Factors 41
2.5.1 Flat-Lying Sediments 41
2.5.2 Lateral Thermal Conductivities Contrasts 44
2.5.3 Sedimentation and Erosion 47
2.5.4 Past Climate 50
2.5.5 Vertical and Horizontal Water Movements 51
2.5.6 Fluid Discharge Trough a Fault 53
2.5.7 Island or Lake 56
2.5.8 Single Mountain Range 58
2.5.9 Modeling of the Temperature Field 60

3 WELLBORE AND FORMATIONS TEMPERATURE DURING DRILLING 64

3.1 Heat Exchange in the Wellbore-Formation System 64
3.1.1 Literature Review 64
3.1.2 Newton's Relationship 69
3.1.3 Overall Heat Transfer Coefficient 70
3.1.4 Effect of the Hydraulic and Rotary Inputs 72
3.1.5 Radial Heat Flow Rate 73
3.1.6 Heat Loss Due to Fluid Loss 74
3.2 Downhole Circulating Mud Temperatures 78
3.2.1 Analytical Methods and Computer Programs 78
3.2.2 Empirical Equation 84
3.2.3 Mud Temperature Control 90
3.3 Drilling Fluid Densities at High Temperatures and Pressures 95
3.3.1 Experimental Data 95
3.3.2 Empirical Formula 96
3.4 Hydrostatic Mud Pressure 101
3.4.1 New Formula 101

3.4.2 Differential Pressure 104
3.5 Drilling Through Hydrates 106
3.6 Formation Temperatures Around the Wellbore 112
3.6.1 Radius of Thermal Influence 112
3.6.2 Adjusted Circulation Time 114
3.6.3 Radial Temperature Distribution 115
3.6.4 Volumetric Average Temperature 116
3.6.5 Application of the Duhamel's Integral 119
3.7 Thermal Stresses in Formations and Casings 121
3.8 Drilling Through Permafrost Interval 125
3.8.1 Estimation of the Permafrost Base 125
3.8.2 Low and High Temperature Permafrost 131
3.8.3 Radius of Thawing 134
3.8.4 Temperature Distribution and the Radius of Thermal Influence . . . 139
3.8.5 Heat Losses from Wells 140
3.8.6 Allowable Shut-in Time 142
3.9 Hole Enlargement Control in Permafrost Areas 145
3.9.1 Field and Experimental Data 145
3.9.2 Washout Diameter 150
3.9.3 Mud Properties Control 154

4 WELLBORE AND FORMATIONS TEMPERATURE DURING SHUT-IN 158

4.1 Determination of the Downhole Shut-in Temperatures 158
4.1.1 Literature Review 158
4.1.2 The Basic Formula 161
4.1.3 Effect of the Formation Thermal Diffusivity 165
4.1.4 The Impact of the Well's Radius 166
4.1.5 Variations in the Shut-in and Circulation Time Ratio 168
4.2 Prediction of the Formations Temperatures 169
4.2.1 "Two Temperature Logs" Method 169
4.2.2 Solution for a Time Dependent Mud Circulation Temperature . . . 175
4.3 Temperature Distribution in Formations 176

4.4 Restoration of the Thermal Equilibrium in Permafrost Areas 179
4.4.1 Results of Long Term Temperature Surveys 179
4.4.2 Dynamics of the Thawed Zone 181
4.4.3 Time of the Complete Freezeback 184
4.4.4 Modification of the "Two Temperature Logs" Method 185
4.4.5 Pressures Generated During Refreezing 190

5 CEMENTING OF CASING 194
5.1 Strength and Thickening Time of Cement 194
5.2 Cement Heat Generation 195
5.2.1 Rate of Heat Generation Versus Time 195
5.2.2 API Class H Cement and API Class A Cement 199
5.3 Temperature Increase Due to Cement Hydration 200
5.3.1 Formula and Table 200
5.3.2 Size of the Annulus 204
5.3.3 Thermal Properties and Temperature of Formations 208
5.4 Bottomhole Fluid Circulating Temperatures 208
5.4.1 Field Data and Empirical Formula 208
5.4.2 Comparison with API Schedules 212
5.5 Designing Cementing Programs for Deep Wells 216
5.5.1 Utilization of MWD Temperature Logs 216
5.5.2 Predicting the Geothermal Gradient in Offshore Areas 219
5.5.3 Production Liners 219
5.6 Cementing of Casing in Permafrost Regions 221

6 PRODUCTION AND INJECTION WELLS 224
6.1 Heat Transfer 224
6.1.1 Overall Coefficient of Heat Loss 224
6.1.2 Time Function 226
6.1.3 Effective Well Radius 228
6.1.4 Heat Losses From Wells 229
6.2 Temperature Profiles in Wells 232
6.3 Water Formation Volume Factor 235

6.4 Temperature Around the Wellbore 238
6.5 Permafrost Thawing and Estimation of Well Thermal Insulation Efficiency . 240
6.6 Thermal Stresses 244

7 INTERPRETATION AND UTILIZATION OF TEMPERATURE DATA 248

7.1 Effect of Free Thermal Convection and Casing 248
7.2 Determination of Formation Temperature 256
7.2.1 Applicability of the Horner Method 256
7.2.2 Analytical Method 259
7.3 Estimation of the Geothermal Gradient 261
7.4 Mud Density Program 264
7.5 Location of the Cement Column Top 266
7.6 The Injectivity Profile 268
7.7 The Use of Thermistors in Temperature Probes 271
7.8 Interpretation of Temperature Surveys in Shallow Wells 276
7.8.1 General Information 276
7.8.2 Elimination of Temporary Variations 277
7.8.3 Elimination of Terrain Relief Effect 279
7.8.4 Common Aspects of Graviational, Magnetic and Temperature Anomalies 281
7.8.5 Description of the Methods Employed by Quantitative Interpretation 284
7.8.6 Calculation of the Inclined Relief Influence 289
7.8.7 Examples of Quantitative Interpretation 290
7.8.8 Further Improvement of the Thermal Near-Surface Technique . . . 294

8 APPENDICES 297

8.1 APPENDIX A. CONVERSION FACTORS 297
8.2 APPENDIX B. THERMAL PROPERTIES OF FORMATIONS 300
8.3 APPENDIX C. COMPUTER PROGRAMS (FORTRAN) 305

REFERENCES 324

INDEX 340

This Page Intentionally Left Blank

Chapter 1

INTRODUCTION

1.1 Scope of the Monograph

The purpose of the monograph is to present in a clear and concise form methods of utilizing the data of temperature surveys in deep boreholes as well as the results of field, laboratory, and analytical investigations in geothermics to the wide range of petroleum reservoir engineers, drilling and production engineers, petroleum geologists, and geophysicists. Although some aspects of this book have been discussed in several monographs (Kappelmeyer and Haenel, 1974; Proselkov, 1975; Cheremenskiy, 1977; Gretener, 1981; Prats, 1982; Jorden and Campbell, 1984; Handbook of Terrestrial Heat-Flow Density Determination, Eds.: Haenel, Rybach, and Stegena, 1988) and numerous papers, at present no monographs on this topic are available to the petroleum engineers.

This monograph is developed mainly from notes used for six years in courses (Applied Geothermics, Impact of Elevated Temperatures and High Pressures on Drilling and Production, Arctic Drilling and Production) given to senior and graduate students at the Petroleum Engineering and Geosciences Department of the Louisiana Tech University. All chapters of the monograph (Introduction, Temperature Field of Reservoirs, Wellbore and Formations Temperatures During Drilling, Wellbore and Formations Temperatures During Shut-in, Cementing and Casing, Production and Injection Wells, Interpretation and Utilization of Temperature Data, Appendix - Thermal Properties of Formations, Computer Programs) are introduced at a level that will make them accessible to field operators and staff. Mathematical formulas are presented

in a concise form and illustrated by tables and numerical examples. Many field examples are provided to develop an understanding of the interpretation and utilization of temperature data.

1.2 Objectives of Monograph

The objective of this monograph is a valid presentation of the state of knowledge and prediction of downhole and formations temperatures during well drilling, well completion, shut-in, and production.
Our intent is to reach drilling engineers (impact of elevated temperatures on well drilling and completion technology, Arctic drilling); production engineers (temperature regime of production, injection, and geothermal wells, Arctic production); reservoir engineers (temperature field of reservoirs, thermal properties of formations and formation fluids); well logging engineers (interpretation of electrical resistance, mud density, and temperature logs); geophysicists and geologists (interpretation of geophysical data, calculation of the terrestrial heat flow, reconstruction of the past climate). The Author also hopes that the monograph will be used as a textbook for senior and graduate petroleum engineering students.

1.3 Potential Applications

Potential applications of data presented in this monograph are given in the following outline.

Well drilling and oil/gas production.
1. Prediction and control of downhole mud properties.
2. Designing deep wells cementing programs.
3. Evaluation of thermal stresses in casings and in surrounding the borehole formations.
4. Logging tools design and log interpretation.
5. Determination of physical properties of reservoir fluids.
6. Prediction of permafrost thaw and refreezing around the wellbore.
7. Determination of the gas hydrate prone zone.
8. Hole enlargement control in permafrost areas.
9. Well planning in Arctic areas (determination of the surface casing

shoe depth, selection of low-temperature cements, design of safe casing strings to avoid pipes buckling during the freezeback).

Geophysics.
1. Interpretation of geophysical data, using the temperature dependence of mechanical and electrical properties of formations.
2. Calculation of the terrestrial heat flow. Extrapolation of temperatures to greater depths in the crust and the upper mantle.
3. Reconstruction of the past climate from the temperature profiles.
4. Determination of the dynamics of the permafrost zone by comparing the values of heat flow in the frozen and unfrozen zones.

Geology.
1. Calculation of the regional heat flow for various tectonic structures.
2. Preparation of regional temperature gradient maps. Evaluation of geothermal energy resources.
3. Evaluation of the rates of erosion and sedimentation from temperature profiles.
4. Studying of underground water movement using the variations of the vertical heat flow in water re-charge and discharge areas.

1.4 Symbols and Units

The Society of Petroleum Engineers has suggested a set of standard symbols for use in petroleum engineering and an effort has been made to adhere to those standards. In the monograph International System (SI) of units is used with practical oilfield units in brackets. When reference data (figures and tables) are used the original units will be maintained. The coefficients in empirical equations are presented in such way that the Reader can use them either with the practical oilfield units (prevalent in many many, including the U.S.), or with the SI set of units. Conversion factors are presented in the Appendix A.

Chapter 2

TEMPERATURE FIELD OF RESERVOIRS

2.1 Thermal Properties of Formations

The temperature field of reservoirs, the heat exchange between boreholes and surrounding formations are very much dependent on the thermal properties of formations. It is known that three macroscopic quantities: pressure (p), density (or specific volume, v) and temperature (T) define the state of a system in thermal and mechanical equilibrium. The relation $f(p, v, T) = 0$ is called the equation of state. A number of thermodynamic properties of a material can be determined from the equation of state.
Unlike pressure or density, the concept of the temperature can not be expressed in simple terms. Indeed, the definition of the temperature as a system property that determines whether bodies (solids, fluids and gases) in a closed system are in thermal equilibrium, provides only a qualitative definition of this variable. From physics is known that the state of thermal equilibrium is reached when the average kinetic energies of particles (atoms and molecules) of all bodies are equal. Thus, quantitatively the temperature of the system can be identified with the average kinetic energy (E_k) of the atoms and molecules. The accepted definition of the temperature is that the temperature is equal to two thirds of E_k,

$$T = \frac{2}{3}E_k = \frac{2}{3}\frac{\overline{mu^2}}{2} = \frac{\overline{mu^2}}{3}, \tag{2.1}$$

where m is the mass of the particle, u is the particle's velocity and the overline sign means that this is the average value of mu^2.

In this case the temperature has the dimension of energy and this is very difficult to use in practice. For this reason a conversion coefficient (k) is introduced and the temperature is expressed in absolute thermodynamic scale – Kelvin scale. One degree (K) in Kelvin scale is defined as a 1/100 of the difference between the temperatures of boiling and freezing of pure water at atmospheric pressure. The conversion coefficient is called Boltzmann constant and shows the amount of energy contained in one degree, $k = 1.380662 \cdot 10^{-23}$ J/K. From the last formula follows that

$$kT = \frac{\overline{mu^2}}{3}, \tag{2.2}$$

It is practically impossible to stop all molecules and atoms and reach the temperature of the absolute zero degree.

The above mentioned relation between energy an temperature will help to Reader to gain a more penetrating insight into physical meaning of formations thermal properties.

Specific heat.

This parameter is defined as the amount of energy required to raise the temperature of a unit of mass of substance by one degree. The specific heat shows the capability of the formations to store heat. The dimension of the specific heat in the SI is J/kg· K. The specific heat can be measured at constant pressure (c_p) or at constant volume (c_v). For an incompressible material the specific heats are equal to one another, $c(T) = c_p(T) = c_v(T)$. The $c(T)$ is a weak function of the temperature and for a wide temperature interval it can be approximated by a linear equation,

$$c(T) = c(T_i) + \beta(T - T_i), \tag{2.3}$$

where T_i is the initial temperature, and β is a coefficient. From experimental data (Somerton, 1958) we calculated parameters in equation (2.3) for several rocks. For the 70°F (21°C) – 620°F (327°C) interval we obtained that for sandstone $c(70°\text{F})$=0.197 Btu/lbm·°F and $\beta = 1.24 \times 10^{-4}$ Btu lbm^{-1} (°F)$^{-2}$. The corresponding values of $c(70°\text{F})$ and β are: for shale 0.190 and 1.43 $\times 10^{-4}$; and for siltstone 0.203 and 1.12 $\times 10^{-4}$. Very often a density and specific heat product (ρc) – volumetric heat capacity is used. For fluid-saturated rocks at high temperatures the effective specific heat of

the reservoir (c_R) can be estimated from the following equations (Prats, 1982),

$$c_R = M_R/\rho_a, \tag{2.4}$$

$$M_R = (1-\phi)M_\delta + \phi(S_oM_o + S_wM_w) + \phi S_g$$

$$\cdot[fM_g + (1-f)(\frac{\rho_s L_v}{\Delta T} + \rho_s C_w)], \quad \Delta T = 1^oC \tag{2.5}$$

$$\rho_a = \rho_\delta(1-\phi) + \phi(S_o\rho_o + S_w\rho_w + S_g\rho_g), \tag{2.6}$$

where ρ_a is the average density, M_R is the effective volumetric capacity, ϕ is porosity, f is the volume fraction of noncondensable gas in the vapor phase; M_δ, M_o, M_w, and M_g are the isobaric volumetric heat capacities of the solid, oil, water, and gas respectively; S_o, S_w and S_g are the saturation of the fluid and gas phases ; L_v is the latent heat of vaporization of water; c_w is the isobaric specific heat capacity of water; ρ_s is the steam density, ρ_δ, ρ_w, ρ_o, and ρ_g are densities of the solid, fluid, and gas phases.

Thermal conductivity.

Thermal conductivity or the thermal conductivity coefficient of a material indicates its ability to transfer heat. Consider an infinite plane wall of a certain material and the thickness of the wall is one unit of length. The wall's sides are maintained at constant temperatures and the temperature difference is equal to one degree. Let us also assume that a sensor can measure the amount of heat per unit of the wall's area per unit of time. In this case the measured amount of heat will be *numerically* equal to the thermal conductivity coefficient (λ) of the given material. The dimension of this quantity in SI is J m^{-1} s^{-1} K^{-1} or W m^{-1} K^{-1}.

It was found experimentally that the amount of heat transferred through the wall (q_A) is proportional to the area (A) and to the temperature difference (ΔT) and wall thickness (Δx) ratio. This statement is known as the Fourier law (equation) of thermal diffusion. In the differential form the Fourier law for a unit of area may be expressed by the formula,

$$q = -\lambda\frac{\partial T}{\partial x}, \tag{2.7}$$

where q is the heat flow rate in direction of x. The negative sign follows from the fact that heat flows in the direction of lower

temperatures. Thus the coefficient of proportionality in the Fourier equation is the thermal conductivity (in the direction of x) coefficient.
In the hydrodynamics of flow of incompressible fluids through porous media an analogous equation was suggested by Darcy. In the Darcy equation the flow rate is proportional to the pressure gradient and the coefficient proportionality is the permeability and hydrodynamic viscosity ratio (mobility). Similarly in the electrical current conduction, according to the Ohm's formula, the current is proportional to the voltage gradient. The coefficient of proportionality here is the specific electrical conductivity. Thus a correspondence exist between thermal conductivity coefficient, mobility, and specific electrical conductivity.

The thermal conductivity of formations is dependent on temperature, pressure, porosity, composition, and properties of pore-filling fluids and gases. Values of thermal conductivity coefficients range widely for rocks and pore-filling substances (Table 2.1).

Table 2.1 Thermal conductivities of some geological materials (Poelchau et al., 1997)

	$Wm^{-1}K^{-1}$	Source
Earth's crust	2.0–2.5	Kappelmeyr and Haenel (1974)
Rocks	1.2–5.9	Sass et al. (1971)
Sandstones	2.5	Clark (1966)
Shales	1.1–2.1	Clark (1966), Blackwell and Steele (1989)
Limestones	2.5–3	Clark (1966), Robertson (1967)
Water	0.6	At 20° C
Oil	0.15	At 20° C
Ice	2.1	Gretener (1981)
Air	0.025	CRC (1974) Handbook
Methane	0.033	CRC (1974) Handbook

All pore filling fluids have lower λ values than rocks and this causes the bulk thermal conductivities to decrease with increasing porosity (Poelchau et al., 1997). Examples for the effect of porosity are presented in Fig. 2.1.

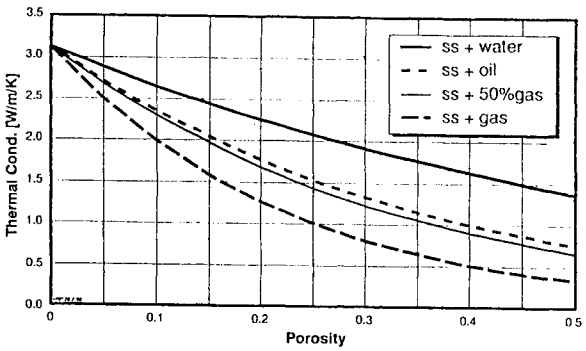


Fig. 2.1. Thermal conductivity of sandstone as a function of porosity and pore fluid at ambient temperature and pressure (Poelchau et al., 1997).

For low porosity formations temperature has the major effect on the variation of thermal conductivity (Fig. 2.2).

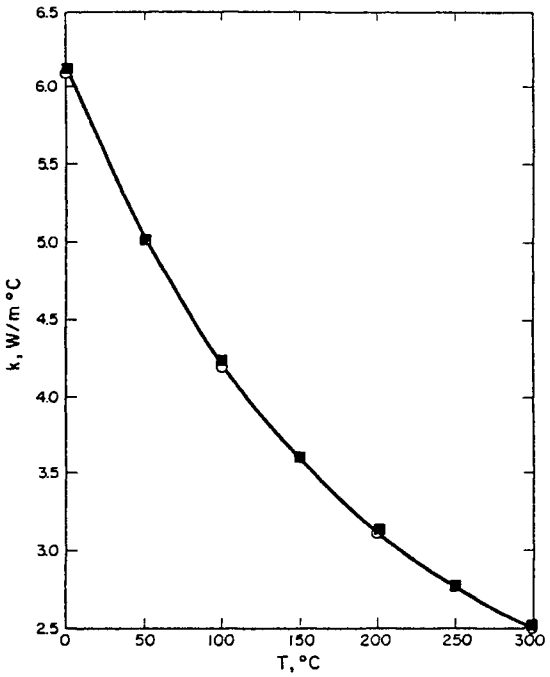


Fig. 2.2. Variation of the thermal conductivity of salt with temperature (Blesh et al., 1983).

Birch and Clark (1940) have suggested that the reciprocal of the thermal conductivity (thermal resistivity) might be a linear function of the temperature. Blesh et al. (1983) found that the agreement between the best-fit line and experimental data for several rocks for temperatures up to 300°C is good with no greater than ±3 percent variation. Coefficients of the equation

$$\lambda^{-1} = a_o + a_1 T \tag{2.8}$$

are presented in Table 2.2.

Table 2.2 Coefficients of least squares fit of thermal conductivities data (Blesh et al., 1983)

Rock	a_o m °C/W	$a_1 \times 10^4$ m/W
Salt	0.1605	7.955
Granite	0.3514	3.795
Basalt	0.8684	6.146
$\text{Shale}_{\parallel}$	0.5297	2.215
$\text{Shale}_{\perp}$	0.7167	2.949

As we can see (Table 2.2) for shale the thermal conductivity parallel to bedding is higher than the vertical thermal conductivity. For sedimentary rocks thermal anisotropy ratios (horizontal to vertical) up to 2.5 were reported (Kappelmeyer and Haenel, 1974; Gretener, 1981; Popov et al., 1995).
Kutas and Gordienko (1971) proposed the following empirical formula for estimating thermal conductivities of sedimentary formations at temperatures up to 300°C,

$$\lambda_T = \lambda_{20} - (\lambda_{20} - 3.3)[\exp(0.725\frac{T-20}{T+130}) - 1] \tag{2.9}$$

where λ_{20} is the thermal conductivity coefficient at 20°C in 10^{-3} cal s^{-1} cm^{-1} °C. The accuracy of the formula is 5-10%. Only one value of λ_T is needed to use the last formula. For example, let us assume that the value of the thermal conductivity coefficient at T=50°C is known. Then from the last equation the value of λ_{20} is calculated. The increase of thermal conductivity with pressure (p) can be accounted for by the following equation (Kappelmeyer and

Haenel, 1974):

$$\lambda = \lambda_o(1 + \delta p) \tag{2.10}$$

where λ_o is the thermal conductivity coefficient at normal pressure, and δ is the pressure coefficient of thermal conductivity.

Very few experiments were conducted to estimate the values of δ. From experiments at pressures up to 10,000–12,000 kg cm^{-2} the calculated values of δ were small: for rocksalt 3.6×10^{-5}; for dry and wet limestone with density of 2.31 g cm^{-3}, 9.5×10^{-5} and 1.35×10^{-5}; and for dry and wet sandstone with density of 2.64 g cm^{-3} respectively 2.55×10^{-4} and 5.7×10^{-5} kg^{-1}cm^2 (Kappelmeyer and Haenel, 1974). However, at smaller pressures (up to 205 kg cm^{-2}) higher values of δ were obtained (Hurtig and Brugger, 1970; see Appendix B, Table B.8).

Thermal diffusivity.
Under transient conditions this parameter determines how fast the temperature field of a solid changes with time. The coefficient of thermal diffusivity (a) is expressed by the formula

$$a = \frac{\lambda}{\rho c} \tag{2.11}$$

The dimension of thermal diffusivity in SI is m^2/s. In hydrodynamics an analogous quantity is hydraulic diffusivity (the ratio of mobility and porosity-total system compressibility product).

Some values of formations thermal properties are presented in the literature (Birch and Clark, 1940; Clark, 1966; Kappelmeyer and Haenel, 1974; Somerton, 1992) and in Appendix B.

2.2 Heat Flow and Temperature

2.2.1 Geothermal Gradient and Heat Flow

The temperature regime of sedimentary formations is influenced by many topographic and geological factors (constant terrain, sedimentation, erosion, lateral conductivity contrasts, underground water movement), past climate, and by the heat flow from the Earth's

interior – terrestrial heat flow. As a result the temperature field of formations is time (t) dependent and three dimensional,

$$T = T(x, y, z, t) \tag{2.12}$$

The time dependence of the temperature is mainly caused by changes in the Earth's surface temperature conditions (past climate) or by the changes in the value of the terrestrial heat flow (q). Calculations after several models of Earth's thermal history have shown that for the crust the value the of q did not practically changed during several million years. The impact of the past climate on the subsurface temperatures is usually limited to several hundreds meters. Thus, for deep depths ($>$ 300–500 m), we can assume that

$$T = T(x, y, z) \tag{2.13}$$

Most of temperature surveys are conducted in boreholes. The total vertical depth of the boreholes ($<$ 10 km) is small in comparison with the radius of the Earth (6370 km) and for this reason the curvature of the Earth's surface can be neglected.

It is a known fact that the formation temperature increases with depth. Only in some offshore-onshore transition areas and permafrost regions at shallow depths (several hundreds meters) the temperature reduces with depth. The rate of the temperature increase is determined by the geothermal gradient (Γ). In a general case the geothermal gradient has three components,

$$\Gamma = \sqrt{\Gamma_x^2 + \Gamma_y^2 + \Gamma_z^2} \tag{2.14}$$

where

$$\Gamma_x = \frac{\partial T}{\partial x}, \qquad \Gamma_y = \frac{\partial T}{\partial y}, \qquad \Gamma_z = \frac{\partial T}{\partial z}$$

Here we want to make a comment: in this study we will follow to the recommendations of the International Heat-Flow Commission (IHFC). It is recommended that the units and symbolism be as follows: K or ^{o}C and T for temperature; Km^{-1} ($\mathrm{mK\ m}^{-1}$) and Γ for geothermal gradient; $\mathrm{W\ m}^{-1}\mathrm{K}^{-1}$ and λ for thermal conductivity; $\mathrm{mW\ m}^{-2}$ and q or HFD for heat-flow density; and $\mathrm{W\ m}^{-3}$ and H for heat production rate (Haenel et al., 1988). In engineering calculations the Rankine, Fahrenheit and Celsius

temperature scales are usually used. The relationships between these scales and Kelvin scale are:

$$T(^oC) = T(K) - 273.15 \tag{2.15}$$

$$T(^oF) = \frac{9}{5}T(^oC) + 32$$

$$T(^oR) = T(^oF) + 459.67$$

The value of HFD determines the amount of heat per unit of area per unit of time which is transmitted by heat conduction from the Earth's interior. For isotropic and homogeneous formations, where coefficient of thermal conductivity is a constant, the value of HFD ($\vec{q}$) can be calculated from the Fourier equation

$$\vec{q} = -\lambda \, grad \, T = -\lambda \, \nabla T \tag{2.16}$$

Here the parameters $\vec{q}$ and ∇T are vectors. For anisotropic rocks, where the coefficient of thermal conductivity in a given point depends on direction, the corresponding equation for HFD is

$$\vec{q} = (q_x, q_y, q_z) \tag{2.17}$$

$$\nabla T = (\Gamma_x, \Gamma_y, \Gamma_z)$$

In an isotropic and homogeneous layer, where $\lambda_x = \lambda_x = \lambda_z = \lambda$ and $\Gamma_x = \Gamma_y = 0$, $\Gamma_z = \Gamma$, the absolute value of HFD is

$$q = \lambda\Gamma \tag{2.18}$$

Thus to calculate the HFD we need to estimate the value of the static (undisturbed) geothermal gradient (Γ) and to measure the thermal conductivity of the formation.

Two methods of combining thermal conductivity and temperature gradient data are used: interval method and the Bullard method (Powell et al., 1988). It is assumed that the effect of climatic changes, relief, underground water movement, subsurface conductivity variations on the temperature gradient (G) have been estimated and the corrected value of G is close to the value of Γ.

In the interval method, for each depth interval a temperature gradient is combined with the representative value of formation thermal conductivity. An example of HFD determination by the interval

Table 2.3 Calculation of heat flow density (HFD), drill site WSR-1 at Woodside, on the Colorado Plateau (after Bodell and Chapman, 1982). Depth interval in m, gradient in mK m^{-1}, conductivity in $Wm^{-1}K^{-1}$, heat flow density in mW m^{-2}

Depth interval	Thermal gradient	Sample type	Conductivity λ	HFD	Mean value
45–105	15.0 ±1.0	core	3.96±0.23	60±5	
105–245	18.0±1.0	core	3.43±0.15	62±4	
245–320	24.8±0.7	core	2.75±0.14	68±4	65±4
320–455	16.0±0.4	core	4.18±0.15	67±3	
455–515	17.2±0.5	core	4.20±0.14	72±3	
515–575	16.5±0.6	core	3.86±0.09	64±3	

method is presented in Table 2.3. Bullard's method can be used for one dimensional conductive heat flow in a flat layered medium. The following expression is used to process the temperature–thermal conductivity data

$$T(z) = T_o + q_o \sum_{i=1}^{N} (\Delta z_i / \lambda_i) \tag{2.19}$$

where T_o is the extrapolated surface temperature, q_o is the constant heat flow density, and λ_i is thermal conductivity in the depth interval Δz_i.
The average value of HFD over continents is about 60 mW m^{-2} (Kappelmeyer and Haenel, 1974; Davies, 1980).

It was considered for a long time that the average values of HFD over continents and oceans are practically the same. At present, taking the non-conductivity component (hydrothermal circulation in the oceanic crust) into account, the average oceanic HFD is estimated to be about 100 mW m^{-2} (Uyeda, 1988).

2.2.2 Temperature and Lithological Profile

For several (N) layers with no heat production the geothermal gradient-coefficient of thermal conductivity product is a constant,

$$\lambda_1 \Gamma_1 = \lambda_2 \Gamma_2 = \cdots = \lambda_N \Gamma_N \tag{2.20}$$

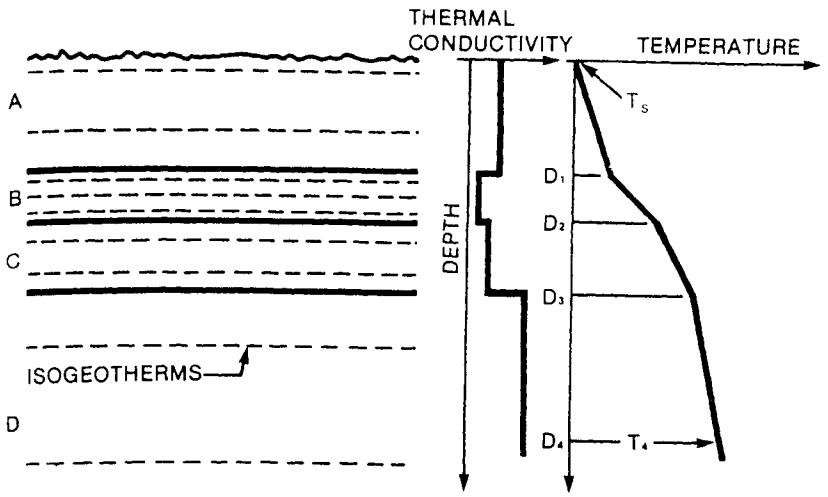


Fig. 2.3. Isogeotherms and formation temperature/depth profile in a hypothetical rock sequence (Jorden and Campbell, 1984).

and to high thermal conductivity formations correspond low values of the geothermal gradient (Fig. 2.3). In this case the temperature of formations can be calculated from the Eq. 2.19. The change of the geothermal gradient with the depth for one wellbore drilled into Precambrian granitic rock in the Jemez Mountains of northern New Mexico is shown on Fig. 2.4. Čermak and Haenel (1988) presented several solutions of the steady-state conductivity equation for temperature-dependent thermal conductivity $\lambda(T)$ and depth-dependent heat production $H(z)$:

$$H(z) + \frac{d}{dz}\left[\lambda(T)\frac{dT}{dz}\right] = 0 \qquad (2.21)$$

with the boundary conditions $T_o = T(z = 0)$ and $q_o = \lambda(dT/dz)_{z=0}$. For one layer with $H = H_o = constant$ and $\lambda(T) = \lambda_o/(1 + CT)$; where C is in the order of 10^{-3} K^{-1}, the solution is

$$T(z) = (1/C)\{(1 + CT_o)\exp[(C/\lambda_o)(q_o z - H_o z^2/2)] - 1\}. \qquad (2.22)$$

When the heat production is depth dependent $H = H_o \exp(-z/D)$; where D is in the order of 10 km, the solution is

$$T(z) = (1/C)[(1 + CT_o)\exp\{(C/\lambda_o)[H_oD^2(1 - \exp(-z/D)) - H_oDz + q_oz]\} - 1]. \quad (2.23)$$

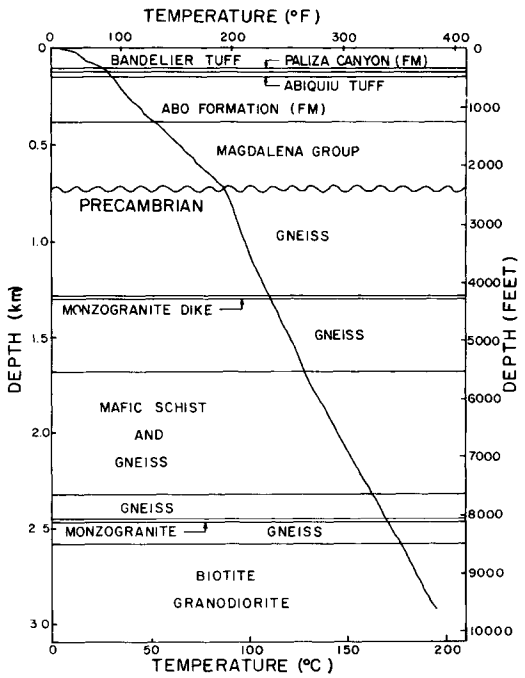


Fig. 2.4. Lithologic log of the well GT-2 showing temperature versus depth (Sibbitt et al., 1979).

2.2.3 Regional Patterns of Heat Flow

There is reason to believe that the major sources of thermal energy in the Earth's crust are radioactive isotopes of uranium, thorium and potassium. Thus the thickness of the crust and the distribution of radioactive isotopes with depth to a large degree effects the heat flow from Earth's interior. In young oceanic areas the non-conductive heat transfer by hydrothermal circulation in the oceanic crust produces variations in values of HFD. With age increase an impermeable sedimentary layer thickens and water circulation is shut off (Uyeda, 1988). Analysis of heat-flow density data shows

that HFD generally decreases from young orogenic zones (120 mW m^{-2}) to Pre-Cambrian shields (40 mW m^{-2}) on land and from mid-oceanic ridges (170 mW m^{-2}) to older basins (50 mW m^{-2}) in the sea (Uyeda, 1988).

An empirical formula is used by many authors to describe the relationship between the HFD and the radiogenic heat component

$$q = q_r + DH_o, \tag{2.24}$$

where DH_o is the contribution from radiogenic heat in the upper crust, q_r is the heat coming from lower crust and upper mantle, and D is the effective thickness of the near-surface radioactive layer when its rate of heat generation (H_o) is assumed to be constant.

Below we present three empirical equations (Rybach, 1988) which can be used to calculate the rock's radioactive heat production rate (H). The first equation can be used when the rock's density and contents of radioactive isotopes are known,

$$H = 10^{-5}\rho(9.52c_U + 2.56c_{Th} + 3.48c_k), \tag{2.25}$$

where c_U, c_{Th}, and c_k are the natural uranium, thorium and potassium contents respectively; ρ (in kg m^{-3}) is the rock's density. In the last formula practical concentrations units are used: weight in ppm (1 ppm = 10^{-6}kg/kg) for uranium and thorium and weight percent for potassium; and value of H is given in $\mu W\ m^{-3}$. The second equation describes the relationship between the velocity of compressional seismic waves (v_p) and heat production rate,

$$\ln H = 16.5 - 2.74v_p, \tag{2.26}$$

where v_p is in km s^{-1}, and H is in $\mu W\ m^{-3}$. This formula is based on laboratory data obtained at 50 MPa pressure and at room temperature. For this reason the v_p values measured *in situ* must be recalculated to match the above mentioned laboratory conditions. In the third formula the relationship between bulk density and heat production rate is used,

$$\ln H = 22.5 - 8.15\rho, \tag{2.27}$$

where ρ is in g cm^{-3}, and H is in $\mu W\ m^{-3}$.
The estimated values of H (at a given D) can be used to calculate the parameter H_o in Equation 2.24.

2.2.4 Annual Temperature Variation

The oscillation of the annual Earth's surface temperature is usually approximated by a periodical function

$$T(t) = T_o + A_o \sin \omega t, \qquad \omega = \frac{2\pi}{P} \tag{2.28}$$

where t is time, T_o is the mean annual air temperature at the Earth's surface, P is the period (1 year), ω is the angular frequency, and A_o is the amplitude of the temperature oscillation at the surface. The amplitude A_o is generally in the range from 10 to 30°C. The surface temperature wave propagates downward with decreasing amplitude and lagging phase. The temperature field $T(z,t)$ in the zone of annual variation can be described by the heat conduction equation for a semi-infinite homogeneous medium with following initial and boundary conditions:

$$\frac{1}{a}\frac{\partial T}{\partial t} = \frac{\partial^2 T}{\partial z^2}, \qquad z > 0, \tag{2.29}$$

$$T(z,0) = T_o + \Gamma z$$

$$T(0,t) = T(t), \qquad T(\infty,t) = T_o + \Gamma z$$

The solution of this equation is known (Carslaw and Jaeger, 1959):

$$T(z,t) = T_o + \Gamma z + A_o \exp\left(-z\sqrt{\frac{\omega}{2a}}\right) \sin\left(\omega t - z\sqrt{\frac{\omega}{2a}}\right), \tag{2.30}$$

where a is the thermal diffusivity. The ratio of the temperature amplitudes $A(z)$ and A_o is

$$\frac{A(z)}{A_o} = \exp\left(-z\sqrt{\frac{\omega}{2a}}\right) \tag{2.31}$$

As can be seen this ratio approaches zero only when $z \to \infty$. In practice, the value of $A(z)$ is generally taken to be equal to the accuracy of temperature measurements (ΔT).

Example.
Let us assume that for some location:
$A_o = 20^o$C, $a = 1.0 \times 10^{-6} m^2/s$, and $\Delta T = 0.01^o$C. The parameters ω and $A(z)/A_o$ are $2\pi/\text{year} = 2.0 \times 10^{-7} s^{-1}$ and 0.01/20=0.0005 respectively. From equation (2.31) we obtain that

$$\ln\ 0.0005 = -z\sqrt{2.0 \times 10^{-7}/2.0 \times 10^{-6}}, \quad 7.6 = z\sqrt{0.1}, \quad z = 24.0\ m$$

This means that at the depth of 24.0 m the temperature oscillations during the year will not exceed 0.01°C.

It was noted by many investigators that, when field temperature–depth curves are extrapolated to the surface, the obtained surface temperatures (T_o^*) usually differ from the mean annual air temperature at the surface (T_o). The values of $b = T_o^* - T_o$ for 125 measurements ranged from -6.9°C to 5°C and the mean value of b was -1.6°C (Van Orstrand, 1941). Here we will not discuss the effect of numerous factors which may contribute to this phenomenon.

2.2.5 Mechanisms of Heat Transfer

There are three mechanisms for heat transfer: conduction, convection, and radiation.

If some parts of a solid body are at different temperatures, the process of temperature equalization will take place. The molecules from "hot" parts of the body with higher kinetic energy will collide with their neighbors – molecules with lower kinetic energy and a portion of energy will be transferred to the "cold" molecules. With time all parts of body will attain an equal temperature. This process of temperature equalization is called heat conduction. Quantitatively the Fourier law (Equation 2.16) describes the heat transfer by heat conduction.

At heat convection the energy is transferred by a flowing fluid or gas. Two types of heat convection are distinguished by their driving force. The free heat convection is caused only by the nonuniform fluid or gas density distribution. At forced heat convection the movement of fluids or gases can be brought by some external factors. For example, in a closed temperature observational well only free heat convection can occur. In a gas producing well the dominant heat transfer mechanism is the forced heat convection and the gas movement is caused by the high reservoir pressure. Usually heat conduction and heat convection occur simultaneously. In practice an effective (apparent) thermal conductivity coefficient λ_e is used,

$$\gamma_c = \frac{\lambda_e}{\lambda} = 1 + \frac{\lambda_c}{\lambda} \tag{2.32}$$

where λ_c is the convective thermal conductivity coefficient, and γ_c

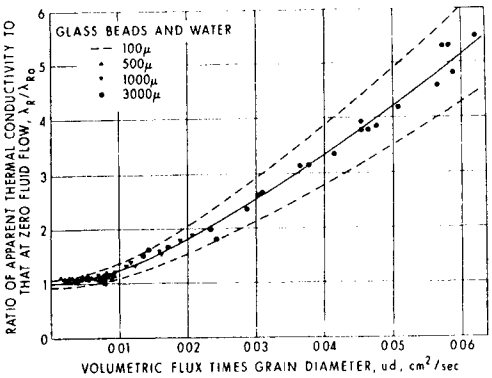


Fig.2.5. Influence of fluid velocity on the longitudinal thermal dispersity of a porous medium (Bia and Comparnous, 1975).

Table 2.4 The γ_c = f(Ra) function (Petrazhitskiy and Bekneva, 1973)

$0.7 \leq Pr \leq 310$; $1.18 \leq \frac{r_2}{r_1} \leq 6.6$	
Ra	γ_c
$\leq 10^3$	1
$10^3 \leq 10^7$	$0.121 \times Ra^{0.287}$
$10^7 \leq 10^{10}$	$0.595 \times Ra^{0.188}$

shows the effect of heat convection on the heat transfer. An example of the effective thermal conductivity increase with fluid velocity is shown in Fig. 2.5. For vertical cylindrical annuluses the value of γ_c can be determined from Table 2.4.

$$Pr = \frac{\nu}{a}; \qquad Ra = \frac{g\beta}{\nu a}(r_2 - r_1)^3 \Delta T, \tag{2.33}$$

where Pr is the Prandtl number, Ra is the Rayleigh number, ν is kinematic viscosity, a is thermal diffusivity, g is gravitational acceleration, β coefficient of volumetric thermal expansion, r_1 is the inner radius (outside radius of the drill pipe), r_2 is the outer radius (inside radius of the casing or well radius), and ΔT is the radial temperature difference.

At radiation heat is transferred by the electromagnetic waves. The rate of radiation heat transfer from a heated surface per unit surface

area is given by the Stefan-Boltzmann law

$$q = \delta \epsilon T^4 \tag{2.34}$$

where $\delta = 5.775 \cdot 10^{-12}$ W cm^{-2}K^{-4} is the Stefan-Boltzmann constant, ϵ is the emissivity of the surface. Radiation heat transfer is not considered to be an important heat transfer mechanism in reservoir formations (Prats, 1982). For steam or hot water injection wells radiation contributes to heat losses (see Chapter 6).

2.3 Basic Heat Transfer Equations

2.3.1 The Differential Heat Conductivity Equation

In this section we will follow the classical monograph by Carslaw and Jaeger (1959).
The differential equation of heat conduction is the mathematical expression of the first law of thermodynamics – the law of conservation of energy. According to this law the rate of increase of the heat content of a small volume (ΔV) with surface area S is equal to the sum of the rate of heat generation in ΔV and the rate of flow of thermal energy into this volume across S.

Consider the case of a solid through which heat is flowing and no heat is generated within of this solid. The temperature T at the point $P(x, y, z)$ and the heat flow will be continuous functions of Cartesian coordinates and time. For a homogeneous solid whose thermal conductivity and volumetric heat capacity are independent of temperature the differential heat conductivity equation may be written

$$\nabla^2 T = \frac{\partial^2 T}{\partial x^2} + \frac{\partial^2 T}{\partial y^2} + \frac{\partial^2 T}{\partial z^2} = \frac{1}{a}\frac{\partial T}{\partial t}, \tag{2.35}$$

where a is the solid's thermal diffusivity coefficient. In this work mainly cylindrical coordinates will be used. In the cylindrical system

$$x = r \cos\theta, \quad y = r \sin\theta$$

and the equation for T becomes

$$\nabla^2 T = \frac{\partial^2 T}{\partial r^2} + \frac{1}{r}\frac{\partial T}{\partial r} + \frac{1}{r^2}\frac{\partial^2 T}{\partial \theta^2} + \frac{\partial^2 T}{\partial z^2} = \frac{1}{a}\frac{\partial T}{\partial t} \tag{2.36}$$

Let us now assume that heat is produced in the solid and at the point $P(x, y, z)$ heat is supplied at the rate $A(x, y, z, t)$ per unit time per unit volume. In this case the equation (2.35) becomes

$$\nabla^2 T + \frac{A(x, y, z, t)}{\lambda} = \frac{1}{a}\frac{\partial T}{\partial t} \tag{2.37}$$

If the thermal conductivity and volumetric heat capacity of the solids are dependent of both position and temperature, the equation (2.37) is replaced by

$$\rho c \frac{\partial T}{\partial t} = \frac{\partial}{\partial x}\left(\lambda \frac{\partial T}{\partial x}\right) + \frac{\partial}{\partial y}\left(\lambda \frac{\partial T}{\partial y}\right) + \frac{\partial}{\partial z}\left(\lambda \frac{\partial T}{\partial z}\right) + A \tag{2.38}$$

As was mentioned by Carslaw and Jaeger (1959), the solution of this equation offers no great difficulty and a number of solutions were obtained for composite solids and for some $\lambda = \lambda(x, y, z)$ functions. If the thermal properties depend on temperature, the differential heat conduction equation becomes non-linear and mainly numerical methods of solutions are used.

2.3.2 Main Assumptions

To mathematically describe the heat exchange between the flowing fluid (or gas) in the wellbore (during drilling, cementing, production, and injection) and the surrounding formations, following assumptions are usually made.

- Formation around wellbore is homogeneous and isotropic.
- There is no flow of fluids across the formation except in the thief zone.
- Heat flow within the formation is due only to conductivity.
- Initially, no radial temperature gradients around the wellbore are present.
- In surrounding the wellbore formations the initial temperature is a known function of depth.
- Thermal properties of fluids and formations are constant. Only in permafrost areas the changes of thermal properties can be caused by freezing or thawing. Similarly, at steam injection the evaporation

of water in surrounding the wellbore formations may change the thermal properties in the "dry" zone.

- The radial temperature distribution in the tubing (drill pipe) and in the annulus is neglected.
- Well flow rate of the fluid (drilling mud, oil, water) or gas is constant.
- Fluid flow in the tubing and the annulus is one-dimensional, vertical.
- The vertical heat conduction in the formation can be neglected compared with the horizontal heat conduction.

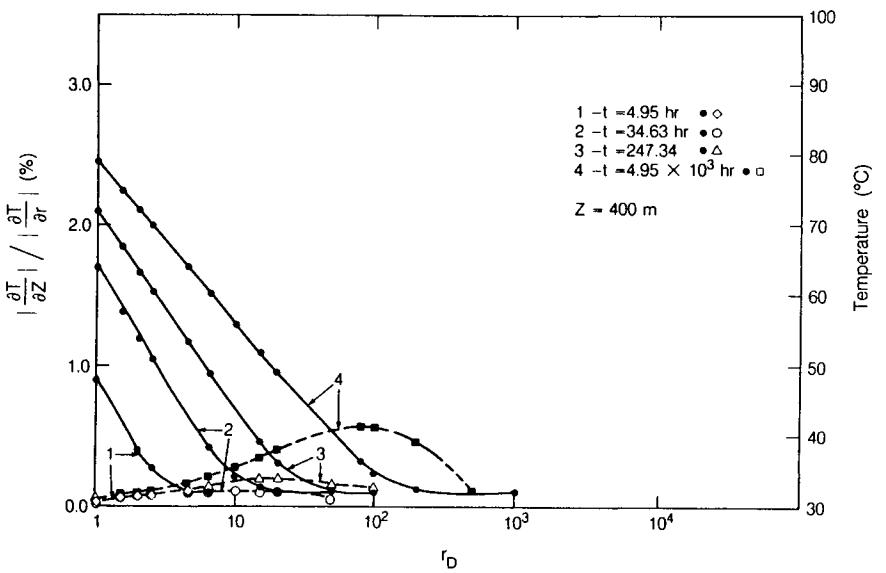


Fig. 2.6. Ratio of vertical and horizontal temperature gradients and temperature distribution in formation (Wu and Pruess, 1988). Courtesy of Society of Petroleum Engineers.

Wu an Pruess (1988) used a numerical solution and examined the last assumption by comparing the horizontal and vertical gradients in the formation. It was shown (Fig. 2.6) that the ratio of veriical and horizontal temperature gradients η is always smaller than 1%. To estimate the value of η Medvedskiy (1971) assummed that a constant linear heat source can approximate the thermal effect of a

drilling/production well. In this case the value of η is approximately

$$\eta = \frac{1}{2u}\int_0^u \{\sqrt{\pi}\,[1 - \Phi(\frac{1}{\sqrt{x}})] - \sqrt{x}[1 - \exp(-\frac{1}{x^2})]\}\,dx \qquad (2.38)$$

where Φ is the error function, $u = 4at/z^2$ is the dimensionless time, a is the thermal diffusivity, z is the depth of the well, and t is the drilling/production time. In the extreme case when $t \to \infty$ the computed value of η is $\sqrt{\pi}/2 = 0.886$. However, if we assume that $t = 50$ years, $a = 0.0040$ m^2/hr, $z = 1000$ m, then $\eta = 0.033$ (Medvedski, 1971).

2.3.3 Laplace Equation

For a steady heat flow in a material with constant conductivity and no heat production $A(x, y, z, t) = 0$ the diffusivity equation becomes

$$\frac{\partial^2 T}{\partial x^2} + \frac{\partial^2 T}{\partial y^2} + \frac{\partial^2 T}{\partial z^2} = 0 \qquad (2.39)$$

This equation is known as Laplace's equation. In cylindrical coordinates the Laplace equation is

$$\frac{\partial^2 T}{\partial r^2} + \frac{1}{r}\frac{\partial T}{\partial r} + \frac{1}{r^2}\frac{\partial^2 T}{\partial \theta^2} + \frac{\partial^2 T}{\partial z^2} = 0 \qquad (2.40)$$

For a one dimensional case the last equation becomes

$$\frac{\partial^2 T}{\partial r^2} + \frac{1}{r}\frac{\partial T}{\partial r} = 0 \qquad (2.41)$$

This equation describes the temperature distribution in a cylindrical wall where heat transfer is only in radial direction. The solution of the equation (2.41) is

$$T = C_1 \ln r + C_2 \qquad (2.42$$

The constants C_1 and C_2 are determined from boundary conditions.

2.3.4 Poisson Equation

For a steady heat flow in a body with constant conductivity and constant internal heat production $A(x, y, z) = const$ the diffusivity

equation becomes

$$\frac{\partial^2 T}{\partial x^2} + \frac{\partial^2 T}{\partial y^2} + \frac{\partial^2 T}{\partial z^2} + A(x, y, z) = 0 \tag{2.42}$$

This equation is called the Poisson equation. In cylindrical coordinates the Poisson equation is

$$\frac{\partial^2 T}{\partial r^2} + \frac{1}{r}\frac{\partial T}{\partial r} + \frac{1}{r^2}\frac{\partial^2 T}{\partial \theta^2} + \frac{\partial^2 T}{\partial z^2} + A(r, \theta, z) = 0 \tag{2.43}$$

2.3.5 Stefan Relationship

The problem of phase change around a cylindrical source occurs in many petroleum engineering designs: underground pipelines and oil/gas production wells in permafrost areas, and steam injection boreholes. During a thawing (evaporation) or freezing (condensation) process the formations around the wellbore will be divided into zones separated by a phase change interface. The energy conservation condition at phase change interface is expressed by the Stefan relationship. For a thawing process the Stefan relationship becomes

$$\lambda_f \frac{\partial T_f}{\partial r} - \lambda_t \frac{\partial T_t}{\partial r} = Lw \frac{dh}{dt}, \tag{2.44}$$

where T_f, T_t are radial transient temperatures in the frozen and thawed zones, L is the latent heat per unit of mass, λ_f, λ_t are the thermal conductivities, $h = h(t)$ is the radius of thawing, and w is the ice mass content per unit of volume. It is also assumed that the density is constant and melting of the substance (ice) occur at a constant temperature. For a freezing process a negative value of L should be used in the last equation.

2.3.6 Initial and Boundary Conditions

To solve the diffusivity equation we assume that in the formations T is a continuous function of x, y, z, and t, and that holds also for the first differential coefficient with regard to t and for second differential coefficients with regard to x, y, and z. At the boundary of the solid, and at the moment of time $t = 0$ these assumptions are not made (Carslaw and Jaeger, 1959). Accordingly, more

simplified assumptions should be made to solve the Laplace or Poisson equation.

Initial conditions.

Any instant can be taken as the origin of the time coordinate. In this case the temperature distribution at this moment of time should be given

$$T(x, y, z, t = 0) = f(x, y, z); \text{ or } T(r, \theta, z, t = 0) = f(r, \theta, z) \quad (2.45)$$

Let us assume a case of radial symmetry: an oil well after some period of production was shut-in for some time. To find the temperature distribution around the wellbore during shut-in, the end of production can be taken as the origin of the time coordinate. In this case the temperature $f(r, z)$ around the wellbore at the end of production should be given. We also can take as a starting instant the moment of time when the well was spudded. Let us also assume that the undisturbed formation temperature is $f_o(z) = T_o + \Gamma z$, then the initial temperature distribution is $T(r, z, t = 0) = f_o(z)$. However, in this case we have to specify boundary conditions during drilling, production, and shut-in periods. Only computer programs can deal with this complex problem.

Boundary or surface conditions

To determine the temperature field of a given body we should also specify its boundary conditions. The four types of boundary conditions are:

- Prescribed surface temperature T_s. In general case this temperature may be constant or a function of time and coordinates $T_s = f(x, y, z, t)$.
- Prescribed heat flow q_s across the surface. The function q_s may be a function of time and position

$$q_s(x, y, z, t) = -\lambda \frac{\partial T}{\partial n}, \quad (2.46)$$

where $\frac{\partial}{\partial n}$ denotes differentiation in the direction of the outward normal to the surface.

- Linear heat transfer at the surface. In this case the heat flow across the surface is proportional to the temperature difference between the surface and the surrounding medium

$$q_s = \alpha(T_s - T_o), \quad (2.47)$$

where T_s is the surface temperature, T_o is the temperature of the surrounding medium, and α is a constant – heat transfer coefficient. As $\alpha \to \infty$ this boundary condition tends to the first boundary condition ($T_s = T_o$).

□ The surface of separation (S) of two media of different conductivities λ_1 and λ_2. Let T_1 and T_2 denote the temperatures in the two media. In this case

$$T_1|_S = T_2|_S, \tag{2.48}$$

$$-\lambda_1 \frac{\partial T_1}{\partial n}|_S = -\lambda_2 \frac{\partial T_2}{\partial n}|_S. \tag{2.49}$$

In practice, however, various modifications of the above mentioned boundary conditions are often used.

2.3.7 Dimensionless Parameters

To reduce the number of variables in solving heat conduction problems the dimensionless quantities are usually used. For example, consider the equation of radial flow of heat from a cylindrical source with a radius r_c.

$$\frac{\partial^2 T}{\partial r^2} + \frac{1}{r}\frac{\partial T}{\partial r} = \frac{1}{a}\frac{\partial T}{\partial t}; \quad r > r_c, \tag{2.50}$$

with initial and boundary conditions

$$T(r,0) = T_o; \quad T(r_c,t) = T_c; \quad T(\infty,t) = T_o \tag{2.51}$$

Let us introduce dimensionless quantities of distance (r_D), temperature (T_D), and time (t_D)

$$r_D = \frac{r}{r_c}; \quad T_D = \frac{T(r,t)}{T_c - T_o}; \quad t_D = \frac{at}{r_c^2} \tag{2.52}$$

Now the equations 2.50 and 2.51 can be replaced by

$$\frac{\partial^2 T_D}{\partial r_D^2} + \frac{1}{r_D}\frac{\partial T_D}{\partial r_D} = \frac{\partial T_D}{\partial t_D}; \quad r_D > 1, \tag{2.53}$$

$$T(r_D,0) = \frac{T_o}{T_c - T_o}; \quad T(1,t_D) = \frac{T_c}{T_c - T_o}; \tag{2.54}$$

$$T(\infty,t_D) = \frac{T_o}{T_c - T_o}$$

2.4 Thermal Regime of Permafrost

2.4.1 Temperature of Frozen Rocks

Permanent ice is found on or beneath approximately twenty percent of the dry land: 75% of Alaska, 63% of Canada, and 47% of Russian Federation are covered by permafrost. Wherever permanent ice is found a necessary condition is satisfied for the existence of permafrost. The permafrost base is defined as the 0^oC isotherm and thickness as the depth from the surface to that isotherm. Hence, an accurate temperature–depth curve is needed to obtain the value of the permafrost thickness. At a given location the permafrost depth depends mainly on following factors: long-term annual mean surface temperature, thermal conductivity, ice (water) content of formations, salinity of unfrozen water, heat flow density (heat flow from the Earth's interior), and past climate. For this reason the thickness of permafrost can vary within wide limits even for close located sites.

Permafrost was formed and exists in definite thermal conditions, characterized in the first place by a field of negative temperatures (in ^{o}C) and phase transitions of water into ice. The temperature field in permafrost regions is formed under the influence of the heat exchange on the surface, the composition and structure of the formations, the heat flow density, local sources of heat, and phase transitions of water. In the permafrost areas the rate of heat flow serves as the main criterion of the steadiness or nonsteadiness of the thermal regime. Indeed, this directly follows from the Stefan's condition at the phase boundary,

$$q_f - q_t = \pm Q \frac{dl}{dt}, \tag{2.55}$$

where q_t and q_f are the heat flow at the phase boundary in the thawed and frozen zone respectively, Q is the amount of heat released (absorbed) per unit of volume at freezing (thawing), l is the thickness of of the frozen formations, and t is the time.
It is clear that the condition $q_f = q_t$ corresponds to a steady regime, the condition $q_f > q_t$ corresponds to a regime of freezing and the condition $q_f < q_t$ corresponds to a thawing regime.

The analysis of geothermal field and laboratory data: determi-

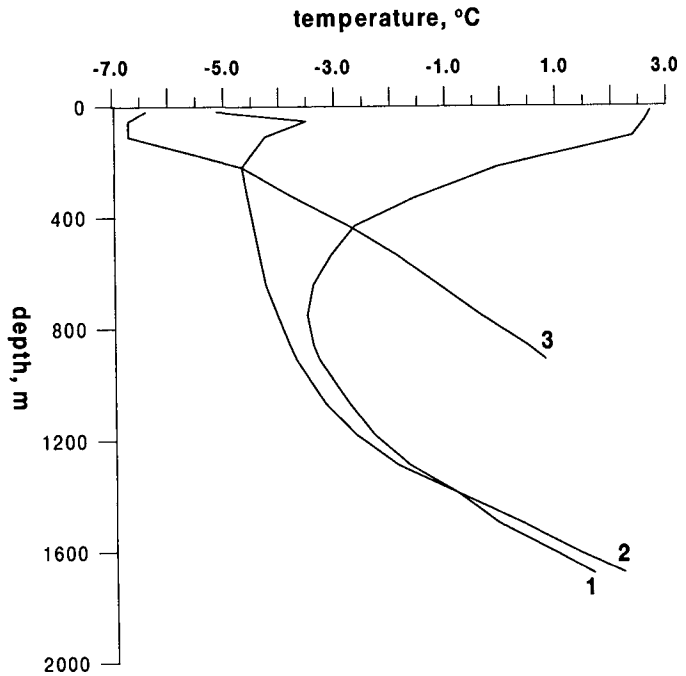


Fig. 2.7. Vertical profiles of the temperature field of rocks west of the East Siberian platform. 1–Markhinskaya well 1; 1–Markhinskaya well 2; 3–well of the "Udachnaya" pipe (Balobayev et al., 1973).

nation of formations thermal properties, estimation values of q_f and q_t have shown that the temperature profiles in permafrost regions can be divided into three groups (Balobayev et al., 1973).

The first group, which comprises the greater part of geothermal data, indicates that the temperature field of permafrost is steady and corresponds to contemporary conditions of heat exchange on the surface and geothermal heat flow ($q_f = q_t$).

Examples of the second group of the geothermal data are presented in Fig. 2.7 . The unusual temperature profiles is due to the fact that the heat flow constantly increases with depth, while in the area of well 1 it even changes sign because of the development of a local surface talik. The analysis of the field data (Fig. 2.7) shows that the absorption of the heat flow due to physicochemical processes may cause change of the heat flow with depth. Subterranean waters

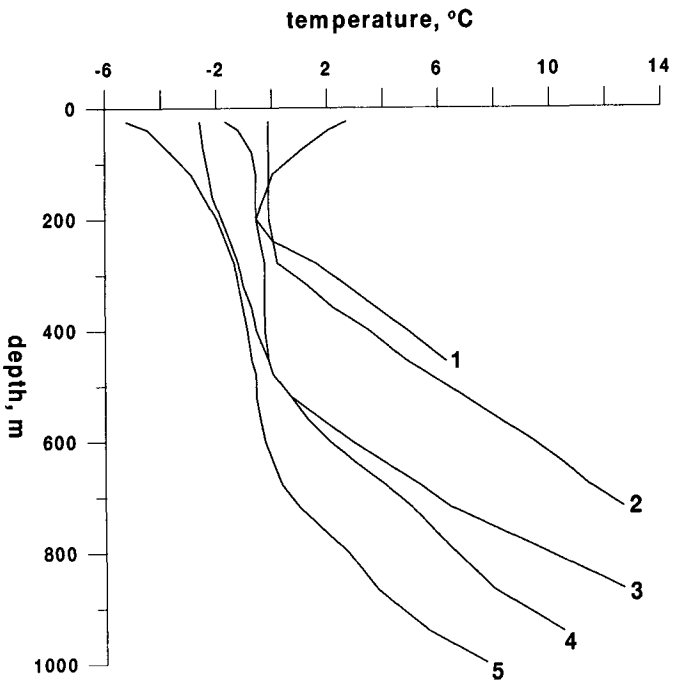


Fig. 2.8. Vertical profiles of a transient temperature field of rocks in different areas. 1–Lower Ob'; 2–Kostrovskii; 3–Middle Vilyui; 4–Namtsy; 5–Bakhynai (Balobayev et al., 1973).

in these areas are brines with a salt content of 250-350 g/l. A number of dissolved substances can be found in saturated condition, and in these conditions processes of crystallization, exchange, and replacement with absorption of heat can take place. It should be noted that the ice bounded formations can be found only in the upper (100-300 m) near-surface part.

The third group of geothermic data (Fig. 2.8) characterizes a clearly transient temperature field accompanied by the thawing at the permafrost base. This shows the existence of a more severe climate in the past. The rate of thawing at the present time can be estimated from Formula 2.56

$$-\frac{dl}{dt} = \frac{q_t - q_f}{Q} \tag{2.56}$$

and its estimated value from field data is 1-2 cm/yr (Melnikov et al.,

1973). Balobayev (Balobayev et al., 1973) obtained an approximate formula which allows one to evaluate the change of the permafrost thickness when the surface temperature is a linear function of time. It is interesting to note, that at present there are no data showing contemporary increase of the permafrost thickness with time.
Thus the temperature profiles in the permafrost contain a record of the change in surface temperature in the past. When interpreted with heat conduction theory, this source can provide important information of patterns of contemporary climate change. Precision measurements in oil wells in the Alaskan Arctic indicate a widespread warming (2°- 4°C) at the permafrost surface during the 20th century (Lachenbruch et al., 1988). It should be noted that the "permafrost surface" is the surface of permafrost which lies beneath an annually thawing (active) layer. In the Section 2.4.4 we present the Berggren formula which allows one to determine the depth of this layer.

2.4.2 Thickness and Dynamics of Permafrost

In this section we present a simple model for permafrost response to climate change. The schematic model is presented in Fig. 2.9. Let us assume that at some moment of time the temperature of permafrost is given by the curve $t = 0$; thereafter the top of ice-bound permafrost is maintained at temperature V_1, and melting temperature of ice is equal to 0°C. When the salinity of frozen formations can be estimated, then the melting temperature at the permafrost base should be specified (Osterkamp, 1984).
For small values of time t we can assume that the heat flow from the base of the permafrost into the frozen zone is equal to heat flow for the case when the base of permafrost remains fixed (Lachenbruch and Marshall, 1977; Lachenbruch et al., 1982; Osterkamp, 1984). In this case, it is necessary to approximate the transient behavior of the temperature in a slab (T_s) of a constant thickness, l_o, with an initial linear temperature distribution and with the upper and lower surfaces maintained at a constant temperatures (V_1 and 0°C) for $t > 0$. The corresponding diffusivity equation is:

$$a_f \frac{\partial^2 T_s}{\partial x^2} = \frac{\partial T_s}{\partial t}; \qquad t > 0, \quad 0 \leq x \leq l_o \tag{2.57}$$

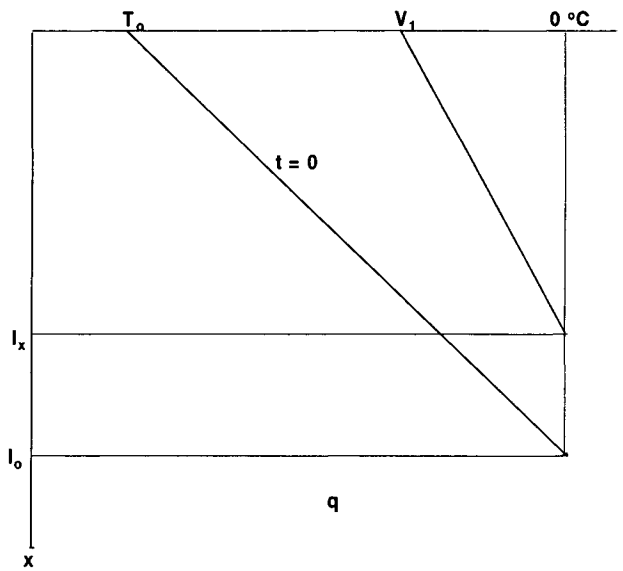


Fig. 2.9. Dynamics of permafrost thickness – a schematic model.

with the initial an boundary conditions

$$T_s = T_o + kx; \qquad k = -T_o/l_o \ \ at \ \ t = 0, \tag{2.58}$$

$$T_s(0,\ t) = V_1; \qquad T_s(l_o,\ t) = 0 \ \ at \ \ t > 0,$$

where l_o is the initial depth of permafrost, T_o is the long-term mean annual temperature at $t = 0$, and V_1 is the long-term mean annual temperature of the top of ice-bounded permafrost at $t > 0$.
The solution of this equation is known (Carslaw and Jaeger, 1959)

$$T_s = V_1 - V_1\frac{x}{l_o} + \frac{2(T_o - V_1)}{\pi}\sum_{n=1}^{\infty}\frac{1}{n}\sin\frac{\pi n x}{l_o}\exp\left(-Fo\ n^2\pi^2\right) \tag{2.59}$$

where the dimensionless time – Fourier number is

$$Fo = \frac{a_f t}{l_o^2}$$

and a_f is the thermal diffusivity of ice-bounded permafrost. The temperature gradient at the base of the permafrost ($x = l_o$) from formula (2.59) is:

$$\Gamma_b = \frac{dT_s}{dx}\Big|_{x=l_o} = -\frac{V_1}{l_o} + \frac{2(T_o - V_1)}{l_o}\sum_{n=1}^{\infty}(-1)^n\exp\left(-Fo\ n^2\pi^2\right) \tag{2.60}$$

Table 2.5 The $\psi = \psi(Fo)$ function

ψ	Fo
0.5	$0.04 \geq Fo > 0$
$0.592 \exp(-4.223Fo)$	$0.06 \geq Fo \geq 0.04$
$\exp(-\pi^2 Fo) - \exp(4\pi^2 Fo)$	$0.15 \geq Fo \geq 0.06$
$\exp(-\pi^2 Fo)$	$Fo \geq 0.15$

The temperatures of frozen formations near the permafrost base are close to 0°C. Hence, the amount of heat which is consumed in warming the permafrost to the melting temperature is small and can be neglected. The value of l_x under these assumptions can be obtained from the thermal balance condition

$$-\lambda_f \int_o^t \Gamma_b \, dt + qt = L_v(l_o - l_x) \tag{2.61}$$

where q is the heat flow density (geothermal flux), L_v is the latent heat of melting per unit of volume of frozen formation, and l_x current depth of the permafrost base.
From formulas (2.60) and (2.61) we obtain

$$l_x = l_o + \frac{\lambda_f(T_o - V_1)}{l_o L_v}(t - \int_o^t \psi \, dt), \tag{2.62}$$

$$\psi = -\sum_{n=1}^{\infty}(-1)^n \exp\,(-Fo\, n^2\pi^2) \tag{2.63}$$

A simple computer program can be used to estimate the value of l_x. For approximate calculations we present Table 2.5. For large values of time, assuming steady-state distribution of temperatures in the frozen zone, the Stefan equation is

$$-\lambda_f \frac{V_1}{l_x} - L_v \frac{dl_x}{dt} = q \tag{2.64}$$

Now the temperature distribution is

$$T_s = V_1 - \frac{V_1}{l_x}x; \qquad x \leq l_x \tag{2.65}$$

The solution of equation (2.64) is

$$t = \frac{L_v}{q^2}[q(l_o - l_x) + \lambda_f V_1 \ln \frac{\lambda_f V_1 + q l_x}{\lambda_f V_1 + q l_o}] \tag{2.66}$$

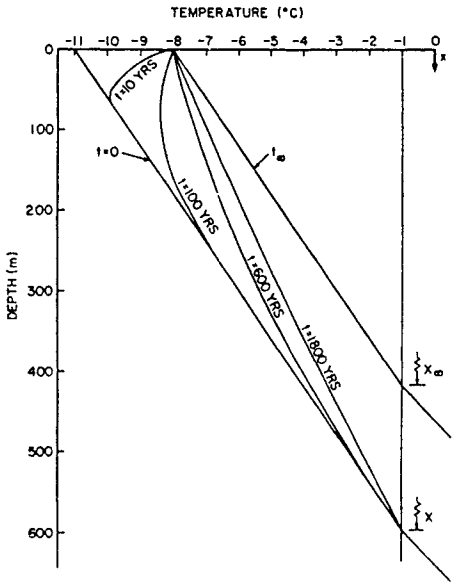


Fig. 2.10 Thermal warming model for the continuous permafrost zone (Osterkamp, 1984).

From equation (2.64) the minimum value of l_x is when $\frac{dl_x}{dt} = 0$ (at $t \to \infty$),

$$l_{x,min} = -\frac{\lambda_f V_1}{q} \tag{2.67}$$

For Prudhoe Bay, Alaska this simple model that illustrates the response of the permafrost to sudden change in the mean annual surface temperature is shown in Fig. 2.10. Note that here the thawing temperature at the permafrost base is assumed to be -1 °C. Melting at the base of the permafrost amounts to $\approx$ 3.5 m during the first 1800 years and is ignored in this graph.

More realistic model of the dynamics of the temperature field and the permafrost thickness, that accounts for the possible time variation in surface temperature, were represented by an expression of the form (Lachenbruch et al., 1982; Lachenbruch et al., 1988)

$$T_o(0,t) = Dt^{n/2}, \qquad 0 < t < t_o \tag{2.68}$$

where D is a constant, n can be any positive integer, and t is the time since the start of the warming; $t = t_o$ represents the

present day. Duchkov et al. (1997) used numerical modeling to predict the possible evolution of the temperature field of permafrost rocks until year 2100. The Authors assumed a stable increase in the permafrost surface temperature at a rate of 0.02-0.06 °C/year. It has been shown that the past climate may considerable accelerate the permafrost degradation in the West-Siberian region. This may cause in the future serious problems in the oil/gas exploration and production.

2.4.3 Offshore Permafrost

During the last transgression which terminated about 5000-6000 years ago, the sea flooded extensive areas of coastal lowlands (Molochushkin, 1973; Lachenbruch and Marshall, 1977). This brought about a substantial change in the thickness and temperature of the permafrost layer. The results of drilling, probing, and geophysical studies have shown that there are substantial areas of permafrost sea (Molochushkin, 1973; Lachenbruch and Marshall, 1977; Osterkamp and Harrison, 1982). To estimate the current depth of permafrost base as a function of time since submergence and transient temperature profiles formulas 2.59-2.67 can be used. In this case l_o is the initial depth of permafrost (on land), and T_o is the long-term mean annual temperature at land surface (prior to submergence) at $t = 0$. Molochushkin (1973) conducted long term (four years) temperature observations in shallow boreholes (up to 20 m) drilled on the island and in the coastal waters of the Laptev sea.

The temperature observations have shown the existence of subsea permafrost in near shore area of the Laptev sea. It was determined that permafrost with a relatively high temperature can bee found in an area of intensive thermal abrasion, even in the sectors with a positive mean annual water temperature at a distance of up to 1.0 - 1.5 km from the shore.

Numerical modeling has shown that the temperature disturbance caused by a sudden change in surface conditions penetrated to a depth of over 100 m during the first 50 years after submergence (Fig. 2.11). Let us consider a general case when it is unknown how many times in the past a selected drilling site was flooded. In this case it is reasonable to assume that the temperature profiles in a

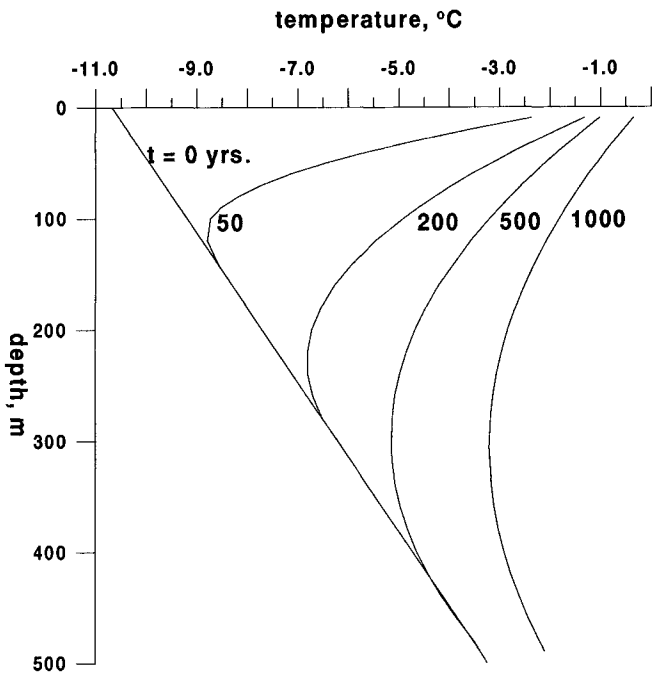


Fig. 2.11. Changes in temperature of continental permafrost under the thermal influence of water with a mean annual temperature of -0.8°C (Molochushkin, 1973), modified.

given area could fall between the hypothetical Curves 1 and 4 in Fig. 2.12. Profile 2 corresponds to a recent offshore-to-onshore transition and Profile 4 corresponds to a onshore-to-offshore transition.

2.4.4 Change of Mechanical Properties at Thawing

The knowledge of mechanical properties of frozen formations is the key to understanding the problem of surface and well stability. Therefore, in this Section we will present some data on this subject. The mechanical properties of frozen formations very strongly depend on moisture content and cryogeneous texture. A knowledge of the ice and unfrozen water content of permafrost is essential in predicting the permafrost behavior during well drilling and production. Ice contents do vary widely and depend primarily on the formation type, and the thermal and depositional history of the formation profile (Smith and Clegg, 1971).

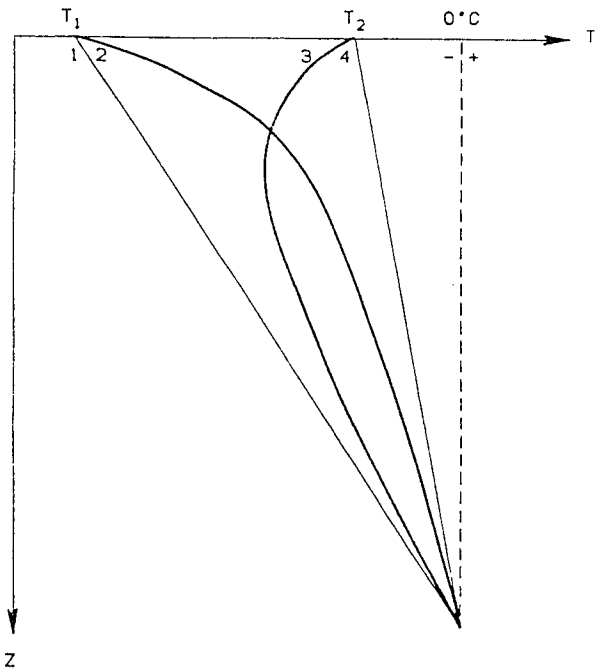


Fig. 2.12. Schematic curves of permafrost temperatures versus depth. 1 – onshore; 2 and 3 – transitional areas; 4 – offshore.

It is known that only a part of the formation's pore water changes to the ice at 0°C. With further lowering of the temperature, phase transition of the water continues, but at steadily decreasing rates. The amount of unfrozen water is practically independent of the total moisture content for a given soil (Tsytovich, 1975). Frozen soils are bodies in which stresses and strains that arise under the influence of an external constant load are not constant, but vary with time, giving rise to relaxation of stresses and creep (an increase in the strains with passage of time). These processes are called rheological. The strong development of rheological processes in frozen soils is due to a peculiarity of their internal bonds in which ice plays a role of major importance (Tsytovich, 1975).

Some values of the instantaneous (C_{inst}) and long term (C_{lt}) cohesion for frozen soils are presented in Table 2.6. In this table W_d is the ratio (in percent) of total ice-water content to dry unit weight of the soil. The impact of sea water on mechanical properties of

Table 2.6 Instantaneous and ultimate long term cohesion (in kg/cm^2) of permafrost, (Tsytovich, 1975)

Type of Soil	W_d	T = -0.3 to -0.4 °C		T = -4.0 to -4.2°C	
	%	C_{inst}	C_{lt}	C_{inst}	C_{lt}
Dense varved clay (mineral inter-layers)	30-40	5.7	1.8	16.0	4.2
Silty heavy loam	36	4.3	0.6	12.0	–
Silty light loam	30	4.1	0.9	11.0	2.0
Heavy silty sandy loam	28-34	4.0-4.5	0.9-1.0	8.0-15.0	2.8-3.2
Same, high moisture	43	6.0	1.8	11.0	2.0
Silty sand	23	11.0	2.1	20.0	3.7-4.5

submerged frozen soil is very important for the upper layer of frozen bottom sediments. The results of experimental studies performed in order to discover the effect of concentration of pore solution on the strength of the frozen ground are presented in Table 2.7 (Tsytovich et al., 1973). Research has shown that the long term compressive strength of frozen soils δ_{lt} is well described as a function of the negative temperature (in °C),

$$\delta_{lt} = a + b\sqrt{-T}, \tag{2.69}$$

where a and b are constants. Figure 2.13 shows the relation between compressive strength and temperature examined for various types of sand at salt concentrations of 0% and 3% and Fig. 2.14 presents a similar relation examined for cohesive soils. The compressive strength of frozen soils is very much dependent on the amount of the unfrozen water. The measured values of unfrozen water content for the samples (Figures 2.13, and 2.14) are presented in Fig. 2.15.

The curves showing the relation between the amount of unfrozen water and temperature show that the amount of unfrozen water is closely related with the specific surface area of each sample (Ogata et al., 1982).

Elastic deformations of frozen soils are governed purely reversible by changes in the crystal lattices of the mineral particles and ice, by the elastic properties of the thin films of unfrozen water, and

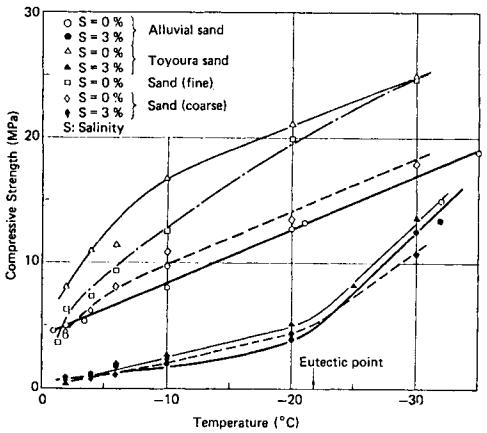


Fig. 2.13. Relation between compressive strength and temperature for sands (Ogata et al., 1982).

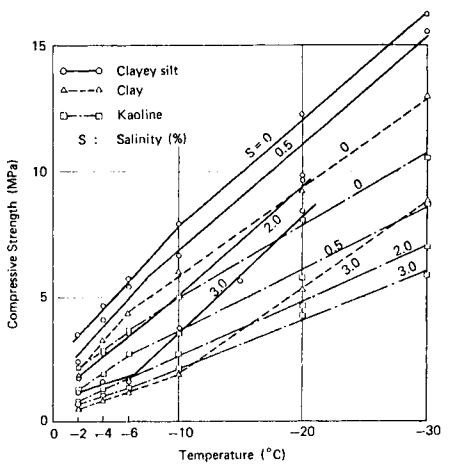


Fig. 2.14. Relation between compressive strength and temperature at various salinity (Ogata et al., 1982).

Table 2.7 Values of C_8 for soil of different granulometric composition (Tsytovich et al., 1973). C_8 is the eight-hour cohesion

Type of soil	Salt concentration percent	C_8 kg/cm^2, T, °C			
		-1	-2	-3	-4
Quartz sand with a silt-	0.0	4.7	5.4	7.9	9.3
clay fraction content	0.26	1.5	3.1	5.7	7.1
of 25 percent	0.52	0.6	1.2	2.3	3.5
	1.04	–	0.6	1.2	2.3
The same with a silt-clay	0.26	2.6	3.7	6.5	7.4
fraction content of	0.52	1.3	2.6	–	–
45 percent	2.6	–	–	0.6	0.7
Hydromica clayey sand	0.23-0.27	2.6	6.1	8.0	12.5
	0.64	2.5	3.7	7.0	11.3
	1.1-1.2	1.2	2.1	5.3	8.7
	2.1-2.5	–	0.4	0.9	1.5
	4.4-5.0	–	–	–	0.4
Quaternary clayey silt	1.35	–	0.64	1.56	2.35
(hydromica with mont-	2.2	–	0.46	0.78	1.05
morillonite admixture)	3.2	–	–	0.54	0.87
	4.3	–	–	–	0.5

by elastic properties of enclosed air bubbles (Tsytovich, 1975). The experiments showed that the modulus of normal elasticity of frozen soils is in tens and hundreds times larger than those of unfrozen soils.

The integrity and stability of pipelines, derricks, and foundations of structures very much depends on the processes of frost heave and surface subsidence. Both frost heave and surface subsidence are associated with volume changes (about 9%) at ice-water-ice transition. In the annual cycle the water phase transitions occur in the active layer – the layer of seasonal thawing (freezing). Hence, the intensity of the frost heave and surface subsidence are very much dependent on the depth of the active layer (h_{al}). To estimate the value of h_{al} the Berggren formula can be used (Pavlov, 1974; Lunardini, 1988)

$$h_{al} = \delta \sqrt{\frac{2\lambda_t T_{et} t_t}{L(w - w_u)}}, \tag{2.70}$$

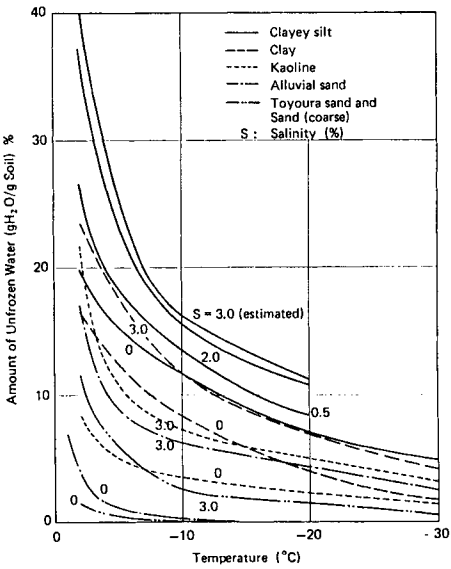


Fig. 2.15. Relation between unfrozen water content and temperature (Ogata et al., 1982).

where λ_t is the thermal conductivity of thawed soil, T_{et} is the mean effective temperature of air in degrees above the freezing point (in ^{o}C), t_t is the time of thawing, L is the latent heat per unit of weight, w is the total moisture content per unit of soil volume, w_u is the content of unfrozen water per unit of soil volume, and δ is a coefficient and can be obtained from Fig. 2.16. The parameters K_t and K_q are:

$$K_t = \frac{T_o - T_{fr}}{T_{et}}; \qquad K_q = \frac{C_f + C_t}{2L(w - w_u)} T_{et}, \tag{2.71}$$

where T_{fr} is the temperature of freezing (in ^{o}C), T_o is the temperature of the layer with zero amplitude of annual temperature change, and C_f, C_t are the volumetric heat capacity of frozen and thawed soil. For calculations the curves $\delta = \delta(K_t, K_q)$ can be approximated by

$$\delta = 1 - 1.6|K_t K_q|; \qquad |K_t K_q| \leq 0.06, \tag{2.72}$$

$$\delta = 1 - 1.278|K_t K_q| + (K_t K_q)^2; \qquad 0.06 < |K_t K_q| < 0.45$$

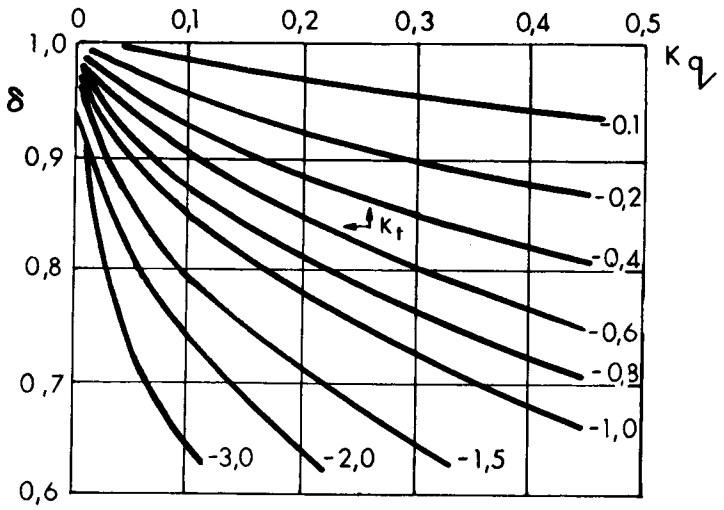


Fig. 2.16. The $\delta = \delta(K_t, K_q)$ coefficient (Pavlov, 1974).

2.5 Temperature Anomalies due to Topographic and Geological Factors

2.5.1 Flat-Lying Sediments

Consider a single uniform horizontal layer. Let us now assume that the formation temperatures at the top ($x = a$) and at the bottom ($x = b$) of this layer are known: $T(a)$ and $T(b)$. In this case one may expect that the temperature within of this layer can be expressed by a linear equation

$$T(x) = T(a) + \frac{T(b) - T(a)}{b - a}(x - a), \qquad a \leq x \leq b, \tag{2.73}$$

where a and b are the layer's top and bottom coordinates. It is logical to assume that when the actual formations temperatures $T^*(x)$ differ from those calculated after equation (2.73), the possibility of heat production or free thermal convection should be considered. The temperature–depth variation $\delta T(x) = T^*(x) - T(x)$ in this case may characterize the effect of one or both of these factors.
Below we will consider a case of heat supply at a constant rate in one layer. This may occur due to radioactivity, water movement,

and chemical reactions.
The corresponding equation of steady flow of heat is

$$\frac{d}{dx}(\lambda\frac{dT}{dx}) = -A = const \tag{2.74}$$

where A is the heat rate per unit time per unit volume. As a general example, we will consider a three-layer case (Carslaw and Jaeger, 1959) in which $\lambda = \lambda_1$, $A = 0$ in $0 < x < x_1$; $\lambda = \lambda_2$, $A = A_2$ in $x_1 < x < x_2$; $\lambda = \lambda_3$, $A = 0$ in $x > x_2$, where λ_1, λ_2, λ_3, A_2 are constants. Then the solution of the equation (2.74) is (Carslaw and Jaeger, 1959)

$$T = T_o + \frac{q_o x}{\lambda_1}, \quad 0 < x < x_1, \tag{2.75}$$

$$T = T_o + \frac{q_o x_1}{\lambda_1} + \frac{q_o(x - x_1)}{\lambda_2} - \frac{A_2(x - x_1)^2}{2\lambda_2}, \quad x_1 < x < x_2, \tag{2.76}$$

$$T = T_o + \frac{q_o x_1}{\lambda_1} + \frac{q_o(x_2 - x_1)}{\lambda_2} - \frac{A_2(x_2 - x_1)^2}{2\lambda_2} + \frac{[q_o - A_2(x_2 - x_1)](x - x_2)}{\lambda_3}, \quad x > x_2 \tag{2.77}$$

where T_o is the surface temperature and q_o is the surface heat flow (at $x = 0$). From equation (2.76) the value of $\delta T(x)$ is

$$\delta T(x) = T(x, A_2) - T(x, A_2 = 0) = -\frac{A_2(x - x_1)^2}{2\lambda_2}, \tag{2.78}$$

Earlier were presented several solutions of the steady-state conductivity equation for temperature-dependent thermal conductivity and depth-dependent heat production (equations 2.21-2.23).
To describe the process of free thermal convection of water in a porous medium, caused by temperature differences, Rayleigh number (Ra) and the Nusselt number (Nu) are used. By means of these numbers it is possible to examine whether or not water convection occurs through porous rocks, thus promoting heat transport (Haenel, et al., 1988). The two dimensionless numbers are given by:

$$Ra = \frac{\rho_w c_w \alpha_v k g z \Delta T}{\nu \lambda_r}; \quad Nu = \frac{\alpha z}{\lambda_r} \tag{2.79}$$

where ρ_w is the density of water, kg m^{-3}, c_w is specific heat capacity of water, J kg $^{-1}$ K^{-1}, α_v is the coefficient of volumetric thermal

expansion of water, K^{-1}; k is permeability to water, m^2; g is the acceleration of gravity, $m^2\ s^{-1}$; ΔT is the temperature difference at vertical distance, K; z is the vertical distance, m; ν is the kinematic viscosity of water $m^2\ s^{-1}$; λ_r is the thermal conductivity of water-saturated rock, $W\ m^{-1}\ K^{-1}$; and α is the coefficient of surface heat transfer, $W\ m^{-2}\ K^{-1}$.

From experimental data (Elder, 1981) it was found that convection of water in a porous medium (Hele-Shaw cell) starts at the critical Rayleigh number $Ra = Ra_c \geq 40$, and that the Nusselt number is given by

$$Nu = \frac{Ra}{40} \tag{2.80}$$

Elder (1981) also estimated the value of the total heat-flow density q_t transmitted from the bottom (z=L) to the top (z=0) of the Hele-Shaw cell

$$q_t = Nu\ \lambda_r\ \frac{\Delta T}{L} \tag{2.81}$$

Thus from this equation the value of $\Delta T = T_L - T_o$ can be determined. From physical considerations is clear that at a given value of q_t the convective process reduces the parameter ΔT and, hence, the temperature gradient. In practice this can be erroneously attributed to the formation's thermal conductivity increase. In the case where $Ra < 40$, the Nusselt number has to be set at $Nu = 1$.

Powell et al. (1988) introduced the first critical number Ra_1^* which defines the onset of fluid convection in a permeable layer of infinite horizontal extent and bounded by two perfectly insulating impermeable formations,

$$Ra_1^* = 4\pi^2 \tag{2.82}$$

Straus and Schubert (1977) have shown that in a real case the value of Ra_1^* is considerably influenced by the variable physical properties and non-Boussinesq behavior of the fluid; in this case the temperature gradient must be specified. Figure 2.17 shows how $Ra_c = Ra_1^*$ varies with the temperature gradient and thickness of the formation in which the physical properties are temperature and pressure dependent.

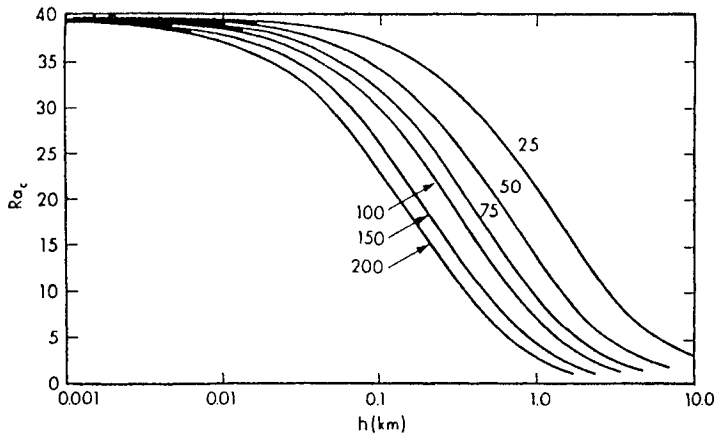


Fig. 2.17. First critical Rayleigh number Ra_c for a geothermal reservoir of thickness h at various gradients in mK m^{-1} and with permeability varying with temperature and pressure (Straus and Schubert, 1977).

It can be concluded from the Fig. 2.17 that free thermal convection is only likely to be important in geothermal regions (Powell et al., 1988).

2.5.2 Lateral Thermal Conductivities Contrasts

Consider a region of a flat relief with a constant heat flow density q. When the lithological profile of a wellbore consists of n uniform horizontal layers, the formation temperature will be a function of the vertical depth only. The geothermal gradient for any formation's layer (Γ_n) can be determined from the condition: $\Gamma_n \lambda_n = q$.

Let us assume that the area of the given region is A, then the total amount of heat per unit of time transferred to the Earth's surface will be $Q = Aq$. Suppose now that near the wellbore a body of anomalous thermal conductivity – a salt dome was discovered. In a this case the increase of the heat flow density (HFD) above salt dome will occur. At the same time a corresponding reduction of HFD will occur at some distances from the salt dome (Fig. 2.18). It is clear that the presence of a salt dome can only change the temperature field of formations but the value of Q will remain constant. The effect of lateral thermal conductivity contrasts,

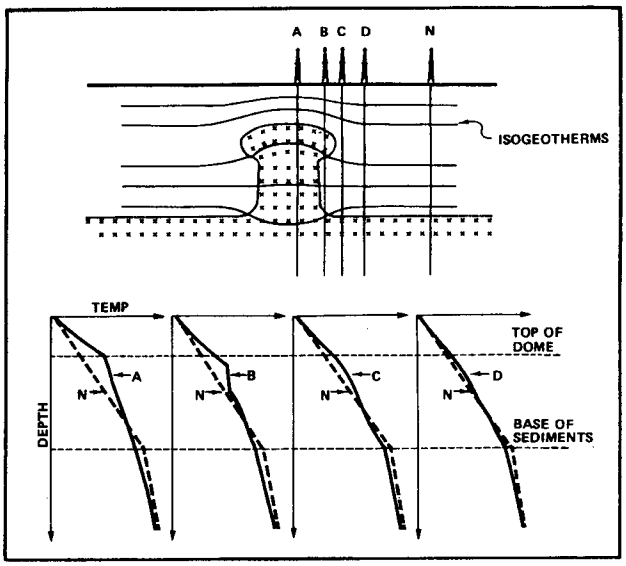


Fig. 2.18. Temperature–depth profiles near a salt dome (Guyod, 1946).

due to anomalously high thermal conductivity of rock salt, on the temperature field of formations near salt domes were discussed in the literature (Guyod, 1946; Kappelmeyer and Haenel, 1974; Cheremenskiy, 1977; Gretener, 1981). The value of HFD through salt domes and salt anticlines is high and causes anomalously high temperature gradients (Fig. 2.19). Guyod (1946) showed that the temperature gradients can reach 0.072 °C/m over the Humble dome (Texas) with salt at 380 m. Gradients from 0.067 to 0.100 °C/m (2 to 3 times the regional average) were recorded with diapiric salt at 150 to 250 m below the seafloor (Gretener, 1981). Interesting results of a numerical modeling were presented by Gretener (1981). He calculated the anomalies of the geothermal gradient and temperature at 150 m below the surface (at different distances from center of the salt dome) for salt rising from 13 km to various depths. The strong dependence of thermal conductivity on temperature (depth) was taken into account at calculations.

The well known solutions (Carslaw and Jaeger, 1959) for a spherical, cylindrical, or an ellipsoidal body of thermal conductivity λ^* immersed in a medium of thermal conductivity λ, in which

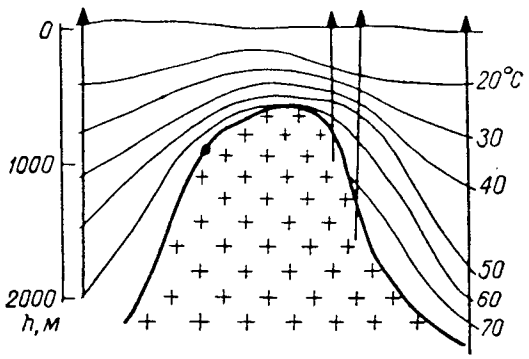


Fig. 2.19. Isogeotherms near a salt dome (Cheremenskiy, 1977).

the undisturbed geothermal gradient is Γ, often can be used for crude estimations of the effect of the lateral thermal conductivities contrasts on the reservoir's temperature field. Below we present these solutions.

The region within the sphere $0 \leq r <$ is of conductivity λ^* and the region outside of conductivity λ. The temperature T tends to $T_o + \Gamma z$ at great distances. The temperatures T^* inside, and T outside, the sphere are

$$T = T_o + \Gamma z + \frac{\Gamma a^3(\lambda - \lambda^*)z}{r^3(2\lambda + \lambda^*)} \tag{2.83}$$

$$T^* = T_o + \frac{3\Gamma\lambda z}{2\lambda + \lambda^*} \tag{2.84}$$

The cylinder $0 \leq r <$ is of conductivity λ^* and has its axis perpendicular to the z-axis. The region outside is of conductivity λ and the temperature in it is $T_o + \Gamma z$ at great distances. The temperatures T^* inside, and T outside, the cylinder are

$$T^* = T_o + \frac{2\Gamma\lambda z}{\lambda + \lambda^*} \tag{2.85}$$

$$T = T_o + \Gamma z - \frac{\Gamma a^2(\lambda - \lambda^*)z}{r^2(\lambda + \lambda^*)} \tag{2.86}$$

An ellipsoid of conductivity λ^* in a medium of conductivity λ. Suppose the ellipsoid is

$$\frac{x^2}{a^2} + \frac{y^2}{b^2} + \frac{z^2}{c^2} = 1 \tag{2.87}$$

and T tends to $T_o + \Gamma z$ at great distances. The temperature inside (T^*) and outside (T) the ellipsoid are

$$T^* = T_o + \frac{\Gamma z}{1 + C_o(\varepsilon - 1)}, \qquad \varepsilon = \frac{\lambda^*}{\lambda} \tag{2.88}$$

$$T = T_o + \Gamma z - \frac{\Gamma(\varepsilon - 1)C_k z}{1 + C_o(\varepsilon - 1)} \tag{2.89}$$

where C_o is the integral C_k (Carslaw and Jaeger, 1959, p.427) with $k = 0$. For prolate and oblate spheroids these integrals can be expressed in terms of elementary functions.

Prolate spheroid, $b = c < a$;

$$e' = \sqrt{\frac{a^2 - b^2}{a^2 + k}} \tag{2.90}$$

where e' is the eccentricity of the confocal ellipse through the external point considered, and e' for $k = 0$ is e, the eccentricity of the generating ellipse.

$$C_k = \frac{1 - e^2}{2e^3}\{\frac{e'}{1 - e'^2} - \frac{1}{2} \ln \frac{1 + e'}{1 - e'}\}. \tag{2.91}$$

Oblate spheroid, $a = b > c$

$$C_k = \frac{\sqrt{1 - e^2}}{e^3}\{\frac{1}{\nu} - \frac{1}{\arctan \nu}\}. \tag{2.92}$$

where

$$\nu = \frac{\sqrt{1 - e'^2}}{e'} \tag{2.93}$$

2.5.3 Sedimentation and Erosion

The effect of processes of sedimentation and erosion on the temperature regime of reservoirs can be estimated from the heat conduction

equation in a moving medium. The effect of erosion at speed U is equivalent to formations below the actual surface moving toward the surface (Jaeger, 1965). Similarly, if material is added by sedimentation, the formations below can be regarded as moving away from the surface.

The heat conduction equation for a material moving with velocity U in the z direction is

$$\frac{\partial T}{\partial t} + U\frac{\partial T}{\partial t} = a\frac{\partial^2 T}{\partial z^2} \tag{2.94}$$

The z axis is taken vertically downward from the surface ($z = 0$), the positive U corresponds to sedimentation, and negative U – to erosion. Let us assume that these processes begin at $t = 0$, when the temperature $T(z, t = 0) = T_o + \Gamma z$, and that subsequently the surface temperature is a linear function of time $T_s(z = 0, t) = T_o + bt$ (for sedimentation with constant temperature $b = 0$). Under these boundary and initial conditions the solution of the equation (2.94) is (Jaeger, 1965):

$$T = T_o + \Gamma(z - Ut) + \frac{1}{2}(\Gamma + b/U)\{(z + Ut)e^{Uz/a} f_1 + (Ut - z) f_2\} \tag{2.95}$$

$$f_1 = \Phi^*\left(\frac{z + Ut}{2\sqrt{at}}\right), \qquad f_2 = \Phi^*\left(\frac{z - Ut}{2\sqrt{at}}\right) \tag{2.96}$$

$$\Phi^*(x) = 1 - \Phi(x), \qquad \Phi(-x) = -\Phi(x) \tag{2.97}$$

here $\Phi(x)$ is the error function and a is the coefficient of thermal diffusivity of formations (sediments). From equation (2.95) the temperature gradient at the surface is (Jaeger, 1965):

$$\frac{\partial T}{\partial z}\Big|_{z=0} = \Gamma + (\Gamma + b/U)\Psi(p) \tag{2.98}$$

$$\Psi(p) = p^2/2 - (1 + p^2/2)\Phi(p/2) - \frac{1}{\sqrt{\pi}}\, p\, \exp(-p^2/4) \tag{2.99}$$

$$p = \frac{Ut}{\sqrt{at}} \tag{2.100}$$

Cheremenskiy (1977) considered a case when the thermal properties of the formations differ from that of the sedimentary layer. It was assumed that the sedimentation process begins at time $t = 0$.

Prior to this moment of time the thermal conductivity of the semi-infinite medium ($0 < z < \infty$, region 1) is λ_1, the coefficient of thermal diffusivity is a_1, and the value of HFD is q_o. At $t > 0$ the sedimentation process starts and a new uniform layer ($-f(t) < z < 0$, region 2) with thermal conductivity of λ_2, and thermal diffusivity of a_2 is formed. In this case the solution of the system of two one dimensional heat conductivity equations with following boundary and initial conditions

$$T_1|_{t=0} = \frac{q_o}{\lambda_1} z; \qquad T_2|_{z=-f(t)} = 0; \tag{2.101}$$

$$T_1|_{z=0} = T_2|_{z=0}; \qquad \lambda_1 \frac{\partial T_1}{\partial z}|_{z=0}, = \lambda_2 \frac{\partial T_2}{\partial z}|_{z=0}, \tag{2.102}$$

should be obtained. When the thickness of the sedimentary layer changes after formula $f(t) = \beta\sqrt{t}$ (β is a constant), the corresponding solutions (Cheremenskiy, 1977) are:

$$T_1 = \frac{q_o}{\lambda_1}[z + \frac{\lambda_1}{\lambda_2} \frac{\beta\sqrt{t}}{u} i\Phi^*(\frac{z}{2\sqrt{a_1 t}})] \tag{2.103}$$

$$T_2 = \frac{q_o}{\lambda_2 u}[\beta\sqrt{t}\, i\Phi^*(\frac{z}{2\sqrt{a_2 t}}) + z\, i\Phi^*(\frac{\beta}{2\sqrt{a_2}}) + \frac{\beta z}{\sqrt{a_2}}] \tag{2.104}$$

$$u = i\Phi^*(\frac{\beta}{2\sqrt{a_2}}) + \frac{\beta}{2\sqrt{a_2}}(1 + \frac{\lambda_1}{\lambda_2}\sqrt{\frac{a_2}{a_1}}) \tag{2.105}$$

where

$$i\Phi^*(x) = \frac{1}{\sqrt{\pi}} \exp(-x^2) - x\Phi^*(x) \tag{2.106}$$

The changes in the geothermal gradients can be calculated (Cheremenskiy, 1977) from formulas (2.103 and 2.104):

$$\Gamma_1 = \frac{q_o}{\lambda_1 u}[\frac{\lambda_1}{\lambda_2} \frac{\beta}{2\sqrt{a_1}} \Phi(\frac{z}{2\sqrt{a_1 t}}) + i\Phi^*(\frac{\beta}{2\sqrt{a_2}}) + \frac{\beta}{2\sqrt{a_2}}] \tag{2.107}$$

$$\Gamma_2 = \frac{q_o}{\lambda_2 u}[\frac{\beta}{2\sqrt{a_2}} \Phi(\frac{z}{2\sqrt{a_2 t}}) + i\Phi^*(\frac{\beta}{2\sqrt{a_2}}) + \frac{\beta}{2\sqrt{a_2}}] \tag{2.108}$$

2.5.4 Past Climate

The effect of surface temperature variations in the past on the temperature field of formations is discussed in the literature (Carslaw and Jaeger, 1959; Jaeger, 1965; Cheremenskiy, 1977; Lachenbruch et al., 1982; Powell et al., 1988).

At present many efforts are made to determine the trends in the paleoclimatic history from geothermal surveys. In this case accurate subsurface temperature measurements are needed to solve this inverse problem – estimation of the unknown time dependent surface temperature.

For petroleum engineers is important to evaluate the effect of the surface temperature variations in the past on the temperature field of formations during the reservoir's life. In some cases this effect may be significant for shallow depths. Below we present several simple methods of evaluation of the perturbations to the temperatures ΔT and geothermal gradients $\Delta\Gamma$ due to past surface temperature changes (Powell et al., 1988). The values of ΔT and $\Delta\Gamma$ due to an instantaneous surface temperature change of surface temperature ΔT_o at time t before now are:

$$\Delta T(z,t) = \Delta T_o \, \Phi^*(\frac{z}{2\sqrt{at}}) \tag{2.109}$$

$$\Delta\Gamma(z,t) = -\frac{\Delta T_o}{\sqrt{\pi at}} \exp(-\frac{z^2}{4at}) \tag{2.110}$$

In Table 2.8 are given the results of calculations after Eqs. (2.109) and (2.110) for a single temperature step $\Delta T_o = 1\,^oC$. It can be seen that for small times only shallow depths are effected by temperature changes. When, for example, ΔT_o=5^oC then the values of ΔT and $\Delta\Gamma$ in Table 2.8 should be increased in 5 times. For several steps the superposition principle can be used to calculate the values of ΔT and $\Delta\Gamma$.

Consider a linear change of surface temperature with T_s constant for time $t < 0$ and changing at constant rate (b) after $t = 0$ ($\Delta T_s = bt$). The half space solutions (Carslaw and Jaeger, 1959; Powell et al., 1988) are:

$$\Delta T(z,t) = bt[(1 + \frac{z^2}{2\sqrt{at}})\Phi^*(\frac{z}{2\sqrt{at}}) - \frac{z}{\sqrt{\pi at}} \exp(\frac{-z^2}{2\sqrt{at}})] \tag{2.110}$$

Table 2.8 Present perturbations to the temperatures ΔT and gradients $\Delta\Gamma$ due to instantaneous surface temperature change of 1°C at various times prior to present.
Thermal diffusivity = 1 mm^2/s, ΔT in °C, $\Delta\Gamma$ in °C/m (Powell et al., 1988)

Depth	10		100		1000		10000 years	
m	ΔT	$\Delta\Gamma$	ΔT	$\Delta\Gamma$	ΔT	$\Delta\Gamma$	ΔT	$\Delta\Gamma$
50	0.05	-0.004	0.53	-0.008	0.84	-0.003	0.95	-0.001
100	0	0	0.21	-0.005	0.69	-0.003	0.90	-0.001
500	0	0	0	0	0.05	-0.001	0.53	-0.001
1000	0	0	0	0	0	0	0.21	-0.001
5000	0	0	0	0	0	0	0	0

$$\Delta\Gamma(z,t) = bt[\frac{z}{at}\,\Phi^*(\frac{z}{2\sqrt{at}}) - \frac{2}{\sqrt{\pi at}}\exp(\frac{-z^2}{2\sqrt{at}})] \qquad (2.111)$$

The perturbations to formations temperatures due to long term sinusoidal surface temperature variation can be determined from the Equation (2.30)

$$\Delta T(z,t) = A_o\,\exp\left(-z\sqrt{\frac{\omega}{2a}}\right)\,\sin\,\left(\omega t - z\sqrt{\frac{\omega}{2a}}\right), \qquad (2.112)$$

where $\omega = 2\pi/P$ is the angular frequency, P is the period, and A_o is the amplitude of the temperature oscillation at the surface.

2.5.5 Vertical and Horizontal Water Movements

Known analytical solutions (Bredehoeft and Papadopulos, 1965; Lubimova et al., 1965; Osterkamp and Gosink, 1984; Haenel et al., 1988), describing the vertical and horizontal steady-state flow of water and heat through an isotropic, homogeneous, porous and saturated horizontal layer, can be used to estimate the effect of water flow on the temperature regime of formations.

Consider a layer with the thickness of h and let z to be the vertical coordinate axis taken as positive downward. Let us assume

that the top ($z = 0$) and the bottom ($z = h$) of this layer are maintained at constant temperatures: $T(0) = T_1$ and $T(h) = T_h$. For the case of a constant vertical flow of fluid the one-dimensional, steady-state, heat transfer equation is (Bear, 1972)

$$\frac{\partial^2 T}{\partial z^2} - \alpha v \frac{\partial T}{\partial z} = 0 \tag{2.113}$$

where v is the constant vertical velocity of water flow and α is parameter which depends on the thermal properties and the porosity of the medium. The solution of Eq. (2.113) for the given boundary conditions: $T(0) = T_1$ and $T(h) = T_h$ (Bredehoeft and Papadopulos, 1965) is

$$T(z, v) = T_1 + \Delta T[\frac{\exp(\alpha v z) - 1}{\exp(\alpha v h) - 1}], \quad \Delta T = T_h - T_1 \tag{2.114}$$

For $v = 0$

$$T(z, v = 0) = T_1 + \Delta T \frac{z}{h}, \tag{2.115}$$

and the temperature disturbance $\delta T(z)$ due to vertical water flow from Eqs. (2.114 and 2.115) is

$$\delta T(z) = T(z, v) - T(z, v = 0) = \Delta T[\frac{\exp(\alpha v z) - 1}{\exp(\alpha v h) - 1} - \frac{z}{h}] \tag{2.116}$$

The total heat flow density q_t which is the sum of conductivity heat-flow density q_d and the convective heat flow density q_v (Haenel et al., 1988) is

$$q_t = q_d + q_v = -\lambda_r \frac{T_h - T(z)}{h} - \phi \rho_w c_w v[T(z) - T_h] \tag{2.117}$$

where ϕ is the porosity, ρ_w is the water density, c_w is the specific heat of water, and λ_r is thermal conductivity of water-saturated rock. The maximum value of q_t occur at $z = 0$ for an upward water flow

$$q_{t,max} = |\lambda_r \frac{T_h - T_z)}{h}| + \rho_w c_w v(T_h - T_1) \tag{2.118}$$

For the case of constant horizontal flow in a horizontal slab, the two-dimensional steady-state heat transfer equation for a saturated, homogeneous and isotropic porous medium is

$$\frac{\partial^2 T}{\partial z^2} - \alpha u \frac{\partial T}{\partial x} = 0 \tag{2.119}$$

where u is the constant horizontal velocity of water flow. When $\partial T/\partial x$ is constant and the boundary conditions are

$$T(z = h) = T_1, \qquad T(z = -h) = T_2 \tag{2.120}$$

then (Osterkamp and Gosink, 1984)

$$T(z) = \frac{\alpha u}{2} \frac{\partial T}{\partial x}(z^2 - h^2) + \frac{T_1 - T_2}{2h} z + \frac{T_1 + T_2}{2} \tag{2.121}$$

Application of Eq. (2.121) requires a knowledge of $\partial T/\partial x$. Therefore, temperature measurements in two wells are needed to determine the horizontal temperature gradient.

2.5.6 Fluid Discharge Trough a Fault

Earlier (Section 2.2.3) we mentioned that in young oceanic areas the non-conductive heat transfer by hydrothermal circulation in the oceanic crust can produce significant variations in values of HFD. For old basins a thick impermeable sedimentary layer exist and water circulation is shut off (Uyeda, 1988).

At geothermal studies in oceanic areas with a thick layer of bottom sediments one sometimes comes across the following pattern: over a wide (when compared with the distance between the observation points) tectonically and geologically homogeneous region; the topography of the region is such that there is no need for making significant topographical corrections, i.e., the heat flow within the given region must be constant everywhere. Nevertheless, for observation points situated at small distances apart (1 to 2 km) the value of HFD at one point may be of several times the value at the other.

In order to interpret such variations in values of HFD a following model was suggested (Yefimov et al., 1975):
on a flat portion of the bottom of the ocean (or sea, or lake) there is a fault through which water rises from some depth H. The velocity of filtration is such that at the point of emergence the temperature of the water T_o is the same as at the depth H. Without loss of generality one can consider that the surface temperature of the sediments (beyond the limits of the fault) is constant and equal T_1. The fault is sufficiently long so that a two-dimensional model

can be considered. The temperature distribution and temperature gradients in a direction perpendicular to the fault were determined for the following two cases: the homogeneous isotropic medium and the two-layer medium with different thermal properties for each layer (Yefimov et al., 1975). The formulation of the problem is somewhat an idealization of the real process, since at the point of emergence of the underground water, the boundary condition is not satisfied. Consequently, the obtained solutions cannot be applied to the immediate vicinity of the source and the solutions give only maximum estimates of the zone of the influence.

The solution for the two-layer case is expressed through a complex equation and for this reason we present here only the solution of the Laplace equation for one layer case. The Laplace equation for the two-dimensional model is

$$\frac{\partial^2 T}{\partial x^2} + \frac{\partial^2 T}{\partial z^2} = 0 \tag{2.122}$$

with boundary conditions

$$T(0,z) = T_o, \quad T(x,0) = T_1, \quad T(x,H) = T_o \tag{2.123}$$

In dimensionless variables

$$\theta(\eta,\xi) = \frac{T(x,z) - T_1}{T_o - T_1}; \quad \xi = \frac{x}{H}; \quad \eta = \frac{z}{H} \tag{2.124}$$

the Laplace equation is

$$\frac{\partial^2 \theta}{\partial \xi^2} + \frac{\partial^2 \theta}{\partial \eta^2} = 0 \tag{2.125}$$

with boundary conditions

$$\theta(0,\eta) = 1, \quad \theta(\xi,0) = 0, \quad \theta(\xi,1) = 1. \tag{2.126}$$

The solution of this problem is known (Tikhonov and Samarsky, 1963) and the expressions for the dimensionless temperatures and temperature gradients are:

$$\theta = \theta_1 + \eta + \frac{2}{\pi}[\arctan\frac{\sin\pi\eta}{\sinh\pi\xi} - \arctan\frac{\sin\pi\eta}{exp(\pi\xi) + \cos\pi\eta}] \tag{2.127}$$

$$\frac{\partial\theta}{\partial\eta} = 1 + 2[\frac{\cos\pi\eta\ \sinh\pi\xi}{\sinh^2\pi\xi + \sin^2\pi\eta} - \frac{1 + e^{\pi\xi}\ \cos\pi\eta}{(e^{\pi\xi} + \cos\pi\eta)^2 + \sin^2\pi\eta}] \tag{2.128}$$

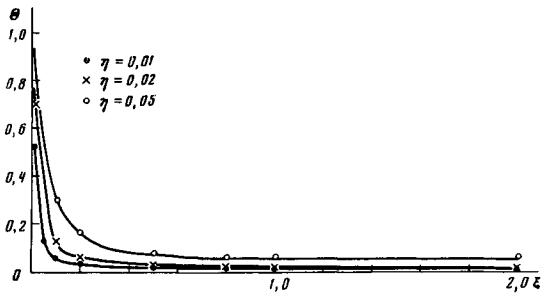


Fig. 2.20. Function θ of ξ for different values of η (Yefimov et al., 1975).

where $\theta_1 = T_1/(T_o - T_1)$. The curves of distribution of θ and $\frac{\partial\theta}{\partial\eta}$ are displayed in Figures 2.20 and 2.21. From numerical calculations the following conclusions were made (Yefimov et al., 1975):
For both variants of the problem when $\eta \leq 0.1$, sharp and fairly large (in magnitude) maximal of the temperature gradients were found. The maximum values can exceed the normal values (Γ) by a factor of more than 10.

The temperature effect decreases fairly rapidly with an increase of the distance from the fissure. Thus, when $\eta = 1$, i.e., at a distance equal to the depth of the water-bearing layer, the dimensionless temperature θ is different from the normal distribution by no more than 10%, the temperature gradient being practically equal to Γ.

Example.
Let us assume that at the distance x=1000 ft (305 m) from the fault, the formation temperature was measured at the depth z=1000 ft. The values of H, T_o and T_1 are:
H=2000 ft (610 m), T_o=160 °F (71.1°C), T_1=60 °F (15.6°C). To estimate the influence of the water discharge trough the fault on the formation temperature and geothermal gradient the dimensionless parameters should be calculated:

$$\eta = \frac{1000}{2000} = 0.5, \quad \xi = \frac{1000}{2000} = 0.5, \quad \theta_1 = \frac{60}{160 - 60} = 0.6$$

The formation temperature and geothermal gradient Γ at $x \to \infty$

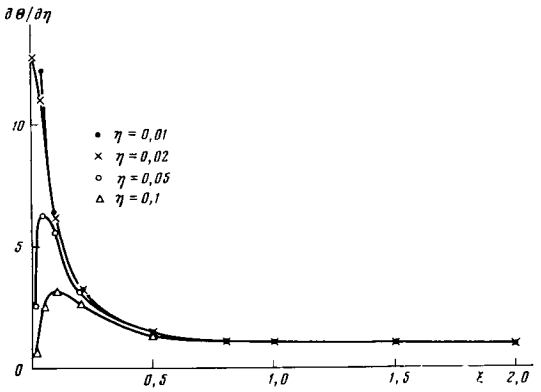


Fig. 2.21. Function $\frac{\partial\theta}{\partial\eta}$ of ξ for different values of η (Yefimov et al., 1975).

are:

$$\Gamma = \frac{160 - 60}{2000} = 0.05(^oF/ft), \quad T(\infty, 1000) = 60 + 50 = 110(^oF)$$

From Eqs. (2.127 and 2.128) we obtain that:

$$\theta(0.5, 0.5) = \frac{T - 60}{160 - 60} = 0.62305; \qquad A = \frac{\partial\theta}{\partial\eta}|_{\xi=0.5,\eta=0.5} = 0.9172$$

and

$$T = 0.62305 \times 100 + 60 = 123.05(^oF),$$

$$\Gamma = 0.9172(160 - 60)/2000 = 0.04586(^oF/ft).$$

Thus the impact of the fault on the formation temperature and geothermal gradient at the given point can be estimated

$$\Delta T = 123.05 - 110 = 13.05^oF \ (7.25^oC),$$

$$\Delta\Gamma = 0.04586 - 0.5000 = -0.00414^oF/ft \ (0.00755^oC/m)$$

2.5.7 Island or Lake

Consider a case when the well site is located in an island. The temperature regime of formations beneath the island's surface is subjected to the thermal influence of the sea. The extent of this

influence depends mainly on the island's dimensions, on the current depth, and on the difference between the long term mean annual temperature at the island surface and the long term mean annual temperature at the sea bottom. We will assume that the island existed for an infinitely large period of time and it was never flooded. Now, we will predict the formation temperatures as a function of depth for the well site. Let us also assume that the well is located on a island of circular shape with a radius R_i. The following designations will be used below:
ρ, z are polar coordinates (ρ is the distance from the center of the island); $T_c = T_c(\rho = 0,\ z)$ is the temperature profile in the center of the island; T_{is} is the long-term mean annual temperature at island surface; T_{ot} is the long-term mean annual temperature of the sea bottom sediments; and Γ is the offshore temperature gradient.

Now suppose that for infinitely large periods of time the island surface is maintained at a constant temperature T_{is} and the sea bottom is maintained at temperature T_{ot} = *constant.* The corresponding solution of Laplace equation for the semi-infinite solid (offshore-onshore) area is (Balobayev and Shastkevich, 1974):

$$T(\rho, z) = T_{ot} + \Gamma z + M(T_{is} - T_{ot}) \tag{2.129}$$

$$M(\rho, z) = 1 - A_1[A_2\ \Pi(\alpha_1^2, k) + A_3\ \Pi(\alpha_2^2, k)] \tag{2.130}$$

$$A_1 = \frac{z}{\pi\sqrt{z^2 + (R_i + \rho)^2}}; \qquad A_2 = \frac{\sqrt{z^2 + \rho^2} - R_i}{\sqrt{z^2 + \rho^2} + \rho} \tag{2.131}$$

$$A_3 = \frac{\sqrt{z^2 + \rho^2} + R_i}{\sqrt{z^2 + \rho^2} - \rho}; \qquad \alpha_1^2 = \frac{2\rho}{r + \rho}; \qquad \alpha_2^2 = -\frac{2\rho}{r - \rho} \tag{2.132}$$

$$r^2 = \rho^2 + z^2; \qquad k^2 = \frac{4\rho R_i}{z^2 + (R_i + \rho)^2} \tag{2.133}$$

where $\Pi(\alpha_1^2, k)$ and $\Pi(\alpha_2^2, k)$ are the complete elliptical integrals of the third order (Byrd and Friedman, 1959).

For the center of the island ($\rho = 0$),

$$M(z) = 1 - \frac{z}{\sqrt{z^2 + R_i^2}} \tag{2.134}$$

The temperature gradient for the well drilled at the center of the can be determined from Eqs. (2.129 and 2.134)

$$\Gamma^* = \frac{dT_c}{dz} = \Gamma - (T_{is} - T_{ot})\left[\frac{R_i^2}{(z^2 + R_i^2)^{3/2}}\right] \tag{2.135}$$

It is easy to see that the Eqs. (2.129-2.135) can be also used to describe the temperature field of formations beneath lakes. In this case R_i is the radius of the lake, T_{is} is the long term mean annual temperature at the lake's bottom, and T_{ot} is the land's surface temperature (temperature at the depth with practically zero oscillation of the annual temperature).

Example.
Consider a lake with R_i=600 m and T_{is}=4.00°C. The regional geothermal gradient is Γ=0.0300°C/m and T_{ot}=24.00°C. Formation temperature at the depth z=300 m was measured in a well located at the center of the lake. What are the magnitudes of the formation temperature and gradient distortions caused by lake?

The undisturbed formation temperature is

$$T(z = 300) = 24.00 + 300 \cdot 0.0300 = 33.00(^oC).$$

From Eqs. (2.129 and 2.134) the values of M and $T(0, 300)$ are

$$M = 1 - \frac{300}{\sqrt{300^2 + 600^2}} = 0.5528; \quad T = 33.00 - 11.06 = 21.94(^oC).$$

The value of Γ^* from Eq. (2.135) is

$$\Gamma^* = 0.0300 - (4 - 24)\frac{600^2}{(300^2 + 600^2)^{3/2}} = 0.05385(^oC/m).$$

Thus for shallow depths the influence of the lake on the geothermal regime of formations is significant. Indeed, (in °C and °C/m) ΔT=21.94-33.00= - 11.06 and $\Delta\Gamma$=0.05385-0.0300=0.02385. Similar calculations for the depth z=1200 m show that $\Delta\Gamma$=0.03298-0.0300=0.00298 and ΔT=57.89-60.00=-2.11.

2.5.8 Single Mountain Range

The effect of the local relief may significantly affect the temperature field of formations. To solve the Laplace equation the surface temperature $T_s(x, y)$ should be specified (here x and y axis are taken in the sea level surface). In practice, the function $T_s(x, y)$ is usually not known, and a linear variation of T_s with height (h) is used (Jaeger, 1965),

$$T_s(x, y) = T_o - g'h(x, y), \tag{2.136}$$

where T_o and g' are constants. The adiabatic atmospheric temperature gradient g' can be estimated from meteorological data. Only several explicit solutions of Laplace equation at boundary condition (2.136) are known. We present below the Lees solution (Jaeger, 1965) for a single mountain range,

$$T(x,z) = T_o + \Gamma z + \frac{A(z+a)}{x^2 + (z+a)^2} \tag{2.137}$$

$$a = H + \sqrt{\frac{H^2}{4} + b^2} \tag{2.138}$$

$$A = H(\Gamma - g')\sqrt{\frac{H^2}{4} + b^2} \tag{2.139}$$

Here H is the height of the single mountain range and $2b$ its width at half its height. From Eq. (2.139) we can calculate the vertical temperature gradient

$$\Gamma = \frac{\partial T}{\partial z} = G + \frac{A[x^2 - (z+a)^2]}{[x^2 + (z+a)^2]^2} \tag{2.140}$$

Example.
Consider a single mountain range with H=600 m and $2b$=120 m. The regional geothermal gradient is Γ=0.0300°C/m, g'=0.004500°C/m, and T_o=20.00°C. Formation temperature at the depth z=300 m was measured in a well located at x=900 m.

What are the magnitudes of the formation temperature and gradient distortions caused by the single mountain range?

The undisturbed formation temperature is
$T(z = 300) = 20.00 + 300 \cdot 0.0300 = 29.00(^oC)$.
From Eqs. (2.138 and 2.139) the values of a and A are

$$a = 600 + \sqrt{600^2/4 + 60^2} = 905.9(m),$$

$$A = (0.0300 - 0.00450) \cdot 600\sqrt{600^2/4 + 60^2} = 4680.9(^oC \cdot m).$$

From Formula (2.137) the value of $T(300, 900)$ is calculated

$$T(300,900) = 20 + 0.0300 \cdot 300 + \frac{4680.9 \cdot (300 + 905.9)}{900^2 + (300 + 905.9)^2} = 31.49(^oC)$$

Finally, the temperature gradient is determined from Eq. (2.140)

$$\Gamma = 0.0300 + \frac{4680.9[900^2 - (300 + 905.9)^2]}{[900^2 + (300 + 905.9)^2]^2} = 0.02941(^oC/m)$$

Thus in this case even for a shallow depth the values of $\Delta\Gamma$ and ΔT are relatively small: $\Delta\Gamma$=0.02941-0.03000=-0.00059(^{o}C/m) and ΔT=31.49-29.00=-2.49(^{o}C).

Lachenbruch (1968) developed a general method which allows to make topographic corrections to geothermal gradients. This method is based on two-dimensional steady-state solution for heat flux through an inclined plane of arbitrary height and slope angle. These two parameters can approximate any real relief. The suggested method can be applied for points close to slopes of any height and inclination.

The results of temperature surveys in deep wells show that usually for deep depths ($> 2 - 3$ km) the topographic correction to geothermal gradients is very small and can be neglected.

2.5.9 Modeling of the Temperature Field

At thermal modeling the study of steady-state or transient heat transfer in formations is conducted on physical models. The theory of similarity is used to process the results of modeling.

Let us assume that n dimensionless parameters $(I_1, I_2 \cdots I_n)$ describe the heat conduction in a reservoir and surrounding formations. In this case the results of modeling should be also expressed in terms of corresponding n dimensionless parameters $(I_1', I_2' \cdots I_n')$. To apply the results of modeling to the actual problem the following conditions should be satisfied:

$$I_1 = I_1', \; I_2 = I_2' \; \cdots \; I_n = I_n'$$

For steady-state heat conduction problems the results of modeling in hydrodynamics of flow through porous media, electrostatic, and current conduction can be utilized (Table 2.9). For example consider a two-dimensional case of a horizontal layer with variable thermal conductivity, $\lambda = \lambda(x, z)$.

Let us assume that the boundary conditions are:

$$T(z_1, x) = T_1, \quad T(z_2, x) = T_2, \quad -l \leq x \leq l \tag{2.141}$$

Table 2.9 Correspondences between the flow of an incompressible liquid through a porous medium, heat conduction, electrostatics, and current conduction (Muskat, 1946)

Hydrodynamics of steady-state flow Hydrodynamics of through porous media(incompressible liquids)	Heat conduction	Electrostatics	Current conduction
Pressure: p	Temperature: T	Electrostatic potential: Φ	Voltage (potential):V
Negative pressure gradient: $-\nabla p$	Negative temperature gradient: $-\nabla T$	Field-strength vector: $\vec{E} = -\nabla\Phi$	Negatine potential gradient: $-\nabla V$
Permeability viscosity ratio: k/μ	Thermal conductivity: λ	Dielectric constant: $\epsilon/4\pi$	Specific conductivity σ
Velocity vector: $\vec{v} = -\frac{k}{\mu}\nabla p$	Rate of heat transfer: $\vec{q} = -\nabla T$	Dielectric displacement: $\frac{\epsilon}{4\pi}\vec{E} = -\frac{\epsilon}{4\pi}\nabla\Phi$	Current vector: $\vec{I} = -\nabla V$
(Darcy's law)	(Fourier's law)	(Maxwell's law)	(Ohm's law)
Equipressure surface: p = const.	Isotherma surface: T = const.	Equipotential surface: Φ = const.	Equipotential surface: V = const.
Impermeable boundary or streamline: $\frac{\partial p}{\partial n} = 0$	Insulated surface or line of heat flow: $\frac{\partial T}{\partial n} = 0$	A tube or line of force: $\frac{\partial\Phi}{\partial n} = 0$	Free or insulated surface of tube or line of flow: $\frac{\partial V}{\partial n} = 0$

$$\frac{\partial T(z,x)}{\partial x}|_{-l} = \frac{\partial T(z,x)}{\partial x}|_{l} = 0 \qquad (2.142)$$

The similarity of the Fouirier's law and the Ohm's law is obvious (Table 2.9), and in this case a current conduction model can be used. The temperature difference $(T_2 - T_1)$ is replaced by the corresponding (proportional) voltage drop $(V_2 - V_1)$, a length scale is selected, and the unit of length is l_s. Now the new dimensionless coordinates and the model dimensions are:

$$x' = \frac{x}{l_s}, \quad z' = \frac{z}{l_s}, \quad z_1' = \frac{z_1}{l_s}, \quad z_2' = \frac{z_2}{l_s}, \quad l' = \frac{l}{l_s}$$

The function $\lambda = \lambda(x, z)$ is substituted by the specific conductivity function $\sigma = \sigma(x', z')$ so that the ratio λ/σ is constant at any point. By the use of electrical integrators any distribution of the specific electrical resistance $(1/\sigma)$ can be specified. The voltage $V = V(x', z')$ is measured and the results are presented in the dimensionless form:

$$V_D(x', z') = \frac{V(x', z') - V_1}{V_2 - V_1} \tag{2.143}$$

For example, let us assume that V_1=0, V_2=10V, T_1=50°C, T_2=100°C, and at some point the value of V_D is 0.3. From Eq. (2.143) the value of $V(x', z')$ is 3.0V. In this example a temperature difference of 1°C corresponds to 0.2V voltage drop, and the temperature at the given point is $50 + 3.0/0.2 = 65(°C)$.

An extreme caution should used in utilization results of non-steady (transient) modeling. Below we present an example. The same diffusivity equation describes the transient flow of incompressible fluid in porous medium and heat conduction in solids. For transient liquid flow models are typical very high values of hydraulic diffusivity coefficient $\eta = k/(\phi\, c_t \mu)$, where k is permeability, ϕ is the porosity, c_t is the total compressibility, and μ is the dynamic viscosity. The analogue of η in heat conduction is the thermal diffusivity coefficient (a). For reservoir formations the values of η and a are within following limits

$$360 < \eta < 18000\ m^2/hr; \qquad 0.0010 < a < 0.020\ m^2/hr.$$

To apply the results of liquid transient flow models to analogues heat conduction problems the dimensionless time in both cases should be equal. The following example shows that this condition is practically impossible to reach.

Let us assume that for a gas well modeling was conducted to determine the distribution of pressure and flow in the reservoir. The production period is $t = 1000$ hours, well radius $r_w = 0.1$ m, and $\eta = 360$ m^2/hr (a low value). In this case the dimensionless time is $t_D = \eta t/r_w^2 = 360 \cdot 1000/0.01 = 3.6 \cdot 10^7$. For the high value of $a = 0.020$ m^2/hr the corresponding value of t_D is $0.20 \cdot 1000/0.01 = 20$ and the results of a transient liquid model in this case can not be applied to an analogues heat conduction problem – heat flow and temperature distribution around a production well.

At modeling of the formations temperature field the selection of the reference surface becomes very important: the temperature field should be independent on surface topography and underground water movements. To specify the boundary conditions in many cases the maps of regional subsurface temperatures and maps of heat flow density can be used (Čermak and Haenel, 1988).

Chapter 3

WELLBORE AND FORMATIONS TEMPERATURE DURING DRILLING

3.1 Heat Exchange in the Wellbore-Formation System

3.1.1 Literature Review

The wellbore temperature during drilling is a complex function of wellbore geometry, wellbore depth, penetration rate, flow rate, duration of the shut-in intervals, pump and rotary inputs, fluid and formation properties, and geothermal gradients.

Edwardson et al. (1962) made the first attempt to evaluate the effect of shut-in periods during drilling on the temperature distribution in wells and surrounding formations. The Authors numerically solved the differential heat conduction equations necessary to predict formation temperature distributions during mud circulation and shut-in periods. The results of calculations were presented in a graphical form, which allows one to determine the formation temperature disturbance around the wellbore. As was mentioned by Sump and Williams (1973), since Edwardson et al. (1962) used assumed formation temperature profiles at the end of circulation, the wellbore temperature can not be calculated directly. Edwardson et al. (1962) took into account that the circulating drilling mud temperature, T_m, at any depth is not constant but rather changes as the well is drilled deeper and the maximum

temperature occurs not at the end of the drill string but somewhere in the annulus. It was suggested that the following formula can be used to approximate the downhole circulating mud temperature

$$T_m = a_o + a_1 z + a_2 z^2, \tag{3.1}$$

where a_o is the outlet temperature of the mud, a_1 and a_2 are constants. At calculations the undisturbed formation temperature T_f was expressed by the relationship

$$T_f = b + \Gamma z, \tag{3.2}$$

where b is the local surface formation temperature. Edwardson et al. (1962) assumed that $z = z_x$ is the depth with the maximum mud temperature, where T_m and T_f are the same. It was also assumed that the bottomhole circulating temperature (at $z = H$) is known

$$T_{bh} = a_o + a_1 H + a_2 H^2, \tag{3.3}$$

In this case the values of a_1 and a_2 can be expressed through the parameter z_x. Finally, the value of z_x can be determine from a quadratic equation. For one depth field data (Table 3.1) were used to estimate the resultant of temperature disturbances. Raymond (1969) developed generalized techniques to predict downhole fluid temperatures in a circulating fluid system during both transient and pseudo-steady state conditions. The fluid circulation in over 70 wells was simulated to generate charts of $\Delta T = T_{bh} - T_{ou}$ (bottomhole and outlet mud temperature) versus the flow rate for oil and water base muds (Raymond, 1969). These charts were obtained for a geothermal gradient of 0.017°F/ft (0.031 °C/m), 4.5 in. drill pipe, and a hole size of 8.625 in. Raymond conducted a sensitivity study and found that the drill pipe and hole sizes have little effect on circulating temperatures.

In the Raymond's model the circulation time was constant for all sections of the well. The well depth was also constant and the initial formation temperatures (prior to circulation) were equal to the geothermal (undisturbed) temperature. Several main characteristics of the drilling process were not taken into consideration in this model.

□ The amount of time that a formation is exposed to drilling fluid circulation depends on the depth (maximum periods of exposure correspond with shallowest depths).

Table 3.1 Circulation history and calculated resultant temperature disturbances at 8812 ft, Montana well (Edwardson et al., 1962)

Drilling depth interval ft	Circul. period	t_E hrs	Circul. time, hrs	ΔT_{fc}, °F	ΔT_s °F	ΔT °F
8812-8949	1	0	17.3	79	0	79
8949-8997	2	21.7	8.5	77	36.1	40.9
8897-9021	3	45.0	6.7	76	21.4	54.6
9021	4	64.8	4.3	76	23.4	52.6
9021-9099	5	85.0	13.0	75	21.1	53.9
9099-9184	6	103.0	18.3	73	37.2	35.8
9184-9200	7	136.0	4.0	72	26.3	45.7
9200	8	151.5	3.0	72	27.0	45.0
9200-9222	9	180.5	5.0	72	22.1	49.8

t_E is the cumulative time of exposure to mud at beginning of a circulation period, ΔT_{fc} is the undisturbed formation temperature minus circulating mud temperature, ΔT_s is the sum of residual temperature disturbances resulting from prior circulation periods, ΔT is the difference between undisturbed formation temperature and actual temperature at annulus-formation interface at the beginning of the circulation period.

- The temperature of the drilling fluid at a given depth depends on the current total depth.
- The discontinuity of the mud circulation process during drilling.
- The presence of the casing strings cemented at various depths.
- The impact of the energy sources caused by drilling.

The influence of energy sources on the temperature distribution in circulating mud columns was considered by Keller et al. (1973). Usually only the thermal energy of the inlet drilling mud is taken into account. However, during drilling heat is generated also by fluid friction in the drill pipe and annulus, by the rotary input needed to rotate the drill string, and by the bit work. It is commonly assumed that during drilling more than 99 percent of mechanical energy (rotary and pump inputs) is transformed into thermal energy. For one Gulf Coast well, the effect of including heat sources in the calculations is shown in Fig. 3.1. It was assumed that the

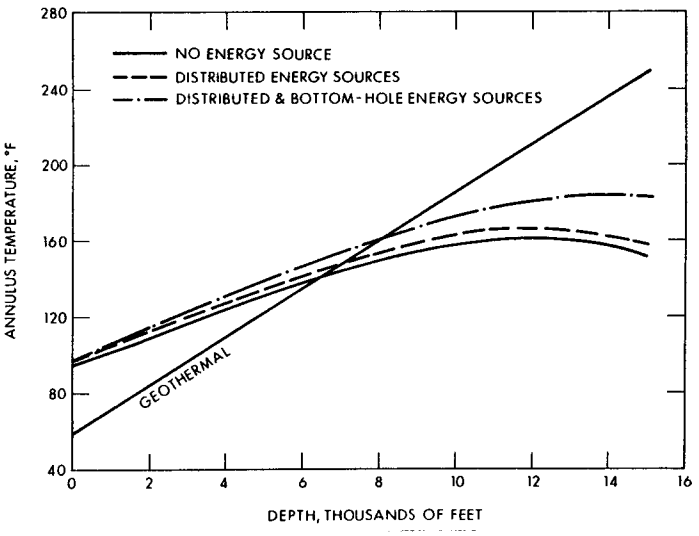


Fig. 3.1. The effect of energy sources on the annulus temperatures in a drilling well (Keller et al., 1973).

casing was initially (prior to the last circulation period) at the same temperature as the geothermal temperature (Keller et al., 1973). For this reason, this example has only an illustrative interest. The lower curve in Fig. 3.1 gives the temperature distribution after 24 hours of mud circulation for no energy sources. The center curve was calculated with a uniform energy source of 8.17 W/m inside the drill string and a uniform source of 15.90 W/m in the annulus. The upper curve was calculated using the same energy sources used for the center curve plus a source of $1.68 \cdot 10^5$W at the bottom of the hole. The pump energy sources used were calculated from pressure drop read from charts. The total pump input was $1.86 \cdot 10^5$W and the rotary input was 125 hp ($9.32 \cdot 10^4$W). Thus these calculations (Keller et al., 1973) indicate that the energy sources terms have a marked effect on the computed downhole temperature (Fig. 3.1).

A comprehensive two dimensional, axisymmetric, transient computer model of wellbore temperatures (WELLTEMP) was created and used to calculate temperatures in wellbore fluids, cement, steel, and surrounding formations as functions of depth and time (Wooley, 1980; Mitchell, 1981, Wooley et al., 1984). WELLTEMP is linked to an another program which computes temperature and pressure dependent fluid properties, fluid pressures, and fluid velocities. Thus

this wellbore thermal simulator can account for several main features of the drilling process: well depth change with time, discontinuity of mud circulation, variation of mud properties with depth and time, and the complexity of the completion design. Beirute (1991) developed a computer simulator which is able to predict downhole temperatures during fluid circulation and shut-in periods. The simulator can be used for any well configuration and handle several fluids in the wellbore at one time.

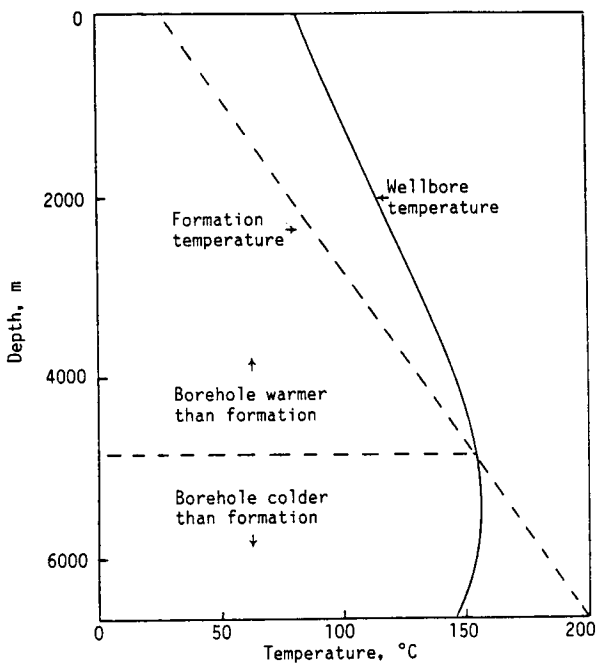


Fig. 3.2. Profiles of wellbore temperature and undisturbed formation temperature in a drilling well (Gogoi, 1986).

It is worth noting that in deep wells the circulating drilling mud system acts as a heat exchanger, cooling the lower part of the well and heating the upper part. For one well (for a current vertical depth) the profiles of the circulating and geothermal temperatures are shown in Fig. 3.2. During drilling the length of well's heated (upper) section increases with time.

3.1.2 Newton's Relationship

The discontinuity of the mud circulation process during drilling poses a serious problem in using the Newton relationship for determining the heat flow from the mud in the drill pipe to the wall of the drill pipe as well as the heat flow through the formation–annulus interface (q_f). According to the Newton relationship

$$q_f = \alpha_{fa}(T_m - T_{fa}), \tag{3.4}$$

where α_{fa} is the film heat transfer coefficient from mud in the annulus to the formation, T_m is the average mud temperature (in annulus section), and T_{fa} is the temperature at the formation–annulus interface.

For a developed turbulent flow the Dittus–Boelter formula is usually used to estimate the value of the film heat transfer coefficient, and for applications in which the temperature influence on fluid properties is significant, the Sieder–Tate correlation is recommended (Bejan, 1993).

On theoretical grounds the Newton equation is applicable only to steady-state conditions. This means that in our case both temperatures (T_{fa}, T_m) cannot be time dependent functions. In practice, however, the Newton relationship is successfully used in many areas when the temperature of the fluids and the temperatures at the fluid-solid wall interfaces are slowly changing with time. Therefore, it is necessary to find out under which conditions Eq. (3.4) can be used to predict the wellbore temperatures during drilling. Indeed, the wellbore temperature during mud circulation is a complex function of time, wellbore geometry, well bore depth, penetration rate, circulation mud rate, fluid and formation properties and geothermal gradients. Drilling records show that the mud is circulating only a certain part of the time required to drill the well (Table 3.1). In this example the cumulative circulation time at the depth 8821 ft was 80.1 hours or 44.3 percent of the drilling time. Some results of field investigations in the USA and Russia have shown that using conventional values of the film heat transfer coefficients in predicting wellbore temperatures during drilling is very questionable (Deykin et al., 1973; Sump and Williams, 1973). Predictions using Raymond's (1969) method, for example, differed from the measured values by 12 percent on the average (Fig. 3.3) and

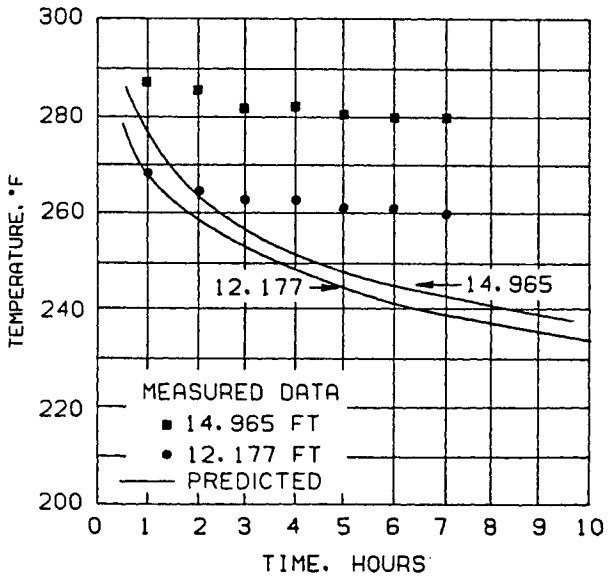


Fig. 3.3. Comparison of measured and predicted mud temperatures from Well 1 (Sump and Williams, 1973).

in one case missed the measured temperature by 65°F (36°C) (Sump and Williams, 1973). In order to get an agreement between measured and predicted temperature values, Sump and Williams (1973) offered to alter the values of the film heat transfer coefficient. Deykin et al. (1973) independently arrived at the same conclusion. It should be noted that in all previous studies (Tragesser et al., 1967; Raymond, 1969; Holmes and Swift, 1970; Keller et al., 1973; Sump and Williams, 1973; Wooley, 1980; Thompson and Burgess, 1985) the Newton relationship was used to describe the heat exchange between the mud in the annulus and formation.

3.1.3 Overall Heat Transfer Coefficient

During mud circulation the thin steel wall of the drill pipe separates two streams of the fluid. To determine the radial heat flow from (or into) the drill pipe to (or from) the annulus, the value of the overall heat transfer coefficient (U) should calculated. The procedure of calculation the value of U is clear from Fig. 3.4. In our case the wall

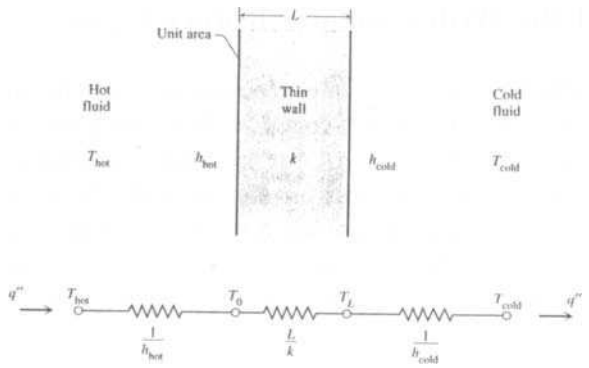


Fig. 3.4. Thin wall sandwiced between two flows: the definition of overall heat transfer coefficient (Bejan, 1993).

thickness and drill pipe radius ratio is very small, and we can assume that the radial heat flow (q'') is constant inside the wall. Besides the maximum deviation between experimental values of heat transfer coefficients (h_{hot}, h_{cold}) and those predicted from the Dittus–Boelter formula can be of the order of 40 percent (Bejan, 1993). From the Newton relationship and Fourier law follows that

$$T_{hot} - T_o = \frac{q''}{h_{hot}} \tag{3.5}$$

$$T_L - T_{cold} = \frac{q''}{h_{cold}} \tag{3.6}$$

$$T_o - T_L = \frac{L}{k} q'' \tag{3.7}$$

From Eqs. (3.5-3.7) we obtain

$$q'' = U(T_{hot} - T_{cold}) \tag{3.8}$$

$$\frac{1}{U} = \frac{1}{h_{hot}} + \frac{L}{k} + \frac{1}{h_{cold}} \tag{3.9}$$

where k is the thermal conductivity of steel, T_{hot} is the bulk mud temperature in the annulus, and T_{cold} is bulk mud temperature in the drill pipe.

3.1.4 Effect of the Hydraulic and Rotary Inputs

To evaluate the influence of the drilling technology on the temperature of the circulating fluid, we will assume that 100 percent of the hydraulic and rotary inputs is spent for heating the drilling mud. Due to frictional losses the mud pump must provide the circulating fluid with a continuous supply of mechanical energy. This amount of energy per unit of time – the hydraulic power output of the pump (H_h) in oilfield units can be expressed by the following formula (Craft et al., 1962).

$$H_h = \frac{q\Delta p}{1714}(hp) \tag{3.10}$$

where H_h is usually expressed in units of horsepower, q is the flow rate in gallons per minute (gpm), and Δp is the discharge pressure (diffrential pressure) developed by the pump in $psig$. To determine the rotary horsepower (R_h) – the amount of energy needed to rotate the drill pipe and penetrate the formations, the surface torque (T_s) and speed of rotation (S_r) should be recorded while drilling. The rotary horsepower in oilfield units can be expressed by the relationship (API Bulletin, 1981).

$$R_h = \frac{T_s S_r}{5250}(hp) \tag{3.11}$$

where the surface torque (bending moment) is in $ft \cdot lbf$ and speed of rotation is in revolutions per minute, rpm. Below we present a field example. The following (averaged) parameters were recorded while drilling the 6200-7800 ft section of an oil well:
$q = 470\ gpm$, $\Delta p = 3000\ psig$, $T_s = 5000\ ft{\cdot}lbf$, and $S_r = 80\ rpm$.
From Eqs. 3.10 and 3.11 we obtain
H_h=470·3000/1714=822.6 (hp); R_h=5000·80/5250=76.2 (hp).
The total input of mechanical energy is 822.6 + 76.2 = 898.8 (hp).
In our case the density of the drilling mud was 9.3 ppg and specific heat capacity was 0.854 Btu/lb ·°F.
Taking into account that 1 hp = 2545 Btu/hr, we obtain that the equivalent average temperature increase (ΔT) of the drilling fluid is

$$\Delta T = \frac{898.8 \cdot 2545}{9.3 \cdot 470 \cdot 0.854 \cdot 60} = 10.2(^oF) = 5.7(^oC)$$

3.1.5 Radial Heat Flow Rate

The results of field and analytical investigations have shown that in many cases the temperature of the circulating fluid (mud) at a given depth $T_m(z)$ can be assumed constant during drilling or production (Lachenbruch and Brewer, 1959; Ramey, 1962; Edwardson et al., 1962; Jaeger, 1961; Kutasov et al., 1966; Raymond, 1969). However for super deep wells (5000-7000 m) the temperature of the circulating fluid is a function of the vertical depth (z) and time (t). Thus the estimation of heat losses from the wellbore is an important factor which shows to what degree the drilling process disturbs the temperature field of formations surrounding the wellbore. It is known that, if the temperature distribution $T(r, z, t)$ or the heat flow rate $q(r = r_w, z, t)$ (r_w is the well radius) are known for a case of a well with a constant bore-face temperature, then the functions $T(r, z, t)$ and $q(r = r_w, z, t)$ for a case of time dependent bore-face temperature can be determined through the use of the Duhamel's integral.

In this section we present an approximate formula which will allow one to calculate the rate of heat losses for wells with a constant bore-face temperature (T_w) at a given depth. Heat flow rate from the wellbore per unit of length is given by:

$$q = 2\pi\lambda(T_w - T_f)q_D(t_D) \tag{3.12}$$

where T_f is the undisturbed formation temperature, λ is the thermal conductivity of the formation, q_D is the dimensionless heat flow rate. Here we introduce the dimensionless mud circulation time t_D

$$t_D = \frac{at}{r_w^2} \tag{3.13}$$

where a is the thermal diffusivity of the formation.

The dimensionless heat flow rate was calculated by Jacob and Lohman (1952). Sengul (1983) computed values of $q_D(t_D)$ for a wider range of t_D and with more table entries. We found (Kutasov, 1987) that the dimensionless heat flow rate can be approximated by:

$$q_D = \frac{1}{\ln(1 + D\sqrt{t_D})} \tag{3.14}$$

$$D = d + \frac{1}{\sqrt{t_D} + b} \tag{3.15}$$

Table 3.2 Comparison of values of dimensionless heat flow rate for a well with constant bore-face temperature.
q_D^* – Sengul (1983); q_D – equation (3.14)

t_D	q_D^*	q_D	$\frac{\Delta q}{q_D^*} \cdot 100$, %
2	0.80058	0.80877	1.02
3	0.71620	0.72402	1.09
5	0.62818	0.63555	1.17
10	0.53392	0.54068	1.27
20	0.46114	0.46730	1.34
50	0.38818	0.39351	1.37
100	0.34556	0.35025	1.36
200	0.31080	0.31484	1.30
500	0.27381	0.27706	1.19
1000	0.25096	0.25366	1.08
2000	0.23151	0.23371	0.95
5000	0.20986	0.21153	0.80
10000	0.19593	0.19727	0.69
20000	0.18370	0.18477	0.58
50000	0.16966	0.17044	0.46
100000	0.16037	0.16098	0.38

$$d = \frac{\pi}{2}; \quad \frac{1}{b} = \sqrt{\pi} - \frac{\pi}{2}; \quad b = 4.9589$$

In Table 3.2 values of q_D calculated after formula 3.14 and the results of a numerical solution are compared. The agreement between values of q_D calculated by these two methods is seen to be good. The suggested formula (3.14) is valid for any values of fluid circulation time.

3.1.6 Heat Loss Due to Fluid Loss

Lost of circulation can be a serious problem in deep drilling. When the fluid loss is detected the drilling operator has to make a decision if the rate of fluid losses can be tolerated without changing the mud program, or mud has to be treated with large quantities of plugging materials.

Filtration of the drilling fluid into high permeability formations can significantly alter the temperature field of formations. To esti-

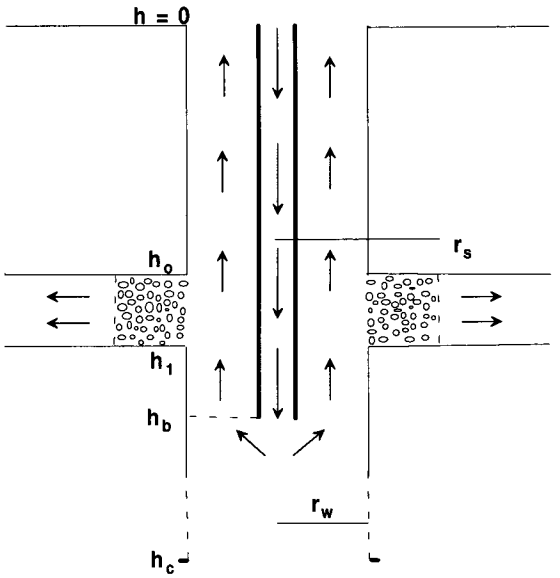


Fig. 3.5. Schematic of a fluid loss model.
h_o – top of thief zone, h_1 – bottom of thief zone, h_b – position of bit, h_c – casing shoe depth, r_w – well (bit) radius, and r_s – skin radius.

mate the amount of thermal energy transported to the formations, the rate of fluid losses (q) and cumulative fluid loss (Q) while drilling should be evaluated. Earlier a method of predicting values of q and Q was presented (Kutasov and Bizanti, 1984; Kutasov, 1995c). It was assumed that the loss of fluids starts while penetrating the top of an interval of high permeability (thief zone). The difference between the mud column pressure and the pore pressure is assumed to be the dominant factor causing filtration at any depth. The impact of the mud cake and mud invasion in the thief zone interval (positive skin factor) and the impact of slight fractures created around the drill bit (negative skin) was accounted for by the introduction of the effective wellbore radius (Uraiet and Raghavan, 1980)

$$r_{wa} = r_w \exp(-s), \tag{3.16}$$

where r_w is the well (bit) radius and s is the skin factor.
Figure 3.5 is a fluid loss schematic diagram of a well with a constant rate of penetration u. At time $t = 0$ the bit reaches the top of thief zone at depth $h = h_o$. As drilling continues, the mud filters into the thief zone, and a radius of ther skin is created (r_s). The rate

of fluid loss will increase until the bit reaches the bottom of the thief zone (h_1) because the area exposed to filtration increases with depth. After the penetration of the thief zone, the rate of fluid loss will gradually decrease, because for any depth the rate of fluid loss per unit of length decreases with time and the exposed area of the thief zone is constant. The mud weight is assumed to remain constant. The thief zone formation is assumed to be a uniform homogeneous medium with high permeability. The porosity and permeability of the thief zone are usually unknown during actual drilling. Only the rate of fluid loss can be recorded by the drilling operator. A computer program "FLOSS" (Appendix C, Table C.1) can be used to generate a set of curves for values of q as a function of current depth (h_b) for various thief zone properties. Then, by the use of conventional methods of curve matching, the permeability and porosity of the thief zone can be estimated.
Below the dimensionless depth is defined by

$$H = \frac{h}{r_w} \tag{3.17}$$

The corresponding dimensionless values for depths are

$$H_o = \frac{h_o}{r_w}, \quad H_1 = \frac{h_1}{r_w}, \quad H_b = \frac{h_b}{r_w}, \quad H_c = \frac{h_c}{r_w} \tag{3.18}$$

The rate of fluid losses per unit of length h_o, h_1, h_b, and h_c are

$$q_e = \frac{2\pi k}{\mu} \Delta\gamma \; h \; q_D, \qquad \Delta\rho = \rho_m - \rho_p \tag{3.19}$$

where k is the formation permeability, μ is the dynamic viscosity, ρ_m is the mud density, ρ_p is the pore fluid density, and h is the vertical depth. The dimensionless rate of fluid losses (q_D) is identical to the dimensionless heat flow rate (Formula 3.14). For $t_D \geq 100$ the function q_d can be described by the approximate formula

$$q_D = \frac{1}{\ln(1 + D\sqrt{t_D})}, \qquad D = \pi/2 = 1.5708 \tag{3.20}$$

The rate of fluid losses for values of $h_b \leq h_1$ is

$$q = \int_{h_o}^{h_b} q_e \, dh, \tag{3.21}$$

and for values of $h_b > h_1$ is

$$q = \int_{h_o}^{h_1} q_e \, dh, \tag{3.22}$$

The general solution (Kutasov and Bizanti, 1984) obtained from integration of equations 3.21 and 3.22 is given as follows:

$$q = \frac{4\pi k}{(D^2 A)^2 \mu} \Delta\rho \, r_w^2 \, J \tag{3.23}$$

For $H_b \leq H_1$, $J = J_1$; for $H_1 < H_b < H_c$, $J = J_2$, and for $H_b = H_c$, $J = J_3$.
Where,

$$\begin{aligned} J_1 = D^2 A H_b [Ei(2x_o) - Ei(x_o) - \ln\ 2] - Ei(4x_o) + Ei(x_o) \\ +2\ \ln\ 2 + 3[Ei(3x_o) - Ei(2x_o) - \ln\ 1.5] \end{aligned} \tag{3.24}$$

$$\begin{aligned} J_2 = D^2 A H_b [Ei(2x_o) - Ei(2x_1) - Ei(x_o) + Ei(x_1)] \\ +Ei(4x_1) - Ei(4x_o) + Ei(x_o) - Ei(x_1) \\ +3[Ei(3x_o) - Ei(2x_o) - Ei(3x_1) + Ei(2x_1)] \end{aligned} \tag{3.25}$$

$$\begin{aligned} J_3 = D^2 A (H_c + \frac{u\Delta t}{r_w}) \, [Ei(2x_2) - Ei(2x_3) - Ei(x_2) \\ +Ei(x_3)] + Ei(4x_3) - Ei(4x_2) + Ei(x_2) \\ -Ei(x_3) + 3[Ei(3x_2) - Ei(2x_2) - [Ei(3x_3) + Ei(2x_3)] \end{aligned} \tag{3.26}$$

$$x_o = \ln\ [1 + D\sqrt{A(H_b - H_o)}\ ] \tag{3.27}$$

$$x_1 = \ln\ [1 + D\sqrt{A(H_b - H_1)}\ ] \tag{3.28}$$

$$x_2 = \ln\ [1 + D\sqrt{A(H_c + \frac{u\Delta t}{r_w} - H_o)}\ ] \tag{3.29}$$

$$x_3 = \ln\ [1 + D\sqrt{A(H_c + \frac{u\Delta t}{r_w} - H_1)}\ ] \tag{3.30}$$

$$A = \frac{k}{u\phi\mu c_t r_w} \tag{3.31}$$

where ϕ is the porosity, c_t is the total compressibilty, and $Ei(x)$ is the exponential integral of a positive argumenet.

The cumulative fluid losses can be computed from the equation

$$Q = \int_o^t q dt \tag{3.32}$$

It is not difficult to perform integration of equation (3.32) but this method of calculation Q is too cumbersome. For this reason in the computer program "FLOSS" summation was used to estimate values of Q by using the equations (3.19-3.32). In the computer program oilfield (practical) units were used:

$$|k| = md, \quad |\rho| = ppg, \quad |u| = ft/hr, \quad |r_w| = ft,$$

$$|t| = hr, \quad |c_t| = 1/psia, \quad |\mu| = cp, \quad |h| = ft, \quad |q| = gpm$$

We present an example of calculation.

Let us assume that a well is drilled with a constant rate of penetration to the depth of 8000 ft. The input parameters are: permeability is 200 md, penetration rate is 50 ft/hr, porosity (fraction) is 0.20, bit radius is 0.52 ft, compressibility is 0.0000036 $1/psia$, viscosity is 27 cp, depth of thief zone bottom is 4500 ft, depth of thief zone top is 4000 ft, drilling mud density is 12.0 ppg, pore fluid density is 9 ppg, skin factors are: -2, -1, 0, +1, +2; and period of time with no penetration is 48 hrs.
The results of calculations after computer program "FLOSS" are presented in Table 3.3. For the case of no skin the cumulative fluid loss after 128 hrs (4000/50+48) of mud circulation (Table 3.3) is $3.45 \cdot 10^5$ gallons or $1.31 \cdot 10^9$ cm^3. For the density of water base mud of 12 ppg (1.44 g/cm^3) the specific heat capacity is 0.53 $cal/g \cdot ^oC$ (Proselkov, 1975).

Let us assume that average (while circulation) mud temperature is 5^oC higher then the undisturbed formation temperature. In our example the total amount of heat loss due to fluid loss is:
$1.31 \cdot 10^9 \cdot 1.44 \cdot 0.53 \cdot 5 = 5.00 \cdot 10^9$ cal.

3.2 Downhole Circulating Mud Temperatures

3.2.1 Analytical Methods and Computer Programs

A prediction of the downhole mud temperatures during well drilling and completion is needed for drilling fluids and cement slurry design,

Table 3.3 Filtration rate and cumulative flow loss for a hypothetical well

Depth, ft	s = -2	s = -1	s = 0	s = +1	s = +2
Filtration rate, gallons per minute					
4100	33.6	25.0	19.9	16.5	14.1
4200	60.8	46.6	37.6	31.5	27.1
4300	87.2	67.6	55.0	46.4	40.1
4400	113.6	88.3	72.4	61.2	53.1
4500	139.8	109	89.8	76.2	66.2
4600	126.9	102	84.9	72.8	63.6
5000	114.7	93.8	79.2	68.5	60.3
5400	109.2	90.1	76.5	66.5	58.8
5800	105.8	87.7	74.8	65.2	57.8
6200	103.3	86.0	73.6	64.2	57.0
6600	101.3	84.6	72.6	63.5	56.4
7000	99.9	83.5	71.8	62.9	55.9
7400	98.6	82.6	71.1	62.3	55.5
7800	97.4	81.8	70.5	61.9	55.2
8000	92.5	78.3	67.9	59.9	53.5
Cumulative fluid loss, gallons					
4200	0.786E+04	0.590E+04	0.471E+04	0.391E+04	0.335E+04
4500	0.439E+05	0.340E+05	0.276E+05	0.233E+05	0.201E+05
5000	0.118E+06	0.936E+05	0.775E+05	0.661E+05	0.577E+05
5800	0.223E+06	0.180E+06	0.151E+06	0.130E+06	0.114E+06
6600	0.322E+06	0.263E+06	0.222E+06	0.192E+06	0.169E+06
7400	0.418E+06	0.343E+06	0.291E+06	0.252E+06	0.223E+06
8000	0.493E+06	0.406E+06	0.345E+06	0.300E+06	0.265E+06

for drilling bit design, and for evaluation of the thermal stresses in tubing and casings.

One of best attempts at predicting the fluid temperature during mud circulation was made by (Raymond, 1969). For the first time a comprehensive technique to predict transient formations profiles and downhole fluid temperatures in a circulating fluid system was developed. The calculating procedure suggested by Raymond can be modified to account for the presence of the casing strings cemented at various depths. As we mentioned before (Section 3.1.1), the main features of the drilling process were not considered in the Raymond's model: change of well's depth with time, the disturbance of the formation temperature field by previous circulation cycles, the

discontinuity of the mud circulation while drilling, and the effect of the energy sources caused by drilling.

However, the Raymond's model allows one to evaluate the effect of circulation time and depth on downhole temperatures, to estimate the effect of mud type on the difference between bottomhole fluid and outlet temperatures. It is very important to note that this model allows also to determine the duration of the circulation period, after which the downhole temperatures calculated from the pseudo-state equations are practically identical with those computed from unsteady state equations.

For these reasons below we present the physical model and differential equations which describe the process of circulating drilling fluid (Raymond, 1969). The process of forward mud circulation has three phases: fluid enters the drill pipe at the temperature T_{do} and passes down the drill pipe; fluid exits the drill pipe through the bit and enters the annulus at the bottom; fluid passes up the annulus and exits the annulus at the surface. The following conventional assumptions were made: axial conduction of heat in fluid is negligible compared with axial convection; there are no radial temperature gradients in the fluid; the properties of fluids do not change with temperature, and heat generation by viscous dissipation in the fluid is negligible.

For a well of a total vertical depth L the following differential equations describe the heat conduction in the drill pipe–annulus–formation system (Raymond, 1969),

$$A_d\rho v_d c_p \frac{\partial T_d(z,t)}{\partial z} + 2\pi r_d U[T_d(z,t) - T_a(z,t)] = - A_d\rho v_d c_p \frac{\partial T_d(z,t)}{\partial t} \tag{3.33}$$

$$A_a\rho v_a c_p \frac{\partial T_a(z,t)}{\partial z} + 2\pi r_d U[T_d(z,t) - T_a(z,t)] + 2\pi r_b h_f[T_f(r_b,z,t) - T_a(z,t)] = A_a\rho c_p \frac{\partial T_a(z,t)}{\partial t} \tag{3.34}$$

$$\frac{\partial T_f(r_b,z,t)}{\partial t} = \frac{k_f}{\rho_f c_{pf}} \frac{1}{r} \frac{\partial}{\partial r}\left[r \frac{\partial T_f(r,z,t)}{\partial r}\right]_{r=r_b}, \tag{3.35}$$

where A_d and A_a are the cross-sectional areas of drill pipe and annulus; T_d, T_a and T_f are the drill pipe, annular, and formation

temperatures respectively; r_d is the radius of the drill pipe, r_b is the radius of the borehole; c_p and c_{pf} are specific heat capacities of the fluid and formations; ρ and ρ_f are the fluid and formation densities; v_d and v_a are drill pipe and annular fluid velocities; U is the overall heat transfer coefficient between drill pipe and annulus; h_f is borehole wall heat transfer coefficient; k_f is the formation heat conductivity; t, r and z are time and cylindrical coordinates.
The boundary and initial conditions are,

$$2\pi r_b h_f[T_f(r_b, z, t) - T_a(z, t)] = 2\pi r_b K_f[\frac{\partial T_f(r, z, t)}{\partial r}]_{r=r_b} \qquad (3.36)$$

$$T_d(z = 0, t) = T_{do}, \quad T_d(z = L, t) = T_a(z = L, t), \qquad (3.37)$$

$$T_f(r \to \infty, z, t) = a + \Gamma z \qquad (3.38)$$

$$T_f(r, z, 0) = T_d(z, 0) = T_a(z, 0) = a + \Gamma z \qquad (3.39)$$

where a is the surface formation temperature and Γ is the geothermal gradient.
The system of equations (3.33-3.35) was solved numerically to obtain the transient circulating fluid temperature profiles for a simulated well (Raymond, 1969).

The input parameters were:
L=20,000 ft, $2r_d$=4.5 in., $2r_b$=8.625 in., T_{do}=135°F
ρ=18 ppg (oil-based mud), a=80°F, and Γ=0.016°F/ft.
The flow rate was held constant at 200 *gpm* during the entire 16 hours of circulation. The main results of calculations are presented below.

- The outlet temperature rises rapidly to 147°F and in the last 9 hours of circulation the outlet temperature was changed by 1°F;
- Practically constant temperature difference between the bottom-hole fluid and rock is set up after 2-3 hours of the circulation process. It continually changes with time and a steady-state condition is never attained.
- The overall effect of circulation has been to heat the upper section $(0 - z_1)$ of the simulated well and cool the lower section $(z_1 - L)$ of the well. This means that at depth z_1 the annular temperature of the drilling mud (for a given circulation time) is equal to geothermal temperature $(a + \Gamma z_1)$. For example, after 2 hours

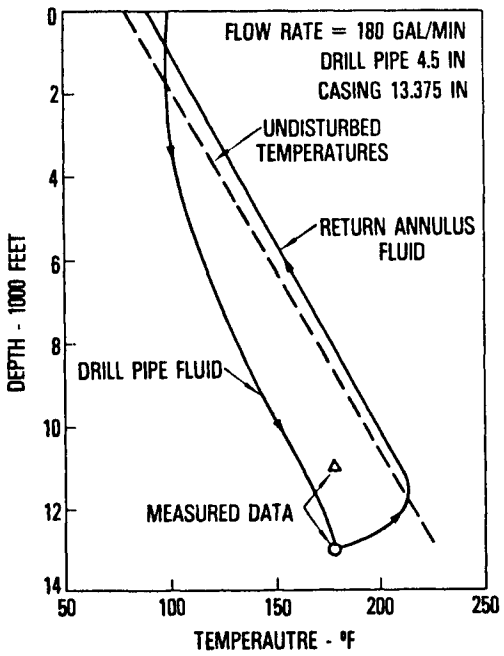


Fig. 3.6. American Petroleum Institute study of a Gulf well – fluid temperature profile after 3 hours (Wooley, 1980).

of mud circulation the value of z_1 was 12,000 ft. The parameter z_1 reduces with circulation time.

□ After a short circulation period (for a constant inlet mud temperature) the unsteady state terms in Eqs. 3.33 and 3.34 can be neglected and a pseudo-state solution can be used. This indicates that the rate of heat flow from formation (or into formation) to annulus becomes a dominant factor.
In this case the Eqs. 3.33 and 3.34 can be written:

$$A_d \rho v_d c_p \frac{\partial T_d(z)}{\partial z} + 2\pi r_d U[T_d(z,t) - T_a(z)] = 0 \tag{3.40}$$

$$A_a \rho v_a c_p \frac{\partial T_a(z)}{\partial z} + 2\pi r_d U[T_d(z) - T_a(z)] + 2\pi r_b h_f[T_f(r_b,t,z) - T_a(z)] = 0 \tag{3.41}$$

It a actual drilling process many time dependent variables influence downhole temperatures. The composition of annular materials

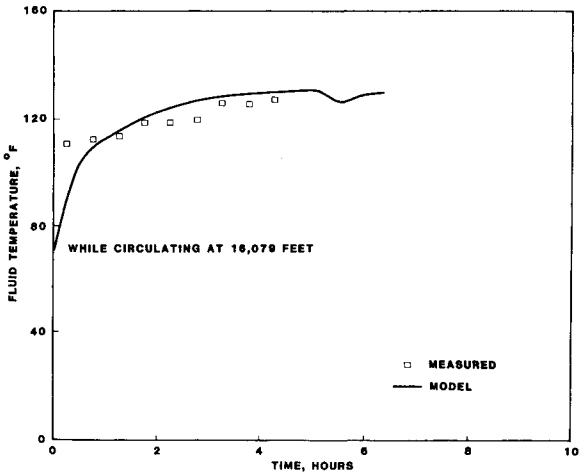


Fig. 3.7. Outlet mud temperature while circulating at 16,079 ft – Mississippi well (Wooley et al., 1984). Courtesy of Society of Petroleum Engineers.

(steel, cement, fluids), the drilling history (vertical depth versus time), the duration of short shut-in periods, fluid flow history, radial and vertical heat conduction in formations, the change of geothermal gradient with depth, and other factors should be accounted for and their effects on the wellbore temperatures while drilling should be determined. It is clear that only transient computer models can be used to calculate temperatures in the wellbore and surrounding formations as functions of depth and time (Wooley, 1980; Mitchell, 1981, Wooley et al., 1984; Beirute, 1991). In the above mentioned references the Reader can find the describtion of several computer thermal simulators. These computer simulators were tested against analytical solutions and in some cases field tests data were used to verify the results of modeling.

We present several examples of circulating temperatures predictions by the WELLTEMP computer code (Figures 3.6-3.8).

As can be seen from Figures 3.6-3.8 the computed circulating temperatures are in a good agreement with the field data. Here we should also take into account that due to incompleteness of the input data (fluid and formations properties, geothermal gradients) some assumptions have to be made before the simulation can be conducted. A drilling simulation was conducted on the geothermal

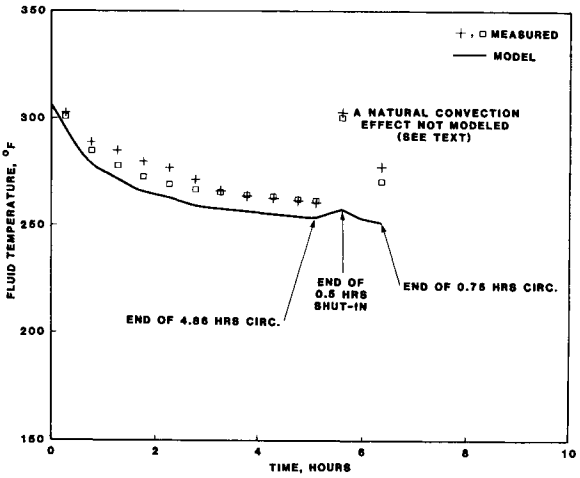


Fig. 3.8. Circulating mud temperature at 16,079 ft – Mississippi well (Wooley et al., 1984). Courtesy of Society of Petroleum Engineers.

Republic 56-30 well (Imperial Valley, California). Table 3.4 summarizes the drilling history of this well. As can be seen from Table 3.4 a thermal simulation of this well requires four different wellbore fluids, four different flow rates, and varying depth (Mitchell, 1981). Mitchell (1981) computed wellbore temperatures for selected time periods (circulation and shut-in), estimated the temperatures at the drill bit over the drilling history of the well, and for two depths calculated the time dependent casing temperature.

3.2.2 Empirical Equation

The temperature surveys in many deep wells have shown that both the outlet drilling fluid temperature and the bottomhole temperature varies monotonically with the vertical depth (Fig. 3.9). It was suggested (Kuliev et al., 1968) that the stabilized circulating fluid temperature in the annulus (T_m) at any point can be expressed as

$$T_m = A_o + A_1 h + A_2 H, \quad h \leq H \tag{3.42}$$

where the values A_o, A_1, and A_2 are constants for a given area, h is the current vertical depth and H is the total vertical depth of the well (the position of the bottom of the drill pipe at fluid circulation).

Table 3.4 Republic 56-30 well: drilling history, fluid properties, and well completion data (Mitchell, 1981)

Drilling hystory				
Time, days	Depth, ft	Circ. rate, gal/min	Circ. time, per day	Fluid*
0	0	480	17.0	1
1	1513	480	5.0	1
2	1513	500	20.0	2
10	5330	360	2.0	3
17	5330	360	17.0	4
24	7520	400	2.0	4
Drilling fluid properties				
Fluid*	Density, lb/gal	Plastic visc., centipoise	Yield point, lb/100 ft^2	
1	8.8	4.0	4.0	
2	9.0	7.0	4.0	
3	8.9	22.0	17.0	
4	8.9	9.0	5.0	
Well completion				
Casing, pipe	Size, inch	Weight, lbf/ft	Setting depth, ft	
Conductor	20	94.0	90.	
Surface	13-3/8	54.5	1503.	
Production	8-5/8	32.0	5320.	
Protective	6-5/8	28.0	7520.	
Drill pipe	3-1/2	9.5	N.A.	

The values of A_o, A_1, and A_2 are dependent on drilling technology (flow rate, well design, fluid properties, penetration rate, etc.), geothermal gradient and thermal properties of the formation. It is assumed that, for a given area, the above mentioned parameters vary within narrow limits. In order to obtain the values of A_o, A_1, and A_2, the records of the outlet fluid (mud) temperature (at $h = 0$) and results of downhole temperature surveys are needed. In Formula 3.42 the value of T_m is the stabilized downhole circulating temperature. The time of the downhole temperature stabilization (t_s) can be estimated from the routinely recorded outlet mud temperature logs. Let us assume that the pump has started to operate at the moment of time $t = 0$. In this case, to get the stabilized values of the outlet mud temperature, one must take readings at

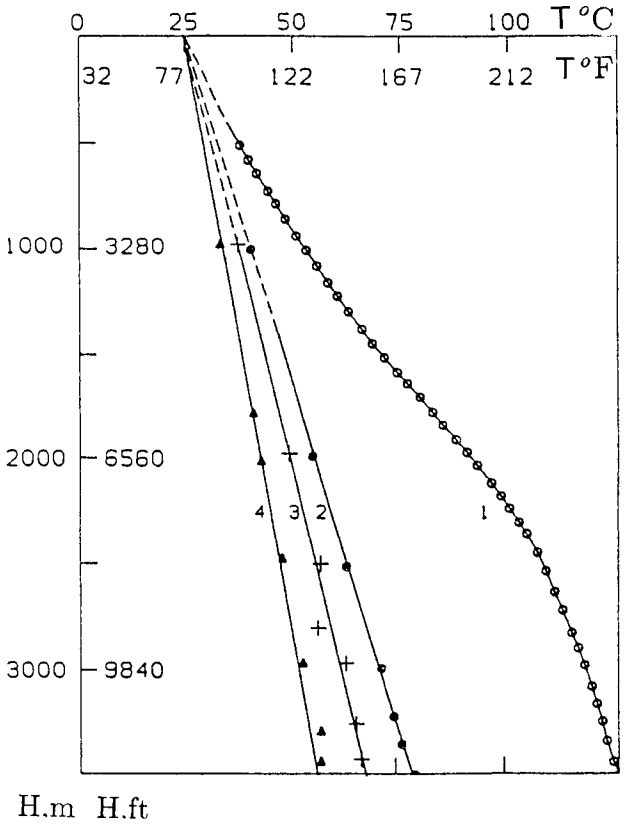


Fig. 3.9. Temperature curves versus current well depth. Well 12-PXC, Stavropol district, Russia (Proselkov, 1975). 1 – geothermal curve, 2 – circulating bottomhole temperature, 3 – outlet drilling mud temperature, 4 – inlet drilling mud temperature.

$t > t_s$. The value of t_s can be obtained from an empirical formula (Kuliev et al., 1968):

$$t_s = b_0 + b_1 H, \tag{3.43}$$

where the values b_0 and b_1 are constants and time t_s is in hours.

Recording the values of the outlet mud temperature (T_{mo}) in time during mud circulation without penetration we can determine the moment of time $t = t_{s1}$, after which the value of T_{mo} is practically constant (Fig. 3.10).

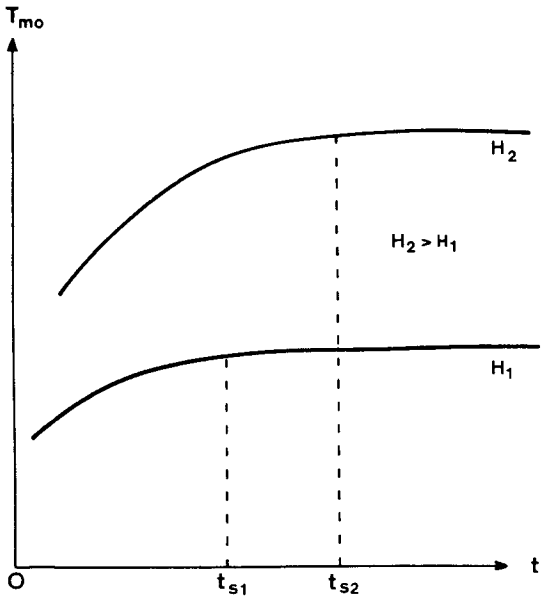


Fig. 3.10. Schematic representation of the outlet temperature versus circulation time.

Hence for $H = H_1$

$$t_{s1} = b_0 + b_1 H_1. \tag{3.44}$$

Similarly for the vertical depth of the well $H = H_2$

$$t_{s2} = b_0 + b_1 H_2. \tag{3.45}$$

From equations 3.44 and 3.45 we obtain

$$b_1 = (t_s 2 - t_s 1) / (H_2 - H_1); \qquad b_0 = t_{s1} - b_1 H_1. \tag{3.46}$$

Equation 3.42 was verified (Kutasov et al., 1988) with more than 10 deep wells, including two offshore wells, and the results were satisfactory ones. Here we are presenting two examples of applying Eq. 3.42 for prediction downhole circulating temperatures. It will be shown that only a minimum of field data is needed to use this empirical method.

Mississippi well.

The results of field temperature surveys and additional data (Table

Table 3.5 Measured (T_m^*) and predicted (T_m) values of wellbore circulating temperature.

Location	h m	H m	T_m^* °C	T_m °C	$T_m^* - T_m$ °C
Mississippi well	4900	4900	129.4	130.7	-1.3
	6534	6534	162.8	163.4	-0.6
	7214	7214	178.3	177.0	1.3
	0	4900	50.0	48.1	1.9
	0	6534	51.7	53.2	-1.5
	0	7214	55.6	55.4	0.2
Webb County, Texas	2805	2805	70.6	71.6	-1.0
	3048	3048	78.3	77.3	1.0
	3449	3449	86.7	86.7	0.0
	0	2805	53.3	53.8	-0.5
	0	3048	60.0	57.9	2.1
	0	3261	60.0	61.6	-1.6

3.5) were taken from the paper by Wooley et al. (1984). The stabilized values of bottomhole circulating temperature were measured at $H = 4900$ m, $H = 6534$ m, and $H = 7214$ m. The outlet mud temperature (at $h = 0$) was also recorded. For the depth of 7214 m (23,669 ft) the actual outlet (flowline) and bottomhole temperatures recorded during logging are presented in Figures 3.11 and 3.12. From plots of outlet mud temperature versus time the values of stabilization time were obtained,

$$t_{s1} = 3.1\ hr \quad at \quad H = H_1 = 4900\ m$$

$$t_{s1} = 4.2\ hr \quad at\ H = H_2 = 7214\ m.$$

From Eq. 3.46 we obtain

$$b_0 = 0.77\ hr; \qquad b_1 = 0.000475\ hr/m.$$

Therefore, the stabilization time for this Mississippi well for any total vertical depth (the position of the end of the drill pipe) can be estimated from Eq. 3.43,

$$t_s = 0.77 + 0.0004754H$$

Three measurements of stabilized bottomhole circulating temperatures and three values of stabilized outlet mud temperatures were

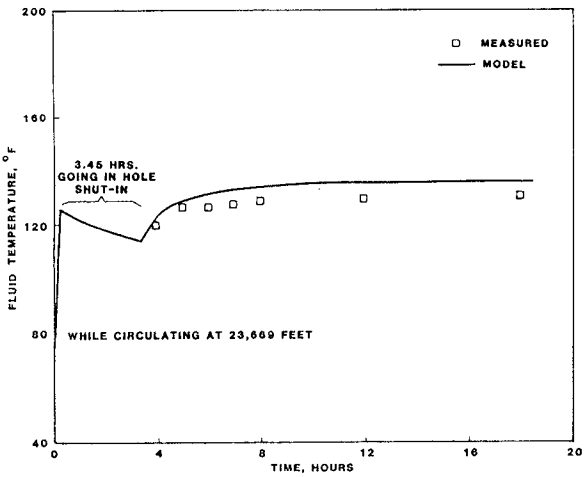


Fig. 3.11. Outlet mud temperature while circulating at 23,669 ft (7214 m) – Mississippi well (Wooley et al., 1984). Courtesy of Society of Petroleum Engineers.

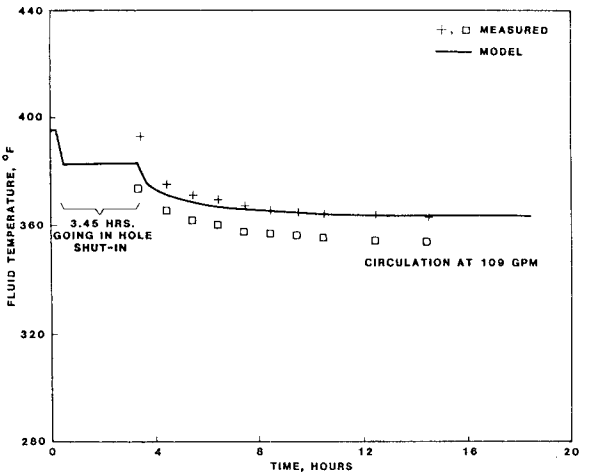


Fig. 3.12. Circulating mud temperature at 23,669 ft (7214 m)– Mississippi well (Wooley et al., 1984). Courtesy of Society of Petroleum Engineers.

run in a multiple regression analysis computer program and the coefficients of the empirical formula (3.42) were obtained

$$A_o = 32.68^oC, \quad A_1 = 0.01685\ ^oC/m, \quad A_2 = 0.003148\ ^oC/m$$

Thus, the equation for the downhole circulating temperature is

$$T_m = 32.68 + 0.01685h + 0.003148H$$

Webb County, Texas.
The temperature measurements (Table 3.5) in this location were obtained from paper by Venditto and George (1984). It was not known whether these measurements were taken in a single well or in the wells in the same area. But since this empirical method can be applied to an entire area as well as to a single well, the data points were used simultaneously to calculate the coefficients in the formula (3.42). By using the multiple regression analysis computer program was obtained,

$$A_o = 5.69^oC, \quad A_1 = 0.00636\ ^oC/m, \quad A_2 = 0.01714\ ^oC/m$$

In Table 3.5 the measured and predicted values of bottom-hole and outlet circulating temperatures are compared and the agreement is seen to be good in both cases. The significant difference in values of A_o, A_1 and A_2 for the Mississippi and the Texas wells indicates that these coefficients are valid only within a given area.

3.2.3 Mud Temperature Control

The high downhole temperatures to a great extent affect the drilling technology of deep wells. A few applications that require a knowledge of the maximum values of bottomhole temperatures include drilling mud program design, bit performance, stability of the well's wall, logging tool design, log interpretation, and thermal stresses in dril pipes and casing. At deep drilling for hydrocarbons and geothermal drilling efforts are made to control and to lower the circulating downhole temperatures. For example, at geothermal drilling bottomhole temperatures (at the producing zone) may range from 300°F (149°C) to 800 °F (427°C) depending on the area, (Edwards et al., 1982).

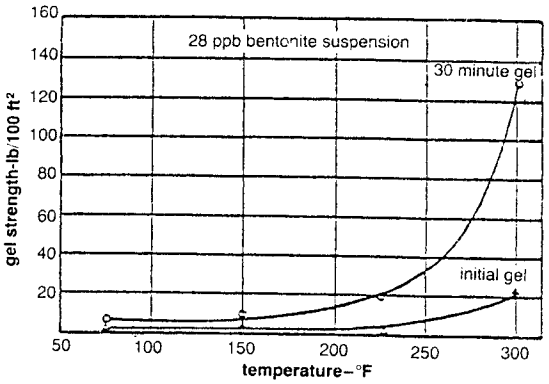


Fig. 3.13. Effects of temperature and bentonite concentration on 30-minute gel strength (Edwards et al., 1982).

For this reason high temperature stability of drilling fluids is a major problem at geothermal exploration. Due to clay colloids flocculation water-based muds start to degenerate significantly at about 150°C and the rate of degeneration increases rapidly with increase in temperature (Edwards et al., 1982). It is seen from Fig. 3.13 that high density muds are more sensitive to high-temperature floccation. Wooley (1980) used a computer model to conduct a sensitivity study – to evaluate the influence of fluid inlet temperature, fluid flow rate, and depth on downhole circulating temperature predictions. A case of forward circulation was considered. Casing and tubing dimensions used for calculations were: tubing 4.5 in. to total depth, production casing, 9.625 in. to total depth, intermediate casing, 13.375 in. to 3,000 ft, and surface casing, 20 in. to 1,000 ft. Some results of calculations are presented in Figures 3.14-3.17.

For the inlet mud temperature of 50°F (10°C) the circulating fluid has a cooling effect on the surrounding formation (Fig. 3.14). The drastic increase of the flow rate (ten times) has a little effect on the bottomhole temperature (Fig. 3.15). In this case the bottomhole temperature was lowered only by 10°F (5.6°C). Bottomhole temperature is presented in Fig. 3.16 for circulation at two depths. As was expected, at the shallow depth a steady state is achieved earlier. Figure 3.17 shows steady temperature profiles for fluid circulation at two depths. Note that the mud circulation system acts as a heat exchanger, and the inlet temperature is close to the outlet temperature for either depth.

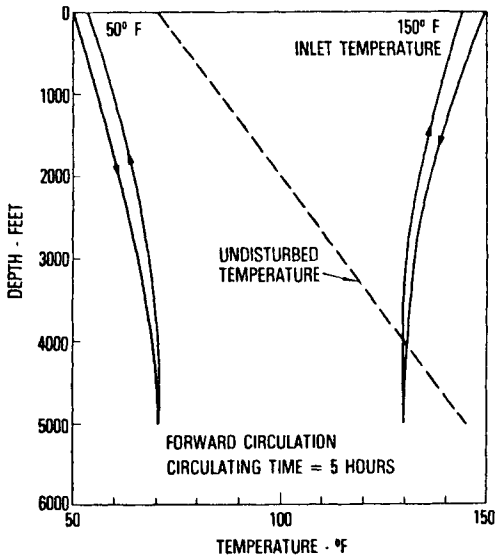


Fig. 3.14. Sensitivity of steady temperature profile to inlet temperature (Wooley, 1980).

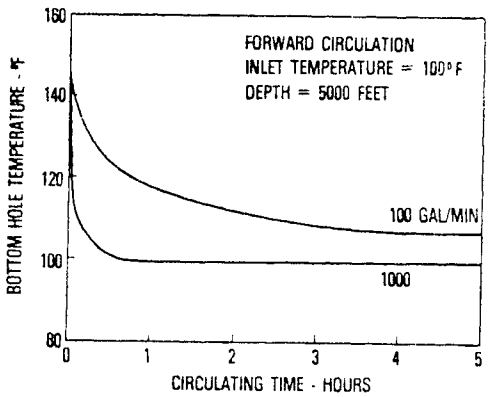


Fig. 3.15. Sensitivity of bottomhole temperature to flow rate (Wooley, 1980).

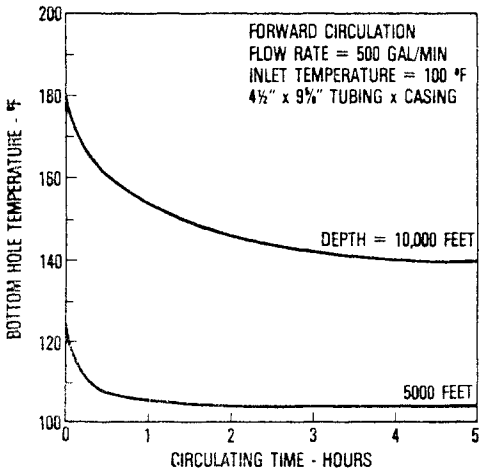


Fig. 3.16. Sensitivity of bottomhole temperature to depth (Wooley, 1980).

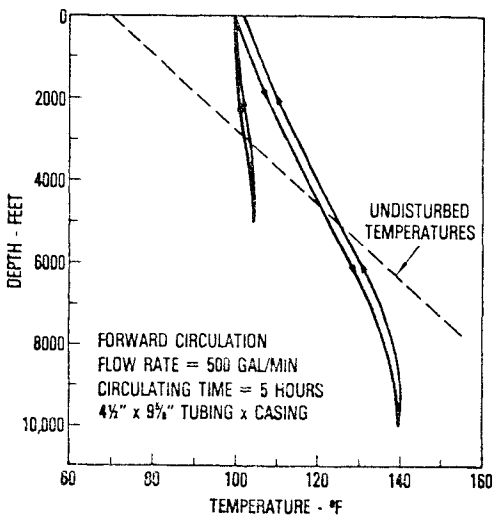


Fig. 3.17. Sensitivity of steady temperature profile to depth (Wooley, 1980).

Table 3.6 Calculated bottomhole circulating temperature (Proselkov, 1975). Well depth – 5000 m, diameter – 300 mm, bottomhole geothermal temperature – 164 °C, the drill pipe-annulus heat transfer coefficient – 4000 $\frac{kcal}{m^2 \cdot hr \cdot °C}$

Flow rate	Inlet temperature °C	Outlet temperature °C	Bottomhole temperature °C
35 l/s (550 *gpm*)	40	45	103
	0	15	95
	-20	0	91
70 l/s (1100 *gpm*)	40	49	76
	0	18	55
	-20	3	44

Calculations for a deep well show (Table 3.6), that surface cooling of drilling fluid with some mixtures (ice + $NaCl$ or ice + $CaCl_2$) has a little effect on the reduction of the bottomhole temperature at even relatively high flow (35 l/s) rates. Hence, the inlet temperatures can be used to control downhole temperatures only if the circulation rates are high. It is more effective to use mud and ice mixtures as drilling fluids. In this case a significant amount of heat will be spent to melt the ice particles. At forward circulation the temperature of the of this mixture in the drill pipe up to some depth (z_o) will remain close to 0°C until melting of the last particles of ice. The value of z_o is a function of the initial ice concentration in the mud and ice mixture, heat transfer coefficient, flow rate, geothermal gradient, thermal properties of surrounding formations, inlet temperature, well depth, drill pipe, and well sizes. Two set of equations describe the heat conduction in the drill pipe-annulus-formation system (Proselkov, 1975). For the 0-z_o section of the well the equations account for the ice-water transition in the drill pipe. The temperature of the fluid in the drill pipe at z_o is equal to 0°C. At deeper depths ($> z_o$) a conventional system of differential equations described the heat conduction process. Proselkov (1975) used a computer program and calculated (for a simulated 3100 m well) transient values of z_o and bottomhole circulating temperature. The cooling effect at the bottomhole increases with the increase of

the mud circulation time. In one run, for example, after one cycle of mud circulation the bottomhole temperature was 69.5°C and the value of z_o was 660 m. After three cycles of mud circulation the corresponding values were 43.3°C and 900 m. It should be mentioned that the bottomhole geothermal temperature was 124.6 °C.

3.3 Drilling Fluid Densities at High Temperatures and Pressures

3.3.1 Experimental Data

In deep and hot wells, the densities of water/oil muds and brines can be significantly different from those measured at surface conditions. Calculations have shown that bottomhole pressures predicted with constant mud densities to be in error by hundreds of *psig* (Hoberock et al., 1982). Determining accurate density of drilling mud under downhole conditions is therefore needed for calculating the actual hydrostatic pressure in a well. Also it is very important to estimate the effect of pressure and temperature on the density of the formation fluid. This will permit a more accurate prediction of differential pressure at the bottomhole and will help to reduce the fluid losses resulting from miscalculated pressure differentials. In areas with high geothermal gradients, the thermal expansion of drilling muds can lead to unintentional underbalance, and a kick may occur.

In the following section we will present an empirical equation of state (pressure-density-temperature dependence) for drilling muds and brines. Below we present information about the data base, which was used to estimate the accuracy of the suggested formula.

McMordie et al. (1982) presented laboratory data on the changes in density of three types of water base muds (fluid numbers 1, 2, and 3) and three types of diesel oil muds (fluid numbers 4, 5, and 6) in the temperature and pressure ranges of 70-400°F (0-204°C) and 0-14,000 *psig* (0-965 bar).

The densities of thirteen sodium chloride solutions in the temperature and pressure ranges of 70-482°F (21-250°C) and 0-29,000 *psig*

(0-2,000 bar) at various molal concentration of $NaCl$ were obtained from tables presented by Potter et al. (1977). Two sodium chloride solutions will be referred below as fluids No. 7 and No. 8.

Reliable established laboratory densities of water (Burnham et al., 1969) were used to compare the densities of $NaCl$ brines and water under downhole conditions. For a 7.0 molal calcium bromide brine (fluid No. 9) density-pressure-temperature data were taken from a plot (Hubbard, 1984).

3.3.2 Empirical Formula

At present, a material balance compositional model is used to predict the density of drilling muds and brines at downhole conditions (Hoberock et al., 1982; Sorelle, et al., 1982). To use this method, only laboratory density measurements for oils and brines at elevated temperatures and pressures are needed because, conventionally the compressibility and thermal expansion of the solid components are assumed to be very small, and therefore can be neglected. But if a significant amount of chemicals is present in the mud, some chemical interaction can cause changes in the solid-fluid system. It is known, for example, that water-based muds start to degenerate at elevated temperatures. In these cases the compositional model can not be used and laboratory density measurements of water base muds and brines at elevated temperatures and pressures are needed.

Here we present an empirical equation of state for drilling muds and brines (Kutasov, 1988b). This simple formula will allow one to predict the density of water/oil base muds and brines at downhole conditions. A minimum of input data is required to calculate the coefficients in this formula. Application of the suggested formula may reduce the time and cost of laboratory density tests.

In physics, pressures encountered in deep wells (up to 30,000 $psia$) are considered only as moderate pressures. Within this range of pressures, the coefficient of isothermal compressibility is a weak function of pressure and can be assumed as a constant for many fluids. Our analysis of laboratory density test data (Hubbard, 1984; McMordie et al.,1982; Potter et al., 1977;) for water and oil base muds and brines has shown that their coefficient of thermal (volumetric) expansion can be expressed as a linear function of

temperature and the coefficient of isothermal compressibility is practically a constant. We have found that the following empirical formula can be used as an equation of state for either water or oil-based drilling muds, or for brines:

$$\rho = \rho_o \, exp[\alpha p + \beta(T - T_s) + \gamma(T - T_s)^2] \qquad or \qquad (3.47)$$

$$\ln \rho = \ln \rho_o + \alpha p + \beta(T - T_s) + \gamma(T - T_s)^2 \qquad (3.48)$$

Where T is the temperature, ^{o}F, p is the pressure, $psig$, $T_s = 59^o\text{F} = 15^o\text{C}$ (International standard temperature), ρ is the fluid density (ppg); ρ_o is the fluid density (ppg) at standard conditions ($p = 0$ $psig$, $T = 59^o$F); α (isothermal compressibility), β, and γ are constants. A regression analysis computer program was used to process density-pressure-temperature data (Tables 3.7-3.9) and to provide the coefficients of Formula 3.47 (Table 3.10).

Table 3.7 Measured (McMordie et al., 1982) ρ^* and predicted ρ densities for two water-based muds

		Fluid No. 1			Fluid No. 3		
P	T	ρ^*	ρ	$\Delta\rho$	ρ^*	ρ	$\Delta\rho$
psig	^{o}F	*ppg*	*ppg*	*ppg*	*ppg*	*ppg*	*ppg*
2000	100	10.75	10.73	-0.02	18.11	18.08	-0.03
2000	200	10.44	10.40	-0.04	17.73	17.70	-0.03
2000	300	9.98	10.00	0.02	17.19	17.19	0.00
4000	100	10.82	10.80	-0.02	18.23	18.19	-0.04
4000	200	10.50	10.47	-0.03	17.81	17.81	0.00
4000	300	10.05	10.07	0.02	17.29	17.29	0.00
4000	400	9.59	9.59	0.00	16.64	16.65	0.01
6000	100	10.87	10.88	0.01	18.32	18.30	-0.02
6000	200	10.55	10.54	-0.01	17.89	17.91	0.02
6000	300	10.11	10.13	0.02	17.38	17.40	0.02
6000	400	9.67	9.66	-0.01	16.76	16.75	-0.01
8000	300	10.17	10.20	0.03	17.47	17.50	0.03
8000	400	9.74	9.72	-0.02	16.87	16.85	-0.02
10000	300	10.23	10.27	0.04	17.56	17.61	0.05
10000	400	9.81	9.79	-0.02	16.98	16.96	-0.02
12000	400	9.88	9.86	-0.02	17.08	17.06	-0.02
14000	400	9.95	9.92	-0.03	17.17	17.16	-0.01

The accuracy of the results was estimated from the the sum of squared residuals and is presented in Table 3.10. In Tables 3.7,

Table 3.8 Measured (McMordie et al., 1982) ρ^* and predicted ρ densities for two oil-based muds

		Fluid No. 4			Fluid No. 6		
P	T	ρ^*	ρ	$\Delta\rho$	ρ^*	ρ	$\Delta\rho$
psig	^oF	*ppg*	*ppg*	*ppg*	*ppg*	*ppg*	*ppg*
2000	100	11.04	10.97	-0.07	18.08	18.02	0.01
2000	200	10.56	10.53	-0.03	17.56	17.52	-0.04
2000	300	10.12	10.14	0.02	17.05	17.05	0.00
4000	100	11.14	11.11	-0.03	18.22	18.21	-0.01
4000	200	10.70	10.67	-0.03	17.73	17.70	-0.03
4000	300	10.29	10.27	-0.02	17.26	17.23	-0.03
4000	400	9.92	9.92	0.00	16.78	16.80	0.02
6000	100	11.24	11.26	0.02	18.35	18.40	0.05
6000	200	10.81	10.81	0.00	17.88	17.89	0.01
6000	300	10.43	10.41	-0.02	17.43	17.41	-0.02
6000	400	10.08	10.05	-0.03	16.99	16.98	-0.01
8000	300	10.55	10.54	-0.01	17.60	17.59	-0.01
8000	400	10.22	10.18	-0.04	17.18	17.15	-0.03
10000	300	10.67	10.68	0.01	17.74	17.78	0.04
10000	400	10.35	10.31	-0.04	17.35	17.33	-0.02
12000	400	10.46	10.45	-0.01	17.54	17.52	-0.02
14000	400	10.57	10.58	0.01	17.69	17.70	0.01

3.8, and 3.9, the measured (ρ^*) and calculated (ρ) values of fluid density are compared. The results show a good agreement between the measured and predicted densities. Results also show that the diesel oil muds are more compressible than the water-based muds. At the same time the oil-based muds are more susceptible to thermal expansion. Sodium chloride brines are widely used during drilling and workover operations to control formation pressure. To obtain the density at various molal concentrations of $NaCl$, the coefficients ρ_o, α, β, and γ in Eq. 3.37 were calculated (Kutasov, 1991). A regression analysis computer program was used to process density-pressure-temperature data (Potter et al., 1977) for a $NaCl$ brine and water (Burnham et al., 1969) and to calculate the coefficients (Table 3.11). The accuracy of the results ($R = |\rho - \rho^*|/\rho^*$) was estimated from the the sum of squared residuals (Table 3.11).

Example.
The following example shows that with a minimum of laboratory density data the coefficients in Eq. 3.47 can be determined, and

Table 3.9 Measured (Potter et al., 1977) ρ^* and predicted ρ densities for two sodium chloride solutions

		Fluid No. 7			Fluid No. 8		
P	T	ρ^*	ρ	$\Delta\rho$	ρ^*	ρ	$\Delta\rho$
psig	^oF	*ppg*	*ppg*	*ppg*	*ppg*	*ppg*	*ppg*
8688	167	8.696	8.692	-0.004	9.889	9.897	0.008
11588	167	8.763	8.792	0.029	9.964	9.985	0.021
8688	212	8.604	8.584	-0.021	9.789	9.783	-0.007
11588	212	8.679	8.682	0.003	9.873	9.869	-0.003
14489	212	8.738	8.782	0.044	9.931	9.957	0.026
11588	257	8.579	8.559	-0.021	9.772	9.750	-0.023
14489	257	8.637	8.657	0.019	9.831	9.836	0.005
18115	257	8.704	8.782	0.077	9.898	9.946	0.048
14489	302	8.521	8.518	-0.003	9.714	9.711	-0.003
18115	302	8.596	8.641	0.045	9.798	9.819	0.021
21741	302	8.688	8.765	0.077	9.881	9.928	0.047
14489	347	8.379	8.366	-0.013	9.597	9.581	-0.016
18115	347	8.462	8.486	0.024	9.681	9.688	0.007
21741	347	8.562	8.608	0.046	9.772	9.796	0.023
18115	392	8.312	8.320	0.007	9.564	9.553	-0.011
21741	392	8.454	8.439	-0.015	9.656	9.659	0.004
25367	392	8.537	8.561	0.023	9.739	9.767	0.028
18115	437	8.153	8.141	-0.012	9.430	9.414	-0.016
21741	437	8.270	8.258	-0.012	9.530	9.519	-0.012
25367	437	8.404	8.377	-0.027	9.631	9.625	-0.006
21741	482	8.103	8.066	-0.037	9.405	9.375	-0.030
25367	482	8.237	8.182	-0.054	9.505	9.479	-0.026
28993	482	8.362	8.300	-0.062	9.606	9.585	-0.021

this equation predicts with a sufficient accuracy the mud density under downhole conditions.

Let us assume that for fluid No. 2 (Table 3.10) only 6 laboratory density tests (instead of 39) were conducted (Table 3.12). By using a regression analysis computer program, the coefficients of Eq. 3.47 are determined to be: $\rho_o = 13.627\ ppg$, $\alpha = 3.597E-06\ 1/psig$,

$$\beta = -1.3063E-04\ 1/^oF, \quad \gamma = -6.6128E-07\ 1/(^oF \cdot ^o F)$$

In Table 3.12 the measured ρ^* and calculated ρ values of fluid density are compared. By assuming that the bottomhole pressure and temperature are: p=6,000 $psig$; T=400^{o}F, from Eq. 3.47, the

Table 3.10 Coefficients in Equation 3.47

Fluid No.	Mud, brine	ρ_o ppg	α $1/psig$ 10^{-6}	β $1/°F$ 10^{-4}	γ $1/(°F \times °F)$ 10^{-7}	$\Delta\rho/\rho$ x 100 %
1	Water base	10.770	3.3815	-2.3489	-4.2366	0.22
2	Water base	13.684	3.2976	-1.7702	-5.2126	0.15
3	Water base	18.079	3.0296	-1.3547	-4.1444	0.16
4	Oil-base	11.020	6.5146	-4.3414	+1.4144	0.32
5	Oil-base	14.257	6.0527	-3.0027	-0.5156	0.34
6	Oil-base	18.049	5.1951	-2.9637	+0.7460	0.21
7	Sodium chloride	8.591	3.9414	-1.6008	-4.5254	0.34
8	Sodium chloride	9.886	3.0519	-2.1967	-1.4840	0.21
9	Calcium bromide	15.227	1.3506	-2.4383	-0.3618	0.20

Table 3.11 Coefficients in Equation 3.47 for sodium chloride brines

Molal concentration	ρ_o ppg	α $1/psig$ 10^{-6}	β $1/°F$ 10^{-4}	γ $1/(°F \times °F)$ 10^{-7}	$\Delta\rho/\rho$ x 100 %
0	8.3723	3.2422	-2.5836	-4.06130	0.22
1	8.3562	4.3447	-1.8070	-4.90363	0.41
3	8.4742	4.1310	-1.7128	-4.67334	0.37
5	8.5908	3.9414	-1.6008	-4.52541	0.34
7	8.7128	3.7431	-1.5436	-4.28340	0.34
9	8.8350	3.5928	-1.5105	-4.05636	0.34
11	8.9624	3.4504	-1.5421	-3.71040	0.35
13	9.0870	3.3187	-1.5505	-3.43119	0.35
15	9.2152	3.2549	-1.5682	-3.21697	0.34
17	9.3472	3.1678	-1.6837	-2.84163	0.33
19	9.4779	3.1076	-1.7719	-2.52752	0.30
21	9.6242	3.0667	-1.8977	-2.18582	0.27
23	9.7504	3.0466	-2.0438	-1.82556	0.24
25	9.8865	3.0519	-2.1967	-1.48402	0.21

Table 3.12 Comparison of measured (McMordie et al., 1982) ρ^* and predicted ρ densities

P *psig*	T ^oF	ρ^* *ppg*	ρ *ppg*	$\Delta\rho$ *ppg*
0	70	13.60	13.61	0.01
0	200	13.22	13.20	-0.02
0	300	12.70	12.71	0.01
4,000	200	13.40	13139	-0.01
8,000	300	13.06	13.08	0.02
14,000	400	12.70	12.69	-0.01

mud density is determined to be:

$$\rho = 13.637 \cdot \exp[(3.5967E-06 \cdot 6,000) - 1.3063E-04 \cdot$$

$$(400-59) - 6.6128E-07 \cdot (400-59)^2] = 12.33 \ (ppg)$$

This value is in a satisfactory agreement with the measured mud density of 12.36 *ppg* (McMordie et al., 1982).

3.4 Hydrostatic Mud Pressure

3.4.1 New Formula

For a static well the pressure at any well's depth is equal to the hydrostatic pressure exerted by the column of the drilling mud. During drilling mud circulation an additional pressure drop is required to overcome friction forces opposing the flow of fluid in the annulus. The total pressure during circulation is expressed through the equivalent circulating fluid density. For a successful drilling the mud weight should conform to two conditions: the static mud weight must be able to control the formation pressures and to provide sufficient support to prevent hole collapse, and the equivalent circulating density during circulation should not exceed the fracture gradient (French and McLean, 1993).

The mud density increases with pressure and reduces with the increase of the temperature. Many drilling operators consider this compensating effect as a basis for the using the surface mud

density for calculation of the hydrostatic pressure. In oilfield units (ppg, $psig$, ft) the following relationship is usually used

$$p = B_c \rho h, \qquad B_c = 0.052 \, \frac{psig}{ppg \cdot ft} \tag{3.49}$$

Below we present a formula for calculating the downhole hydrostatic mud pressure. It will be shown that in many cases the effect of the temperature and depth on drilling mud density should be taken into account at downhole mud pressure predictions.
From physics is known that

$$dp = \rho g \, dh \tag{3.50}$$

where dp is the increment given to pressure, $\rho(T,p)$ is the mud density, g is acceleration constant due to gravity, and dh is the increment given to the vertical depth. As we mentioned before (Section 3.2), the stabilized values of downhole circulating temperatures can be approximated by a linear function of depth

$$T = a_o + a_1 h \tag{3.51}$$

where a_o and a_1 are coefficients. Let us now introduce a variable x

$$x = T - T_s = a_o + a_1 h - T_s, \quad dx = a_1 \, dh, \quad T_s = 15^o C \tag{3.52}$$

From Eqs. 3.47 and 3.50-3.52 we obtain

$$-\frac{1}{\alpha}[\exp(-\alpha p) - 1] = \int_o^{a_1 h} \exp(\beta x + \gamma x^2) \, dx \tag{3.52}$$

The values of γx^2 and αp are very small and we assume that

$$\exp(\gamma x^2) \approx 1 + \gamma x^2 \tag{3.53}$$

$$\exp(-\alpha p) \approx 1 - \alpha p + \frac{(\alpha p)^2}{2} \tag{3.54}$$

Now the integral 3.52 can be evaluated by using tables for the following integral (Gradshtein and Ryzhik, 1965)

$$\int x^2 \, \exp(ax) \, dx = e^{ax} \, (\frac{x^2}{a} - \frac{2x}{a^2} + \frac{2}{a^3}) \tag{3.55}$$

From Eqs. 3.52-3.55 we obtain

$$p^2 - \frac{2p}{\alpha} + \frac{2F}{\alpha} = 0 \tag{3.56}$$

Table 3.13 The effect of mud density-depth variation on downhole hydrostatic pressure predictions

		Fluid No.1		Fluid No.5		Fluid No.8	
h	T	p	Δp	p	Δp	p	Δp
ft	^oF	*psig*	*psig*	*psig*	*psig*	*psig*	*psig*
1000	117.2	552	-7	730	-11	508	-6
2000	123.6	1104	-15	1462	-19	1016	-11
3000	130.1	1656	-22	2195	-27	1523	-18
4000	136.5	2208	-30	2931	-31	2031	-23
5000	142.9	2761	-36	3668	-35	2539	-29
6000	149.3	3313	-44	4408	-36	3048	-33
8000	162.2	4417	-59	5892	-33	4064	-44
10000	175.0	5520	-75	7384	-22	5081	-55
12000	187.8	6623	-91	8885	-2	6098	-65
14000	200.7	7725	-108	10394	25	7115	-75
16000	213.5	8827	-125	11911	61	8132	-85
18000	226.4	9927	-144	13438	107	9150	-94
20000	239.2	11027	-162	14974	162	10169	-102

$$p = \frac{1}{\alpha} - \sqrt{\frac{1}{\alpha^2} - \frac{2F}{\alpha}} \tag{3.57}$$

where

$$F = B_o(B_1 B_2 - A_o) \tag{3.58}$$

$$A_o = 1 + \gamma[(a_o - T_s)^2 - \frac{2}{\beta}(a_o - T_s) + \frac{2}{\beta^2}] \tag{3.59}$$

$$B_o = \frac{\rho_o g}{a_1 \beta} \exp[\beta(a_o - T_s)] \tag{3.60}$$

$$B_1 = \exp(\beta a_1 h) \tag{3.61}$$

$$B_2 = 1 + \gamma[(a_o + a_1 h - T_s)^2 - \frac{2}{\beta}(a_o + a_1 h - T_s) + \frac{2}{\beta^2}] \tag{3.62}$$

The values of hydrostatic pressures were calculated after formula 3.56 for three types of muds (Table 3.10) and compared with the pressures p^*, $\Delta p = p - p^*$ (Table 3.13) calculated by the conventional method (Formula 3.49). The values of the coefficients ρ_o, α β, and γ were presented in Table 3.10. From Table 3.13 follows that for deep and hot wells the change of mud density with depth should be taken into account in calculations of the downhole mud pressure.

3.4.2 Differential Pressure

The hydrostatic mud pressure required to prevent the influx of reservoir fluid into the well is equal to the formation pressure plus a safe overbalance. Let us consider a simple case when the formation pore pressure is equal to the hydrostatic pressure of the formation fluid. In this case the pore pressure can be calculated from Eq. 3.57. The differential pressure — downhole mud pressure minus the pore pressure can be calculated, and a safe overbalance can be selected. When, according to the drilling mud program, the density (or the type) of the inlet fluid is changed, new values of coefficients ρ_o, α β, and γ are introduced and the Eq. 3.57 is used again. However, for high temperature, high pressure (HTHP) wells the pore pressure depends on many factors and may increase drastically with depth. For example, for HTHP wells drilled in the Central Graben (North Sea) a sharp increase in pore pressure over a short vertical interval, sometimes less than 100 ft (30 m), was observed (MacAndrew et al., 1993). In this case the Eq. 3.57 can be used only to evaluate the pressure change due to mud and formation density variation with depth. To speed up calculations after Eq. 3.57 we prepared a computer program "HYDIF" (Appendix C, Table C.2). In this program the formation fluid is water or sodium chloride brine with density of 9 *ppg* (1.1 g/cm^3) at normal conditions. However, by the introducing new values of the coefficients ρ_o, α β, and γ in the "Data" statement, the program can be used for any formation fluid. In the program the downhole mud hydrostatic pressures computed from Eq. 3.57 are compared with those calculated by the conventional constant-surface-mud-density method (Eq. 3.49). We should only to note that in the "HYDIF" program a more accurate value of the conversion factor B_c (0.051947 instead of 0.052) is used.
Below we present three examples which will show that in deep, hot wells the actual mud column pressure (p) can be hundreds of *psi* less then those calculated by the conventional (constant mud density) method (p^*). Let us assume that the water base mud No. 2 (Table 3.10) is used. The "HYDIF" program was utilized to calculate bottomhole hydrostatic mud pressures (Table 3.14) for various geothermal gradients (Γ), outlet (T_{mo}) and bottomhole (T_{mb}) mud temperatures.
The values of T_{mb} were estimated from an empirical formula (Ku-

Table 3.14 The downhole hydrostatic mud pressure predictions for water base fluid No. 2. Total well's vertical depth – 20,000 ft

Γ °F/100 ft	T_{mo} °F	T_{mb} °F	p *psig*	$p - p^*$ *psig*	ρ *ppg*	$\rho - \rho_o$ *ppg*
1.0	110.8	239.2	14151	-66	13.65	0.03
1.2	113.3	276.7	14056	-161	13.46	0.23
1.4	119.5	310.5	13955	-262	13.26	0.42
1.6	129.3	340.8	13849	-368	13.07	0.61
1.8	142.4	367.6	13741	-476	12.90	0.78
2.0	159.2	390.8	13628	-589	12.74	0.94

tasov and Targhi, 1987; see Section 5.4). It was assumed that the surface temperature of formations is 75°F (24 °C).

Example 1.
The permeability of a gasbearing formation is low enough to allow drilling at underbalance. Let us assume that the differential pressure is: -300 *psig*. Fluid No. 2 is used, the geothermal gradient is 1.4 °F/100 ft (Table 3.14). Assume that pore pressure (equivalent density) at 20,000 ft is 13.707 *ppg*, then the needed mud column hydrostatic pressure (using the conventional formula) is:

$$0.052 \cdot 13.707 \cdot 20,000 - 300 = 13,955(psig)$$

and the equivalent mud density is:

$$13,955 : (0.052 \cdot 20,000) = 13.418(ppg)$$

From Table 3.14 we find that mud with surface density of 13.648 *ppg* will produce the hydrostatic pressure of 13,955 *psig*. Thus the additional underbalance is:

$$(13.418 - 13.684) \cdot 0.052 \cdot 20,000 = -277(psig)$$

and the actual underbalance is: $-277 + (-300) = -577(psig)$. This underbalance may be large enough to cause a kick.

Example 2.
Drilling is conducted at overbalance and the differential pressure is: +200 *psig*. Geothermal gradient is 1.4 °F/100 ft. Assume that pore pressure (equivalent density) at 20,000 ft is 13.226 *ppg*, then

the needed mud column hydrostatic pressure is:

$$0.052 \cdot 13.226 \cdot 20,000 + 200 = 13,955(psig)$$

and the equivalent mud density is:

$$13,955 : (0.052 \cdot 20,000) = 13.418(ppg)$$

From Table 3.14 we find that mud with surface density of 13.648 *ppg* will produce the hydrostatic pressure of 13,955 *psig*. Thus the differential pressure change is:

$$(13.418 - 13.684) \cdot 0.052 \cdot 20,000 = -277(psig).$$

The actual differential pressure is: -277 + 200 = -77(*psig*) and drilling is conducted at underbalance instead of overbalance.

Example 3.
Drilling is conducted at overbalance and the differential pressure is: +200 *psig*. Geothermal gradient is 2.0 °F/100 ft. Assume that the equivalent density at 20,000 ft is 12.912 *ppg*, then the needed mud column hydrostatic pressure is:

$$0.052 \cdot 12.912 \cdot 20,000 + 200 = 13,628(psig)$$

and the equivalent mud density is:

$$13,628 : (0.052 \cdot 20,000) = 13.104(ppg)$$

From Table 3.14 we estimate that mud with surface density of 13.648 *ppg* will produce the hydrostatic pressure of 13,628 *psig*. Thus the differential pressure change is:

$$(13.104 - 13.684) \cdot 0.052 \cdot 20,000 = -603(psig)$$

and the actual differential pressure is: -603 + 200 = -403(*psig*). In this case drilling is conducted at underbalance instead of overbalance and the underbalance may be large enough to cause a kick.

3.5 Drilling Through Hydrates

Gas hydrates are solid mixtures of natural gas and water which can be formed at various combinations of the temperature and pressure.

Drilling through the hydrate-bearing formations can pose problems and a downhole mud density and temperature control is required.

Due to drastic increase in the gas volume at hydrate decomposition, the hydrate zones may cause the drilling mud become highly gasified, resulting in an intense gas kick. High collapse strength casing should be used to case off the hydrate bearing formations. Billy and Dick (1974) described the first experience of drilling through gas hydrate zones. In two exploratory wells (Imperial Oil Ltd., Mackenzie Delta area, Canada) significant gas shows were observed in the drilling mud while penetrating what was considered to be gas-bearing reservoirs (Billy and Dick 1974). The results of logging and formations tests have shown that gas is in hydrate form. Water-based drilling fluids contain many sites for crystal nucleation and this creates favorable conditions for formation of hydrates. Hydrate formation in water-based fluids was first observed while drilling offshore wells (California, Gulf of Mexico) and a number of water-based mud formulations have been suggested as inhibitors (Sloan, 1991).

The composition of natural gases is the major factor which determines the ranges of pressure and temperature required for formation or decomposition of hydrates (Fig. 3.18) From the temperature-pressure stability diagram follows that if hydrates are contained in a confined space and the temperature is raised, high pressures can be generated. For example, when methane hydrate forms at 0^{o}C, and then decomposes due to heating to a temperature of 100^{o}C (in a confined space) the pressure increases from 2.6 MPa to 2500 MPa (Gritsenko and Makogon, 1983). The depth of hydrate stability in the earth can be obtained through a plot of the geothermal gradient and the hydrate temperature-depth (pressure) stability envelope (Fig. 3.19).

The knowledge of the mean earth surface temperature and the geothermal gradient is needed to predict the hydrate-prone zone (Fig. 3.20). For an Arctic site with mean surface temperature of -16^{o}C, a geothermal gradient of 65 mK/m is necessary for no hydrates, whereas at 0^{o}C a gradient of 15 mk/m will ensure their absence (Judge, 1982).

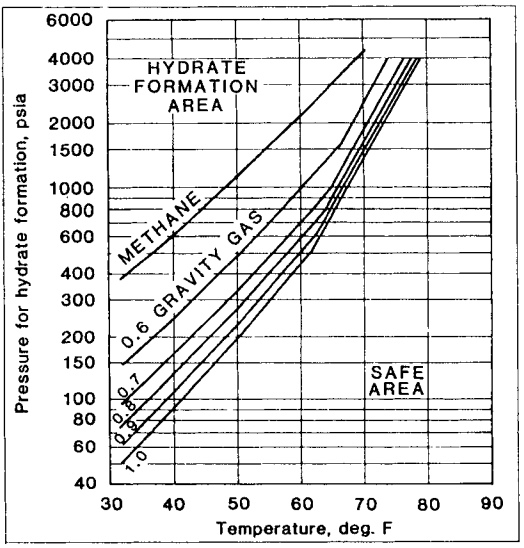


Fig. 3.18. Temperature-pressure diagram of natural gas hydrates formation (Katz, 1945).

Goodman and Franklin (1982) suggested to control the hydrate gas influx by increasing the decomposition temperature through the use of high density drilling muds.

A computer program (WELLTEMP) has been used to simulate the drilling of an Arctic offshore Panarctic well. For the heat transfer calculations WELLTEMP program requires to specify for each day the duration of the circulating and shut-in periods. For this reason the projected drilling schedule was simplified for the computer simulation. The depth-drilling time plot (Fig. 3.21) was divided into sections of constant drilling penetration rate. Two temperature gradients were used for the Panarctic simulation. The sea surface temperature is 28°F (-2°C) and sea floor temperature is 32°F (0°C). Below the sea floor geothermal gradient is constant to 5282 ft (1610 m) where the temperature is 102.2°F (39°C). The mud density was 10 *ppg* (1200 kg/m^3), the porosity of formations is 10 percent, and latent heat for the soil-hydrate composite is 15.2 cal/g. The annulus mud temperature at the hydrate depth 2200 ft (671 m) was predicted as a function of drilling time (Fig 3.22). The jump at 24 days is due to the increase in mud inlet temperature from 48°F (8.9°C) to 55°F (12.8°C). The hydrate decomposition

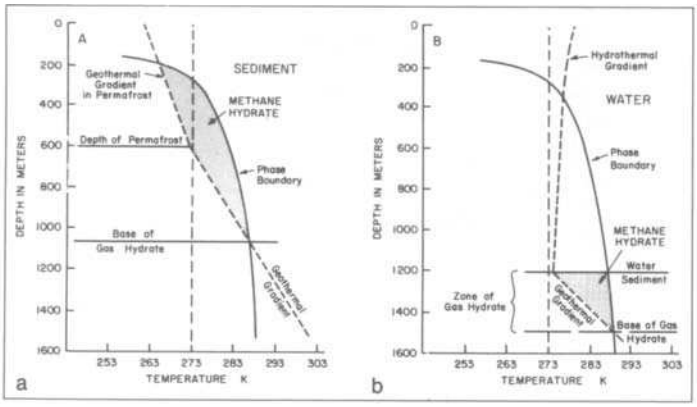


Fig. 3.19. Methane hydrate stability depths in (A) permafrost and (B) ocean environments (Kvenvolden, 1988).

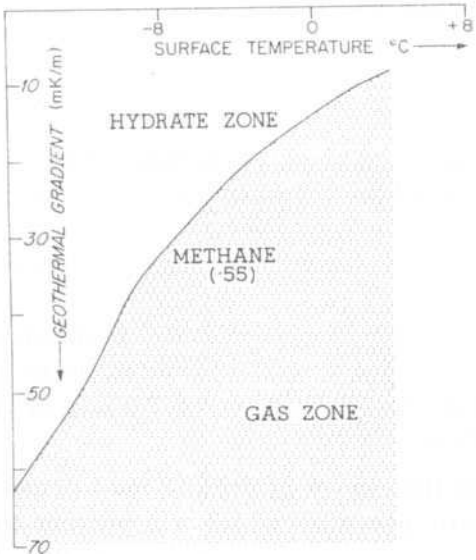


Fig. 3.20. Relationship between mean surface temperature and temperature gradient for the occurrence of methane gas hydrate (Judge, 1982).

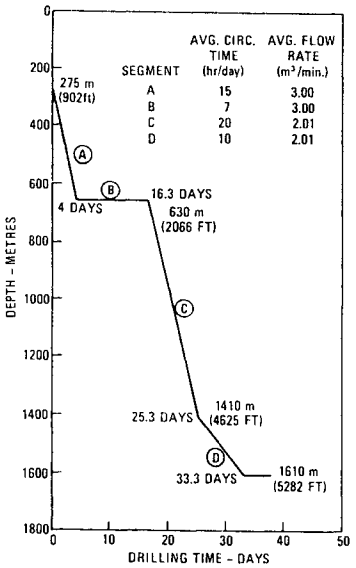


Fig. 3.21. The depth-time plot used in drilling simulation (Goodman and Franklin, 1982).

does not begin until after 24 days of drilling (Fig. 3.22), but then increases rapidly, reaching a radius of 1.82 ft (0.55 m) after 33.6 days (Goodman and Franklin, 1982). To prevent the hydrate decomposition the density of the drilling mud should be increased according to the pressure-temperature stability diagram (Fig. 3.18). As was shown, for example, by Goodman and Franklin (1982) an increase of 3.6 *ppg* (432 kg/m^3) used by Panarctic is more than enough to inhibit hydrate decomposition for 2.6 day of circulation and shut-in at bottomhole.

Figure 3.23 presents the curves of drilling mud densities necessary to ensure hydrostatic pressures which will prevent the decomposition of hydrates of a natural gas (specific gravity 0.6) depending on the depth and on the mud temperature (Gritsenko and Makogon, 1983). Bondarev et al. (1976) presented equations describing the decomposition of hydrates around the wellbore when the bore-face is maintained at a constant temperature or at a constant radial heat flow rate.

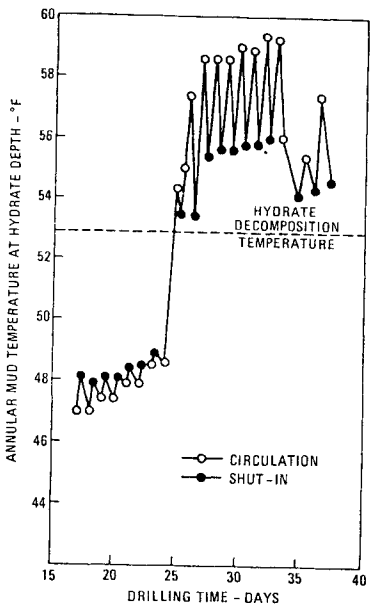


Fig. 3.22. Mud temperature opposite hydrate zone (Goodman and Franklin, 1982).

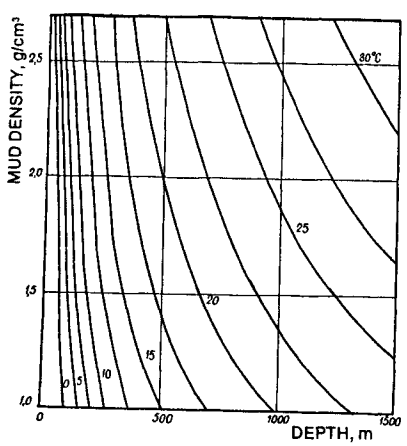


Fig. 3.23. Minimum mud density to prevent decomposition of natural gas (Gritsenko and Makogon, 1983).

3.6 Formation Temperatures Around the Wellbore

3.6.1 Radius of Thermal Influence

Interpretation of electric logs, evaluation of the thermal stresses arising due to the difference between the wellbore temperature and undisturbed formation temperature, and estimation of static formation temperatures from well logs requires knowledge of the temperature disturbance of formations produced by the circulating drilling mud. The drilling process greatly alters the temperature field of formations surrounding the wellbore. The temperature change is affected by the duration of fluid circulation (depth penetration, hole cleaning, cementing), the duration of shut-in periods (tripping of drill pipe, running of casing, logging), the temperature difference between the formation and drilling mud, the well radius, the thermal properties of formations, and the drilling technology used. The results of field and analytical investigations have shown that in many cases the effective temperature (T_w) of the circulating fluid (mud) at a given depth can be assumed constant during drilling or production (Lachenbruch and Brewer, 1959; Ramey, 1962; Edwardson et al., 1962; Jaeger, 1961; Kutasov et al., 1966; Raymond, 1969). Here we should to note that even for a continuous mud circulation process the wellbore temperature is dependent on the current well depth and other factors. The term "effective fluid temperature" is used to describe the temperature disturbance of formations while drilling. Lachenbruch and Brewer (1959) have shown that the wellbore shut-in temperature mainly depends on the amount of thermal energy transferred to (or from) formations. Thus for every depth a value of T_w can be estimated from shut-in temperature logs. In theory the drilling process affects the temperature field of formations at very long radial distances. There is, however, a practical limit to the distance – the radius of thermal influence (r_{in}), where for a given circulation period ($t = t_c$) the temperature $T(r_{in}, t_c)$ is practically equal to the geothermal temperature T_f. To avoid uncertainty, however, it is essential that the parameter r_{in} must not to be dependent on the temperature difference $T(r_{in}, t_c) - T_f$. For this reason we used the thermal balance method to calculate the radius of thermal influence.

The results of modeling, experimental works, and field observations have shown the temperature distribution around the wellbore during drilling can be approximated by the following relation (Kutasov, 1968; Kutasov, 1976):

$$\frac{T(r,t)-T_f}{T_w-T_f}=1-\frac{\ln\ r/r_w}{\ln\ r_{in}/r_w},\qquad r_w\le r\le r_{in} \tag{3.63}$$

Introducing the dimensionless values of circulation time, radial distance, radius of thermal influence, and temperature

$$t_D=\frac{at_c}{r_w^2},\quad r_D=\frac{r}{r_w},\quad R_{in}=\frac{r_{in}}{r_w},\quad T_D(r_D,t_D)=\frac{T(r,t)-T_f}{T_w-T_f} \tag{3.64}$$

we obtain

$$T_D(r_D,t_D)=1-\frac{\ln\ r_D}{\ln\ R_{in}},\qquad 1\le r_D\le R_{in} \tag{3.65}$$

It is known that the cumulative heat flow from the wellbore per unit of length is give by:

$$Q=2\pi\rho c r_w^2(T_w-T_f)Q_D \tag{3.66}$$

where ρ is the density of formations, c is the specific heat of formations, r_w is the well radius, and Q_D is the dimensionless cumulative heat flow. The time dependent function Q_D can be expressed as

$$Q_D=\int_1^{R_e}(1-\frac{\ln\ r_D}{\ln\ R_{in}})\ r_D\ dr_D \tag{3.67}$$

The last integral is evaluated by using the table for the following integral (Gradshtein and Ryzhik, 1965)

$$\int x^n\ \ln\ x\ dx=\frac{x^{n+1}}{n+1}(\ln\ x-\frac{1}{n+1}) \tag{3.68}$$

where n is a positive integer. From Eqs. 3.67 and 3.68 we obtain

$$Q_D=\frac{R_{in}^2-1}{4\ \ln\ R_{in}}-\frac{1}{2} \tag{3.69}$$

The results of a numerical solution (Jaeger, 1956) for a cylindrical source with a constant wall temperature were used to obtain the

values of $Q_D(t_D)$. From the last equation we found that the dimensionless radius of thermal influence can be approximated by:

$$R_{in} = 1 + D_o\sqrt{t_D}, \tag{3.70}$$

$$D_o = 2.184, \quad 5 \leq t_D < 10^4,$$
$$D_o = 2.143, \quad 5 \leq t_D < 10^6$$

3.6.2 Adjusted Circulation Time

In his classical paper Henry Ramey (1962) drawed the attention of petroleum engineers to the fact that three solutions: for a cylinder losing heat at constant temperature, for a constant heat flow line source, and for a cylinder losing heat under the convection boundary, practically converge after some time. The simple solution for a constant fluid flow (or heat flow) line source is expressed through the exponential integral, and is widely used in reservoir engineering. To use this solution for any value of circulation time, we introduce below the adjusted circulation time.

Let us assume that at a given depth the fluid circulation started at the moment of time $t = 0$ and stopped at $t = t_c$. The corresponding values of the dimensionless heat flow rates (Formula 3.14) are

$$q_D(t = 0) = \infty, \qquad q_D(t = t_c) = q_D$$

and the values of the dimensionless cumulative heat flow are $Q_D(0) = 0$ and $Q_D(t_c) = Q_D$. Assuming that during the circulation period $0 < t \leq t_c$ the value of of $q_D(t) = q_D = constant$, then the dimensionless adjusted circulation time is

$$t_D^* = \frac{Q_D}{q_D}, \quad or \quad Q_D = q_D \cdot t_D^* \quad t > 0 \tag{3.71}$$

The actual adjusted circulation time is $t_c^* = t_D^* \, r_w^2/a$. The values of Q_D are presented in the literature (Van Everdingen and Hurst, 1949; Jacob and Lohman, 1952; Edwardson, et al., 1962; Sengul, 1983). Using these data we obtained:

$$t_D^* = t_D[1 + 1/(1 + AF)], \quad t_D \leq 10 \tag{3.72}$$

$$F = [\ln(1 + t_D)]^n; \quad n = 2/3, \quad A = 7/8$$

Table 3.15 Comparison of values of dimensionless cumulative heat flow for a well with constant bore-face temperature. Q_D^* – Van Everdingen and Hurst (1949); Q_D – equation (3.71)

t_D	Q_D^*	Q_D	$\frac{\Delta Q_D}{Q_D^*} \cdot 100, \%$
2	0.2447×10^1	0.2455×10^1	0.32
3	0.3202×10^1	0.3212×10^1	0.32
5	0.4539×10^1	0.4565×10^1	0.57
10	0.7411×10^1	0.7512×10^1	1.37
20	0.1232×10^2	0.1240×10^2	0.65
50	0.2486×10^2	0.2516×10^2	1.22
100	0.4313×10^2	0.4382×10^2	1.61
200	0.7579×10^2	0.7710×10^2	1.73
500	0.1627×10^3	0.1650×10^3	1.39
1000	0.2935×10^3	0.2966×10^3	1.04
2000	0.5341×10^3	0.5382×10^3	0.77
5000	0.1192×10^4	0.1198×10^4	0.52
10000	0.2204×10^4	0.2213×10^4	0.42
20000	0.4096×10^4	0.4110×10^4	0.36
50000	0.9363×10^4	0.9390×10^4	0.29
100000	0.1759×10^5	0.1763×10^5	0.24

$$t_D^* = t_D \frac{\ln t_D - \exp(-0.236\sqrt{t_D})}{\ln t_D - 1}, \quad t_D > 10 \tag{3.73}$$

The dimensionless cumulative heat flow is calculated from Eqs. 3.71, 3.72, 3.73, and 3.14. The values of Q_D are presented in Table 3.15 and compared with the results of a numerical solution.

3.6.3 Radial Temperature Distribution

To determine the temperature distribution $T(r,t)$ in formations near a wellbore with a constant bore-face temperature it is necessary to obtain a solution of the diffusivity equation for the following boundary and initial conditions:

$$T(r,0) = T_f; \qquad r_w \leq r < \infty, \qquad t > 0$$

$$T(r_w,t) = T_w; \qquad T(\infty,t) = T_f$$

It is well known that in this case the diffusivity equation has a solution in a complex integral form (Jaeger, 1956; Carslaw and

Jaeger, 1959). Jaeger (1956) presented results of a numerical solution for the dimensionless temperature $T_D(r_D, t_D)$ with values of r_D ranging from 1.1 to 100 and t_D ranging from 0.001 to 1000. We used these data to verify the Formula 3.63 (Table 3.16) The Table 3.16 shows that the suggested formula can be used to determine the formation temperatures with a sufficient accuracy.

We also have found that the exponential integral (a tabulated function) can be used to describe the temperature field of formations around a well with a constant bore-face temperature

$$T_D(r_D, t_D) = \frac{T(r,t) - T_f}{T_w - T_f} = \frac{Ei(-r_D^2/4t_D^*)}{Ei(-1/4t_D^*)} \tag{3.74}$$

$$t_D = \frac{at}{r_w^2}; \qquad r_D = \frac{r}{r_w}$$

In Table 3.16 values of T_D calculated after Formula 3.74 and the results of a numerical solution are compared. The agreement between values of T_D calculated by these two methods is seen to be good.

3.6.4 Volumetric Average Temperature

Knowledge of volumetric average temperature of formations T_{vol} for a given radius of investigation (r_{inv}) is needed to estimate the electrical resistance of the formation water and to evaluate the temperature-density dependence of formations. The dimensionless volumetric average temperature of formation T_{vD} can be described by the following equation:

$$T_{vD} = \frac{T_{vol} - T_f}{T_w - T_f} = \frac{1}{R_{inv}^2 - 1} \int_1^{R_{inv}} T_D(r_D, t_D)\, r_D\, dr_D, \tag{3.75}$$

where $R_{inv} = r_{inv}/r_w$ is the dimensionless radius of investigation. The last integral is evaluated by using the table of the following integral (Gradshtein and Ryzhik, 1965)

$$\int_0^p Ei(\beta\, x)\, dx = pEi(\beta\, x) + \frac{1 - e^{\beta p}}{\beta} \tag{3.76}$$

Using the substitution $x = r_D^2$, from Eqs. 3.74, 3.75 and 3.76 we obtain

$$T_{vD} = \frac{-pEi(\beta R_{inv}^2) + Ei(\beta) - (e^{\beta p} - e^{\beta})/\beta}{(1 - R_{inv}^2)Ei(\beta)} \tag{3.77}$$

Table 3.16 Dimensionless temperature $T_D(r_D, t_D)$ for a well with constant bore-face temperature, first line – formula 3.63; second line – formula 3.74; third line – numerical solution (Jaeger, 1956)

t_D	$T_D \times 1000$									
	Dimensionless distance, r_D									
	1.1	1.2	1.5	2.0	3.0	5.0	7.0	10.0	20.0	30.0
5.0	946	897	771	609	380	92	0	0	0	0
	934	875	726	543	310	97	26	2	0	0
	940	886	746	568	332	101	24	2	0	0
10.0	954	912	804	665	469	222	59	0	0	0
	945	896	771	614	404	180	77	18	0	0
	949	903	784	631	422	188	77	16	0	0
20.0	960	923	829	708	538	323	181	31	0	0
	953	912	804	668	481	266	148	59	1	0
	956	916	813	681	497	277	153	57	1	0
50.0	966	935	855	752	608	425	305	178	0	0
	961	926	837	723	564	370	253	144	18	1
	963	929	843	731	574	381	260	146	16	1
100.0	970	942	870	778	649	486	378	264	42	0
	966	935	856	755	613	437	326	216	55	11
	967	937	860	760	621	446	334	222	53	10
200.0	972	947	883	800	683	535	438	335	135	18
	969	942	871	780	653	493	390	285	109	39
	970	943	874	784	658	500	397	291	110	38
300.0	974	950	889	811	700	560	468	371	181	70
	971	945	879	793	673	522	424	323	144	65
	972	946	881	796	677	528	430	328	146	64
500.0	976	953	896	823	719	588	502	411	234	130
	973	949	887	807	695	554	462	365	190	102
	974	950	889	810	699	559	468	372	194	104
700.0	977	955	900	830	730	605	522	435	265	165
	974	951	892	815	708	573	484	392	219	129
	975	952	893	818	712	578	490	397	223	132
1000.0	978	957	904	837	741	621	542	458	295	200
	975	953	897	824	721	591	506	417	249	159
	976	954	898	826	724	596	511	422	254	162

$$\beta = -\frac{1}{4t_D^*} \tag{3.78}$$

The volumetric average temperature is is given by:

$$T_{vol} = (T_w - Tf)T_{vD} + T_f \tag{3.79}$$

A computer program "TEMVOL" (Appendix C, Table C.3) is prepared to calculate functions T_{vol} and $T_{rf} = T(r_{inv}, t_c)$. Tables have been constructed that allow prediction of values T_{vD} and T_D at various distances from the wellbore (Kutasov, 1989a).

Example.
The example well was drilled to a depth of 12,490 ft (3,807 m) in Webb County, Texas (Venditto and George, 1984). The values of the static temperature of formations and circulating temperature at the bottomhole are:

$$T_f = 306^oF\ (152.2^oC), \qquad T_w = 251^oF\ (121.7^oC).$$

Let us assume that after 20 hours of mud circulation an electrical log was run (near the bottomhole) and the radius of investigation, bit diameter, and the thermal diffusivity of formations are:

$$r_{inv} = 17.5\ in. = 0.445\ m; \quad 2r_w = 8.75\ in.\ (0.222\ m),$$

$$a = 0.04\ ft^2/hr\ (0.00372\ m^2/hr)$$

The following steps are needed to calculate the radial temperature ($r = r_{inv}$) and the volumetric average temperature of formations for t_c= 20 hr.
Step 1. Compute the dimensionless circulation time and dimensionless radius of investigation,

$$t_D = \frac{20 \cdot 0.04 \cdot (2 \cdot 12)^2}{8.75^2} = 6.0, \qquad R_{inv} = \frac{17.5 \cdot 2}{8.75} = 4.0$$

Step 2. From tables (Kutasov, 1989a), or from computer program "TEMVOL", or from formulas 3.74 and 3.77 determine the values of $T_D(4.0, 6.0) = 0.2011$ and $T_{vD}(4.0, 6.0) = 0.4114$.
Step 3. Compute the value of T_{vol} and $T_{rf} = T(r = r_{inv}, t_c)$,

$$T_{vol} = 0.4114 \cdot (251 - 306) + 306 = 283.4(^oF) = 139.7(^oC),$$

$$T_{rf} = 0.2011 \cdot x(251 - 306) + 306 = 294.9(^oF.) = 146.1(^oC)$$

3.6.5 Application of the Duhamel's Integral

Until now we considered cylindrical heat sources with a constant (at a given depth) bore-face temperature. However, for very deep wells (5,000–10,000 m) the circulating temperature is a function of time. Let us now assume that the bore-face temperature is a prescribed function of time. The solution of the thermal diffusivity equation for this case (no heat production in the formations) can be deduced from that for constant surface conditions by the use of Duhamel's theorem namely, (Carslaw and Jaeger, 1959, p.30):
If $v = F(x, y, z, \lambda, t)$ *represents the temperature at* (x, y, z) *at the time* t *in a solid in which the initial temperature is zero, while the surface temperature is* $\phi(x, y, z, \lambda)$*, then the solution of the problem in which the initial temperature is zero, and the surface temperature is* $\phi(x, y, z, t)$*, is given by*

$$v = \int_0^t \frac{\partial}{\partial t} F(x, y, z, \lambda, t - \lambda)\, d\lambda \tag{3.80}$$

In the Duhamel's theorem the parameter λ is the variable of integration and the term "zero initial temperature" means that the initial temperature is a constant. In our case $T(r, 0) = T_f$ and in the Eq. 3.80 the function v should be replaced by $v - T_f$. When the function $\phi(x, y, z, t)$ can be approximated by a sequence of discrete constant temperatures the principle of superposition is used. This approach is widely used in pressure and flow well testing. Gogoi (Gogoi, 1986; Gogoi and Kutasov, 1986) used the principle of superposition to determine the temperature distribution around an uncased well when the fluid circulation (with a constant temperature) while drilling was followed by a short production period. The simple Formula 3.63 was extended to the production period by superpositioning in time domain the effect of temperature change. The validity of the method was demonstrated by comparison with an "exact" numerical solution (Carslaw and Jaeger, 1959).

We used the Duhamel's integral to determine the temperature distribution around the wellbore when the circulating fluid temperature (at a given depth) is a linear function of time

$$T_c = B_o + B_1 t, \quad 0 < t \leq t_c \tag{3.81}$$

where B_o and B_1 are constants.
For the well wall temperature (Formula 3.81) an approximate ana-

Table 3.17 Formulas for the Ei(x) function

x	y	$Ei(x)$
0.05 - 0.50	$A_o + A_1(\ln x) + A_2(\ln x)^2 + A^3(\ln x)^3$ $A_0 = 1.7016,\ A_1 = 2.0320$ $A_2 = 0.36002,\ A_3 = 0.45141$	$Ei(x) = y$
0.50 - 3.10	$A_o + A_1 x + A_2 x^2 + A_3 x^3$ $A_0 = -1.3059,\ A_1 = 3.9669$ $A_2 = -1.1115,\ A_3 = 0.34609$	$Ei(x) = y$
3.10 - 10.0	$A_0 + A_1/x + A_2/x^2 + A_3/x^3 + A_4/x^4$ $A_o = 1.2049,\ A_1 = -4.4332$ $A_2 = 51.311,\ A_3 = -158.07$ $A_4 = 154.79$	$Ei(x) = ye^x/x$

lytical solution, which describes the temperature distribution $T(r,t)$ in formation surrounding the wellbore during the fluid circulation period (Kutasov, 1976) is:

$$T(r,t) - T_f = \left(1 - \frac{\varphi_1}{\Psi_1} \ln\ r_D\right)(\Psi_1 - T_f), \tag{3.82}$$

$$\Psi_1 = B_o + B_1 t,$$

$$\varphi_1 = \frac{2B_1}{D^2}[Ei(2\ln R_{in}) - Ei(\ln R_{in})] + \frac{B_o}{\ln R_{in}},$$

$$R_{in} = 1 + D_o\sqrt{t_D}, \qquad D_o = 2.184,$$

$$D = D_o\frac{\sqrt{a}}{r_w}, \qquad t_D = \frac{at_c}{r_w^2},$$

where $Ei(x)$ is the exponential integral of a positive argument (a tabulated function) and a is the thermal diffusivity of formations. In order to simplify calculations we used tables of the $Ei(x)$ function (Abramowitz and Stegun, 1972) and derived a set of approximate formulas (Table 3.17). The dimensionless radius of the thermal influence $R^*_{in} = r^*_{in}/r_w$ is:

$$R^*_{in} = e^{\Psi_1/\varphi_1}. \tag{3.83}$$

Thus, for the moment of time $t = t_c$ the temperature distribution in and around the wellbore is:

$$\left.\begin{array}{ll} T_c, & 0 \le r_D \le 1, \\ T(t_c, r), & 1 < r_D \le R^*_{in}, \\ T_f, & r_D > R^*_{in} \end{array}\right\}. \tag{3.84}$$

3.7 Thermal Stresses in Formations and Casings

Knowledge of the stresses in casings and around the wellbore is needed for the analysis of wellbore stability. In addition to the weights of the overburden and the wellbore fluid, the difference in temperatures at the wellbore and the undisturbed formations adds to the stresses around the wellbore, as thermal stress. The total formation stresses (in normally pressured areas) can be determined by calculating the thermal stresses separately and then superposing them on the stresses resulting from the overburden weight and wellbore fluid pressure. Stresses around the borehole of a deep well may be determined by applying the theory of elasticity. It is necessary to assume that the rock is elastic and obeys Hooke's law, has a modulus of elasticity (E), and has a Poisson's ratio (ν). After a well is drilled, the wellbore may be considered as the inside of a cylinder with a very thick wall – approaching an infinite thickness. The pressure at the inside of the well is equal to the weight of the wellbore fluid. Gogoi (1986) obtained equations for determining the thermal stresses around the wellbore during drilling and production periods. The derivation of these equations is based on Borsei et al.'s (1978) derivation of stresses for a thick-walled cylinder (Fig. 3.24)

The Formula 3.63 was used to approximate the radial temperature distribution in formations during drilling mud circulation. Thermal stresses around the wellbore during drilling can be determined from the following equations (Gogoi, 1986):

$$\sigma_{r,th} = \frac{\alpha E}{1-\nu}(T_m - T_f)[\frac{\ln\ r_D}{2\ \ln\ R_{in}} - \frac{1}{2}(1-\frac{1}{r_D^2})(1+\frac{1}{2\ \ln\ R_{in}})] \quad (3.85)$$

$$\sigma_{\theta,th} = \frac{-\alpha E}{1-\nu}(T_m - T_f)[1 - \frac{\ln\ r_D}{2\ \ln\ R_{in}} - \frac{1}{2}(1-\frac{1}{r_D^2})(1+\frac{1}{2\ \ln\ R_{in}})] \quad (3.86)$$

$$\sigma_{z,th} = \frac{-\alpha E}{1-\nu}(T_m - T_f)(1 - \frac{\ln\ r_D}{\ln\ R_{in}}) \quad (3.87)$$

where, $\sigma_{r,th}$, $\sigma_{\theta,th}$, $\sigma_{z,th}$ are normal thermal stress components in cylindrical coordinates; T_m is the wellbore temperature during drilling; T_f is the undisturbed formation temperature; r_D is the dimensional distance measured in units of wellbore radius, and R_{in} is the dimensionless radius of thermal influence. Some parameters

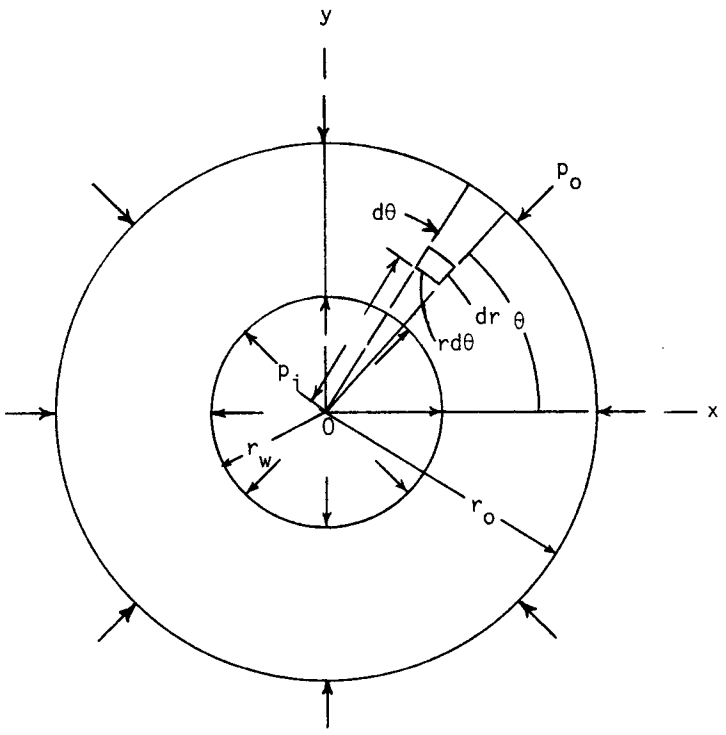


Fig. 3.24. Stresses in a thick-walled cylinder. Thin annulus of thickness dz perpendicular to the plane of the figure (Borsei et al., 1978).

used in Eqs 3.85, 3.86 and 3.87 are presented in Table 3.18. As an example, thermal stresses around the wellbore (sandstone) are calculated (Tables 3.19 and 3.20, Fig. 3.25) for the following conditions:

$$z = 1524\,m, \quad r_w = 0.1\,m, \quad T_m - T_f = 25^oC$$

The steel casing string can be considered as an elastic body with a constant ratio between the applied stress and the resulting strain. This ratio, Young's modulus of elasticity (E), for steel with a coefficient of thermal linear expansion $\alpha = 6.9 \cdot 10^{-6}\ {}^oF^{-1}$ is equal to $3.0 \cdot 10^7\ psi$ (Craft et al., 1962). The change of length (elongation) ΔL of casing of length L due to temperature change ΔT is

$$\Delta L = \alpha L \Delta T \tag{3.88}$$

Table 3.18 Average thermo-elastic properties of rocks (Tuman, 1962)

Rocks	ρ $\frac{g}{cm^3}$	E, 10^9 Pa	ν	α, 10^{-6} $\frac{1}{^oC}$	c $\frac{cal}{g^oC}$	λ, 10^{-3} $\frac{cal}{cm\ s^oC}$	a $\frac{m^2}{hr}$
Sandstone	2.5	16.237	0.25	10	2.5	8.2	0.00537
Limestone	2.7	51.573	0.27	8	2.7	5.2	0.00315
Dolomite	2.9	51.158	0.25	7	2.9	5.2	0.00293
Gypsum	2.3	26.2	0.3	19	2.3	3.0	0.00181
Anhydride	2.9	26.2	0.3	19	2.9	3.5	0.00197
Shale	2.4	24.821	0.4	5.8	2.4	3.52	0.00202

Table 3.19 Radial thermal stresses $\sigma_{r,th}$ in MPa around the a wellbore in sandstone formation (Gogoi, 1986)

r_D	Mud circulation time, hours				
	24	120	240	720	1440
1	0	0	0	0	0
2	-1.635	-1.735	-1.765	-1.802	-1.821
3	-1.593	-1.799	-1.861	-1.938	-1.976
4	-1.398	-1.687	-1.773	-1.881	-1.935
5	-1.195	-1.551	-1.658	-1.790	-1.857
6	-1.010	-1.421	-1.544	-1.697	-1.774
7	-0.843	-1.301	-1.439	-1.610	-1.695
8	-0.693	-1.193	-1.343	-1.529	-1.622
9	0	-1.094	-1.254	-1.454	-1.555
10	0	-1.004	-1.174	-1.386	-1.493

Table 3.20 Circumferential thermal stresses $\sigma_{\theta,th}$ in MPa around the a wellbore in sandstone formation (Gogoi, 1986)

r_D	Mud circulation time, hours				
	24	120	240	720	1440
1	-5.412	-5.412	-5.412	-5.412	-5.412
2	-2.056	-2.392	-2.493	-2.619	-2.681
3	-1.091	-1.577	-1.722	-1.903	-1.994
4	-0.572	-1.115	-1.331	-1.548	-1.657
5	-0.220	-0.878	-1.074	-1.320	-1.442
6	0.047	-0.670	-1.885	-1.152	-1.286
7	0.263	-0.504	-0.733	-1.018	-1.163
8	0.445	-0.364	-0.607	-0.908	-1.060
9	0	-0.245	-0.499	-0.815	-0.973
10	0	-0.140	-0.404	-0.732	-0.897

The product $\alpha\Delta T$ is the strain, a fractional change in length, and the change in axial stress σ_{aT} (in psi) in a casing fixed at both ends is

$$\sigma_{aT} = \alpha E \Delta T = (6.9 \cdot 10^{-6})(3.0 \cdot 10^{7}) = 207\Delta T, \qquad (3.89)$$

where the temperature change is in ^{o}F. Hence a temperature change of $\Delta T = 40^{o}$F will cause an axial stress change of more than 8,000 psi and this may contribute to the buckling tendency of casing. Let us now assume that a casing string is fixed at both ends and capable of slight lateral movement and free longitudinal movement between the fixed ends. With a temperature increase the string will elongate and, due to constrains, an end force F will exist. The function F depends on the elongation, casing length, radial clearance between casing and open hole, cross-sectional casing area and other parameters . Calculations show that the end forces may reach very large magnitudes and the helically deformation of casing can occur (Leutwyler and Bigelow, 1965).

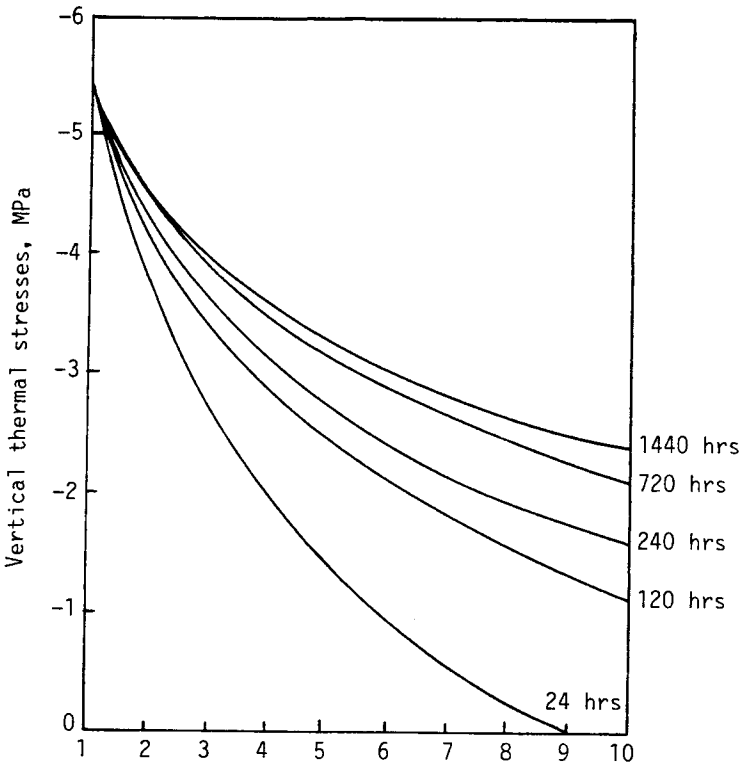


Fig. 3.25. Vertical thermal stresses around a wellbore (Gogoi, 1986).

3.8 Drilling Through Permafrost Interval

3.8.1 Estimation of the Permafrost Base

The development of rapid methods of predicting permafrost temperatures and thickness is essential to progress in the areas of geophysics, well drilling, oil or gas production, and mining. At drilling is very important to know the thickness of the permafrost with sufficient accuracy because the casing shoe has to be placed at a definite distance below the permafrost base.

Let us assume, for example, that the thickness of permafrost is underestimated. In this case, the casing cannot protect the

whole permafrost interval. When drilling resumes, a possibility exists for extensive washouts in the unprotected permafrost. This may result in the loss of shoe joints. Now let us assume that the permafrost thickness is overstated. In this case, the permafrost interval is exposed to the drilling fluid for more time, inducing hole enlargement (washouts) and a poor primary cementing.
In some cases the thickness of permafrost can be estimated from resistivity, sonic, and surface seismic velocity logs. The permafrost properties sought by borehole logging measurements include the permafrost base, the type of soil, and amount of material in the pore space. Because deep wells in permafrost areas are usually drilled with a warm mud, there is some unknown degree of formation thawing around the well. Thus, the borehole correction required for log interpretation can become quite large and is often undeterminate. The base of the permafrost can be detected with resistivity and sonic logs. The transition from higher resistivity and velocity readings to lower values can be considered as the base of the permafrost. The electric resistivities of frozen sediments are affected to a greater extent than are seismic velocities. Seismic velocities may increase by 2 to 10 times in transition to a frozen state, whereas the electrical resistivity may increase by 30 to 300 times in the same temperature interval (Hnatiuk and Randall, 1977). Laboratory data for the electric and acoustic response of frozen soils have shown that the significant variables affecting these parameters are salinity, surface area of soils per unit of volume, temperature, and water content. Thus, the laboratory data should be used to interpret the log response. Since it is difficult to perform such laboratory studies, the temperature logs are commonly used to determine the permafrost temperature and thickness.

When wells are drilled through permafrost, the natural temperature field of the formations (in the vicinity of the borehole) is disturbed and the frozen rocks thaw for some distance from the borehole axis. To determine the static temperature of the formation and permafrost thickness, one must wait for some period after completion of drilling before making geothermal measurements. This is so-called restoration time, after which the difference between the temperature of the formation and that of the fluid is less than the needed measurement accuracy. The presence of permafrost has a marked effect on the time required for the near-well-bore formations

to recover their static temperatures.
The duration of the refreezing of the layer thawed during drilling is very dependent on the natural temperature of formation; therefore, the rocks at the bottom of the permafrost refreeze very slowly. A lengthy restoration period of up to ten years or more is required to determine the temperature and thickness of permafrost with sufficient accuracy (Lachenbruch and Brewer, 1959; Judge, 1973; Melnikov et al. 1973; Taylor and Judge, 1977; Judge et al. 1979; Taylor et al 1982).
In this section we present a "two point method" (Kutasov, 1988a) which permits one to determine the permafrost thickness from short term (in comparison with the time required for temperature restoration) downhole temperature logs.

The slow return to thermal equilibrium in the section of the well within permafrost creates serious difficulties in determining the permafrost temperature and thickness. It is clear that in the sections of the borehole below the permafrost, the static (undisturbed) formation temperatures can be predicted from temperature logs taken at relatively short shut-in times. The proposed "two point method" of predicting the permafrost thickness is based on determining the geothermal gradient in a uniform layer below the permafrost zone (Fig. 3.26). Therefore, a lithological profile for the $h_2 - h_p$ section of the well must be available. Only temperature measurements for two depths are needed to determine the geothermal gradient. The position of the permafrost base is predicted by the extrapolation of the static formation temperature–depth curve to 0°C (Fig. 3.26). It should be noted that here the permafrost base is defined as the 0°C isotherm. The existence of a more severe climate in the past or transgression of the Arctic Shoreline results in warming and thinning of the permafrost (Balobayev et al. 1973; Lachenbruch et al. 1982). Due to slow movement of the permafrost base, the temperature field in the section of the well below the permafrost is also disturbed. An approximate equation which permits one to estimate the thickness of the disturbed zone (if the rate of permafrost thinning is known) was presented by Balobaev (Melnikov et al., 1973). Thus the accurate value of the geothermal gradient can be determined only from temperature measurements below this disturbed zone. Our experience has shown that if the condition $h_1 - h_p > 20\ m$ (Fig. 3.26) is satisfied, the geothermal gradient can be estimated with a

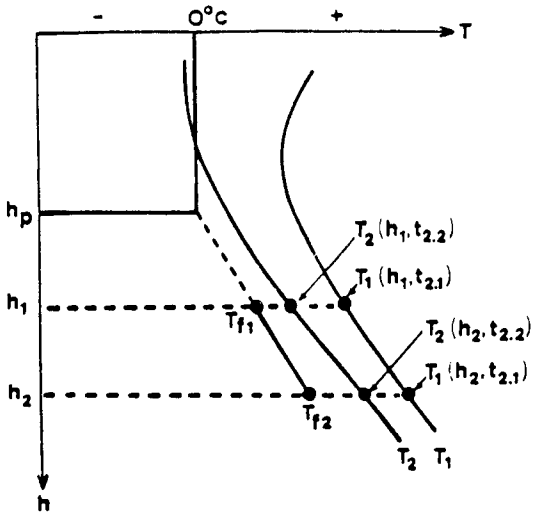


Fig. 3.26. Permafrost base prediction – a schematic model.

good accuracy.
The mathematical model of the "two point method" is based on the assumption that in deep wells the effective temperature of drilling mud at a given depth can be considered constant during the drilling process (Kutasov 1968; Kutasov 1976).

Earlier we suggested a "Two temperature logs" method which allows to estimate the formation temperatures from two logs (Kutasov, 1968; Kutasov, 1976, Kritikos and Kutasov, 1988; Section 4.2.1). According to this method, if two measured temperatures (T_{s1}, T_{s2}) are available for a given depth with shut-in times $t_s = t_{s1}$ and $t_s = t_{s2}$, the formation temperature T_f is

$$T_f = T_{s2} + \gamma(T_{s1} - T_{s2}), \quad \gamma = \gamma(t_c, t_s) \tag{3.90}$$

where t_c is the disturbance (drilling) time and γ is a correlation coefficient. The disturbance time at given depth is:

$$t_c = t_d - t_h$$

where t_d is the total drilling time, t_h is the period of time needed to reach the given depth. The values of t_h can be determined from drilling records. If the drilling records are not available the following formula can be used:

$$t_c = t_d(1 - \frac{h}{H}) \tag{3.91}$$

where h is the given depth and H is the total vertical depth of the well. To determine the geothermal gradient, one should calculate the static formation temperature at two different depths (Fig. 3.26). From Formula 3.90 we obtain:
for $h = h_1$, $T_f = T_{f1}$; and for $h = h_2$, $T_f = T_{f2}$.
Thus the geothermal gradient is:

$$\Gamma = \frac{T_{f2} - T_{f1}}{h_2 - h_1} \tag{3.92}$$

Finally, the position of the permafrost base (h_p) is estimated by extrapolation (Fig. 3.26).

$$h_p = h_1 - \frac{T_{f1}}{\Gamma} \tag{3.93}$$

Precise temperature measurements (Taylor and Judge 1977; Judge et al. 1979) taken in 15 deep wells located in Northern Canada (Arctic Islands and Mackenzie Delta) were used to verify the proposed method. The total depth of the wells (H), drilling time (t_d), shut-in time (time between termination of drilling and logging) for two randomly selected depths (h_1) and (h_2) are presented in Table 3.21. The transient temperatures for depths $h = h_1$ and $h = h_2$ at shut-in times $t_2 = t_{2.1}$ and $t_2 = t_{2.2}$ were taken from previously mentioned references and are also presented in Table 3.21. It should be noted that the interpolation was often used to get values of temperature at the same depth for two different shut-in times.
A general computer program "PERMB" (Appendix C, Table C.4) was prepared to calculate the permafrost thickness. The results of calculations are presented in Table 3.22. The predicted formation static temperatures for two depths are also presented in Table 3.22. Permafrost thickness (h_p^*) obtained from temperature logs after long shut-in times (t_2^*) were compared to those determined by the "two point method" (Table 3.22). Comparison indicates that the proposed "two point method" can be used to predict permafrost thickness with a good accuracy. The accuracy of the suggested method can be improved if more than two depths are selected in the section of the well below the permafrost. In Table 3.23, the values of h_p are presented for six combinations of h_1 and h_2 (four depths). The average value of permafrost thickness is 276.3 m. If one assumes that the "exact" value of permafrost thickness (h_p^*)

Table 3.21 Input data (Taylor and Judge, 1977; Judge, et al., 1979).
$T_{11} = T_1(h_1, t_{2.1})$, $T_{21} = T_2(h_1, t_{2.2})$,
$T_{12} = T_1(h_2, t_{2.1})$, $T_{22} = T_2(h_2, t_{2.1})$

Well No.	H m	t_d days	$t_{2.1}$ days	$t_{2.2}$ days	h_1 m	h_2 m	T_{11} ^oC	T_{21} ^oC	T_{12} ^oC	T_{22} ^oC
86	3375	240	265	634	325.0	350.0	3.38	2.53	4.45	3.67
155	3925	119	190	431	475.0	500.0	4.69	2.97	5.71	4.32
158	3177	73	82	320	450.0	500.0	3.33	1.69	5.98	4.60
167	4361	179	26	106	152.4	213.4	9.88	6.56	11.87	9.67
168	4000	97	99	491	613.0	652.6	3.91	2.42	5.21	3.82
169	2281	65	104	479	275.0	300.0	3.84	2.31	5.27	3.69
170	1829	28	132	372	381.8	427.6	3.77	3.05	6.27	5.45
175	3845	145	53	440	550.0	575.0	9.35	3.98	10.73	5.41
178	3205	94	23	250	375.0	400.0	5.15	1.70	5.73	2.43
192	3689	188	35	321	149.4	195.1	9.56	4.27	11.11	6.04
193	4704	237	16	62	375.0	400.0	7.74	5.09	8.52	6.12
196	4383	133	41	395	785.0	814.7	3.49	2.13	4.10	2.93
272	3305	53	83	158	335.0	365.8	4.93	3.43	5.73	4.33
274	3295	61	60	135	411.2	456.9	4.36	2.97	5.96	4.53
275	3295	116	8	88	386.2	457.2	9.24	4.48	11.03	6.35

Note: Well number is the Earth Physics Branch (Department of Energy, Mines and Resources, Ottawa, Canada) file number.

for this well is 259 m (Table 3.22), then the proposed short shut-in time method determines the permafrost thickness with a relative accuracy of 6.5% (compare with 12%, Table 3.22). It should be noted that, in this example, temperature logs with relatively small shut-in times and drilling time ratios were used. Indeed, for well 272 this ratio is $t_{2.2}/t_d$ =158/53=3 and the "exact" value of h_p^* = 259 m is obtained at t_2^*/t_d =31, (Table 3.22). It is also clear that the predicted values of the permafrost thickness are very dependent on the accuracy of the temperature logs in deep wells (Table 3.23). Application of the suggested method may reduce the time and cost of permafrost surveys in Arctic areas.

Table 3.22 Permafrost thickness for 15 Northern Canadian wells

Well No.	T_{f1} °C	T_{f2} °C	h_p m	h_p^* m	t_2^*/t_d	$\Delta h/h_p^*$ ·100, %
86	1.78	2.97	288	306	8.7	5.9
155	1.41	3.06	454	445	25	2.0
158	1.00	4.02	433	429	24	0.9
167	3.44	6.47	83	86	17	3.5
168	1.95	3.38	559	577	28	3.1
169	1.78	3.15	242	256	19	5.5
170	2.64	4.98	330	336	105	1.8
175	2.72	4.18	503	502	18	0.2
178	0.98	1.71	341	354	29	3.7
192	2.18	4.12	98	95	15	3.2
193	1.21	2.61	353	341	12	3.5
196	1.85	2.68	719	726	14	1.6
272	1.49	2.51	290	259	31	12.0
274	1.43	3.09	372	258	26	3.9
275	2.40	4.33	320	320	10	0.0

Note: t_2^* is the time between drilling completion and latest log; h_p^* is the permafrost thickness determined from a series logs (at $t_2 \leq t_2^*$). Temperature measurements within the permafrost zone were used (Taylor et al. 1982).

3.8.2 Low and High Temperature Permafrost

The development of oil and gas reserves in permafrost areas has required new drilling and well completions technology to deal with the impact of frozen soils. Drilling through permafrost raises some unique difficulties: intensive washouts, caving of frozen soils, fill on the bottom, stuck pipe, and poor primary cement jobs. When the well is shut-in, it will be subjected to the potential hazards of external freezeback pressures, internal freezeback pressures, and thaw consolidation. As permafrost is not homogeneous but varies in thickness, lithology, mechanical and thermal properties, it often happens that drilling methods successful in one area cannot be used in another (Goodman, 1978; Kutasov and Bates, 1980).

As was mentioned before, the mechanical properties of frozen formations vary significantly with the temperature. This variation in mechanical properties with temperature is particularly evident in fine-grained, high clay content soils where all of the water does

Table 3.23 Permafrost thickness, well 272,
$t_{2.1}$ = 83 days, $t_{2.2}$ = 158 days.
$T_{11} = T_1(h_1, t_{2.1})$, $T_{21} = T_2(h_1, t_{2.2})$,
$T_{12} = T_1(h_2, t_{2.1})$, $T_{22} = T_2(h_2, t_{2.1})$

h_1 m	h_2 m	T_{11} ^oC	T_{21} ^oC	T_{12} ^oC	T_{22} ^oC	$Tf1$ ^oC	$Tf2$ ^oC	A $^oC/100m$	h_p m
335.0	365.8	4.93	3.43	5.73	4.33	1.49	2.51	3.31	290.0
335.0	396.2	4.93	3.43	6.71	5.26	1.49	3.38	3.09	286.8
335.0	426.7	4.93	3.43	7.71	6.13	1.49	4.09	2.84	282.5
365.8	396.2	5.53	4.33	6.71	5.26	2.51	3.38	2.86	278.0
365.8	426.7	5.73	4.33	7.71	6.13	2.51	4.09	2.59	268.9
396.2	426.7	6.71	5.26	7.71	6.13	3.38	4.09	2.33	251.4

not freeze at 0°C. The initial temperature profile in the permafrost interval also influences the extent of thawing during drilling and the speed with which the formations refreeze after completion of drilling operations. A typical example of low temperature (cold) permafrost can be described by looking at the temperature profile of the Prudhoe Bay area (Fig. 3.27). High temperature (warm) permafrost is characterized by the profiles of the Medvezhe area (Fig. 3.28) and of the Beaufort sea (Fig. 3.27). The temperature of the permafrost section in each of the warm permafrost profiles is very near to 0°C. At negative temperatures close to 0°C a significant part of water is in unfrozen state and as a result the strength of formations is low. There are three primary problems which occur during the drilling of cold permafrost wells. They are freezeback, washouts, and cementing. The phenomenon of freezeback occurs when a formation which has been heated by circulation of warm drilling fluid begins to cool after cessation of circulation. Since the fluid will expand upon freezing, the pipes which are left in the hole become exposed to large compressive loading which can lead to buckling. This phenomenon was observed in wells in which drilling was temporarily suspended. Collapsed casing was not observed at depths greater than 150 m nor at temperatures warmer than -2°C (Gryaznov, 1978). Suprisingly, washouts can present a severe problem in cold permafrost regions. This is possible even in cases where the predicted radius of thawing is quite small in areas where the formations are unconsolidated (Perkins et al., 1974; Gryaznov,

1978). Consolidated formations are not susceptible to washout problems.

The last major problem observed in cold permafrost regions occurs during cementing. Because of the quick recovery of temperature in cold permafrost, a layer of frozen mud soon develops, particularly in washouts. This prevents good bonding to the formation in these zones. Cement set up is also hampered by the low temperature, and special low temperature cements should be used (Goodman, 1978).

Several problems occur repeatedly in warm permafrost environments which include washouts, surface caving, and cementing. Washouts and surface caving are significantly greater problems in the warm permafrost areas than they are in cold permafrost areas. Typical wells in the Medvezhe natural gas deposit (Tyumen district, Russia) completely fill the reserve pit (150 m^3) with cuttings in matter of days. Computations indicate that the volume of material removed is several times greater than would be indicated by the radius of thawing. Thus this fact can only be explained by additional volume of material added to the hole by caving of frozen soils due to reduction of their strength with an increase of the temperature during drilling. It is interesting to note that in many cases the drilling operators in the Medvezhe field observed crystals of ice in the cuttings. The hole enlargement caused caving of the soil around the well head during drilling through permafrost. In some long term drilling wells, the derricks were repositioned (Kutasov and Bates 1980). The second major problem observed in high temperature permafrost is cementing. In many wells in the Medvezhe deposit, gas migration to the surface has been observed shortly after completion (Kutasov and Bates, 1980).

3.8.3 Radius of Thawing

When wells are drilled through permafrost, the natural temperature field of the formations (in the vicinity of the borehole) is disturbed, and the frozen rocks thaw out for some distance from the borehole axis. For frozen soils, ice serves as a cementing material, and therefore the strength of frozen soils is significantly reduced at ice-water transition. If the thawing soil cannot withstand the load of overlying layers, consolidation will take place, and the corresponding

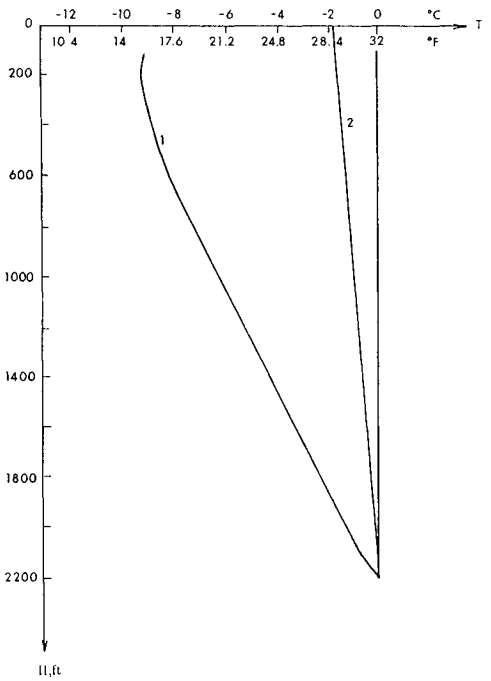


Fig. 3.27. Vertical temperature profie: 1 - Prudhoe Bay, Alaska (Gold and Lachenbruch, 1973); 2 - Beaufort sea (estimate).

settlement can cause significant surface shifts. The settlement in the vertical direction has a greater significance when the shear stress acts downward on the casing causing compressive stresses which can deform the casing (Palmer 1978). The approximate estimates show that the magnitude of the settlement (the center displacement of the thawing soil ring) and the axial compressive stress are proportional to the squared values of the radius of thawing (Palmer 1978). Thus, for long term drilling, the radius of thawing (h) should be estimated to predict platform stability and the integrity of the wellbore. The radius of thawing value also has significant effect on the thermal regime of wells during drilling and cementing. This circumstance has to be taken into account when selecting the oil well cement and mud. To estimate the radius of thawing we will assume that the mud temperature at a given depth (T_m) during drilling is equal to its mean value in time. The results of field and analytical investigations provide support for this assumption if the circulation period is more

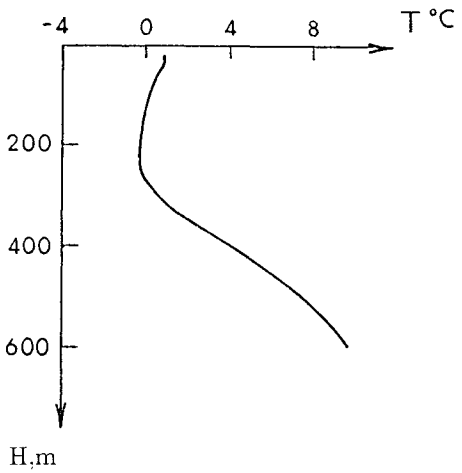


Fig. 3.28. Vertical temperature profie; Medvezhe, well 314, Tyumen district, Russia, (Rusakov and Kononov, 1976).

than several hours (Kutasov 1976).

Consider a simple case: the temperature of the permafrost is equal to the melting temperature of ice-bounded permafrost 0°C and the surface casing is yet not set in the wellbore. We will also assume a steady-state temperature distribution in the thawed zone. In this case the well known solution of the Stefan equation is

$$\frac{t_D}{I_f} = \frac{H^2}{2} \ln H - \frac{1}{4}(H^2 - 1) \tag{3.94}$$

$$t_D = \frac{a_t t}{r_w^2}; \quad I_f = \frac{a_t L w}{T_m \lambda_t}; \quad H = \frac{h}{r_w}$$

where: t_D is dimensionless mud circulation time, I_f is dimensionless latent heat of the formations, H is dimensionless radius of thawing, a_t is thermal diffusivity of thawed formation, λ_t is thermal conductivity of thawed formation, L is latent heat of ice, and w is ice content per unit of formation volume.

Let us assume that the depth of the surface casing shoe (below the permafrost base) is l, and v is the average penetration rate. The duration of mud circulation at the given depth z is equal to:

$$t = \frac{l - z}{v} \tag{3.95}$$

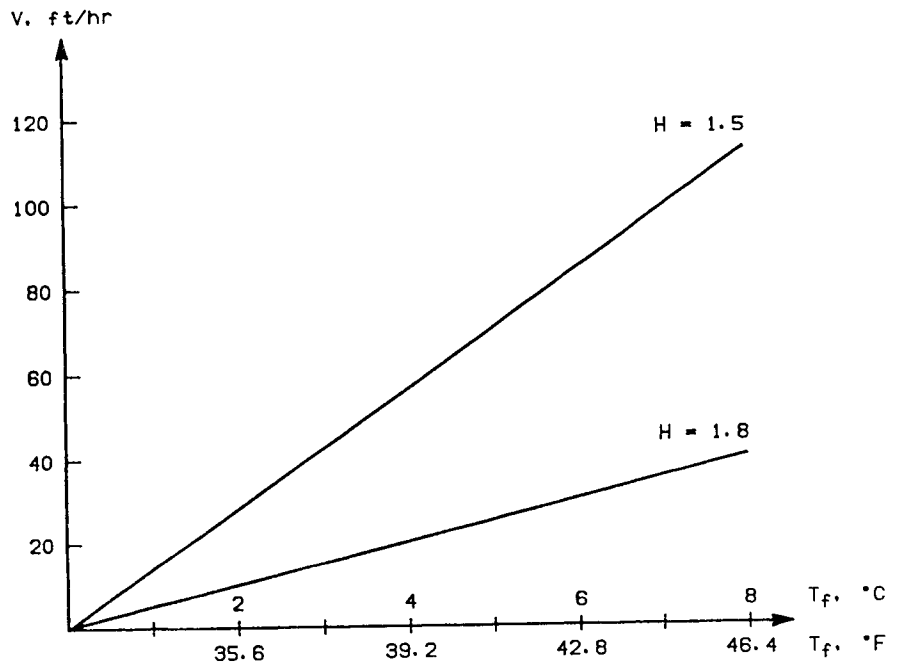


Fig. 3.29. Penetration rate versus drilling mud temperature.

From formulas (3.94, 3.95) we obtain (Kutasov, 1993a)

$$\frac{v}{T_m} = \frac{4B_t(l-z)}{2H^2 \ln H - (H^2-1)} \tag{3.96}$$

$$B_t = \frac{\lambda_t}{r_w^2 L w}$$

The results of calculations after Formula 3.96 for one example are presented in Fig. 3.29. For this example: $w = 370\ kg/m^3$, $\lambda_t = 2.4\ kcal/m \cdot hr \cdot {}^oC$, $z = 305$ m (1000 ft), $r_w = 0.222$ m, and $l = 671$ m (2200 ft). As shown by Fig. 3.29, the most effective way to reduce the permafrost thawing is lowering the drilling mud temperature. Indeed, to maintain the value of $H = 1.8$ at a mud temperature of 6.0^oC (42.8^oF) the penetration rate should be 9.14 m/hr (30 ft/hr) or higher. With a lowering of mud temperature to 2.0^oC (35.6^oF), the penetration rate of only 3.05 m/hr (10 ft/hr) will produce the same effect.

Let us now consider a more general case: the temperature of the

permafrost T_f is lower than 0°C and the surface casing is set in the wellbore. A computer program was used to obtain a numerical solution of a system of differential equations of heat conductivity (for casing-cementing layer, frozen and thawed zones) and the Stefan equation (Kutasov et al., 1977a). The results of computer calculations were combined with the results of a hydrodynamical modeling (Kutasov, 1976) to develop an empirical expression for the ratio of heat flows (M) at the thawed zone-frozen zone interface

$$M = \frac{q_t}{q_f} = 1 + \frac{A}{\sqrt{H-1}} \tag{3.97}$$

$$A = a_o \exp\left(-\frac{a_1\theta}{\sqrt{I_f}} - a_2\theta J\right), \tag{3.98}$$

$$\theta = \frac{-T_f}{T_m}, \quad J = \frac{\lambda_t}{\lambda_{ef}} ln\frac{r_w}{r_{ci}}$$

$$\lambda_{ef} = \frac{ln(r_w/r_{ci})}{\frac{1}{\lambda_s}\ln(r_{co}/r_{ci}) + \frac{1}{\lambda_c}\ln(r_w/r_{co})}$$

$$a_o = 5.7934, \quad a_1 = 2.646, \quad a_2 = 1.425$$

where q_t and q_f are the rates of heat flows for thawed and frozen zones respectively; λ_{ef} is the effective thermal conductivity of the casing-cement layer; r_{ci}, r_{co} are the inside and the outside radii of casing; λ_s, λ_c are the thermal conductivities of steel and cement. Introducing this equation (3.97) into the Stefan relationship (Eq. 2.44), and assuming the a steady-state temperature distribution in the casing, cementing ring, and in the thawed zone, we obtain the following equation

$$\frac{1}{I_f(1+\theta)\ \ln(H+J)}\left(1 - \frac{\sqrt{H-1}}{\sqrt{H-1}+A}\right) = H\frac{dH}{dt_D} \tag{3.99}$$

The solution of this equation is

$$\frac{t_D}{(1+\theta)I_f} = \frac{1}{A}(F_1 + JF_2) + F_3 + JF_4 \tag{3.100}$$

$$F_1(x) = \frac{2}{3}[x^3 \ln\ (x^2+1) - \frac{2}{3}x^3 + 2x - 2\arctan\ x] +$$

$$\frac{2}{5}[x^5 \ln\ (x^2+1) - \frac{2}{5}x^5 + \frac{2}{3}x^3 - 2x + 2\arctan\ x] \tag{3.101}$$

Table 3.24 The functions F_1, F_2, F_3, and F_4

H	F_1	F_2	F_3	F_4	H	F_1	F_2	F_3	F_4
1.4	0.55	0.21	0.09	0.48	4.0	11.78	9.70	7.34	7.50
1.6	0.75	0.42	0.21	0.78	4.5	17.44	13.53	10.42	9.63
1.8	1.00	0.71	0.39	1.12	5.0	24.72	18.13	14.12	12.00
2.0	1.32	1.07	0.64	1.50	5.5	33.80	23.55	18.47	14.63
2.2	1.72	1.51	0.95	1.92	6.0	44.86	29.81	23.50	17.50
2.4	2.23	2.03	1.33	2.38	6.5	58.07	36.98	29.23	20.63
2.6	2.85	2.64	1.79	2.88	7.0	73.62	45.07	35.67	24.00
2.8	3.62	3.35	2.33	3.42	7.5	91.66	54.13	42.86	27.63
3.0	4.53	4.15	2.94	4.00	8.0	112.36	64.20	50.79	31.50
3.2	5.60	5.05	3.65	4.62	8.5	135.87	75.31	59.50	35.63
3.4	6.85	6.05	4.43	5.28	9.0	162.37	87.49	68.99	40.00
3.6	8.28	7.15	5.31	5.98	9.5	192.00	100.78	79.28	44.63
3.8	9.92	8.37	6.28	6.72	10.0	224.91	115.20	90.38	49.50

$$F_2(x) = \frac{2}{5}x^5 + \frac{2}{3}x^3 \tag{3.102}$$

$$F_3(x) = \frac{(1+x^2)^2}{2}[\ln\,(x^2+1) - \frac{1}{2}] + \frac{1}{4} \tag{3.103}$$

$$F_4(x) = \frac{(1+x^2)^2}{2} - \frac{1}{2} \tag{3.104}$$

$$x = \sqrt{H-1} \tag{3.105}$$

To simplify calculations after formula (3.100) we present the Table 3.24. As may be seen from Table 3.25 the Formula 3.100 approximates with a sufficient accuracy the results of a numerical solution. In some works (Bondarev and Krasovitskiy, 1974; Dubina and Krasovitskiy, 1983) the heat transfer coefficient was used to describe the heat exchange between the wellbore and formations. The temperature distribution in frozen zone was approximated by

$$T_f(r,t) = b_1\ \ln\ r + b_2 + b_3 r \tag{3.106}$$

The coefficients b_1, b_2, and b_3 are functions of the thawing radius and of the radius of thermal influence (r_{in}). The Authors obtained a system of differential equations and a numerical method of its solution was suggested to determine the transient values of h and r_{in}.

Table 3.25 Comparison of calculated values of H and H^*; H – Formula 3.100, H^* – numerical solution

t_D	I_f	θ	J	H^*	H
20.63	0.526	0.0526	12.047	2.00	2.26
54.54	0.526	0.0526	12.047	3.00	3.26
168.6	0.526	0.0526	12.047	5.00	5.14
347.2	0.526	0.0526	12.047	7.00	6.93
0.596	0.500	0.0775	0.000	2.05	2.09
1.317	0.500	0.0775	0.000	2.50	2.60
2.536	0.500	0.0775	0.000	3.01	3.15
28.12	2.500	0.2500	0.000	4.00	3.82
96.20	2.500	0.2500	0.000	6.00	5.73
401.9	2.500	0.2500	0.000	10.00	9.47
1398.	2.500	0.2500	0.000	16.00	14.97
2487.	2.500	0.2500	0.000	20.00	18.57
100.6	4.290	0.4290	3.165	2.00	2.05
662.0	4.290	0.4290	3.165	4.00	3.87
1934.	4.290	0.4290	3.165	6.00	5.68
5635.	4.290	0.4290	3.165	9.00	8.41

3.8.4 Temperature Distribution and the Radius of Thermal Influence

To describe the temperature distributions in the thawed and frozen zones simple approximate formulas can be used (Kutasov, 1976). For the thawed zone (the ice melting temperature is 0^oC) the radial temperature profile can be approximated by the following formula,

$$T_t(r,t) = T_m \frac{\ln\ h/r}{\ln\ h/r_w} \qquad r \leq h, \tag{3.107}$$

and the radius of thermal influence (r_{in}) is introduced for the frozen zone,

$$r_{in} = h + 2.184\sqrt{a_f t} \tag{3.108}$$

where a_f is the thermal diffusivity of frozen formations. The temperature in the frozen zone can be approximated by the equation,

$$T_f(r,t) = T_f \frac{\ln\ r/h}{\ln\ r_{in}/h} \qquad r > h \tag{3.109}$$

In Tables 3.26 and 3.27 temperatures calculated after formulas (3.107, 3.109) and the results of a numerical solution (Taylor, 1978) are compared for a case when $T_m = 10.00\ ^oC$, $T_f = -5^oC$, and $I_f = 1.062$. The agreement between the temperatures calculated by these two methods is seen to be good.

3.8.5 Heat Losses from Wells

To calculate the maximum heat flow rate per unit of area (q_t^*) from the wellbore (into thawed formations) we will assume that a constant fluid mud temperature is maintained at the wellbore's wall. This case occur when the flow rate is very large and the heat transfer coefficient from the fluid to the wall of the wellbore is approaching to infinity.
In the dimensionless form the temperature distribution in the thawed zone is given by

$$T_{tD} = 1 - \frac{\ln\ r_D}{\ln\ H}, \quad T_{tD} = \frac{T_t(r,t)}{T_m}, \qquad r \leq h, \tag{3.110}$$

Table 3.26 Temperature distribution $T_t(r,t)$ in the thawed zone. First line – numerical solution (Taylor, 1978); second line – Formula (3.107)

t_D	h/r_w	r_{in}/h	Dimensionless distance, r/r_w							
			1.2	1.5	2.0	2.5	3.0	4.0	5.0	7.0
7.29	2.856	3.06	8.10	5.79	2.96	1.11				
			8.26	6.14	3.38	1.27				
14.57	3.332	3.50	8.47	6.59	4.17	2.30	0.84			
			8.49	6.63	4.24	2.39	0.87			
36.43	4.326	3.96	8.74	7.21	5.22	3.69	2.43	0.52		
			8.76	7.23	5.27	3.74	2.50	0.53		
72.86	5.179	4.60	8.94	7.63	5.96	4.65	3.59	1.91	0.26	
			8.89	7.53	5.79	4.43	3.32	1.57	0.21	
145.71	7.200	4.66	9.07	7.93	6.47	5.33	4.41	2.95	1.83	
			9.08	7.95	6.49	5.36	4.43	2.98	1.85	
364.28	9.391	5.44	9.19	8.19	6.90	5.91	5.09	3.81	2.81	1.31
			9.19	8.19	6.91	5.91	5.09	3.81	2.81	1.31

Table 3.27 Temperature distribution $-T_f(r,t)$ in the frozen zone. First line – numerical solution (Taylor, 1978); Second line – Formula 3.109

t_D	Dimensionless distance, r/r_w									
	4.0	5.0	7.0	10.0	12.0	15.0	20.0	25.0	30.0	40.
7.29	2.01	2.99	4.16	4.81						
	1.50	2.50	4.01	5.00						
14.57	0.87	1.87	3.25	4.33	4.69					
	0.73	1.62	2.96	4.39	5.00					
36.43		0.61	1.97	3.26	3.84	4.38	4.81			
		0.51	1.75	3.04	3.70	4.51	5.00			
72.86			0.94	2.28	2.94	3.65	4.37	4.71		
			0.99	2.15	2.76	3.49	4.43	5.00		
145.71				1.28	1.98	2.78	3.67	4.20	4.53	4.85
				1.07	1.67	2.38	3.32	4.04	4.64	5.00
364.28				0.41	0.85	1.59	2.53	3.20	3.69	4.32
				0.17	0.73	1.39	2.23	2.89	3.43	4.28

From the last equation we obtain

$$\frac{dT_{tD}}{dr_D}|_{r_D=1} = -\frac{1}{\ln\ H} \tag{3.111}$$

Introducing now the dimensionless temperature V_t

$$V_t = \frac{T_t(r,t) - T_f}{T_m - T_f} \tag{3.112}$$

we obtain an expression for the dimensionless heat flow rate per unit of area (q^*_{tD}) from the wellbore

$$q^*_{tD} = \frac{dV_t}{dr_D}|_{r_D=1} = \frac{1}{1+\theta}\ \frac{T_{tD}}{dr_D}|_{r_D=1} = -\frac{1}{\ln\ H}\ \frac{1}{1+\theta} \tag{3.113}$$

The last formula was tested against values of q^*_{tD} obtained from a numerical (computer) solution (Kutasov et al., 1977a). It was found that a correction coefficient $D_c = 0.96$ for values of $\theta \leq 0.4$ must be introduced and the suggested formula for q^*_{tD} is

$$q^*_{tD} = -\frac{D_c}{\ln\ H}\ \frac{1}{1+\theta} \tag{3.114}$$

From this formula follows that for a given variant the product $q^*_D(\ln\ H)$ is practically a constant (Table 3.28).

Table 3.28 Values of $y = q_D^* \cdot (\ln\ H)$ for two variants

A: $I_f = 23.3,\ \theta = 2.33$			B: $I_f = 10.0,\ \theta = 0.25$		
H	t_D	y	H	t_D	y
1.025	0.0083	0.3018	2.00	7.065	0.7820
1.050	0.0379	0.3014	3.00	35.08	0.7775
1.100	0.1848	0.3011	4.00	91.18	0.7754
1.150	0.4707	0.3010	6.00	308.3	0.7730
1.200	0.9157	0.3010	8.00	691.8	0.7717
1.250	1.543	0.3010	10.00	1267.	0.7709
1.300	2.380	0.3010	12.00	2054.	0.7704
1.350	3.456	0.3004	14.00	3070.	0.7699
1.400	4.803	0.3005	16.00	4332.	0.7693
1.450	6.456	0.3005	18.00	5853.	0.7690
1.500	8.453	0.3004	20.00	7649.	0.7687

In dimensional form the heat flow rate per unit of area is

$$q_t^* = -\ \lambda_t\ \frac{T_t(r,t)}{dr}|_{r=r_w} = -\ \frac{D_c \lambda_t T_m}{(1+\theta) r_w\ \ln\ h/r_w} \tag{3.115}$$

3.8.6 Allowable Shut-in Time

If a well is shut-in during drilling, the water base fluids in casing-casing, drill pipe-casing or tubing-casing annuli will refreeze and generate radial loads in the borehole. This process, termed internal freezeback, is distinguished from external freezeback of thawed permafrost and water base fluids outside of the casing (Goodman 1978). In some cases, high enough pressures may develop to cause casing and drill pipe damage (Gryaznov 1978; Kutasov and Bates 1980). If the water in permafrost soils freezes at 0°C, the internal freezeback starts only when the external freezeback is completed. It is known, however, that in the freezing of soils, and especially in fine soils, by no means does all of the pore water change to ice at the freezing temperature of the soils, but only part of it. With further lowering of temperature (°C), phase transition of water continues, but at steadily decreasing rates (Tsytovich 1975).

Freezeback could be a problem if it becomes necessary to temporarily abandon drilling operations. The drilling engineer needs to be able to determine the amount of time he can suspend fluid

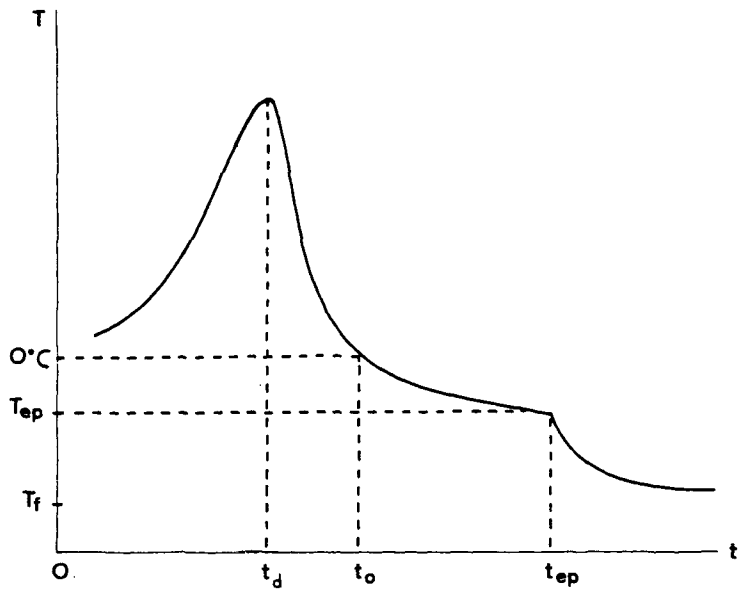


Fig. 3.30. Downhole temperature versus time for a given depth - schematic curve.

circulation without the drilling mud freezing. If the shut-in period is more than the "safety period" (free from freezing of drilling mud in the well), the water base mud in the permafrost section has to be replaced by oil mud or a low freezing-point fluid.

An empirical formula is presented below which allows one to predict the safety shut-in time (t_{sp}) at various drilling times and permafrost temperatures (T_f). Let us assume that the well is temporarily shut-in and the mud circulation is stopped at the moment of time $t = t_d$ (Fig. 3.30). From physical considerations it is clear that the radius of thawing will increase for a definite period of time ($t_o - t_d$) at the expense of heat stored in the thawed zone during drilling. This period of time may be called the safety shut-in period. During this time the temperature of the drilling mud in the wellbore will be greater than 0^oC, and drill pipe will not freeze with mud. The question may arise, "why not consider the period of time ($t_{ep} - t_d$) as a safety period" (Fig. 3.30). It should be noted that at the moment of time $t = t_{ep}$, the phase transition between water and ice is practically completed. As was mentioned above, the

presence of unfrozen water at temperatures less than 0^oC leads to the conclusion that only a part of water freezes at 0°C. Therefore, it is possible that for moments of time $t < t_{ep}$, a significant amount of water in the formation will remain unfrozen and in the same time the drilling mud may be in a frozen state, because it was assumed that the drilling mud freezes at 0°C. Geothermal investigations in permafrost areas have shown that even at -1^oC the freezing of formations continues for a large section of permafrost.

The magnitude of the "safety period" depends mainly on the duration of the thermal disturbance (drilling time) and on the static temperature of permafrost (Kutasov 1976; Kutasov and Strickland 1988). Precise temperature measurements (61 logs) conducted by the Geothermal Service of Canada in 32 deep shut-in wells in Northern Canada (Taylor and Judge, 1977; Judge et al., 1979; Judge et al., 1981; Taylor et al., 1982) were used to estimate the values of t_{sp} (Kutasov and Strickland 1988). The total drilling time (t_t) for these wells ranged from 4 to 404 days, the total vertical depth (h_t) ranged from 1356 m (4,450 ft) to 4704 m (15,430 ft), and the depth of permafrost (h_p) ranged from 74 m (243 ft) to 726 m (2,380 ft).

We have found that the duration of the "safety period" t_{sp} for a given depth can be approximated with sufficient accuracy as a function of two independent variables: time of thermal disturbance at the given depth (drilling time) and permafrost static temperature (T_f). A regression analysis computer program was used to process field data. It was revealed that the following empirical formula can be used to estimate the safety shut-in period:

$$t_{sp} = 3.06\, t_d^{0.817}\, (-T_f)^{-1.5} \tag{3.116}$$

where: t_d is the thermal disturbance time at a given depth. The value t_d is: $t_d = t_t - t_h$ where t_h is the period of time needed to reach the given depth. The values of t_h can be determined from drilling records. A safety factor of 2 was introduced in Eq. 3.116 to compensate for the largest differences between observed and calculated values of t_{sp}. The accuracy of the results (Eq. 3.116 without the safety factor) is $\Delta(\ln t_{sp}) = 0.664$ and was estimated from the sum of squared residuals. It should be remembered that in Eq. 3.116, time is in days and temperature in °C.

Example.
A well is drilled offshore in the Beaufort sea near Prudhoe Bay. The

temperature-depth curve is presented in Fig. 3.27. Only three days were spent penetrating the permafrost section of the well. After 40 days drilling has to be discontinued at the depth 8,000 ft. Can the well be shut-in for 2 weeks?

Step 1. From Fig. 3.27 one can determine that the surface permafrost temperature is -1.8^oC
Step 2. Assuming that for the upper permafrost section $t_d \approx t_t =$ 40 days. From Formula 3.116 one can estimate that the value of $t_{sp} = 26$ days. Thus, the well can be shut-in for 2 weeks and the drilling fluid will not freeze.

3.9 Hole Enlargement Control in Permafrost Areas

3.9.1 Field and Experimental Data

A number of problems occur during Arctic drilling: hole and surface instability, and poor cementing jobs intimately associated with washed out formation. During drilling, the formation is heated by circulation of a warm drilling fluid. As a result, the strength of soils around the well is significantly reduced by the melting of the ice. Heating of frozen soils without thawing also sharply reduces the shear strength of soils and results in the initiation of washouts. Experimental investigations have shown that the shear strength of permafrost depends mainly on the negative temperature, the value of external pressure, and the time of load action. During drilling operations the increase of the temperature of permafrost (increase of the unfrozen water content) can result in a significant reduction of cohesion, which accounts for a substantial part of the total shear strength of frozen soils. Thus the hole enlargement due to caving of frozen soils is possible even when the temperature of the drilling mud is maintained below 0^oC. The field experience and experimental data have shown that three main causes may be responsible for hole enlargement in permafrost areas (Kutasov et al., 1977b; Goodman, 1978; Kutasov and Bates 1980):
a. Frozen soil impermeability, which hinders filter cake build-up and limits differential pressure (overbalance) needed for well bore

support.
b. Filtration of fluid from drilling mud into the thawed zone, which reduces the intergranular cohesion forces and tends to fluidize thawed soils.
c. Caving of frozen soils due to sharp reduction of their strength properties with the increase of temperature during drilling.

Experience has shown that consolidated frozen soils are not susceptible to washouts problems. Caliper logs at the Prudhoe Bay field have shown that a gauge hole could not be obtained when drilling the permafrost interval (Perkins et al. 1974). The interval 100-450 ft. (mostly well graded gravel with some strata of silty sand) was especially sensitive to washout (Fig. 3.31).

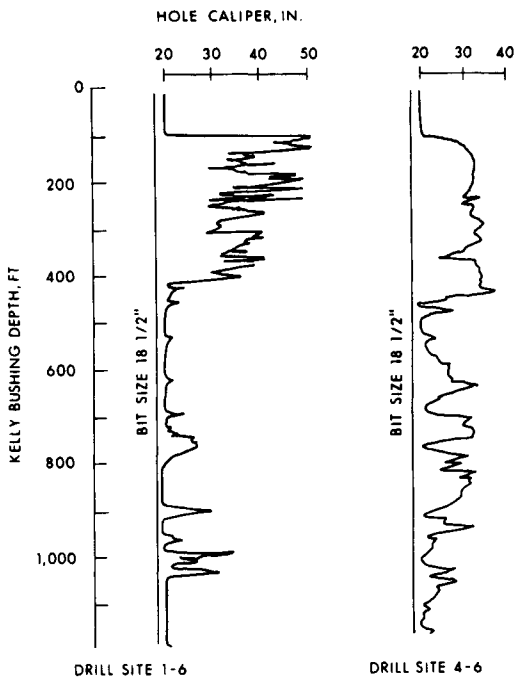


Fig. 3.31. Caliper logs through permafrost at Prudhoe Bay (Perkins et al., 1974).

The Russian experience (Gryaznov 1978; Kutasov and Bates, 1980) has shown that washout can present a severe problem even in areas where the main body of the permafrost is at temperatures

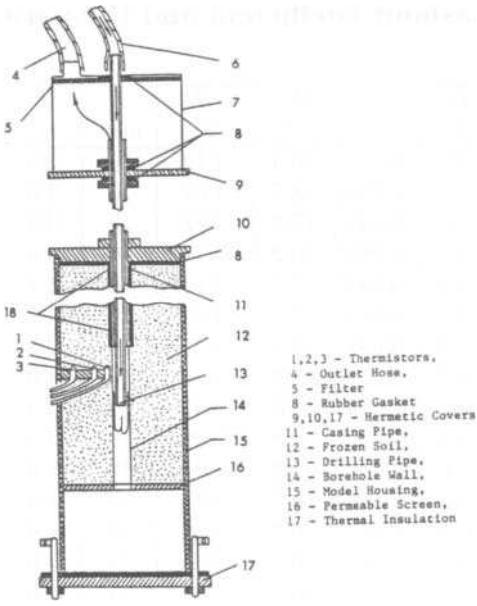


Fig. 3.32. Model of the borehole.

below $-3°C$ and where the predicted radius of thawing was quite small. Especially extensive washouts occur in high temperature permafrost (Kutasov and Bates 1980), where the temperatures of unconsolidated frozen soils (shaley sands with about 20% of ice content) are close to $0°C$.

For better understanding of such complex phenomena as washout formation in permafrost intervals of wells, an experimental investigation was conducted (Kutasov et al., 1977b). The model of the borehole is presented in Fig. 3.32 and a detailed description of laboratory apparatus and the experimental procedure is given in the above mentioned reference. In this study, sand was used as a permafrost formation. The washout diameters were measured and its average value for the interval (in the model), where the washouts were eroded, was calculated. The "drill pipe" was stationary (no rotation) and therefore, the section below the end of the "drill pipe" was not taken into account. For this section, the washout coefficient K (washout diameter and well diameter ratio) was 1.5-2 times larger than the calculated values of K. Mechanical erosion

Table 3.29 Washout coefficient and the parameters of runs

Run #	T_m °C	v_o m/s	W %	$-T_f$ °C	t min	K
8	4.1	0.224	20.4	3.12	10	2.6
9	4.1	0.224	18.7	3.04	10	2.6
14	4.1	0.345	17.5	3.17	10	3.0
18	4.2	0.980	16.2	3.72	10	4.0
19	4.3	0.592	17.7	4.12	10	3.7
20	4.2	0.384	17.2	4.05	10	3.1
24	2.3	0.698	17.3	5.22	10	2.5
25	6.2	0.553	20.3	5.15	10	3.9
26	6.1	0.941	19.3	5.07	10	4.9
29	2.4	1.020	17.8	5.23	10	3.4
27	6.1	0.823	19.2	4.92	10	1.0
28	6.3	0.863	19.2	4.95	42	1.0
35	6.3	0.975	20.2	5.16	12	1.0
37	3.1	1.870	10.7	9.31	5	3.0
38	2.7	1.920	10.4	7.55	5	4.0
39	2.0	2.090	13.1	6.42	5	4.0
40	2.2	2.080	12.1	6.63	5	4.1
41	2.2	2.080	10.3	6.55	5	3.9
42	2.2	1.820	10.3	6.57	4	3.9
43	2.1	2.048	10.0	6.34	5	3.3
50	8.7	1.450	8.0	5.29	10	1.0
51	4.5	1.550	11.6	5.39	15	1.0
53	6.2	1.470	24.0	5.00	3.5	2.5

due to high turbulence of the fluid at the end of the "drill pipe" may be responsible for this result. It is seen from Table 3.29 (runs 18-20, and 24-26) that washout diameter increases with increased flow rate or fluid temperature. In the Table 3.29 v_o is the annular fluid velocity at the beginning of fluid circulation and W is the ratio of the ice content in a unit of volume to the soil's density.

In the second set of experiments (runs 27, 28, 35, Table 3.29), solar oil was used as a drilling fluid. The most unexpected outcome of the above set of experiments was the discovery of the dominant role of fluid infiltration into the thawed zone in the washout formation process. Indeed, the comparison between runs 27 and 28 (where the circulation time was increased by more than four times) shows that no hole enlargement is caused even by intensive soil thawing. This

means that even at relatively high soil ice contents, the cohesion forces in thawed soils can provide a sufficient borehole wall stability if the infiltration of drilling fluid in the thawed zone can be avoided. The experimental evidence points to the fact that the diameter of washouts is minimized when water-based drilling fluids have very small water losses or when oil-based drilling fluids are used. It should be noted that frozen soils are impermeable and only a thin ring of thawed soils around the wellbore is permeable. The filtration into the thawed zone persists as long as the state of saturation in the thawed zone is reached. In order to fluid loss to occur, the pressure inside the wellbore must be higher than the pore pressure inside the thawed zone. Thus the density of drilling fluids should be minimal so that the flow of filtrate into the thawed zone is minimized. The maximum value of the Reynolds number for the first and second sets of experiments was equal 3400. This means that the experiments were conducted at laminar and transitional regimes of flow.

For the third and fourth sets of runs 37-53, Table 3.29, the annular flow velocity was increased and the maximum value of the Reynolds number was equal to 8300. Hence, the experiments were conducted at the turbulent, transitional and laminar regimes of fluid flow. The high annular fluid velocities were typical for the third set of experiments (runs 37-43, Table 3.29), where water was used as a circulating fluid. As may be seen from Table 3.29 the washout coefficients are large even at low temperatures of frozen sands.

In the fourth set of experiments (runs 50-53, Table 3.29), the bentonite mud with the density of 1080 kg/m^3 (9 ppg) was used. Interesting results were obtained from runs 50 and 51. In these cases, the mud cake was built up, serving as a effective barrier to the fluid filtration into the thawed zone and a gauge well was obtained. In the next run 53, where the soil's ice content was increased and the circulation time was sharply reduced, no mud cake was observed. We attribute this result to the significant reduction of cohesion of sand particles at the borehole wall. It is also important that in this case (high porosity), the bentonite particles could not prevent the flow between the sand particles in the thawed zone. Thus the bentonite mud can be designed for use at penetration through low ice content permafrost (up to 12 percent for sands).

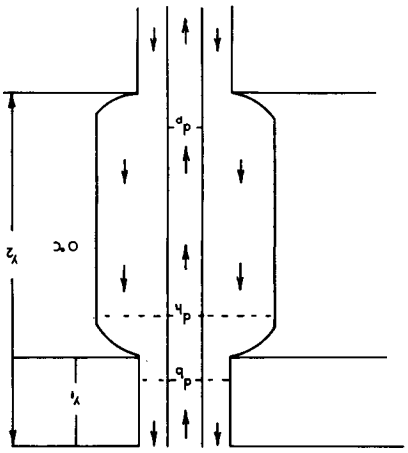


Fig. 3.33. Maximum washout diameter – schematic model.

3.9.2 Washout Diameter

In this section we will show the impact of drilling technology (flow rate, duration of mud circulation, bit and drill pipe diameter) and fluid properties on the hole enlargement. To estimate the radius of washouts, we considered an extreme case when ice is the only cementing material of frozen soils, and the initial temperature of the formation is equal to the temperature of ice melting (0^oC). We also assumed that during drilling the thawed material is removed from the borehole by the mud circulation system. In this case the radius of washouts will be equal to the maximal value of the thawing radius. In practice, this model can be applied only in high temperature permafrost areas with unconsolidated (high ice content) formations. Let us now assume that the washouts are eroded in the $Y_2 - Y_1$ section of the well (Fig. 3.33). The temperature of the drilling mud at given depth (T_m) has been assumed to be equal to the mean value of that in well section $Y_2 - Y_1$ during the circulation period. It is also clear that the duration of mud circulation t at a given depth is not constant; it is minimum for the upper sections of the well and minimum for the lower sections. The position of the moving mud-

frozen soils interface can be obtained from the Stefan equation:

$$\frac{Lw}{2}\frac{dd_h}{dt} = h_c T_m \tag{3.117}$$

where $L = 335\ kJ/kg$ is the latent heat of fusion for ice, h_c is the convective heat transfer coefficient and d_h is thawed hole diameter (washout diameter).
The values of the convective heat transfer coefficients for laminar and turbulent flow were taken from the literature. For laminar flow (Thompson and Burgess, 1985):

$$h_c = \frac{4k_m}{d_h - d_p} = 4 \tag{3.118}$$

where k_m is thermal (molecular) conductivity of drilling mud and d_p is drill pipe (outer) diameter. For the turbulent flow the value of h_c was calculated from the Dittus-Boelter equation (McAdams, 1954). We obtained formulas which allow one to predict the maximum value of the washouts diameter (Kutasov and Caruthers, 1988). For laminar flow:

$$K = \frac{1}{D} + \sqrt{(1 - \frac{1}{D})^2 + \frac{16T_m k_m t}{Lwd_b^2}} \tag{3.119}$$

Where the washout coefficient, the bit diameter and drill pipe outside diameter ratio are defined by

$$K = \frac{d_h}{d_b}; \qquad D = \frac{d_b}{d_p} \tag{3.120}$$

where d_b is the bit diameter.
For turbulent flow:

$$\frac{Bt_D}{I_l} = F(KD) - F(D) \tag{3.121}$$

$$F(x) = \frac{5}{14}(x+1)^{2.8} - \frac{10}{9}(x+1)^{1.8} \tag{3.122}$$

$$B = 0.046(\frac{4q}{\pi\nu d_p})^{0.8}(\frac{\nu}{a})^{0.4} \tag{3.123}$$

$$t_D = \frac{at}{d_p^2}; \qquad I_l = \frac{Lwa}{T_m k_m} \tag{3.124}$$

where t_D is dimensionless mud circulation time, I_l is dimensionless latent heat of the formations, a is the thermal diffusivity of drilling mud, ν is kinematic viscosity of drilling mud, and q is volumetric flow rate. It is clear that for a gauge borehole ($K = 1$) the following condition should be satisfied

$$\frac{Bt_D}{I_l} \longrightarrow 0 \tag{3.125}$$

or in dimensional form

$$\frac{0.0558q^{0.8}a^{0.6}T_m\rho ct}{d_p^{2.8}\nu^{0.4}Lw} \longrightarrow 0 \tag{3.126}$$

where ρ is the mud density and c is the specific heat of the drilling mud. Equations 3.119 and 3.121 were obtained for Newtonian fluids. It is customary to assume (Proselkov, 1975) that for non-Newtonian fluids the same convective heat transfer coefficients can be used if the value of ν is substituted by the ratio μ_{pv}/ρ (μ_{pv} is the plastic viscosity).

Prior to using formulas 3.119 and 3.121 it is necessary to determine the fluid flow regime in the annulus. Due to hole enlargement during drilling, the turbulent flow can undergo a transition to laminar flow, providing that the flow rate remains the same. For Newtonian fluids the value of critical Reynolds number for transition to turbulent flow is approximately equal to 2000. In our case the Reynolds criterion (number) is defined by

$$Re = \frac{v(d_h - d_p)}{\nu} \tag{3.127}$$

where v is the fluid velocity in the annulus. It is commonly assumed that the values of $2000 < Re < 5000$ are typical for the transitional regime of flow and at $Re > 5000$ a developed turbulent flow exists. For Newtonian fluids, the rotation of the drilling pipe significantly speeds up the laminar-turbulent transition (Kaye and Elgar, 1958). This means that at values $Re < 2000$ the turbulent regime of flow can exist. The Taylor number Ta enables us to estimate the impact of drill pipe rotation on the drilling fluid flow. The Taylor number is defined by

$$Ta = \omega r_m^{0.5}\, b^{1.5}\, \nu^{-1} \tag{3.128}$$

$$b = (d_h - d_p)/2; \qquad r_m = (d_h + d_p)/2$$

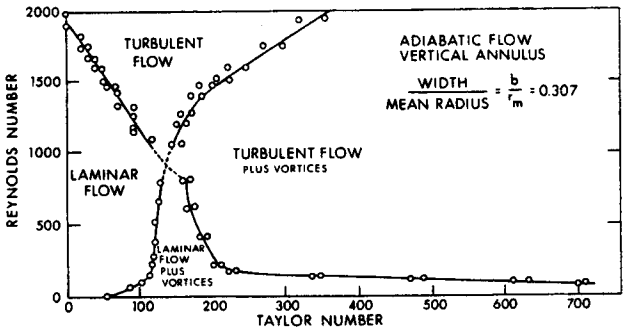


Fig. 3.34. Four flow regions for wide annulus (Kaye and Elgar, 1958).

where ω is the speed of rotation, (1/s). The experiment demonstrated that four different regions of flow were possible in the annulus between the stationary outer cylinder and a rotating inner cylinder, if the axial fluid velocities are superimposed at the various rotating speeds (Kaye and Elgar, 1958). The experimental results for the wide annulus ($b/r_m = 0.307$) are summarized in the Fig. 3.34 showing the four separate regions of flow. In turbo drilling the speed of rotation of the drill pipe is equal to zero. Taking into account the nonconcentricity of the well circulation system and the borehole wall roughness, it can be assumed that $Re = 2000$ is the transition point between laminar and turbulent regimes of flow. Let us now assume that the initial value of the Reynolds criterion (at $K = 1$) is $Re^o > 2000$, then the transition to laminar flow will occur at $K = K_1$ (Fig. 3.35). If Re_r^o is the initial value of the Reynolds criterion for rotary drilling, then the transition to laminar flow will occur at $K = K_2$ (Fig. 3.35). For non-Newtonian and viscoelastic liquid flow, Ryan and Johnson introduced a Reynolds number-type dimensionless grouping termed Z value, which identifies the flow regime as being laminar or turbulent (Walker and Korry, 1974). The Z parameter is computed as a function of radius. If the Z value near the borehole's wall is greater than 800, the annular flow is assumed to be turbulent. It is interesting to note that the effects of drill pipe rotation upon Z value are seldom significant.

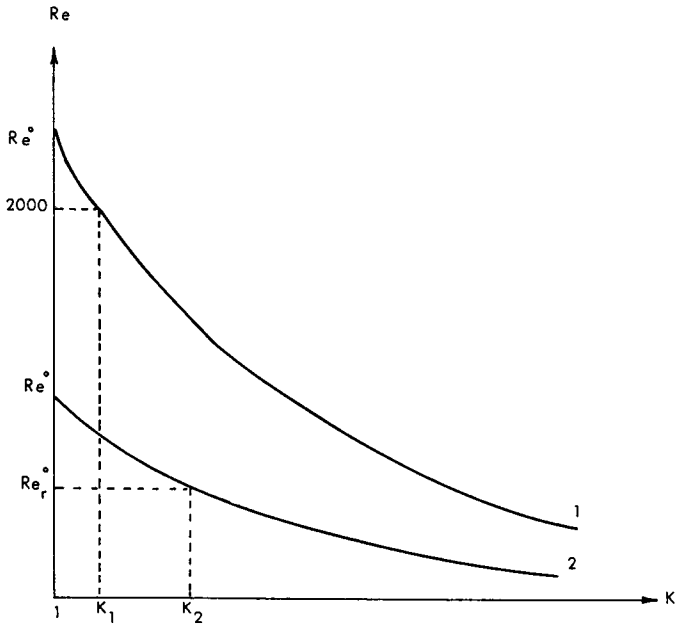


Fig. 3.35. Turbulent-laminar flow transition: 1 – turbo drilling, 2 – rotary drilling.

3.9.3 Mud Properties Control

From Formula 3.119 follows that for laminar flow in the annulus, the hole enlargement can be minimized when the thermal conductivity of the drilling fluid is low, the penetration rate is high, and the temperature is maintained as close to 0^oC as possible.
As can be seen from the Formula 3.126, the washout coefficient decreases with reduction in flow rate and increasing fluid viscosity. Both the minimum annular fluid velocity and fluid viscosity are controlled by the ability of drilling fluids to carry cuttings out of the borehole. It is also clear that the reduction in the time of mud circulation (increasing the penetration rate) is not a controllable factor. At first blush, it would appear that the use of drill pipes with large diameters would have a significant impact on the hole enlargement, but this is not a case, because the function F (Eq. 3.122), is strongly dependent on the value of D (bit diameter to drill pipe overall dimension ratio). Below, through the use of an example of calculation, we will demonstrate that the washout coefficient

Table 3.30 Washout coefficient for different drilling pipe overall dimensions (in inches), $T_m = 2^oC$

t, hr	5.000	6.625	8.625
1	1.110	1.118	1.131
2	1.202	1.214	1.234
5	1.418	1.436	1.464
10	1.679	1.700	1.732
20	2.047	2.069	2.104
30	2.321	2.344	2.378
40	2.545	2.568	2.602
50	2.738	2.760	2.794
60	2.908	2.931	2.964
80	3.203	3.225	3.258
100	3.455	3.477	3.509

practically does not depend on the drill pipe size. Thus, it is clear that for turbulent flow in the annulus, the lowering of drilling fluid parameters (temperature, density and specific heat) is most effective in reducing the washout diameter.

Example.

Let us assume that water was used as a drilling fluid. The parameters are: $\rho = 1,000\ kg/m^3$, $w = 400\ kg/m^3$

$$c = 4.187\ kJ/kg \cdot K,\quad a = 0.135\ mm^2/s,\quad \nu = 1.51\ mm^2/s,$$

$$d_b = 438\ mm\ (17.5in.),\quad q = 0.02524\ m^3/s\ (400\ gpm)$$

a. Let us assume that drill pipes with d_p=5.000 in., 6.625 in., and 8.625 in. were used. The temperature of mud was maintained at 2^oC. The results of calculations (Formulas 3.121-3.123) are presented in Table 3.30. From this example one can see that washout diameter practically does not depend on drill pipe size.

b. Let us now assume that d_p=5.000 in. and the temperature of drilling fluid varies from 1^oC to 5^oC. The results of calculations are shown in Table 3.31. It is easy to see that lowering of the drilling fluid temperature has a significant effect on washout diameter. The reduction of mud density or specific heat reduces the washout coefficient in the same manner as the lowering of mud temperature (Formula 3.126). Now we will briefly discuss the use of brines with inlet temperatures below 0^oC as drilling fluids. It is obvious that in order to prevent thawing and initiation of washouts, the annular

Table 3.31 Washout coefficient at various drilling mud temperatures

t, hr	$1°C$	$2°C$	$3°C$	$5°C$
1	1.058	1.110	1.158	1.243
2	1.110	1.202	1.282	1.418
5	1.243	1.418	1.559	1.785
10	1.418	1.679	1.880	2.192
20	1.679	2.047	2.321	2.738
30	1.880	2.047	2.645	3.134
40	2.047	2.321	2.908	3.455
50	2.192	2.545	3.134	3.729
60	2.321	2.738	3.334	3.971
80	2.545	2.908	3.667	4.387
100	2.738	3.455	3.791	4.741

mud temperature must be maintained below 0°C. High penetration rates while drilling the permafrost interval require high power inputs on the bit. It is commonly assumed that during drilling, more than 99 percent of the mechanical energy (rotary and pump input) is transformed into thermal energy. Experience in the Russian Federation, where conventional water base muds were used, has shown that the outlet drilling mud temperature was, in many cases, close or even higher than the inlet mud temperature during drilling the permafrost interval (Gryaznov, 1978). In the McKenzie Delta area (Canada), the XKB (XC polymer, KCl, bentonite) system was applied to drilling permafrost (Hanni, 1973). The original concept was to use KCl in the mud system to lower the mud freezing point below 0°C. It was hoped that by using a cooled mud the thawing of permafrost could be prevented. During drilling it was found virtually impossible to maintain the annular mud temperature below 0°C (Hanni, 1978). The main point is that at high rates of heat generation on the bit, the small variations in the inlet mud temperature (which can be achieved by using brines) have an insignificant effect on permafrost thawing around the well. From this point of view, only with reverse mud circulation should the possibility of using brines be considered. It is also known that ice disintegrates if it is exposed to brines. With the passage of time the soil's cohesion will be significantly reduced due to breaking off bonds between ice and soil particles. Under this condition it is

very difficult to make a good cementing job. Because of this, fresh water has to be used (causing thawing) to clean up the well before cementing.

Chapter 4

WELLBORE AND FORMATIONS TEMPERATURE DURING SHUT-IN

4.1 Determination of the Downhole Shut-in Temperatures

4.1.1 Literature Review

The modeling of primary oil production and design of enhanced oil recovery operations, well log interpretation, well drilling and completion operations, and evaluation of geothermal energy resources require knowledge of the undisturbed reservoir temperature. Temperature measurements in wells are mainly used to determine the temperature of the Earth's interior. The drilling process, however, greatly alters the temperature of the reservoir immediately surrounding the well. The temperature change is affected by the duration of drilling fluid circulation, the temperature difference between the reservoir and the drilling fluid, the well radius, the thermal diffussivity of the formations, and the drilling technology used. Given these factors, the exact determination of reservoir temperature at any depth requires a certain length of time in which the well is not in operation. In theory, this shut-in time is infinitely long. There is, however, a practical limit to the time required for the difference in temperature between the well wall and surrounding reservoir to become vanishingly small.

The first attempt to determine theoretically the required shut-in time of a well for a given accuracy of formation temperature was made by Sir Edward Bullard (1947), who approximated the thermal

effect of drilling by a constant linear heat source. This energy souce is in operation for some time t_c and represents the time elapsed since the drill bit first reached the given depth. For a continuous drilling period the value of t_c is identical with the duration of mud circulation at a given depth.
Bullard (1947) used the principle of superposition and obtained the following equation for shut-in temperature $T_s(t, r = r_w)$

$$T_{sD} = \frac{T_s(r_w, t_s) - T_f}{T_m - T_f} = \frac{Ei(-\frac{r_w^2}{4a(t_c+t_s)}) - Ei(-\frac{r_w^2}{4at_c})}{Ei(-\frac{r_w^2}{4at_c})} \tag{4.1}$$

The logarithmic approximation of the Ei-function (with a good accuracy) is valid for small arguments

$$Ei(-x) = \ln x + 0.5772, \qquad x < 0.01 \tag{4.2}$$

where 0.5772 is the Euler's constant. Then

$$\frac{T_s(r_w, t_s) - T_f}{T_m - T_f} = \frac{\ln (1 + t_c/t_s)}{\ln (4at_c/r_w^2) - 0.5772} \tag{4.3}$$

From this formula Bullard concluded that for accurate geothermal measurements the shut-in time of a well is very long. For example, at a given depth the shut-in time (t_s) must be longer than the circulation time of the drilling fluid by factor of 10 to 20, if the required relative accuracy of measurement is 0.01.

In their classical work Lachenbruch and Brewer (1959) investigated the effect of variation with time of the heat source strength on the shut-in temperatures (Table 4.1). In this table $t = t_c + t_s$ is the total time, $\bar{q}$ represents the mean value of the radial (at $r = r_w$) flow rate $q(t)$ at $0 < t < t_c$, and Q is identified with $\bar{q}t_c$. The term t_c/t shows the relative error that would result for large value of time ($t >> t_c$). It should be noted that the total amount of heat is the same in all six assumed distributions of heat source strength with time. The first case (Table 4.1) gives the axial temperature, due to an instantaneous linear source of strength, Q units of heat per unit depth released at time $t = t_o$ (λ is thermal conductivity of the formation). The fourth case corresponds the to the assumption made by Bullard (1947). From the drilling data the Authors concluded that the effective temperature of the walls of the hole at a given depth might have been considered constant

Table 4.1 Comparison of cooling formulas based on six different distributions of source strength with time (Lachenbruch and Brewer, 1959)

Case	Description	Axial temperature $t > t_o$ *or* $t > t_c$	Error from treating by case IV, $t >> t_c$
I	Instantaneous $t_o = 0$	$\frac{Q}{4\pi\lambda t}$	$1 - \frac{t_c}{2t} + 0(\frac{t_c}{t})^2$
II	Instantaneous $t_o = t_c$	$\frac{Q}{4\pi\lambda(t-t_c)}$	$1 + \frac{t_c}{2t} + 0(\frac{t_c}{t})^2$
III	Instantaneous $t_o = t_c/2$	$\frac{Q}{4\pi\lambda(t-t_c/2)}$	$1 + 0(\frac{t_c}{t})^2$
IV	Continuous $q = \bar{q},\ 0 > t > t_c$	$\frac{\bar{q}}{4\pi\lambda}\ \ln\ \frac{t}{t-t_c}$	1
V	Continuous $q = 2\bar{q}(1 - t/t_c),\ 0 < t < t_c$	$\frac{\bar{q}}{2\pi\lambda}[(1 - t/t_c)\ln\ \frac{t}{t-t_c} + 1]$	$1 - \frac{t_c}{6t} + 0(\frac{t_c}{t})^2$
VI	Continuous $q = \bar{q}\sqrt{t_c/t},\ 0 > t > t_c$	$\frac{\bar{q}}{8\pi\lambda}\sqrt{t_c/t}[\ln\ \frac{t}{t-t_c} +$ $2\ \ln(1 + \sqrt{t_c/t})]$	$1 - \frac{t_c}{6t} + 0(\frac{t_c}{t})^2$

during drilling. The results of temperature surveys in deep wells have shown that this assumption is valid (Jaeger 1961; Kutasov et al 1966; Kutasov, 1968). Lachenbruch and Brewer (1959) suggested that a limiting case of the heat source distribution might be given by the heat flux through the surface of a region bounded internally by a circular cylinder, where this surface is maintained at a constant temperature (for $0 < t < t_c$).

Hence the cases V and VI (Table 4.1) are more realistic and represent cases where the source strength is decreasing with time. Comparing cases IV, V, and VI we can conclude that treating the effect of variation of heat source strength by case IV should introduce a relative error not greater than $-t_c/6t$ for $t >> t_c$. From Eq. 4.3 we obtain

$$T_s(t_s, r = r_w) = T_f - B\ \ln\ (1 + t_c/t_s), \tag{4.4}$$

$$B = \frac{T_f - T_m}{\ln\ (4t_D) - 0.5772}, \qquad t_D = \frac{at_c}{r_w^2}$$

where B is an unknown parameter. The last relationship (temperature Horner plot) is used for predictions of formation temperature

from bottomhole temperature (BHT) surveys (Timko and Fertl, 1972; Dowdle and Cobb, 1975). However, in many cases, the dimensionless circulation time is small and the logarithmic approximation of the Ei-function cannot be used. The evaluation and limitations of the Horner technique are discussed in the literature (Dowdle and Cobb, 1975; Drury, 1984; Beck and Balling, 1988).

Middletton (1979) and Leblanc et al. (1981) assumed that near the bottom of the well the circulation time is small and the temperature disturbance of formations can be neglected. They suggested models to simulate short-term temperature disspation in mud column near the bottomhole. It was assumed that the thermal properties of the drilling mud and formation are identical. We should also to note that in the practice, due to sedimentation of cuttings, it is very difficult for the temperature probes to reach the bottomhole (Kutasov et al., 1966).
An interesting method, the formation temperature estimation (FTE) model, was suggested by Cao et al. (1988). In this model to determine the value of formation temperature the nonlinear inverse techniques are used. It is not required to know the mud circulation time. To use the FTE model more than two BHT measurements are required. The FTE model is implemented numerically and the following parameters (five) can be determined: formation temperature, mud temperature at the time the mud circulation stops; radius of thermal influence, the formation thermal conductivity; and the fractional factor for heating the mud (in a purely conductive case this factor is equal to 1). Field and synthetic data were used to verify the FTE method (Cao at al., 1988). The Authors concluded that is possible to determine accurately the formation temperature and roughly to estimate the other (four) parameters, providing that input BHT data are of high quality.

4.1.2 The Basic Formula

To determine the temperature in the well ($r = 0$) after the circulation of fluid ceased, we used the solution of the diffusivity equation that describes cooling along the axis of a cylindrical body with known initial temperature distribution (T_D), placed in an infinite

medium of constant temperature (Carslaw and Jaeger, 1959; p.260).

$$T_{sD} = \frac{1}{2at_s} \int_0^\infty exp(-\frac{\tau^2}{4at_s})\ T_D'(\tau, t_D)\ \tau\ d\tau \tag{4.5}$$

$$T_{sD} = \frac{T_s(0,t_s) - T_f}{T_w - T_f} \tag{4.6}$$

$$T_D'(\tau, t_D) = T_D(\tau, t_D); \quad r \geq r_w \quad (Eq.\ 3.74, \tau = r_D, \quad t = t_c)$$

$$T_D'(\tau, t_D) = 1; \quad r < r_w$$

where τ is the variable of integration. From Eq. (4.5), we obtained the following expression for T_{sD} (Kutasov, 1989b).

$$T_{sD} = 1 - \frac{Ei[-\beta(1 + t_D^*/t_{sD})]}{Ei(-\beta)}, \qquad t_{sD} = \frac{at_s}{r_w^2} \tag{4.7}$$

where

$$\beta = \frac{1}{4t_D^*}, \qquad t_D^* = Gt_D \tag{4.8}$$

The values of the $G(t_D)$ function can be calculated from Eqs. 3.72 and 3.73. To simplify calculations we present Table 4.2. For large values of t_D the G function is given by

$$G = \frac{\ln\ t_D}{\ln\ t_D - 1}, \quad t_D > 1000 \tag{4.9}$$

At derivation of the formula (4.7) it is assumed that the thermal diffusivity is the same both within the well and in surrounding formations. The values T_{sD} for t_D = 1, 10, 100, and 1000 are presented in Table 4.3. The good agreement between Jaeger's numerical solution and calculated values of T_{sD} shows that formula (4.7) can be used for temperature predictions during the shut-ion period. Using the logarithmic approximation of the Ei-function for small arguments

$$\beta(1 + t_D^*/t_{sD}) \ < \ 0.01 \tag{4.10}$$

Then

$$Ei(-\beta) = \ln\ t_D^* + \ln\ 4 - 0.5772 \tag{4.11}$$

$$Ei[(-\beta(1 + t_D^*/t_{sD})] = \ln\ t_D^* - \ln\ (1 + t_c^*/t_s) + \ln\ 4 - 0.5772$$

where $t_c^* = t_c G(t_D)$. And from Eqs. (4.7-4.11) we obtain

$$T_s = T_f - M\ \ln\ (1 + t_c^*/t_s) \tag{4.12}$$

Table 4.2 Function $G = G(t_D)$

t_D	G	t_D	G	t_D	G	t_D	G
1	1.5933	25	1.3122	75	1.2624	400	1.1986
2	1.5177	27	1.3078	80	1.2599	420	1.1968
3	1.4789	29	1.3039	85	1.2575	440	1.1952
4	1.4541	31	1.3004	90	1.2553	460	1.1937
5	1.4365	33	1.2973	95	1.2532	480	1.1922
6	1.4230	35	1.2945	100	1.2512	500	1.1908
7	1.4122	37	1.2919	110	1.2475	520	1.1895
8	1.4034	39	1.2894	120	1.2441	540	1.1882
9	1.3959	41	1.2872	130	1.2410	560	1.1870
10	1.4037	43	1.2851	140	1.2382	580	1.1858
11	1.3883	45	1.2831	150	1.2355	600	1.1847
12	1.3761	47	1.2813	160	1.2330	620	1.1837
13	1.3661	49	1.2795	170	1.2306	640	1.1826
14	1.3578	51	1.2779	180	1.2284	660	1.1817
15	1.3507	53	1.2763	190	1.2264	680	1.1807
16	1.3447	55	1.2747	200	1.2244	700	1.1798
17	1.3393	57	1.2733	220	1.2207	720	1.1789
18	1.3346	59	1.2719	240	1.2174	740	1.1781
19	1.3304	61	1.2706	260	1.2144	760	1.1773
20	1.3267	63	1.2693	280	1.2116	800	1.1757
21	1.3233	65	1.2680	300	1.2090	840	1.1742
22	1.3201	67	1.2668	320	1.2066	880	1.1729
23	1.3173	69	1.2657	340	1.2044	920	1.1716
24	1.3146	71	1.2645	360	1.2023	960	1.1703
25	1.3122	73	1.2634	380	1.2004	1000	1.1692

Table 4.3 Values of the dimensionless shut-in temperature T_{sD}

	$t_s/t_c = 0.1$		$t_s/t_c = 1.0$	
t_D	Jaeger(1956)	Formula 4.7	Jaeger(1956)	Formula 4.7
1	0.988	0.9858	0.543	0.5155
10	0.722	0.7315	0.252	0.2446
100	0.477	0.4570	0.143	0.1432
1000	0.324	0.3104	0.098	0.0983

where

$$M = (T_f - T_m)/Ei(-\beta) \tag{4.13}$$

At large circulation times $t_D^*/t_D = t_c^*/t_c \to 1$ (see formula 4.9) and from Eq. (4.12) we obtain

$$T_s = T_f - M \ \ln\ (1 + t_c/t_s) \tag{4.14}$$

This relationship is identical to Eq. 4.4. However, in many cases the dimensionless circulation time is small and the logarithmic approximation of the Ei-function cannot be used. In this case the formula (4.7) should be used for predicting the undisturbed temperature of formations.

Let us assume that two temperature measurements (T_{s1}, T_{s2}) are available for a given depth with $t_s = t_{s1}$ and $t_s = t_{s2}$. From formula (4.7) we obtain

$$\frac{T_{s1} - T_f}{T_{s2} - T_f} = \gamma$$

$$T_f = \frac{T_{s1} - T_{s2}}{1 - \gamma} \tag{4.15}$$

$$\gamma = \frac{Ei(-\beta) - Ei[-\beta(1 + t_c^*/t_{s1})]}{Ei(-\beta) - Ei[-\beta(1 + t^*/t_{s2})]} \tag{4.16}$$

In the bottomhole temperature stabilization model suggested by Leblanc et al. (1981) the temperature disturbance of formations is neglected and the shut-in temperature is given by

$$T_s = T_f - (T_f - T_m)[1 - \exp(-\frac{r_w^2}{4at_s})] \tag{4.17}$$

Here it also assumed that the thermal diffusivity of the mud in the well is equal to the thermal diffusivity of formations. The temperature of the circulating mud (T_m) is not known and therefore two measurements of the shut-in temperature are needed to predict the value of T_f.

Example.

This example is from Kelley Hot Springs geothermal reservoir, Moduc County of California. Depth 1035 m (Roux, et al., 1980). The parameter $a/r^2 = 0.27$/hr, $t_c = 12$ hrs. The results of temperature measurements and predicted formation temperatures are presented in Table 4.4. The static formation temperature for this depth was later found to be 115°C (239 °F).

Table 4.4 Predicted values of T_f

t_{s1}	t_{s2}	T_{s1}	T_{s2}	$T_f, ^oC$		
hrs	hrs	^oC	^oC	Eq.4.17	Eq.4.14	Eq.4.15
14.3	22.3	83.9	90.0	101.3	104.7	106.7
14.3	29.3	83.9	94.4	104.8	108.1	109.9
22.3	29.3	90.0	94.4	108.9	111.9	113.6

4.1.3 Effect of the Formation Thermal Diffusivity

Many investigators believe that the thermal properties of formations measured in the laboratory differ substantially from those in natural (*in situ*) conditions. As a consequence of this some transient temperature anomalies may be associated with the variation of thermal diffusivity of formations. Formula 4.7 can be used to estimate the effect of formation diffusivity on the shut-in temperatures. Some values of $T_{sD} = T_{sD}(t_s, t_c, a, \ r_w = 0.1 \ m)$ are presented in Table 4.5.

Example.
Drilling fluid with a temperature of T_m=50.0°C was circulated at the bottomhole for 20 hours. After 10 hours of shut-in a temperature survey was conducted and the measured temperature was T_s=80.0°C. The bit radius is 0.10 m and it is known that thermal diffusivity of the formation (a) lie within the range 0.0030 to 0.0050 m^2h^{-1}. What is the accuracy ΔT_f of the computed static (undisturbed) formation temperature T_f? For formation thermal diffusivity of $a = 0.0030 \ m^2h^{-1}$ the value of T_{sD} is 0.4246 (Table 4.5). Hence

$$80.0 - T_f = 0.4246(50.0 - T_f); \qquad T_f = 102.1(^oC)$$

For the value of $a = 0.0040 \ m^2h^{-1}$; $T_{sD} = 0.3926$ and

$$80.0 - T_f = 0.3926(50.0 - T_f); \qquad T_f = 99.4(^oC)$$

Similarly, for $a = 0.0050 \ m^2h^{-1}$ and T_{sD}=0.3702

$$80.0 - T_f = 0.3702(50.0 - T_f); \qquad T_f = 97.6(^oC)$$

Thus if the average value of $T_f = 99.7^oC$ is taken as the formation temperature, then $\Delta T_f \approx \pm 2.2^oC$

Table 4.5 The effect of formation diffusivity on the dimensionless shut-in temperature, $T_{sD} \cdot 10,000$

a	Shut-in time, hours							
m^2/hr	1.0	2.0	3.0	5.0	7.0	10.0	15.0	20.0
Circulation time 10 hours								
0.002	9356	8157	7195	5845	4945	4035	3103	2528
0.003	8875	7478	6487	5182	4345	3518	2688	2181
0.004	8479	7002	6018	4764	3976	3206	2440	1976
0.005	8154	6645	5678	4469	3719	2991	2271	1836
0.006	7884	6365	5417	4246	3526	2831	2146	1733
0.007	7655	6138	5208	4070	3375	2706	2048	1653
0.008	7459	5948	5035	3926	3251	2604	1969	1589
Circulation time 20 hours								
0.002	9476	8479	7658	6466	5637	4764	3821	3206
0.003	9069	7884	7021	5845	5058	4246	3386	2831
0.004	8727	7459	6591	5445	4693	3926	3120	2604
0.005	8443	7136	6274	5158	4435	3702	2936	2447
0.006	8203	6878	6027	4937	4237	3532	2796	2329
0.007	7996	6662	5821	4756	4075	3391	2681	2230
0.008	7817	6482	5651	4607	3943	3277	2588	2151
Circulation time 50 hours								
0.002	9588	8794	8127	7136	6424	5646	4764	4156
0.003	9253	8287	7570	6568	5876	5136	4310	3748
0.004	8964	7916	7184	6193	5522	4812	4026	3494
0.005	8722	7630	6896	5922	5269	4583	3828	3318
0.006	8515	7400	6670	5712	5075	4408	3678	3186
0.007	8338	7210	6486	5543	4919	4269	3559	3081
0.008	8183	7049	6331	5402	4791	4155	3461	2995

4.1.4 The Impact of the Well's Radius

Let us now assume that the records of a downhole temperature logs were processed and Formula 4.7 was used for formation temperature predictons. At this time a caliper log was not yet conducted and it was assumed that the well diameter is equal to the bit size. After some time a caliper log was conducted and hole enlargement was observed. In this case Formula 4.7 can be used to estimate the effect of the well radius r_w variation on the shut-in temperatures. Some values of $T_{sD} = T_{sD}(t_s, t_c, r_w, a = 0.0040\ m^2h^{-1})$ are presented in Table 4.6.

Table 4.6 The effect of the well radius on the dimensionless shut-in temperature, $T_{sD} \cdot 10,000$

r_w	Shut-in time, hours							
m	1.0	2.0	3.0	5.0	7.0	10.0	15.0	20.0
Circulation time 10 hours								
0.08	7823	6304	5361	4199	3485	2797	2119	1711
0.10	8157	6445	5355	4035	3252	2528	1849	1459
0.12	8479	7002	6018	4764	3976	3206	2440	1976
0.14	8974	7607	6618	5301	4452	3609	2760	2241
0.16	9335	8124	7159	5810	4912	4007	3080	2509
0.18	9585	8556	7642	6290	5357	4397	3400	2778
0.20	9752	8910	8067	6738	5784	4780	3719	3050
Circulation time 20 hours								
0.08	8149	6820	5971	4888	4193	3493	2765	2302
0.10	8727	7459	6591	5445	4693	3926	3120	2604
0.12	9154	7998	7140	5957	5162	4338	3462	2897
0.14	9458	8450	7626	6433	5606	4736	3797	3186
0.16	9666	8821	8051	6873	6027	5120	4126	3472
0.18	9803	9120	8419	7277	6425	5490	4448	3755
0.20	9888	9356	8734	7646	6798	5845	4764	4035
Circulation time 50 hours								
0.08	8469	7350	6621	5666	5033	4371	3645	3158
0.10	8964	7916	7184	6193	5522	4812	4026	3494
0.12	9324	8386	7676	6673	5976	5228	4392	3821
0.14	9575	8772	8104	7113	6402	5628	4749	4144
0.16	9741	9076	8460	7493	6777	5981	5065	4428
0.18	9849	9319	8766	7842	7131	6323	5378	4714
0.20	9915	9507	9023	8154	7456	6645	5678	4991

Example.

The drilling fluid with a temperature of T_m=50.0°C was circulated at the bottomhole for 20 hours. After 15 hours of shut-in a temperature survey was conducted and the measured temperature was T_s=80.0°C. The bit radius is 0.14 m and the thermal diffusivity of the formation $a = 0.0040\ m^2h^{-1}$. After this a caliper log was conducted and it was found that the well radius is 0.18 m. What is the accuracy ΔT_f of the calculated formation temperature T_f? For the well radius 0.14 m the value of T_{sD} is 0.3797 (Table 4.6). Hence,

$$80.0 - T_f = 0.3797(50.0 - T_f); \qquad T_f = 98.4(^oC)$$

For the value of $r_w = 0.18$ m from Table 4.6 we obtain that $T_{sD} = 0.4448$ and

$$80.0 - T_f = 0.4448(50.0 - T_f); \qquad T_f = 104.0(^oC)$$

Thus the formation temperature was initially determined with an accuracy $\Delta T_f = 5.6^oC$

Reduced speed of temperature recovery was observed in sections of a deep well (7,200 m) where caliper log detected large washouts (Wilhelm et al., 1995). In the 3,400-3,450 m interval the diameter of the wellbore was increased from 390 mm to up to 650 mm. The temperature logs in this well were conducted after 24, 47, 96, and 152 hours of shut-in. The maximum temperature anomaly due to washouts of 3°C was observed from the first temperature survey. After 152 hours of shut-in the temperature anomaly was reduced to approximately 0.5°C.

4.1.5 Variations in the Shut-in and Circulation Time Ratio

Let consider a more general case. The function T_{sD} (Eq. 4.7) can be expressed as function of two dimensionless parameters: the dimensionless disturbance (fluid circulation) time (t_D) and the shut-in and circulation time ratio (n). In this case the function T_{sD} (Table 4.7) can be used to estimate the shut-in time which is needed to determine the value of T_f with a specified accuracy. Below we present an example of calculations.

Example.
The drilling fluid with a temperature of T_m=50.0°C was circulated at the bottomhole for 100 hours. After t_s=50 hours of shut-in a temperature survey was conducted and the measured temperature was T_s=95.0°C. The bit radius is 0.20 m, thermal diffusivity of the formation $a = 0.0040\ m^2h^{-1}$, and the specified accuracy is 1°C. Is this value of t_s sufficient to estimate the formation temperature with $\Delta T_f = 1^oC$? Firstly we have to calculate the dimensionless parameters

$$t_D = \frac{0.0040 \cdot 100}{0.20^2} = 10.0, \qquad n = \frac{50}{100} = 0.50$$

Table 4.7 The effect of the shut-in and circulation time ratio on the dimensionless shut-in temperature, $T_{sD} \cdot 10,000$

	Shut-in time and circulation time ratio							
t_D	0.05	0.10	0.20	0.30	0.40	0.50	0.70	1.00
2.0	9888	9356	8157	7195	6445	5845	4945	4035
5.0	9265	8154	6645	5678	4991	4469	3719	2991
10.0	8443	7136	5646	4764	4156	3702	3061	2447
20.0	7521	6193	4812	4026	3494	3102	2552	2031
50.0	6402	5179	3975	3307	2860	2533	2076	1647
100.0	5691	4572	3492	2898	2503	2213	1811	1434
200.0	5092	4074	3101	2569	2216	1958	1600	1265
500.0	4447	3546	2690	2225	1916	1691	1379	1089
1000.0	4050	3224	2442	2017	1735	1530	1247	983

From Table 4.7 the value of $T_{sD} = T_{sD}(t_D, n)$ is 0.3702 and

$$80.0 - T_f = 0.3702(50.0 - T_f); \quad T_f = 97.6(^oC)$$

Thus, the shut-in time of 50 hours is not sufficient to estimate the value of T_f with the specified accuracy of 1^oC.

4.2 Prediction of the Formations Temperatures

4.2.1 "Two Temperature Logs" Method

The mathematical model of the "Two temperature logs" method is based on the assumption that in deep wells the effective temperature of drilling mud (T_w) at a given depth can assumed to be constant during the drilling process. As was shown before, for moderate and large values of the dimensionless circulation time ($t_D > 5$) the temperature distribution function $T_{cD}(r_D, t_D)$ in the vicinity of the well can be described by a simple formula (3.65). Thus the dimensionless temperature in the wellbore and in formation at the end of mud circulation (at a given depth) can be expressed as:

$$T_{cD}(r_D, t_D) = \begin{cases} 1, & 0 \le r_D \le 1 \\ 1 - \ln r_D / \ln R_D, & 1 \le r_D \le R_{in} \\ 0, & r_D > R_{in} \end{cases} \qquad (4.18)$$

where

$$T_{cD}(r_D, t_D) = \frac{T(r_D, t_D) - T_f}{T_w - T_f}$$

To determine the temperature in the well ($r = 0$) after the circulation of fluid ceased, we used the radial temperature profile (Eq. 4.18) and performed integration of the integral (4.5). We obtained the following expression for T_{sD}

$$T_{sD} = \frac{T(0, t_s) - T_f}{T_w - T_f} = 1 - \frac{Ei(-pR_{in}^2) - Ei(-p)}{2\ ln\ R_{in}}, \qquad t_D > 5 \quad (4.19)$$

where

$$p = \frac{1}{4nt_D}; \qquad n = \frac{t_s}{t_c} \quad (4.20)$$

It was assumed that for deep wells the radius of thermal influence is much larger than the well radius, and, therefore, the difference in thermal properties of drilling muds and formations can be neglected. As we mentioned before, in the analytical derivation of the Eq. 4.19 two main simplifications of the drilling process were made: it was assumed that drilling is a continuous process and the effective mud temperature (at a given depth) is constant. For this reason field data were used to verify the Eq. 4.19. Long term temperature observations in deep wells of Russia, Belarus, and Canada were used for this purpose (Kutasov, 1968; Djamalova, 1969; Bogomolov et al., 1972; Kritikos and Kutasov, 1988). The shut-in times for these wells covered a wide range (12 hours to 10 years) and the drilling time varied from 3 to 20 months.

The observations showed that Eq. 4.19 gives a sufficiently accurate description of the process by which temperature equilibrium comes about in the borehole. Figure 4.1 presents the temperature versus shut-in time curve at the depth of in Namskoe deep well (Yakutia republic, Russia; depth is 3003 m, total drilling time is 578 days). The T_f and T_w values were determined from observed temperatures at $t_s = 200$ days and 3210 days. At this depth determination of the formation (undisturbed) temperature with an accuracy of 0.1^oC requires a shut-in time of about eight years.
In practice, for deep wells (large t_D and small p) we can assume that

$$R_{in} \approx D_o\sqrt{t_D} \quad (4.21)$$

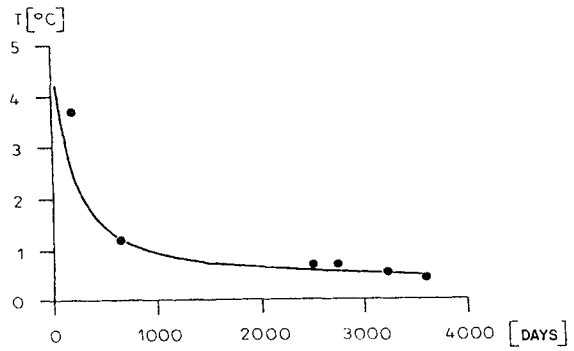


Fig. 4.1. Rate of the temperature recovery at 500 depth in the Namskoe well, (sand $a = 0.0020\ m^2h^{-1}$). Solid curve – Formula 4.19; points – measurements, (Kutasov, 1968).

$$Ei(-p) \approx -\ ln\ t_D - \ ln\ n - \ ln\ 4 + 0.5772 \tag{4.22}$$

Introduction of Eqs. 4.21 and 4.22 into Formula 4.19 yields:

$$\frac{T(0,t_s) - T_f}{T_w - T_f} = -\frac{Ei(-D/n) + \ ln\ n - D_1}{2\ \ ln\ t_D + 2\ \ ln\ D_o} \tag{4.23}$$

where

$$D = D_o^2/4 = 1.1925; \quad D_1 = 0.5772 + \ ln\ D = 0.7532$$

If two measured shut-in temperatures (T_{s1}, T_{s2}) are available for the given depth with $t_2 = t_{s1}$ and $t_s = t_{s2}$ we obtain:

$$\frac{T_{s1} - T_f}{T_{s2} - T_f} = \frac{Ei(-D/n_1) + \ ln\ n_1 - D_1}{Ei(-D/n_2) + \ ln\ n_2 - D_1} \tag{4.24}$$

Therefore:

$$T_f = T_{s2} - \gamma(T_{s1} - T_{s2}) \tag{4.25}$$

where

$$\gamma = \frac{Ei(-D/n_2) + \ ln\ n_2 - D_1}{Ei(-D/n_2) - Ei(-D/n_1) + \ ln\ \frac{n_2}{n_1}} \tag{4.26}$$

$$n_1 = \frac{t_{s1}}{t_c}; \qquad n_2 = \frac{t_{s2}}{t_c} \tag{4.27}$$

Thus the well radius and thermal diffusivity of the formation have no influence on value of T_f, as the unknown parameters T_w and

Table 4.8 Calculated formation temperatures, well Rechitskaya 17-P (Kutasov et al., 1971)

H, m	T_{s1}	T_{s1}	$-\gamma$	$\gamma(T_{s1} - Ts2)$	T_f
500	24.9	24.21	0.215	-0.15	24.06
700	25.5	27.45	0.206	0.40	27.85
900	27.5	29.99	0.194	0.48	30.47
1100	29.35	32.84	0.183	0.64	33.48
1400	31.7	36.49	0.166	0.80	37.29
1600	33.8	39.09	0.154	0.81	39.90
1800	35.65	41.70	0.140	0.85	42.55
2000	37.4	44.32	0.128	0.88	45.20
2300	42.05	52.82	0.105	1.13	53.93
2600	46.0	57.49	0.082	0.95	58.44

t_D have been eliminated. The quantities r_w and a, however, affect the value of T_f through T_{s1} and T_{s2}. The correlation coefficient γ monotonically changes with depth. As an example we present the Table 4.8 for the well Rechitskaya 17-P (Rechitskaya oil field, Belarus). Fig. 4.2 presents the results of calculations of values T_f for the well 1225 (Kola peninsula, Russia). Measured temperatures observed at t_{s1}=4.5 days and t_{s2}=20 days were used (a total of seven temperature logs were made with $0.5 \leq t_s \leq 63$ days). The total drilling time of this well was 94 days. The field data and the calculated T_f values show that, for a depth range 200-500 m, a shut-in time of two months is adequate if the accuracy in the determination of T_f is 0.03^oC.

The temperature gradient is a differential quantity, hence the process by which the geothermal (undisturbed) gradient (Γ) is restored is distinct from temperature recovery process. Now the question arises: how accurately is the value of Γ determined from temperature measurements taken a short time after cessation of drilling. On the basis of the Eq. 4.19 we will derive a relationship linking the geothermal gradient with the transient vertical temperature gradients. Two cases will be considered.

1. The average temperature of the circulating fluid while penetrating some section of the well (ΔH) is not known. Let us assume that two temperature logs $T_{s1} = T(0, t_{s1})$ and $T_{s2} = T(0, t_{s2})$ are

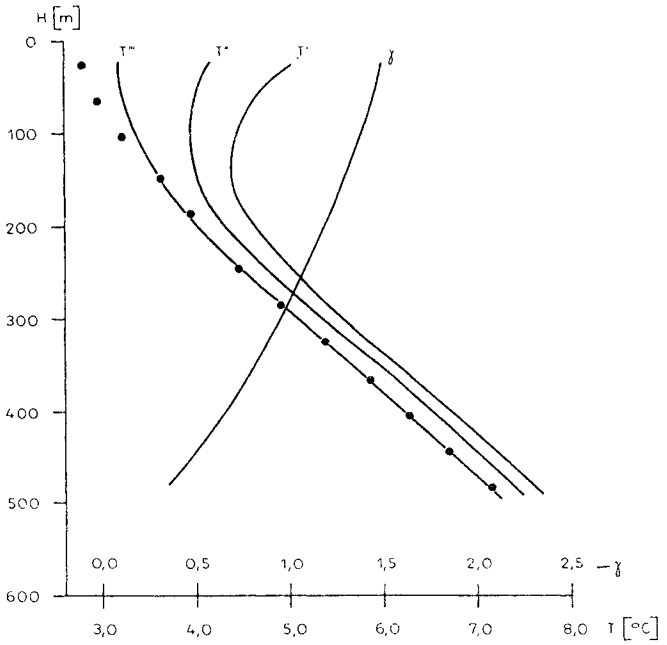


Fig. 4.2. Rate of the temperature recovery in the well 1225. Termograms T', T'', T' were observed at $t_s = 0.5$; 4.5; and 63 days correspondingly. Points – calculated values of T_f, γ – correlation coefficient, (Kutasov, 1968).

available and the parameters for two points (depths) are:

$$H + \Delta H, \quad t_c, \quad r_w, \quad T_w, \quad a, \quad t_D = \frac{at_c}{r_w^2};$$

$$H, \quad t_c', \quad r_w', \quad T_w', \quad a, \quad t_D' = \frac{at_c}{(r_w')^2}$$

Substituting these parameters into Eq. 4.19 we obtain a system of equations

$$\frac{T_{s1} - T_f}{T_{s2} - T_f} = \frac{T_{sD}(t_D, \frac{t_{s1}}{t_c})}{T_{sD}(t_D, \frac{t_{s2}}{t_c})} = \gamma_1 \tag{4.28}$$

$$\frac{T_{s1}' - T_f'}{T_{s2}' - T_f'} = \frac{T_{sD}(t_D', \frac{t_{s1}}{t_c'})}{T_{sD}(t_D', \frac{t_{s2}}{t_c'})} = \gamma_1' \tag{4.29}$$

From this system of equations we obtain

$$\Gamma = \frac{A_1 - \gamma_1' A_2}{1 - \gamma_1'} + \frac{(T_{s1} - T_{s2})(\gamma_1 - \gamma_1')}{\Delta H(1 - \gamma_1')(1 - \gamma_1)} \tag{4.30}$$

$$\Gamma = \frac{T_f - T_f'}{\Delta H}, \quad A_1 = \frac{T_{s1} - T_{s1}'}{\Delta H}, \quad A_2 = \frac{T_{s2} - T_{s2}'}{\Delta H} \tag{4.31}$$

2. The average temperature of the circulating fluid is known. Then only one temperature log is needed to determine the value of Γ. From the following system of equations

$$\frac{T_{s1} - T_f}{T_w - T_f} = T_{sD}(t_D, \frac{t_{s1}}{t_c}) = T_{sD} \tag{4.32}$$

$$\frac{T_{s1}' - T_f'}{T_w' - T_f'} = T_{sD}(t_D', \frac{t_{s1}}{t_c'}) = T_{sD}' \tag{4.33}$$

we obtain

$$\Gamma = A_1 \frac{1}{1 - T_{sD}'} + \frac{T_{s1}(T_{sD} - T_{sD}') + T_{sD}T_{sD}'(T_w - T_w') + (T_{sD}'T_w' - T_{sD}T_w)}{\Delta H(1 - T_{sD}')(1 - T_{sD})} \tag{4.34}$$

For small values of ΔH we can assume that $T_w = T_w'$. Then

$$\Gamma = A_1 \frac{1}{1 - T_{sD}'} + \frac{(T_{s1} - T_w)(T_{sD} - T_{sD}')}{\Delta H(1 - T_{sD}')(1 - T_{sD})} \tag{4.35}$$

The determination of the geothermal gradient in the 407-467 m depth interval in well 1225 (Fig. 4.3) showed that the geoterhermal gradient can be determined with an accuracy of 10% just after two days after drilling ceases, and with an accuracy of 3% after 20 days. In the depth range of 500-700 m in the Namskoe well, the geothermal gradient can be estimated with an accuracy of 6% after only 50 days. The rate of the temperature gradient recovery depends on many parameters (a, r_w, T_w, , t_c) that may vary over wide ranges. This circumstance must be taken into account at interpretation field data, so that the temperature anomalies associated with the thermal recovery process do not get attributed to some peculiarities of the geological structure. For example, in the upper section of well 1225, the temperature gradient for small values of t_s was near zero. This might br misinterpreted as a water encroachment or as an ore body.

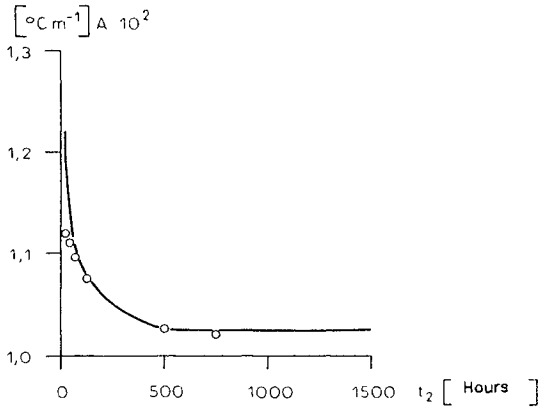


Fig. 4.3. Temperature gradient recovery in the 407-467 m section of the well 1225 (diorites, $a = 0.0027\ m^2h^{-1}$). Solid curve – calculated, open circles – from field data, (Kutasov, 1968).

4.2.2 Solution for a Time Dependent Mud Circulation Temperature

We determined the temperature distribution in and around the wellbore (Eq. 3.84) when the circulating fluid temperature (at a given depth) is a linear function of time (Eq. 3.81). For the temperature distribution (Eq. 3.84) we obtained the following formula for the wellbore shut-in temperature T_s (Kutasov, 1976):

$$\frac{T_s(t_s,0)-\Psi_1}{T_f-\Psi_1}=\frac{Ei(-pR_{in}^{*2})-Ei(-p)}{2\ln R_{in}^*}, \tag{4.36}$$

$$p=\frac{1}{4nt_D};\quad n=\frac{t_s}{t_c}$$

or

$$T_f=\frac{2(T_s-\Psi_1)\ln R_{in}^*}{Ei(-pR_{in}^{*2})-Ei(-p)}+\Psi_1, \tag{4.37}$$

The dimensionless radius of the thermal influence R_{in}^* and the function Ψ_1 are given by Formulas 3.82 and 3.83.

The derivation of equation (4.36) assumes that the difference in thermal properties of drilling mud and formations can be neglected. Although this is a conventional assumption even for interpreting

Table 4.9 Shut-in temperatures at the depth 4,900 m versus shut-in time

t_{sh}, hr	T_s, °C	$T_f - T_s$, °C	t_s, hr	T_s, °C	$T_f - T_s$, °C
1	138.75	15.15	30	143.92	9.98
2	139.55	14.35	40	144.42	9.48
5	140.89	13.01	50	144.81	9.09
10	142.03	11.87	70	145.40	8.50
15	142.72	11.18	100	146.04	7.86
20	143.21	10.69	150	146.76	7.14
25	143.60	10.30	200	147.27	6.63

bottomhole temperature survey (Timko and Fertl, 1972; Dowdle and Cobb, 1975), when the circulation periods are small, Eq. 4.37 should be used with caution for very small shut-in times.

Field example.
Extensive downhole and outlet mud temperature data taken during drilling and completing of a super deep Mississippi well and the well's drilling history (Wooley et al., 1984) were used to determine the coefficients in Eq. 3.81 for the 4,900-6,535 m section of the well

$$B_0 = 130.67^oC, \qquad B_1 = 0.00178\ ^oC/hr$$

The static (undisturbed) temperature of formations the depth of 4,900 m was estimated and T_f =153.9°C (Wooley et al., 1984). The radius of the well is $r_w = 0.0984\ m$ (bit size=7.750 in.) and the value of thermal diffusivity of formations is a=0.0040 m^2/hr (assumed).
In this case the value of T_f is known and formula (4.37) was used to calculate the shut-in temperatures (Table 4.9).

4.3 Temperature Distribution in Formations

Knowledge of the temperature distribution around the wellbore as a function of the circulation time, shut-in time, and the radial distance is needed to estimate the electrical resistance of the formation water. This will permit to improve the quantitative interpretation of electric logs. The temperature distribution around a shut-in

well is an important factor affecting thickening time of cement, rheological properties, compressive strength development, and set time. For the fluid circulating period an approximate analytical solution was obtained (Eq. 3.74), which describes with high accuracy the temperature field of formations around a well with a constant bore-face temperature. Using the principle of superposition for the shut-in period we present an approximate analytical solution which describes the temperature distribution in formation surrounding the wellbore during the shut-in period

$$T_{sD} = \frac{T(r,t_s) - T_f}{T_w - T_f} = \frac{Ei(-\frac{r_D^2}{4(t_D^*+t_{sD})}) - Ei(-\frac{r_D^2}{4t_{sD}})}{Ei(-\frac{1}{4t_D^*})} \qquad (4.38)$$

$$t_D = \frac{at}{r_w^2}, \quad t_{sD} = \frac{at_s}{r_w^2}, \quad r_D = \frac{r}{r_w}, \quad t_D^* = Gt_D$$

where, t_D^* is the adjusted dimensionless circulation time (see Section 3.6.2) and G is a function of t_D (Table 4.2 and Eq. 4.9). The values of dimensionless radial temperature of formations calculated after Formula 4.38 are in good agreement with the results of a numerical solution (Table. 4.10). A computer program "SHUTEMP" (Appendix C, Table C.5) has been used to calculate the function $T_{sD} = T_{sD}(r_D, t_D, t_{sD})$ and tables have been constructed that allow one to determine the radial temperature at several dimensionless radial distances during the shut-in period (Kutasov, 1993b).

Example.

A well was drilled to a depth of 12,490 ft in Webb County, Texas (Venditto and George, 1984). The values of the static temperature of formations and circulating temperature at the bottomhole are: $T_f = 306\ ^oF$ and $T_m = T_w = 251^oF$. Let us assume that after 50 hours of mud circulation the well was shut-in for 100 hours and after that an electrical log was run (near the bottomhole); radius of investigation, bit diameter, and the thermal diffusivity of formations are:

$$r_{inv} = 22\ in., \quad 2r_w = 8.75\ in., \quad a = 0.04\ ft^2/hr$$

The following steps are needed to calculate the radial temperature.

Step 1. Compute the dimensionless circulation time, dimensionless shut-in time, and dimensionless radial distance (dimensionless

Table 4.10 Dimensionless shut-in temperature $T_{sD} \times 1000$. First line – Formula 4.38, second line – numerical solution (Taylor, 1978)

		Dimensionless shut-in time, t_{sD}							
t_D	r_D	5	10	20	30	40	50	70	100
10	1	374	248	151	109	86	71	52	38
		369	247	150	108	85	70	52	–
	2	344	236	147	107	84	70	52	37
		342	235	146	106	84	69	51	–
	3	301	217	140	103	82	68	51	37
		300	216	139	103	81	67	50	–
	5	199	167	120	93	75	63	48	35
		199	166	119	92	75	63	48	–
100	1	569	458	349	290	251	222	181	144
		–	459	352	292	251	223	182	144
	2	545	446	344	287	248	220	180	143
		–	447	346	289	250	221	181	143
	3	509	427	335	281	244	217	178	142
		–	429	337	283	246	218	179	142
	5	418	374	308	263	231	207	172	138
		–	377	310	265	233	208	173	138

radius of investigation)

$$t_D = \frac{50 \cdot 0.04 \cdot (2 \cdot 12)^2}{8.75^2} = 15, \quad t_{sD} = \frac{100 \cdot 0.04 \cdot (2 \cdot 12)^2}{8.75^2} = 30,$$

$$r_D = \frac{22.0 \cdot 2}{8.75} = 5$$

Step 2. From Formula 4.38 determine the value of function T_{sD} for $t_D = 15$, $t_{sD} = 30$, and $r_D = 5$. The value of T_{sD} is 0.115 and

$$T_s(r_{inv}, t_s) = 0.115 \cdot (251 - 306) + 306 = 300(^oF)$$

Step 3. From Formula 4.38 estimate the function T_{sD} at $r = r_w$. The value of T_{sD} is 0.134 and

$$T_s(r_w, t_s) = 0.134 \cdot (251 - 306) + 306 = 299(^oF)$$

Thus, in this example the radial temperature of formations changes from 299°F at the wellbore face to 300 °F at $r_{inv} = 22$ in. The temperatures are close to the static temperature of 306 °F (152 °C)

rather than to the value of the circulating temperature 251°F (122°C). This should be taken into account at interpretation of electric logs.

4.4 Restoration of the Thermal Equilibrium in Permafrost Areas

4.4.1 Results of Long Term Temperature Surveys

Investigations of the temperature field of permafrost zone and determination of the permafrost thickness are based mainly on the results of temperature surveys in deep boreholes. Due to thawing of surrounding the wellbore formations, representative data can be obtained only by repeated observations over a long period of time. During the last several decades long term temperature observations in deep boreholes were conducted in Alaska, Canada, and Russia (Lachenbruch and Brewer, 1959; Melnikov et al., 1973; Taylor et al., 1982). The temperature observations in deep wells have shown that that only after a lengthy shut-in period the temperature of frozen formations can be estimated with a sufficient accuracy. Hence a single temperature log cannot be reliable.

Let us examine the restoration of the natural temperature field by the example of the Bakhynay borehole 1-R (Melnikov et al., 1973). The borehole was drilled for 23 months (1956-1958) to a depth of 2824 m. Sands and weakly cemented sandstones with clay and siltstone partings were revealed in the range from 19 to 1500 m. Nine temperature logs were performed over a shut-in period of 10 years, but the difference between the temperature of formations and that in the borehole was still greater than the measurement accuracy (0.03-0.05°C). After a shut-in period of 1.5 years the the thickness of permafrost was estimated as 470 m instead of 650 m. The restoration of the temperature regime was accompanied by formation of practically zero temperature gradient intervals (Fig. 4.4). Therefore, if the shut-in time is insufficient, one may incorrectly attribute the zero temperature gradient intervals to some geological-geographical factors, an example of which in this case is the warming effect of the Lena river (the drilling site is the

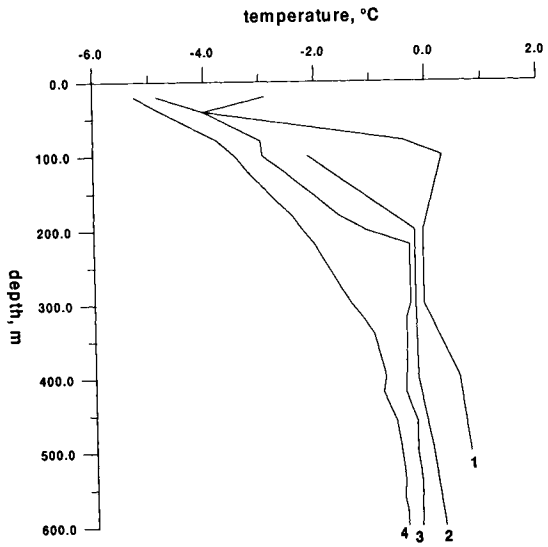


Fig. 4.4. Restoration of temperature profile in the Bakhynay borehole 1-R (Melnikov et al., 1973). Temperature surveys 1, 2, 3, and 4 were conducted at shut-in times of 0.4, 1.5, 3.4 and 10.4 years respectively.

bank of the river).

Temperature observations in the Amga borehole (Central Yakutia, Russia; well depth 1109 m, drilling time 13 months) for a period of 14 years (Fig. 4.5) have shown that 8-9 years were required determine the position of the permafrost base. Extensive temperature measurements in the Northern Canada were conducted by the Geothermal Service of Canada (Judge et al., 1981; Taylor et al., 1982). As an example, in Fig. 4.6 we present results of temperature surveys in the well Kamik D-48 (Mackenzie delta, Canada). The well was drilled for 102 days, drilling operations stoped on April 4, 1976 and the total depth is 3235 m. The field data also show that the duration of refreezing of formation thawed out during drilling significantly depends on its natural (undisturbed) temperature. For low temperature permafrost the refreezing period is relatively short (Fig. 4.7).

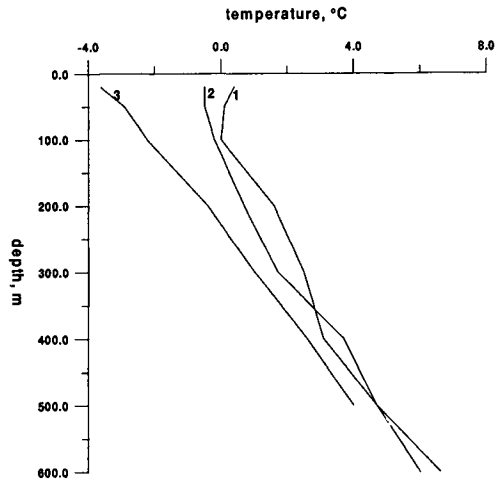


Fig. 4.5. Restoration of temperature profile in the Amga borehole (Kutasov, 1976). Temperature surveys 1, 2, and 3 were conducted at shut-in times of 15, 465, and 4460 days respectively.

4.4.2 Dynamics of the Thawed Zone

After the cessation of the drilling process the radius of thawing and the radius o thermal influence will increase for a definite period of time Δt_o at the expense of the heat accumulated in the thawed zone. The parameter Δt_o is a function of many variables and its value can be estimated from the following formula (Kutasov, 1976)

$$\Delta t_o = \frac{h^2}{5.8 a_t} \ln\left[\frac{1.6\ J_o(2.405/H)\ \theta_\lambda\ \ln\ R_{in}/H}{\ln\ H}\right] \tag{4.39}$$

$$\theta_\lambda = -\frac{\lambda_t T_m}{\lambda_f T_f}, \quad H = \frac{h}{r_w}$$

where $J_o(x)$ is the Bessel function of the first kind of order zero, λ_t, λ_f are the thermal conductivities of the formation in thawed and frozen state, and a_t is the thermal diffusivity of thawed formation. The radius of thermal influence and radius of thawing ratio ($R_{in}/H = r_{in}/h$) can be determined from the graph (Fig. 4.8). To simplify calculations we present some values of the $J_o(x)$ function (Table 4.11). Hydrodynamical modeling (Kutasov, 1976) has

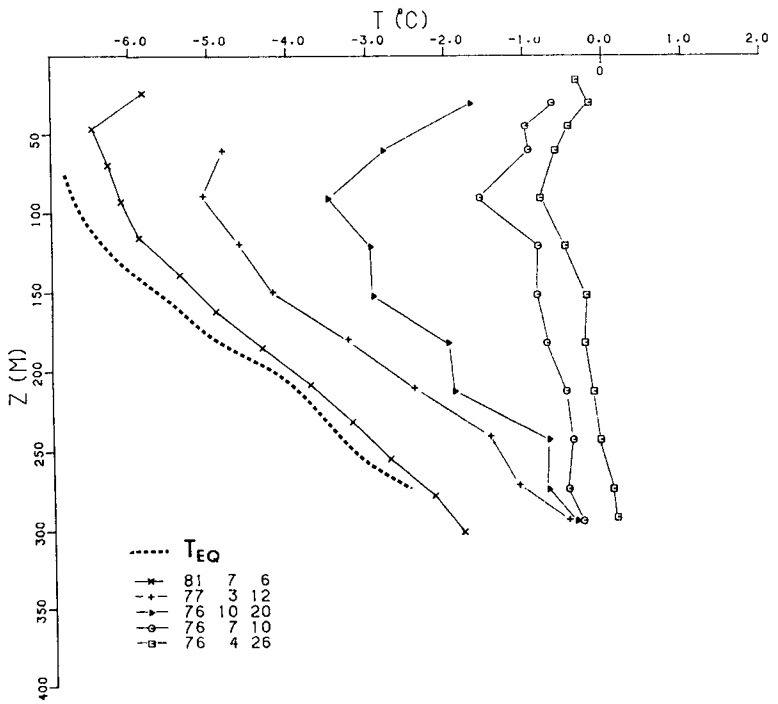


Fig. 4.6. Temperature profiles in the well Kamik D-48, T_{EQ} – the predicted temperature versus depth curve (Taylor et al., 1982).

shown that maximum value of the thawing radius can be given by

$$h_{max} = h(t_c + \Delta t_o) \approx (1 + 0.43\frac{\Delta t_o}{t_c})h(t_c) \qquad (4.40)$$

Example.
The results of one run of the hydrodynamical modeling are presented on Fig. 4.9. The input parameters are:

$$t_c = 2200\ hrs, \quad T_m = 8^oC, \quad T_f = -2^oC, \quad r_w = 0.1\ m$$

$$a_t = 0.0030\, m^2/h, \quad \lambda_t = 2.0\, kcal/(h{\cdot}m{\cdot}^oC), \quad \lambda_f = 2.5\, kcal/(h{\cdot}m{\cdot}^oC)$$

From Figures 4.8 and 4.9 we obtain that $h(t_c) = 1.12$ m, $R_{in}/H = 10$, $J_o(2.405/11) = 0.99$, and

$$\ln\ 10 = 2.30, \quad \ln\ 11.2 = 2.42, \quad \theta_\lambda = -\frac{2.0 \cdot 8}{2.5 \cdot (-2)} = 3.20$$

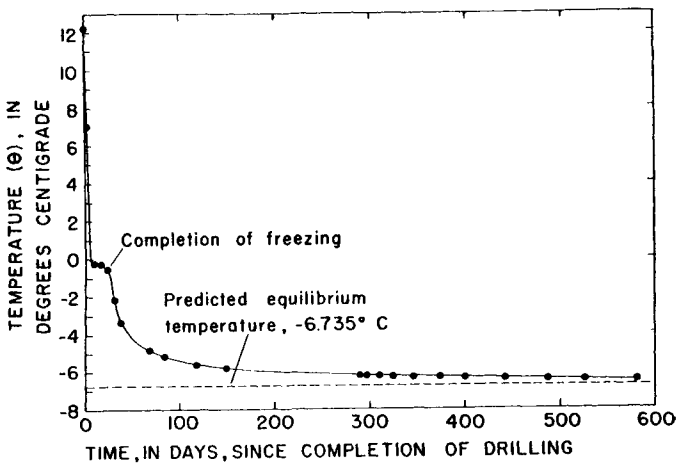


Fig. 4.7. Cooling of South Barrow (Alaska) well 3, 595-foot depth depth curve (Lachenbruch and Brewer, 1959).

Table 4.11 The $J_o(x)$ function

x	$J_o(x)$	x	$J_o(x)$	x	$J_o(x)$
0.0	1.00	0.5	0.94	0.9	0.81
0.2	0.99	0.6	0.91	1.0	0.76
0.3	0.98	0.7	0.88	1.9	0.72
0.4	0.96	0.8	0.85	1.2	0.67

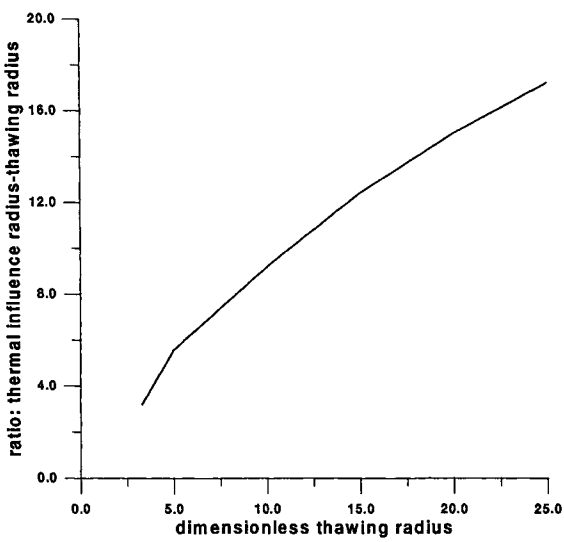


Fig. 4.8. The $R_{in}/H = f(H)$ curve.

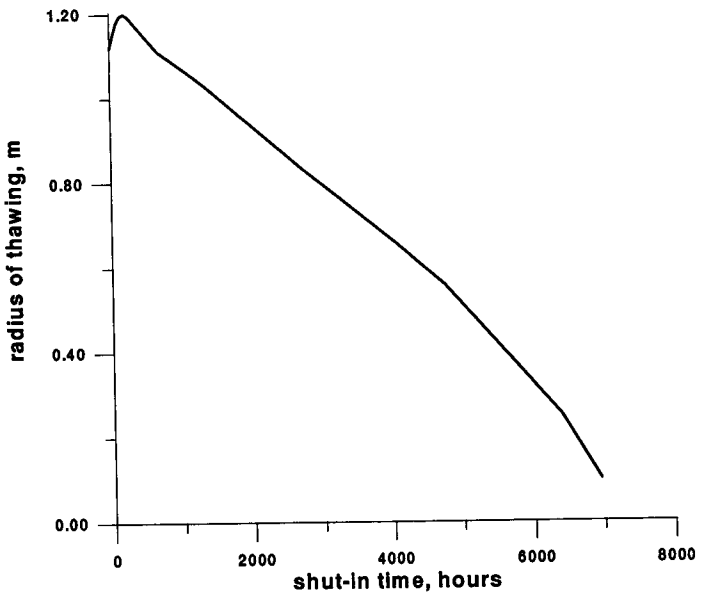


Fig. 4.9. Dynamics of the thawed zone.

From equations (4.39) and (4.40) we obtain

$$\Delta t_o = \frac{1.12^2}{5.8 \cdot 0.0030} \ln \left(\frac{1.6 \cdot 3.20 \cdot 2.30 \cdot 0.99}{2.42}\right) = 113 \ (hrs)$$

$$h_{max} = 1.12(1 + 0.43\frac{113}{2200}) = 1.14 \ (m)$$

4.4.3 Time of the Complete Freezeback

Refreezing of the thawed zone starts at the moment of time $t = t_o$ and ends at $t = t_{ep}$ (Fig. 3.30). To calculate the duration of the freezeback period $t_{fb} = t_{ep} - t_o$ we assumed that the heat flow (at $t > t_o$) from the thawed zone to the thawed zone-frozen zone interface can be neglected. The results of hydrodynamical modeling have shown that this is a valid assumption. In this case the Stefan equation – energy conservation condition at phase change interface ($r = h$) is

$$\lambda_f \frac{dT_f(r,t)}{dr}|_{r=h} = Lw\frac{dh}{dt} \tag{4.41}$$

Assuming the semi-steady temperature distribution in frozen zone (a conventional assumption) we obtain

$$T_f(r,t) = T_f \frac{\ln\ r/h}{\ln\ r_{if}/h} \tag{4.42}$$

where r_{if} is the radius of thermal influence during the freezeback period. The ratio $D_f = r_{if}/h$ was determined from a numerical solution. A computer program was used to obtain a numerical solution of a system of differential equations of heat conductivity for frozen and thawed zones and Eq. 2.44 (Kutasov et al., 1977a). It was found that

$$D_f = 2.00 + 0.25\ \ln(I_{fb} + 1) \tag{4.43}$$

$$1.5 < I_{fb} \leq 400, \qquad 1.25 < H_{max} < 23.4$$

where

$$I_{fb} = -\frac{Lwa_f}{T_f \lambda_f}, \qquad H_{max} = \frac{h_{max}}{r_w}$$

From Eqs. 4.41-4.43 and the the initial condition $h(t_o) = h_{max}$ we obtain

$$t_{fD} = \frac{D_f I_{fb}}{2}(H_{max}^2 - H^2), \qquad t_{fD} = \frac{a_f(t - t_o)}{r_w^2} \tag{4.44}$$

We should to note that, due to assumption (zero heat flow from the thawed zone), the last formula can not be used at $H \to H_{max}$. At $h = r_w$ we obtain the relationship for the duration of complete freezeback, $t_{cf} = t_{ep} - t_o$ (Fig. 3.30)

$$t_{cfD} = \frac{D_f I_{fb}}{2}(H_{max}^2 - 1), \qquad t_{cfD} = \frac{a_f t_{cf}}{r_w^2} \tag{4.45}$$

For three runs the the the values of t_{fD} calculated by Formula 4.44 and results of a numerical solution t_{fD}^* are compared (Table 4.12).

4.4.4 Modification of the "Two Temperature Logs" Method

At the moment of time $t = t_{ep}$ the phase transitions (water-ice) in formations ends and at $t > t_{ep}$ the cooling process is similar to that of temperature recovery in sections of the well below the permafrost

Table 4.12 Freezback dynamics for three runs

H	$I_{fb} = 200$ $H_{max} = 10.1$		$I_{fb} = 10$ $H_{max} = 7.1$		$I_{fb} = 2$ $H_{max} = 8.95$	
	t^*_{fD}	t_{fD}/t^*_{fD}	t^*_{fD}	t_{fD}/t^*_{fD}	t^*_{fD}	t_{fD}/t^*_{fD}
9.0	5965	1.171	-	-	-	-
8.0	11340	1.115	-	-	31.72	1.155
7.0	16380	1.076	17.97	1.020	54.14	1.307
6.0	20980	1.046	142.4	1.315	76.84	1.306
5.0	25100	1.020	267.1	1.236	100.2	1.251
4.5	26970	1.008	331.3	1.183	111.9	1.217
4.0	28690	0.997	391.7	1.142	123.4	1.181
3.5	30280	0.986	449.6	1.103	134.7	1.146
3.0	31710	0.976	504.3	1.067	145.7	1.110
2.5	32980	0.966	555.1	1.034	156.1	1.076
2.0	34090	0.956	601.2	1.003	165.8	1.044
1.5	35020	0.947	641.7	0.975	174.7	1.014
1.0	35750	0.940	675.6	0.951	182.4	0.987

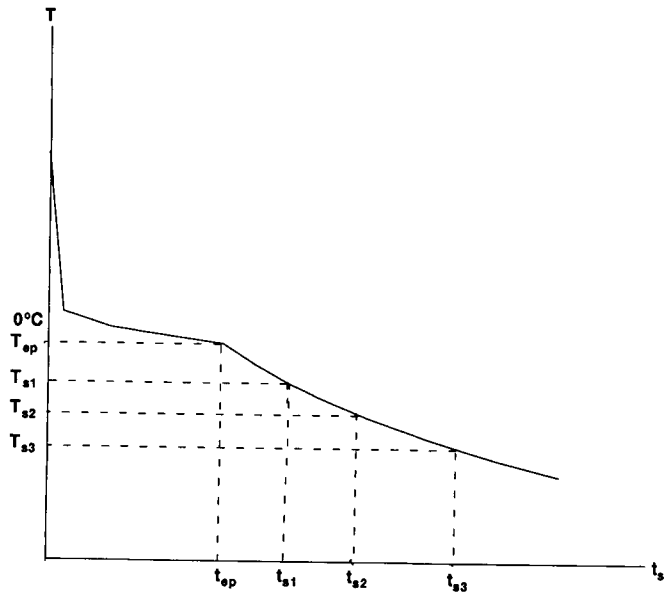


Fig. 4.10. Shut-in temperatures at a given depth – schematic curve.

base. As we mentioned before, the freezing of the water occurs in some temperature interval (Fig. 4.10). In practice, however, the moment of time $t = t_{ep}$ can not be determined. This can be done only by conducting long term continuous temperature observations in deep wells. Below we present a method of predicting formation temperatures in deep wells drilled in permafrost regions.

Let us assume that three shut-in temperatures T_{s1}, T_{s2}, and T_{s3} are measured at a given depth (Fig. 4.10). We can consider that the period of time $t_c^* = t_c + t_{s1}$ as a new "thermal disturbance" period. Then the "shut-in times" are

$$t_{s1}^* = t_{s2} - t_{s1}, \qquad t_{s2}^* = t_{s3} - t_{s1}$$

Now the wellbore temperature in formations can be determined from the integral 4.5 at the following dimensionless temperature distribution

$$T_{cD}^*(r_D, t_{xD}) = \begin{cases} 1, & 0 \le r_D \le 1 \\ 1 - \ln r_D / \ln R_x, & 1 \le r_D \le R_x \\ 0, & r_D > R_x \end{cases} \tag{4.46}$$

$$R_x = 1 + 2.184\sqrt{t_{xD}} \tag{4.47}$$

$$T_{cD}^*(r_D, t_{xD}) = \frac{T_c(r,t) - T_f}{T_{s1} - T_f}, \tag{4.48}$$

$$r_D = \frac{r}{r_{wx}}, \quad t_{xD} = \frac{a_f t_c^*}{r_{wx}^2}, \quad R_x = \frac{r_{ix}}{r_{wx}}$$

where r_{wx} is the radius of a cylindrical source with a constant wall temperature (T_{s1}) during the thermal disturbance period (t_c^*) and r_{ix} is the radius of thermal influence.

The temperature distributions 4.18 and 4.46 are similar and, therefore, the following equation is identical to Eq. 4.19

$$T_{sD}^* = \frac{T(0, t_s^*) - T_f}{T_{s1} - T_f} = 1 - \frac{Ei(-p^* R_x^2) - Ei(-p^*)}{2 \ln R_x}, \tag{4.49}$$

where

$$p^* = \frac{1}{4n^* t_{xD}}; \qquad n^* = \frac{t_s^*}{t_c^*} \tag{4.50}$$

By using measurements T_{s2}, T_{s3} and Eq. (4.49) we can eliminate the formation temperature T_f. After simple transformations we obtain

$$\frac{T_{s2} - T_{s1}}{T_{s3} - T_{s1}} = \frac{Ei(-p_1^* R_x^2) - Ei(-p_1^*)}{Ei(-p_2^* R_x^2) - Ei(-p_2^*)}, \tag{4.51}$$

where

$$p_1^* = \frac{1}{4n_1^* t_{xD}}, \quad p_2^* = \frac{1}{4n_2^* t_{xD}}, \quad n_1^* = \frac{t_{s1}^*}{t_c^*}, \quad n_2^* = \frac{t_{s2}^*}{t_c^*} \tag{4.52}$$

Substituting the value of R_x (relationship 4.47) into Eq. 4.51 we can obtain a formula for calculating the dimensionless disturbance time, t_{xD}. After this is possible to determine values of T_f, R_x, and $A = a_f/r_{wx}^2$. To speed up calculations we prepared a computer program "PERMTEMP" (Appendix C, Table C.6). In many cases this program was utilized to process field and laboratory data. Two examples are presented below.

Example 1.

Temperature measurements to a depth of 595 feet were made during a period of 6 years after drilling. The well was drilled for 63 days to a total depth of the well is 2,900 ft. The predicted by Lachenbruch and Brewer (1959) equilibrium formation temperatures are: -8.835^{o}C, -7.830^{o}C, and -6.735^{o}C (Fig. 4.7) for depths 355, 475, 595 ft respectively. On the average of 0.2^{o}C our results differ from these values. Our model does not take into account the effect of the geothermal gradient on the restoration of the natural temperature field of formations. This may contribute to difference of 0.2^{o}C. We should only to note that at calculations of T_f (Table 4.13) we used temperature measurements with short shut-in times. Let us estimate the values of r_{wx} and r_{ix} for the depth of 595 ft. From the first line (Table 4.13) we find that $A = a_f/r_{wx}^2 = 0.1721/day$. Let assume that the thermal diffusivity of the frozen formation is $a_f = 0.0030\ m^2/hr$, then

$$r_{wx} = \sqrt{24 \cdot 0.0030/0.1721} = 0.647\ (m)$$

$$r_{ix} = 0.647 + 2.184 \cdot 0.647 \cdot \sqrt{13.8} = 7.47\ (m)$$

Example 2.

An electrical heater was used by Dr. V. Devyatkin to simulate

Table 4.13 Observed shut-in temperatures T_{s1}, T_{s2}, and T_{s3} (Lachenbruch and Brewer, 1959) and calculated formation temperature T_f. Alaska, South Barrow Well 3

	T_{s1} °C	T_{s2} °C	T_{s3} °C	t^*_{s1} day	t^*_{s2} day	t^*_{s3} day	t_{xD}	A 1/day	R_x	T_f °C
depth 595 ft.						t_c **= 50 days**				
1	-2.163	-3.345	-4.829	80	87	117	13.8	0.1721	9.10	-6.541
2	-2.163	-3.345	-5.155	80	87	133	13.7	0.1712	9.08	-6.552
3	-2.163	-3.345	-5.542	80	87	167	13.8	0.1726	9.12	-6.536
4	-2.163	-3.345	-5.764	80	87	197	13.6	0.1701	9.06	-6.567
5	-2.163	-3.345	-6.191	80	87	338	13.3	0.1667	8.98	-6.609
6	-3.345	-4.829	-5.155	87	117	133	6.59	0.0758	6.61	-6.574
7	-3.345	-4.829	-5.542	87	117	167	6.89	0.0792	6.73	-6.533
8	-3.345	-4.829	-5.764	87	117	197	6.55	0.0752	6.59	-6.580
9	-3.345	-4.829	-6.191	87	117	338	6.27	0.0721	6.47	-6.621
depth 475 ft.						t_c **= 51 days**				
10	-2.741	-3.780	-4.452	74	81	88	8.66	0.1164	7.43	-7.648
11	-2.741	-3.780	-5.751	74	81	118	8.65	0.1161	7.42	-7.654
12	-2.741	-3.780	-6.079	74	81	134	8.69	0.1167	7.44	-7.638
13	-2.741	-3.780	-6.517	74	81	168	8.61	0.1156	7.41	-7.669
14	-2.741	-3.780	-6.752	74	81	199	8.59	0.1153	7.40	-7.677
15	-2.741	-3.780	-7.219	74	81	339	8.49	0.1140	7.36	-7.712
16	-3.780	-4.452	-5.751	81	88	118	8.05	0.0993	7.20	-7.376
17	-3.780	-4.452	-6.079	81	88	134	7.87	0.0970	7.13	-7.437
18	-3.780	-4.452	-6.517	81	88	168	7.57	0.0933	7.01	-7.542
19	-3.780	-4.452	-6.752	81	88	199	7.46	0.0920	6.97	-7.582
20	-3.780	-4.452	-7.219	81	88	339	7.25	0.0894	6.88	-7.666
depth 355 ft.						t_c **= 56 days**				
21	-4.550	-5.565	-6.122	79	86	93	9.92	0.1257	7.88	-8.845
22	-4.550	-5.565	-7.141	79	86	123	10.5	0.1335	8.09	-8.702
23	-4.550	-5.565	-7.380	79	86	139	10.8	0.1361	8.16	-8.658
24	-4.550	-5.565	-7.706	79	86	173	10.9	0.1378	8.20	-8.632
25	-4.550	-5.565	-7.890	79	86	204	10.9	0.1375	8.20	-8.636
26	-4.550	-5.565	-8.289	79	86	344	10.6	0.1341	8.11	-8.692
27	-5.565	-6.122	-7.141	86	93	123	9.06	0.1050	7.57	-8.435
28	-5.565	-6.122	-7.380	86	93	139	8.93	0.1036	7.53	-8.463
29	-5.565	-6.122	-7.706	86	93	173	8.73	0.1012	7.45	-8.509
30	-5.565	-6.122	-7.890	86	93	204	8.58	0.0995	7.40	-8.544
31	-5.565	-6.122	-8.289	86	93	344	8.18	0.0948	7.24	-8.649

Table 4.14 Experimental shut-in temperatures T_{s1}, T_{s2}, T_{s3} (Kutasov, 1976) and calculated formation temperature T_f

	T_{s1} °C	T_{s2} °C	T_{s3} °C	t_{s1} hrs	t_{s2} hrs	t_{s3} hrs	t_{xD}	A 1/hr	R_x	T_f °C
1	-1.35	-2.21	-2.82	54	57	66	125.	0.864	25.4	-4.35
2	-1.35	-2.21	-3.03	54	57	72	117.	0.805	24.6	-4.42
3	-1.35	-2.21	-3.09	54	57	78	140.	0.969	26.9	-4.24
4	-1.35	-2.21	-3.33	54	57	96	141.	0.974	27.0	-4.23
5	-1.35	-2.21	-3.49	54	57	120	149.	1.028	27.7	-4.18
6	-1.35	-2.21	-3.60	54	57	144	152.	1.045	27.9	-4.17
7	-2.21	-2.82	-3.33	57	66	96	33.7	0.228	13.7	-4.15
8	-2.21	-3.03	-3.49	57	72	120	49.6	0.335	16.4	-4.06
9	-2.21	-3.09	-3.60	57	78	144	30.3	0.205	13.0	-4.15
10	-2.52	-2.82	-3.33	60	66	96	21.4	0.142	11.1	-4.09
11	-2.52	-3.03	-3.49	60	72	120	26.7	0.177	12.3	-4.05
12	-2.52	-3.09	-3.60	60	78	144	16.1	0.107	9.77	-4.16
13	-0.37	-1.35	-2.21	51	54	57	23.2	0.164	11.5	-9.11
14	-0.37	-1.35	-2.52	51	54	60	30.9	0.217	13.1	-7.27
15	-0.37	-1.35	-2.71	51	54	63	36.0	0.253	14.1	-6.56

the drilling process (Kutasov, 1976). The heater operated for 91 hours in a model of a well placed in the underground (depth 15 m) laboratory of Permafrost Institute (Yakutsk, Russia). High temperature-sensitive thermistors were used to monitor the shut-in temperatures in the "borehole" (Table 4.14) and surrounding formations (sands). It was determined that only at -1°C the freezing of the water is practically completed. The last three runs (Table 4.14) show that, when a temperature measurement (-0.37°C) is taken while the refreezing process continues, the value of T_f cannot be determined with a sufficient accuracy.

4.4.5 Pressures Generated During Refreezing

Field studies have shown that external pressures will rise as thawed formations around the wellbore are refrozen (Perkins et al., 1974; Gryaznov, 1978). The limiting pressure values are very much dependent on natural temperature and composition of frozen formations, unfrozen water content, and salinity (Ruedrich and Perkins, 1974;

Dubina, 1988). As we mentioned earlier (Section 2.4.4), frozen formations are rheological bodies, in which an external constant load produces time dependent stresses and strains. To describe the behavior of frozen rocks, it is necessary to have access to the rheological equation of state that determines the correlation between stresses, strains, and time. However, due to experimental complexity, it is difficult to develop a rheological equation of state for *in situ* permafrost. Interesting results were obtained by the use of a mathematical simulation method in describing the pressure development process for elastic-plastic and viscous-elastic models (Dubina and Krasovitskiy 1983; Dubina, 1988).
Below we present an extreme case with a large safety factor: the deformation of frozen soils will be not considered and the maximum external pressure is a function of the formation temperature and mud salinity (Kutasov, 1995b).

Arctic drilling experience has shown that extensive washouts occur in the permafrost interval. Because of this the drilling mud can not be properly displaced prior to the surface casing. When a well is shut-in after drilling, thawed permafrost and water base fluids outside the casing will refreeze and generate inward radial loads around the well bore. The ability of the outer frozen permafrost to compress and accommodate the phase change expansion (about 9 percent volume increase at water-ice transition) determines the magnitude of the load around the well bore. Freezeback pressures will build up continuously during the refreeze process. Complete freezeback is not required for pressures to reach significant levels. Thus, in some cases large compressive loading can lead to buckling of the casing. As the pressure increases, the temperature of freezing (T_{fr}) of the water base mud decreases according to the empirical Bridgman-Tamman equation. In this case, when the difference between T_{fr} and the static temperature of permafrost T_f vanishes, the freezing process of water is terminated. Thus, the maximum pressures upon the casing are dependent on the permafrost temperature. If the collapse resistance of casing is known the corresponding critical temperature of casing (T_{cr}) can be estimated. For the 13.375 in. casing, which is usually used to protect the permafrost interval, the values of T_{cr} are calculated. To avoid collapsing of casing it is suggested to lower the mud freezing temperatures by utilization of a salt solution. A method of calculating the concentration of sodium chloride at which

the buckling of casing is impossible is presented.

The empirical Bridgman-Tamman formula (4.53) can be used to calculate values of T_{fr} at various freezeback pressures

$$P = 1 - 127T_{fr} - 1.519T_{fr}^2 \tag{4.53}$$

In Eq. 4.53, pressure (P) is in kgf/cm^2 and temperature is in ^{o}C. The Eq. 4.53 can be rewritten in the following form:

$$T_{fr} = -41.80 + \sqrt{1747.24 - 0.6583(P-1)} \tag{4.54}$$

It was shown that for small quantities of sodium chloride in the solution the freezing temperature-pressure-salt concentration relationship may be approximated by the following equation (Kutasov, 1977c)

$$T(C,P) = T(C,0) + T(0,P) \tag{4.55}$$

where, C is the quantity of sodium chloride in kilograms per 1000 liters (l) of water, $T(C,0)$ is the freezing temperature of the salt solution at atmospheric pressure, in ^{o}C,

$$T(C,0) = MC, \;\; M = -1000\, l{\cdot}^oC/17\, kg, \;\; T(C,0) > -10^oC \tag{4.56}$$

Here $T(0,P) = T_{fr}(P)$ is the freezing temperature according to the Bridgman-Tamman equation.

To determine the salt concentration C for which buckling of casing is impossible, we assume that $T(C,P) = T_f$ and $T(0,P) = T_{cr}$.

The critical temperatures T_{cr} for the 13.375 in. outside diameter (OD) casing were calculated from Formula 4.54 by assuming that the pressure (1 kgf/cm^2=14.22 psi) is equal to collapse resistance of the casing (Table 4.15). In this table the values of inside diameters (ID) are the standard ID sizes of the American Petroleum Institute (Halliburton Cementing Tables, 1979).

From Eqs. 4.55 and 4.56 we obtain

$$C = (T_f - T_{cr})/M \tag{4.57}$$

It is known that for slow freezing, the formed ice represents pure frozen water, while the salt ions remain in the unfrozen zone of the washouts. As the transition of the quantity of water into ice increases, the concentration of salt in the unfrozen portion of the washouts increases. But this means that, for practical purposes, it

Table 4.15 Critical temperatures for 13.375 in. casing

Grade casing	ID in.	P_{cr} *psi*	T_{cr} °F	T_{cr} °C
H-40	12.715	770	31.2	-0.42
J-55	12.615	1,130	30.9	-0.62
J-55	12.515	1,540	30.5	-0.85
J-55	12.415	1,950	30.0	-1.09
K-55	12.615	1,130	30.9	-0.62
K-55	12.515	1,540	30.5	-0.85
K-55	12.415	1,950	30.0	-1.09
C-75	12.347	2,590	29.4	-1.45
N-80	12.347	2,670	29.3	-1.50
C-95	12.347	2,820	29.2	-1.58

is impossible to attain values of the collapse resistance (pressure) if the original concentration of the solution is calculated from Formula 4.57. Also, the collapse rating of permafrost casing must be greater than the difference between external freezeback pressure and internal packer fluid pressure. This provides an additional safety factor against freezeback collapse; in our calculations the internal fluid pressure is neglected.

Example.
Let us assume that the grade N-80 casing (Table 4.15) is used to protect the permafrost interval. From the caliper log data it was determined that the drilling mud at some depth was not completely displaced prior to the surface casing, and the static temperature of permafrost at this depth is - 4.0°C (24.8°F). From Formula 4.57 we obtain the sodium chloride concentration

$$C = (-4.0^{o}C + 1.50^{o}C) \cdot (-17kg)/(1000l \cdot {}^{o}C), \quad C = 0.0425\ kg/l$$

Thus, the drilling fluid behind the casing should have a sodium chloride concentration of $C = 0.0425\ kg/l = 0.355\ ppg$.

Chapter 5

CEMENTING OF CASING

5.1 Strength and Thickening Time of Cement

In this Chapter we will consider methods of downhole temperature prediction while cementing of casing. It will be shown that for deep and hot wells the heat generation during cement hydration may cause a substantial temperature increase in the annulus. This factor must be taken into account in cement slurry design.
Temperature and pressure are two basic influences on the downhole performance of cement slurries. Temperature has the more pronounced influence (Swayze, 1954). The downhole temperature controls the pace of chemical reactions during cement hydration resulting in cement setting and strength development. The shut-in temperature affects how long the slurry will pump and how well it develops the strength to support the pipe. As the formation temperature increases, the cement slurry hydrates and sets faster and develops strength more rapidly. Cement slurries must be designed with sufficient pumping time to provide its safe placement in the well. At the same time the cement slurry can not be overly retarded as this will prevent the development of satisfactory compressive strength. The thickening time of cement is the time that the slurry remains pumpable under set conditions. The specifications of circulation temperature in the design of thickening times for oil well cement is very important. Two examples illustrate this point (Shell and Tragesser, 1972). A neat cement was tested at simulated bottomhole temperatures of 51.7°C (125°F) and 62.2°C (144°F). At 51.7°C it had a thickening time of 4 hr, 54 min and at 62.2°C the thickening time was only 2 hr, 57 min. Increasing the temperature

by 10.5°C decreased the thickening time by nearly 2 hr. Another cement, designed for greater depths, was tested at schedules which go to 96.7°C (206°F) and 120°C (248°F). At the lower temperature, it pumped for 3 hr, 2 min. The 23.3°C increase to 120°C reduced the pumping time by 88 min to 1 hr, 34 min. While retardes can extend thickening times, the thickening time for a given concentration of retarder is still very sensitive to changes in temperature. Slurries designed for erroneously high circulating temperatures can have unacceptably long setting times at lower temperatures. Another example, taken from files of the API Committee on Standardization of Oil-Well Cements, shows the importance of temperature on compressive strength development (Shell and Tragesser, 1972). One neat cement has an 8-hr compressive strength of 1,575 *psi* at 230°F (110°C), but, it did not set in that time at 200°F (93°C).
The effect of temperature on compressive strength development and thickening time for portland cements is shown in Figures 5.1 and 5.2.

5.2 Cement Heat Generation

5.2.1 Rate of Heat Generation Versus Time

When cement is mixed with water, an exothermic reaction occurs and a significant amount of heat is produced. This amount of heat depends mainly on the fineness and chemical composition of the cement, additives, and ambient temperature. The results of laboratory investigations of heat of hydration of pure cement compounds are presented in Table 5.1. Tricalcium silicate

Table 5.1 Heat of hydration of pure cement compounds (Smith, 1974)

Component	cal/g	Btu/lb
$3CaO \cdot Al_2O_3 (C_3A)$	207	373
$3CaO \cdot SiO_2 (C_3S)$	120	216
$4CaO \cdot Al_2O_3 \cdot Fe_2O_3 (C_4AF)$	100	180
$2CaO \cdot SiO_2 (C_2S)$	62	112

($CaO \cdot Al_2O_3$="C_3A") hydrates rapidly and is the main contribu-

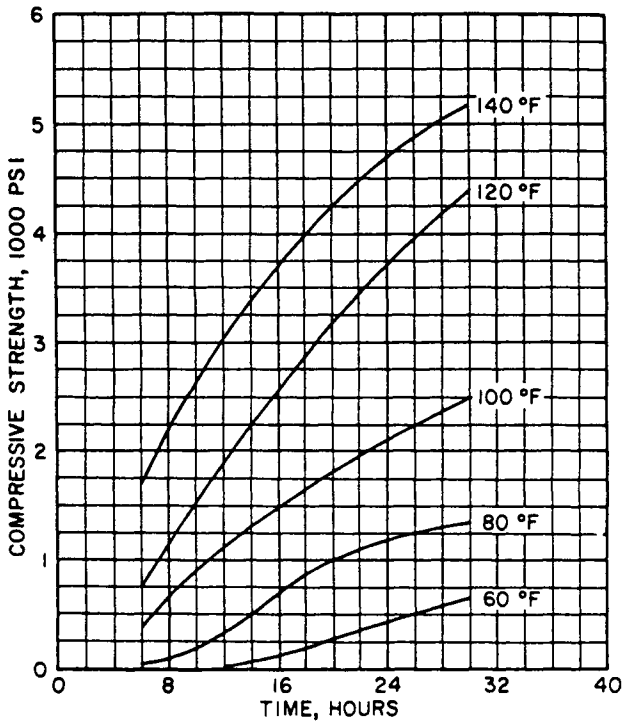


Fig. 5.1. Compressive strength of neat Class A cement (Davis and Faulk, 1952).

tor to the strength of the cement. In portland cement the average tricalcium silicate content is 45 to 65% with a maximum of 67% for high early-strength cement (Craft et al., 1962). From Table 5.1 one can see that tricalcium silicate is the main contributor to the heat of hydration. As in any exothermic reaction, the rate of heat generation during cement hydration increases with the increase of the ambient temperature. Previous studies of cement hydration have primarily measured only the total amount of heat generation over a long time periods. However, cement hydration reactions are complicated and the rate of heat generation is not constant (Fig. 5.3). Figure 5.4 depicts hypothetical relationships between temperature differences (caused by cement hydration) versus time. Referring to Fig. 5.4, Curve 1 corresponds to the high temperatures and Curve 2 to the low temperatures. For setting time t_s, we get $\Delta T_1 >> \Delta T_2$. Therefore, for deep wells heat generation during

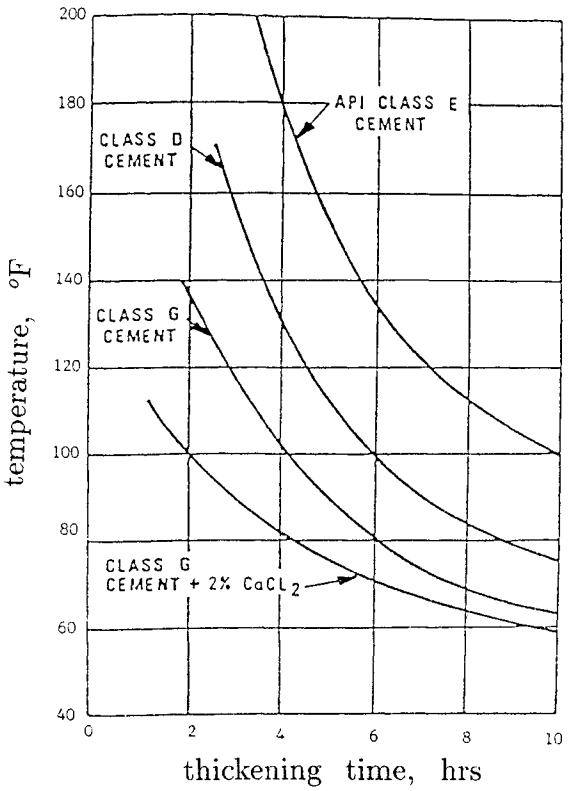


Fig. 5.2. The Influence of temperature on thickening time of typical portland cements at atmospheric pressure (Bearden, 1959).

cement hydration has to be taken into account at cement slurry design. The experimental data show that the maximum value of heat generation occurs during the first 5 to 15 hours. During this period the maximum temperature increase can be observed in the annulus.

It was found that a quadratic equation can be used for this time period to approximate the rate of heat generation (q) as a function of time (Targhi, 1987)

$$q = \pi(r_w^2 - r_c^2)\rho_c q_r q_D \tag{5.1}$$

$$q_D = a_o + a_1 t + a_2 t^2 \tag{5.2}$$

where r_c is the outside radius of casing, ρ_c is the density of cement, q_r is the reference rate of heat generation per unit of length, q_D is

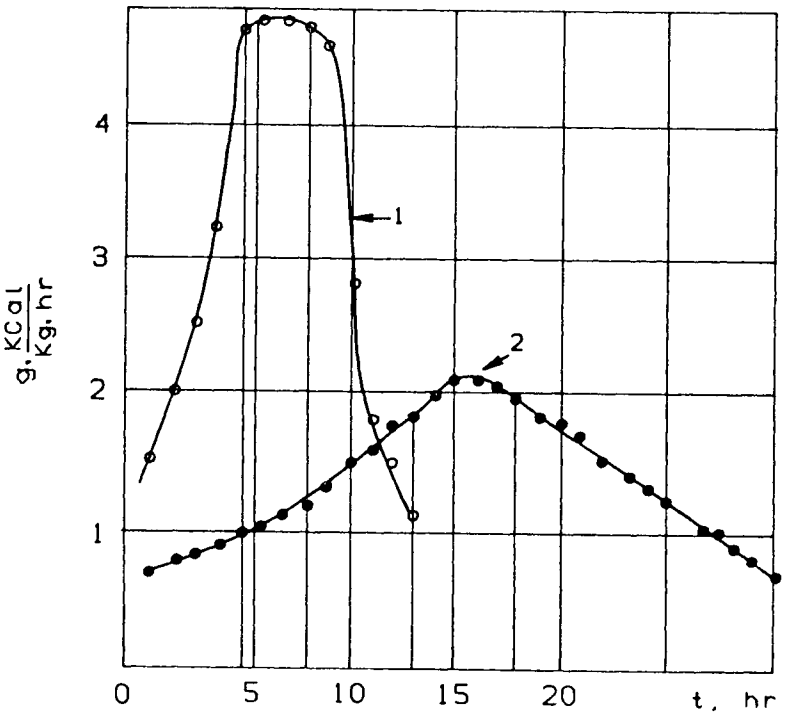


Fig. 5.3. Rate of heat generation versus time of hydration for portland cement (Proselkov, 1975). 1 – at temperatures 50-70°C, 2 – at temperatures 20-40°C.

the dimensionless rate of heat generation per unit of length, and a_o, a_1, a_2 are coefficients.

The reference rate of heat generation is an arbitrary parameter and, for simplicity, we assumed that $q_r = 1\ kcal/kg \cdot hr$. We also assumed that cement slurry starts to generate heat only when the pumping of cement is finished at time $t = 0$. In practice, however, cement slurry starts to generate heat during the final stages of pumping. Due to this assumption a_o, $= 0$ and

$$q_D = a_1 t + a_2 t^2 \tag{5.3}$$

Let now assume that at the moment of time $t = t_x$ the maximum value of $q = q_m$ is estimated from experimental data (Fig. 5.3). Usually the heat generation rate versus time is given per unit of

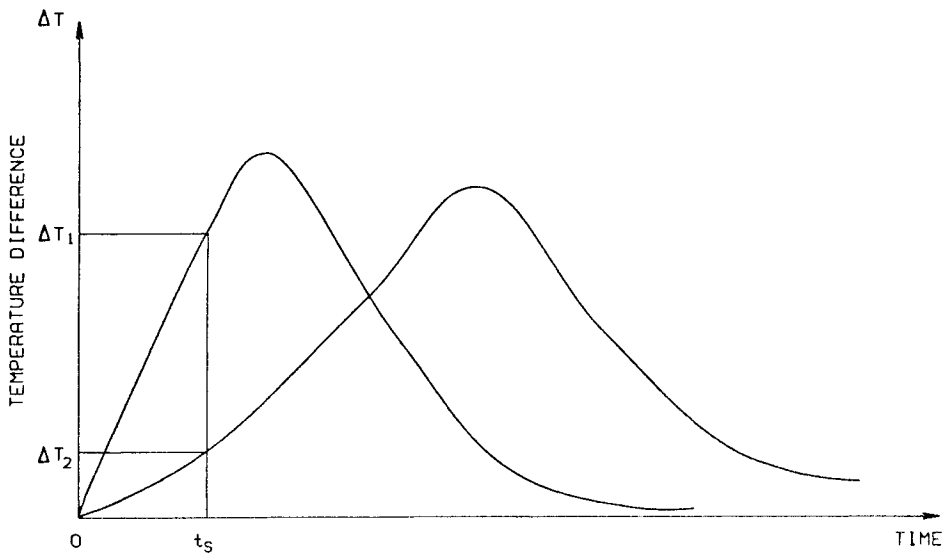


Fig. 5.4. Temperature difference between formation and cement temperatures during cement hydration.
1 – at high temperatures, 2 – at low temperatures

annulus area and per unit of density. Then

$$a_1 t_x + a_2 t_x^2 = q_{mD}, \qquad a_1 + 2a_2 t_x = 0 \tag{5.4}$$

$$a_1 = \frac{2q_{mD}}{t_x}, \qquad a_2 = \frac{q_{mD}}{t_x^2}, \qquad q_{mD} = \frac{q_m}{q_r}$$

Below we present the results of calculations coefficients a_1 and a_2 for two types of cement. It should be remembered that the shape of $q = q(t)$ curves depends mainly on the ambient (formation) temperature (Fig. 5.3) and chemical composition of the cement slurry. For this reason presented below calculations can be used only for illustrational purposes.

5.2.2 API Class H Cement and API Class A Cement

The API Class H cement can be used for a wide range of depths and temperatures. To determine the rate of heat generation for the API Class H Cement, Targhi (1987) used the $q = q(t)$ curve of the cement type A_1 (Milestone and Rogers, 1981). Cement type

A_1 has the closest properties to those of the Class H cement. It was found from the $q = q(t)$ curve that the maximum value of $q_m = 2.65\ Kcal/kg{\cdot}hr$ is reached after 7.2 hours of cement hydration (Targhi, 1987). Using Eqs. 5.4 we obtain

$$a_1 = 0.7361\ \frac{1}{hr}, \qquad a_2 = -\ 0.05112\ \frac{1}{hr^2}$$

$$q_D = 0.7361t - 0.05112t^2 \tag{5.5}$$

For API cement Class A the curves of Fig. 5.3 have been selected to determine the values of the coefficients a_1 and a_2.

For ambient temperatures of 50^o-70^oC we found from Fig. 5.3 (Curve 1) that the maximum value of $q_m = 4.950\ Kcal/kg \cdot hr$ was reached after 6.5 hours. Solving Eqs. 5.4 we obtain

$$a_1 = 1.5077\ \frac{1}{hr}, \qquad a_2 = -\ 0.1160\ \frac{1}{hr^2}$$

$$q_D = 1.5077t - 0.1160t^2 \tag{5.6}$$

Similarly, for ambient temperatures of 20^o-40^oC we found (Fig. 5.3, Curve 2) that the maximum value of $q_m = 2.14\ Kcal/kg \cdot hr$ was observed after 16.1 hours of cement hydration. From Eqs. 5.4 we obtain

$$a_1 = 0.2658\ \frac{1}{hr}, \qquad a_2 = -\ 0.008255\ \frac{1}{hr^2}$$

$$q_D = 0.2658t - 0.008255t^2 \tag{5.7}$$

5.3 Temperature Increase Due to Cement Hydration

5.3.1 Formula and Table

Temperature surveys following the cementing operation are used for locating the top of the cement column behind casing. Field experience shows that in some cases the temperature anomalies caused by the heat of cement hydration can be very substantial (Fig. 5.5). However, even in such cases it is very important to

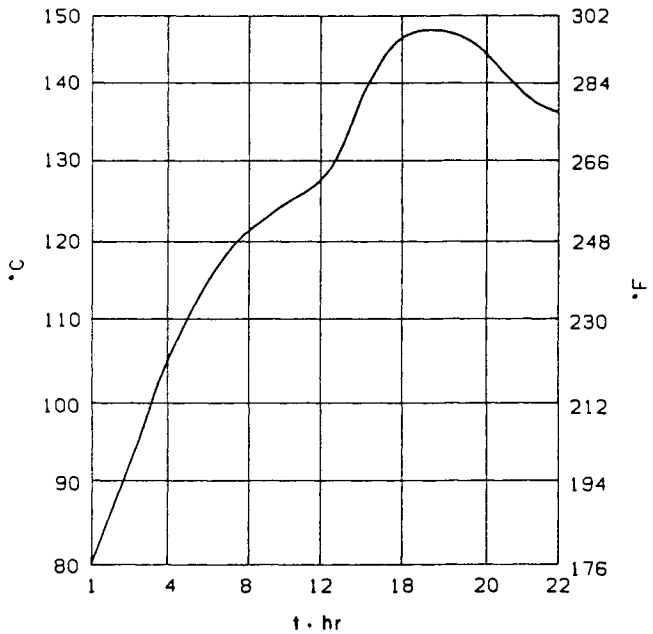


Fig. 5.5. Temperature during WOC (wait on cement setting), well 38, depth 2500 m; Stavropol district, Russia (Proselkov, 1975).

predict the temperature increase during the cement setting. This will allow to determine the optimal time lapse between cementing and temperature survey.

Below we present a formula which will allow one to estimate the temperature increase versus setting time. This formula is based on an approximate solution which describes the transient temperature at the cylinder's wall, while at the surface of the cylinder the radial heat flow rate (into formations) is a quadratic function of time. The suggested solution was validated by a comparison with the results of a numerical solution. Due to complexity of the obtained formula we present here a generalized relationship (Eq. 5.8) and Table 5.2.

$$\Delta T_{ch} = \frac{B\Delta T_{chD}}{4\pi\lambda_f} \tag{5.8}$$

$$\Delta T_{chD} = A_1 F_1 + A_2 F_2 \tag{5.9}$$

$$A_1 = \frac{a_1 r_c^2}{a_f}, \quad A_2 = \frac{a_2 r_c^4}{a_f^2}, \quad t_D = \frac{a_f t}{r_c^2} \tag{5.10}$$

$$B = \pi \rho_c q_r (r_w^2 - r_c^2) \tag{5.11}$$

where ΔT_{ch} is the temperature increase due to cement hydration, ΔT_{chD} is its dimensionless value, λ_f is the thermal conductivity of formations, F_1 and F_2 are dimensionless functions (Table 5.2), a_f is thermal diffusivity of formations, r_c is the outside radius of casing, and ρ_c is the density of cement slurry. We present below an example of calculation.

Example.
A temperature survey was conducted to locate the top of the cement column behind casing. The rate of heat generation is presented in Fig. 5.3 (Curve 1), setting time t=8.0 hrs, and the surrounding wellbore formation is clay. What is the value of ΔT_{ch}? The input parameters are: $2r_w = 12.250\ in.$,

$$a_1 = 1.5077\ 1/hr, \quad a_2 = -0.1160\ 1/hr^2, \quad 2r_c = 8.625\ in.$$

$$\rho_c = 1874\ kg/m^3, \quad a_f = 0.0015\ m^2/hr, \quad \lambda_f = 1.30\ kcal/hr \cdot m \cdot {}^oC$$

Step 1. Compute the dimensionless values of A_1 and A_2

$$A_1 = \frac{1.5077(8.625 \cdot 0.0254)^2}{0.0015 \cdot 4} = 12.06,$$

$$A_2 = -\frac{0.1160(8.625 \cdot 0.0254)^4}{0.0015^2 \cdot 2^4} = -7.422$$

Step 2. Determine the dimensionless cement setting time

$$t_D = \frac{0.0015 \cdot 8.0 \cdot 4}{(8.625 \cdot 0.0254)^2} = 1.00$$

Step 3. Using the Table 5.2 calculate the dimensionless parameter ΔT_{chD}. From Table 5.2 $F_1(1.00)$=0.355, $F_2(1.00)$=0.299 and

$$\Delta T_{chD} = 12.06 \cdot 0.355 - 7.422 \cdot 0.299 = 2.062$$

Step 4. Calculate the value of B

$$B = 3.1416 \cdot 1874 \cdot (12.250^2 - 8.625^2) \cdot 0.0254^2/4 = 71.855\ (kcal/m \cdot hr)$$

Step 5. And, finally, the temperature increase due to cement hydration is

$$\Delta T_{ch} = \frac{71.855 \cdot 2.062}{4 \cdot 3.1416 \cdot 1.30} = 9.07(^oC) = 16.3(^oF)$$

For this example we also calculated values of ΔT_{ch} for various cement setting times (Table 5.3). It is interesting to note that for several hours the temperature increase is practically constant ($\approx 9^o$C).

5.3.2 Size of the Annulus

From physical considerations it is clear that the maximum temperature anomaly (caused by cement hydration) depends on the actual well radius. For a gauge well the well diameter is equal to the bit size and the amount of cement slurry behind the casing can be estimated. In this case the transient temperatures while cement hydration can be determined from Formulas 5.8–5.11, providing that all input parameters are known. However, when some well sections are washout, the interpretation of temperature anomalies becomes difficult and a caliper log should be conducted prior to the cementing operations.

To demonstrate the impact of the annulus size on the maximum temperature increase we conducted calculations after Formulas 5.8-5.11 for a well drilled with a bit size of 12.250 in. and the outside diameter of casing is 8.625 in. It was assumed that due to washouts the well diameter can be increased by up to 8 inches. The rate of heat generation is presented in Fig. 5.3 (Curve 1), the density of cement slurry is $\rho_c = 1874\ kg/m^3$, and the surrounding wellbore formation is sandstone with the following thermal properties

$$a_f = 0.0034\ m^2/hr, \quad \lambda_f = 1.90\ kcal/hr \cdot m \cdot {}^oC$$

The results of calculations are presented in Fig. 5.6. As can be seen from Fig. 5.6, the hole enlargement significantly affects the maximum value of ΔT_{ch}.

An interesting experimental study of temperature anomalies, associated with cement setting behind casing, was conducted by Gretener (1968). In the experimental set the thickness of the inner annulus could be varied from 1/2 to 3 inches, the outer radius was 12 inches, and the height was 24 inches. In the outer annulus either sand and water (high thermal conductivity) or polyfoam and water (low thermal conductivity) simulated the formations. Maximum temperature anomalies ranging from less than 5^oC to as high 35^oC were observed during setting of Lone Star class A cement and Atlas portland class A cement. The experiments have shown that the maximum value of ΔT_{ch} rises almost linearly with the increase of the cement ring thickness (Gretener, 1968).

Table 5.2 The F_1 and F_2 functions

t_D	F_1	F_2	t_D	F_1	F_2	t_D	F_1	F_2
0.2	0.038	0.006	8.2	5.501	39.77	16.2	12.66	183.9
0.4	0.100	0.033	8.4	5.669	42.01	16.4	12.85	189.0
0.6	0.176	0.088	8.6	5.837	44.31	16.6	13.04	194.2
0.8	0.262	0.175	8.8	6.005	46.68	16.8	13.23	199.5
1.0	0.355	0.299	9.0	6.175	49.11	17.0	13.42	204.8
1.2	0.454	0.460	9.2	6.345	51.62	17.2	13.61	210.2
1.4	0.559	0.663	9.4	6.516	54.19	17.4	13.80	215.7
1.6	0.668	0.908	9.6	6.688	56.83	17.6	13.99	221.2
1.8	0.782	1.198	9.8	6.860	59.54	17.8	14.18	226.9
2.0	0.899	1.534	10.0	7.033	62.32	18.0	14.37	232.6
2.2	1.020	1.917	10.2	7.207	65.17	18.2	14.56	238.4
2.4	1.143	2.350	10.4	7.381	68.08	18.4	14.75	244.2
2.6	1.270	2.832	10.6	7.556	71.07	18.6	14.94	250.2
2.8	1.399	3.366	10.8	7.731	74.13	18.8	15.14	256.2
3.0	1.530	3.952	11.0	7.907	77.26	19.0	15.33	262.3
3.2	1.664	4.591	11.2	8.084	80.45	19.2	15.52	268.4
3.4	1.800	5.284	11.4	8.261	83.72	19.4	15.72	274.7
3.6	1.938	6.031	11.6	8.439	87.06	19.6	15.91	281.0
3.8	2.078	6.834	11.8	8.617	90.47	19.8	16.10	287.4
4.0	2.220	7.694	12.0	8.796	93.96	20.0	16.30	293.9
4.2	2.363	8.611	12.2	8.975	97.51	20.2	16.49	300.5
4.4	2.509	9.585	12.4	9.155	101.1	20.4	16.69	307.1
4.6	2.655	10.62	12.6	9.336	104.8	20.6	16.88	313.8
4.8	2.803	11.71	12.8	9.517	108.6	20.8	17.08	320.6
5.0	2.953	12.86	13.0	9.698	112.4	21.0	17.28	327.5
5.2	3.104	14.07	13.2	9.880	116.4	21.2	17.47	334.4
5.4	3.256	15.34	13.4	10.062	120.4	21.4	17.67	341.5
5.6	3.409	16.68	13.6	10.245	124.4	21.6	17.86	348.6
5.8	3.564	18.07	13.8	10.428	128.5	21.8	18.06	355.7
6.0	3.720	19.53	14.0	10.612	132.8	22.0	18.26	363.0
6.2	3.877	21.05	14.2	10.796	137.0	22.2	18.46	370.4
6.4	4.035	22.63	14.4	10.981	141.4	22.4	18.65	377.8
6.6	4.194	24.28	14.6	11.165	145.8	22.6	18.85	385.3
6.8	4.354	25.99	14.8	11.351	150.3	22.8	19.05	392.9
7.0	4.515	27.76	15.0	11.537	154.9	23.0	19.25	400.5
7.2	4.678	29.60	15.2	11.723	159.6	23.2	19.45	408.3
7.4	4.841	31.50	15.4	11.909	164.3	23.4	19.65	416.1
7.6	5.004	33.47	15.6	12.096	169.1	23.6	19.84	424.0
7.8	5.169	35.51	15.8	12.284	174.0	23.8	20.04	431.9
8.0	5.335	37.61	16.0	12.472	178.9	24.0	20.24	440.0

Table 5.2 – continued

t_D	F_1	F_2	t_D	F_1	F_2	t_D	F_1	F_2
24.2	20.44	448.1	32.2	28.60	840.1	40.2	37.02	1365.
24.4	20.64	456.4	32.4	28.81	851.6	40.4	37.23	1380.
24.6	20.84	464.7	32.6	29.02	863.1	40.6	37.45	1394.
24.8	21.04	473.0	32.8	29.22	874.8	40.8	37.66	1410.
25.0	21.24	481.5	33.0	29.43	886.5	41.0	37.87	1425.
25.2	21.44	490.0	33.2	29.64	898.3	41.2	38.09	1440.
25.4	21.65	498.6	33.4	29.85	910.2	41.4	38.30	1455.
25.6	21.85	507.3	33.6	30.06	922.2	41.6	38.51	1470.
25.8	22.05	516.1	33.8	30.27	934.3	41.8	38.73	1486.
26.0	22.25	525.0	34.0	30.47	946.4	42.0	38.94	1501.
26.2	22.45	533.9	34.2	30.68	958.6	42.2	39.16	1517.
26.4	22.65	543.0	34.4	30.89	971.0	42.4	39.37	1533.
26.6	22.86	552.1	34.6	31.10	983.4	42.6	39.59	1549.
26.8	23.06	561.2	34.8	31.31	995.8	42.8	39.80	1564.
27.0	23.26	570.5	35.0	31.52	1008.	43.0	40.01	1580.
27.2	23.47	579.8	35.2	31.73	1021.	43.2	40.23	1596.
27.4	23.67	589.3	35.4	31.94	1034.	43.4	40.44	1613.
27.6	23.87	598.8	35.6	32.15	1047.	43.6	40.66	1629.
27.8	24.08	608.4	35.8	32.36	1060.	43.8	40.87	1645.
28.0	24.28	618.0	36.0	32.57	1072.	44.0	41.09	1662.
28.2	24.48	627.8	36.2	32.78	1086.	44.2	41.30	1678.
28.4	24.69	637.6	36.4	32.99	1099.	44.4	41.52	1695.
28.6	24.89	647.5	36.6	33.20	1112.	44.6	41.74	1711.
28.8	25.10	657.5	36.8	33.41	1125.	44.8	41.95	1728.
29.0	25.30	667.6	37.0	33.62	1139.	45.0	42.17	1745.
29.2	25.51	677.8	37.2	33.84	1152.	45.2	42.38	1762.
29.4	25.71	688.0	37.4	34.05	1166.	45.4	42.60	1779.
29.6	25.92	698.35	37.6	34.26	1179.	45.6	42.82	1796.
29.8	26.12	708.75	37.8	34.47	1193.	45.8	43.03	1813.
30.0	26.33	719.24	38.0	34.68	1207.	46.0	43.25	1830.
30.2	26.53	729.82	38.2	34.89	1221.	46.2	43.46	1848.
30.4	26.74	740.47	38.4	35.11	1235.	46.4	43.68	1865.
30.6	26.95	751.21	38.6	35.32	1249.	46.6	43.90	1882.
30.8	27.15	762.03	38.8	35.53	1263.	46.8	44.11	1900.
31.0	27.36	772.93	39.0	35.74	1277.	47.0	44.33	1918.
31.2	27.56	783.91	39.2	35.95	1292.	47.2	44.55	1936.
31.4	27.77	794.98	39.4	36.17	1306.	47.4	44.77	1953.
31.6	27.98	806.13	39.6	36.38	1321.	47.6	44.98	1971.
31.8	28.19	817.36	39.8	36.59	1335.	47.8	45.20	1989.
32.0	28.39	828.68	40.0	36.81	1350.	48.0	45.42	2008.

Table 5.3 The values of ΔT_{ch} versus time

t	t_D	q_D	ΔT_{ch}	ΔT_{ch}
hrs			°C	°F
5.0	0.625	4.639	6.72	12.09
6.0	0.750	4.870	7.80	14.04
6.5	0.813	4.899	8.24	14.83
7.0	0.875	4.870	8.60	15.48
8.0	1.000	4.638	9.07	16.33
8.6	1.075	4.387	9.19	16.54
8.8	1.100	4.285	9.20	16.56
9.0	1.125	4.173	9.19	16.54
9.2	1.150	4.053	9.17	16.50
9.4	1.175	3.923	9.13	16.43
10.0	1.250	3.477	8.91	16.04
11.0	1.375	2.549	8.21	14.77
12.0	1.500	1.388	7.06	12.71

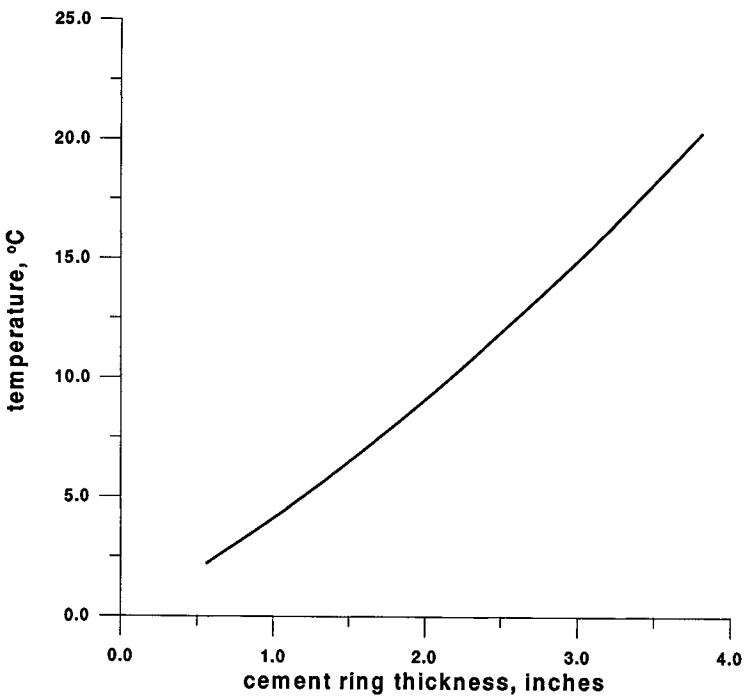


Fig. 5.6. Maximum temperature increase versus cement ring thickness.

5.3.3 Thermal Properties and Temperature of Formations

From Formulas 5.8-5.11 follows that the value of ΔT_{ch} depends on thermal diffusivity and thermal conductivity of formations. We conducted a set of numerical calculations to estimate the effect of thermal parameters of formations on the transient temperatures during cement hydration. In all cases we used the Curve 1 (Fig. 5.3) and the sizes of the annulus varied in wide ranges. An unexpected outcome of these calculations is the conclusion that, for typical reservoir formations, variations of thermal properties has a small effect on the values of ΔT_{ch} (Table 5.4). Targhi (1987) approximated the thermal effect of cement hydration by a linear source whose strength is a quadratic function of time. Targhi conducted calculations of ΔT_{ch} for all practically possible combinations of bit and casing sizes. It was also shown that the impact of variation of thermal properties on temperature increase is not substantial (Targhi, 1987).
To determine the effect of formations (ambient) temperatures and pressures on the values of T_{ch} the rate heat flow $q = q(t)$ should be measured in the laboratory at temperatures and pressures which are close to those in downhole conditions. For illustration we conducted calculations of the temperature increase for two ambient temperature ranges (Table 5.5). Again, the Formulas 5.8-5.11 and Fig. 5.3 (Curve 1) were utilized at calculations. From Table 5.5 follows that at low formation temperature the cement setting time can be very large and it is more difficult to detect the top of the cement column by a temperature survey.

5.4 Bottomhole Fluid Circulating Temperatures

5.4.1 Field Data and Empirical Formula

In 1941 Farris developed bottomhole temperature charts based on measurements of mud circulating temperatures in five Gulf coast wells. These charts were then used by the American Petroleum Institute (API) to develop a pumping test procedure to predict bottomhole temperatures during mud circulation (T_{mb}). In 1977 the API task group presented new casing cementing and well-

Table 5.4 The influence of formations thermal properties on the temperature increase during hydration of the API cement Class A

Formation	a $\frac{m^2}{hr}$	λ_f $\frac{kcal}{hr \cdot m \cdot {}^oC}$	t hrs	ΔT_{ch} ^oC
sandstone	0.0034	1.90	4.0	4.99
			6.0	7.05
			8.0	8.04
			10.0	7.71
			12.0	5.86
clay shale	0.0022	1.40	4.0	5.79
			6.0	8.29
			8.0	9.56
			10.0	9.28
			12.0	7.22
clay	0.0015	1.30	4.0	5.40
			6.0	7.80
			8.0	9.08
			10.0	8.91
			12.0	7.06

Table 5.5 Temperature increase due to hydration for two ambient temperature ranges. Formation – sandstone, bit size – 12.250 in., casing size – 8.625 in.

$50^o - 70^oC$			$20^o - 40^oC$		
t hrs	ΔT_{ch} ^{o}C	ΔT_{ch} ^{o}F	t hrs	ΔT_{ch} ^{o}C	ΔT_{ch} ^{o}F
4.0	5.81	10.46	10.0	2.94	5.29
5.0	7.14	12.86	12.0	3.45	6.21
6.0	8.22	14.79	14.0	3.87	6.96
7.0	8.97	16.15	16.0	4.18	7.53
8.0	9.37	16.87	18.0	4.39	7.90
9.0	9.38	16.89	20.0	4.47	8.05
10.0	8.98	16.16	22.0	4.43	7.97
11.0	8.13	14.64	24.0	4.25	7.66
12.0	6.82	12.28	26.0	3.94	7.10

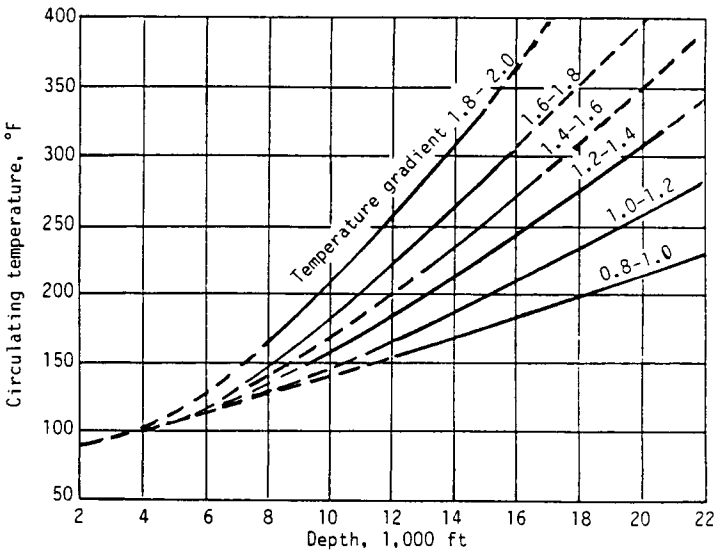


Fig. 5.7. API Test Schedules (New Cement Test..., 1977).

simulation test schedules (New Cement Test..., 1977). Fourty-one measurements of bottomhole circulating temperature in water muds were available to estimate thew correlation between the values of T_{mb}, geothermal gradient Γ, and vertical depth. Curves were fitted through the measured points for each of the geothermal gradient ranges, thus developing a family of curves (Fig. 5.7). From the curves in Fig. 5.7, schedules were developed to provide laboratory test procedures for simulating cementing of casing (New Cement Test..., 1977; API Specifications..., 1982).

Although some studies (Venditto and George, 1984; Jones, 1986) show an overall agreement with the API schedules, some operators feel that these schedules overestimate the bottomhole circulating temperatures in deep wells and will modify them (Bradford, 1985). It should be also be mentioned that for high geothermal gradients and deep wells, the API circulating temperatures are estimated by extrapolation (Fig. 5.7). Because of the higher temperatures encountered in geothermal wells, cement design is similar to that for deep oil or gas wells having high bottomhole temperatures (Edwards et al., 1982). Here one should to note that the current API correlations which are used to determine the bottomhole circulating

temperature permit prediction in wells with geothermal gradients up to only $2^oF/100ft$ ($3.6^oC/100m$); whereas in geothermal wells average temperature gradients up to $5 - 8^oC/100m$ are common.

Since 1977 new measurements of bottomhole circulating temperatures have been conducted (Sump and Williams, 1973; Venditto and George, 1984; Wooley et al., 1984; Jones, 1986). These data and information gathered by the API task group on bottomhole circulating temperatures (Shell and Tragesser, 1972) were used to modify the API bottomhole circulation temperature-geothermal gradient-vertical depth relationships (Kutasov and Targhi, 1987). It was found that the bottomhole circulating temperature (T_{mb}) can be approximated with sufficient accuracy as a function of two independent variables: the geothermal gradient (Γ) and the the bottomhole static (undisturbed) temperature (T_{fb}). Assuming that for deep wells T_{mb} is a linear function of T_{fb}, we found that the following empirical expression can be used for predicting bottomhole circulating temperature

$$T_{mb} = a_1 + a_2\Gamma + (a_3 - a_4\Gamma)T_{fb} \tag{5.12}$$

For 79 field measurements (Kutasov and Targhi, 1987), a multiple regression analysis computer program was used to obtain the coefficients of formula (5.12)

$$a_1 = 50.64^oC\ (-102.1^oF); \qquad a_2 = 804.9\ m\ (3354\ ft);$$

$$a_3 = 1.342; \qquad a_4 = 12.22\ m^oC^{-1}\ (22.28\ ft\ ^oF^{-1})$$

These coefficients are obtained for

$$74.4^oC\ (166^oF)\ \leq T_{fb}\ \leq 212.2^oC\ (414^oF)$$

and

$$1.51^oC/100m\ (0.83^oF/100ft)\ \leq \Gamma\ \leq 4.45^oC/100m\ (2.44^oF/100\ ft)$$

Therefore, equation (5.12) should be used with caution for extrapolated values of T_{fb} and Γ. The accuracy of the results (Formula 5.12) is 4.6^oC (8.2^oF) and was estimated from the sum of squared residuals. The values of T_{fb} can also be expressed as a function of average surface temperature (T_o) and total vertical depth (H)

$$T_{fb} = T_o + \Gamma H \tag{5.13}$$

In Formulas 5.12 and 5.13 Γ is an averaged geothermal gradient. The values of T_o for North America are presented in literature (Jorden and Campbell, 1984). In Table 5.6 the measured and calculated values of bottomhole circulating temperatures for wells with $T_{fb} \geq 139^oC$ are compared. The measurements 1-7 (West Texas, Gulf Coast of Texas and Louisiana), 8-23 (Texas, Lousiana), 24, 25-27 (Mississippi) and 28-32 (Table 5.6) were taken from Shell and Tragesser (1972), Venditto and George (1984), Jones (1986), Wooley et al. (1984) and Sump and Williams (1973) respectively.

5.4.2 Comparison with API Schedules

In Table 5.7 the API test schedules (New cement test..., 1977) and values of T_{mb} calculated by formulas (5.12) and (5.13) are compared. It can be concluded that for deep wells and high temperature gradients the API bottomhole circulating temperatures are too high. We recommend the use of Eq. 5.12 for estimating the bottomhole circulating temperature (Table 5.8). It is possible that the coefficients in Formula 5.12 should be corrected to account for very high geothermal gradients which are common for geothermal wells.

Table 5.6 Measured T^*_{mb} and predicted T_{mb} bottomhole circulating temperatures. T_{fb} – bottomhole static temperature, $\Delta T = T^*_{mb} - T_{mb}$

#	Well	H m	G $^oC/100m$	T_{fb} ^oC	T^*_{mb} ^oC	T_{mb} ^oC	ΔT ^oC
1	8	6050	3.01	205	177	173	4
2	9	6926	2.08	167	146	147	-1
3	10	4237	4.45	212	145	154	-9
4	12	4876	3.14	176	146	143	3
5	16	3747	3.70	162	121	123	-2
6	16	3461	3.44	143	112	109	3
7	16	4887	3.30	185	140	149	-9
8	4	3962	3.37	160	130	125	5
9	5	4454	3.24	171	134	137	-3
10	16	5333	2.46	158	128	133	-5
11	22	4206	2.90	148	118	119	-1
12	27	3352	3.54	145	106	109	-3
13	27	3535	3.52	151	113	115	-2
14	35	3627	3.68	160	131	121	10
15	36	5427	2.48	161	131	136	-5
16	38	5056	2.64	160	138	133	5
17	38	5529	2.57	168	148	143	5
18	38	5898	2.68	184	165	158	7
19	40	3266	3.44	139	110	105	5
20	46	4389	3.17	165	141	132	9
21	47	4079	3.63	175	137	135	2
22	47	4518	3.43	181	142	144	-2
23	51	3806	3.30	152	121	118	3
24	4	3718	3.28	145	112	112	0
25	MS	4900	2.72	153	129	126	3
26	MS	6534	2.55	187	163	162	1
27	MS	7214	2.57	206	178	182	-4
28	1	4578	2.86	157	137	128	9
29	2	4971	2.95	169	142	139	3
30	3	4571	2.92	156	123	127	-4
31	8	5486	3.46	211	179	171	8
32	9	6926	2.11	167	146	148	-2

Table 5.7 Bottomhole circulating temperature. First line: prediction by the empirical formula, second line: API Test Schedules (Oil and Gas Journal, 25 July 1977), surface temperature 23.9°C (75°F)

Depth	Geothermal gradient, $°C/100\ m$								
m/ft	1.640	2.005	2.3695	2.734	3.099	3.463	3.828	4.192	4.557
1,219	-	-	-	-	-	38.0	41.8	45.3	48.4
4,000	37.2	37.8	38.3	38.9	39.4	40.0	-	-	-
1,829	-	-	39.2	45.8	51.9	57.3	62.2	66.5	70.2
6,000	37.2	37.8	38.3	38.9	39.4	40.0	-	-	-
2,438	-	45.3	54.4	62.6	70.1	76.7	82.6	87.7	92.0
8,000	52.2	53.9	57.2	60.0	63.3	71.1	-	-	-
3,047	46.9	58.7	69.6	79.4	88.3	96.1	103.0	108.9	113.8
10,000	60.6	61.1	70.0	75.0	82.2	93.3	-	-	-
3,657	58.3	72.1	84.8	96.2	106.5	115.5	123.4	130.1	135.6
12,000	68.3	73.9	85.0	91.7	102.8	119.4	-	-	-
4267	69.7	85.5	100.0	113.0	124.6	134.9	143.8	151.3	157.4
14,000	76.1	86.1	101.7	111.7	125.6	145.0	-	-	-
4876	81.1	98.9	115.2	129.8	142.8	154.3	164.2	172.5	179.2
16,000	83.9	98.9	118.3	132.2	150.0	171.1	-	-	-
5486	92.5	112.3	130.4	146.6	161.0	173.7	184.6	193.7	201.0
18,000	92.8	112.2	136.1	153.3	175.0	196.1	-	-	-
6095	104.0	125.7	145.6	163.4	179.2	193.1	205.0	214.9	222.8
20,000	101.7	126.1	155.6	175.6	200.0	221.7	-	-	-

Table 5.8 Bottomhole circulating mud temperature, (Formula 5.12)

T_{fb}	Geothermal gradient, $°C/100\ m$							
$°C$	1.5	2.0	2.5	3.0	3.5	4.0	4.5	5.00
80	54	53	52	51	50	49	48	48
85	59	58	57	56	55	54	52	51
90	65	64	62	61	59	58	56	55
95	71	69	67	66	64	62	60	59
100	77	75	73	71	68	66	64	62
105	83	80	78	75	73	71	68	66
110	88	86	83	80	78	75	72	69
115	94	91	88	85	82	79	76	73
120	100	97	93	90	87	83	80	77
125	106	102	99	95	91	88	84	80
130	112	108	104	100	96	92	88	84
135	117	113	109	105	100	96	92	88
140	123	119	114	110	105	100	96	91
145	129	124	119	114	110	105	100	95
150	135	130	124	119	114	109	104	99
155	140	135	130	124	119	113	108	102
160	146	141	135	129	123	118	112	106
165	152	146	140	134	128	122	116	110
170	158	152	145	139	132	126	120	113
175	164	157	150	144	137	130	124	117
180	169	162	156	149	142	135	128	121
185	175	168	161	153	146	139	132	124
190	181	173	166	158	151	143	136	128
195	187	179	171	163	155	147	139	132
200	193	184	176	168	160	152	143	135
205	198	190	181	173	164	156	147	139
210	204	195	187	178	169	160	151	143
215	210	201	192	183	174	164	155	146
220	216	206	197	188	178	169	159	150

5.5 Designing Cementing Programs for Deep Wells

5.5.1 Utilization of MWD Temperature Logs

Thus, to estimate the bottomhole circulating temperature and to design a cementing program, the values of the geothermal gradient and the bottomhole static temperature should determined with a sufficient accuracy. However, when drilling operations are conducted in offshore or new areas, these parameters are usually not known.

Oil and gas companies routinely conduct downhole and bottomhole temperature measurements while drilling (MWD). However, the well shut-in periods are usually very short and it is difficult to use these data for determination of the formation temperature and geothermal gradient. To use the results of temperature surveys, we present below a method of utilization MWD temperature logs deep wells (up to 7000 m). The suggested method allows one to estimate bottomhole formation (undisturbed) temperatures and the geothermal gradient. This method combines the use of an empirical formula (5.12) and of some analytical relationships. Three cases will be considered:

A. Let us assume that at some vertical depth H_A during drilling were measured the stabilized value of bottomhole circulating temperature T_{cA} and one value of shut-in temperature T_{sA} (at a short shut-in time). In this case for the depths H_A and H_B ($H_A < H_B$) the method allows to estimate values of T_{fA}, T_{fB}, T_{cB}, and Γ.

B. Let us assume that at two depths H_A and H_B during drilling were measured stabilized values of bottomhole circulating temperatures T_{cA} and T_{cB} In this case for the depths H_A, H_B and H_C ($H_A < H_B < H_C$) the method allows to estimate values of T_{fA}, T_{fB}, T_{fC}, T_{cC}, and Γ.

C. Let us now assume that at two depths H_A and H_B during drilling were measured values of shut-in temperatures; or one downhole temperature log is available. In this case for the depths H_A, H_B, and H_C the method allows to estimate values of T_{fA}, T_{fB}, T_{cB}, T_{cA}, and Γ. To illustrate the application of the proposed method four field examples are presented below.

As we mentioned earlier (Section 3.2.2), the temperature surveys in many deep wells have shown that both the outlet drilling mud temperature and the bottomhole circulating temperatures after some period of mud circulation – stabilization time (Eq. 3.43) becomes practically constant. For a constant well wall temperature a solution which describes the dimensionless temperature distribution in formation surrounding the wellbore during the fluid circulation is given by Eq. 3.74. The Eq. 3.74 can be is expressed in a general form

$$T_D = \frac{T_(r,t) - T_f}{T_c - T_f} = f(t_D, r_D); \qquad r_D \geq 1 \tag{5.14}$$

where t_D is the dimensionless mud circulation time at a given depth and r_D is the dimensionless radial distance.
It was also shown that Formula 4.7 with good accuracy approximates the dimensionless downhole shut-in temperature T_{sD}.

$$T_{sD} = \frac{T_s - T_f}{T_c - T_f} = \gamma(t_D, t_{sD}), \qquad t_{sD} = \frac{at_s}{r_w^2} \tag{5.15}$$

where t_{sD} is the dimensionless shut-in time.
By the use of several field examples we will show the technique of utilization Formulas 5.12-5.15 in determining values of the geothermal gradient and bottomhole static (undisturbed) temperature.

In the first example (Table 5.9a.) we assumed that the well was shut-in for 12 hrs. The values of T_{cA} and T_{sA} (Wooley, et. al., 1984) were used to calculate parameter T_{fA} after Formula 5.15. In this case four equations were used to determine the values T_{fA}, T_{fB}, T_{cB}, and Γ. From Formula 5.15 one obtains

$$\gamma_A = \frac{T_{sA} - T_{fA}}{T_{cA} - T_{fA}}, \tag{5.16}$$

and following equations can be written as:

$$T_{cA} = a_1 + a_2\Gamma + (a_3 - a_4\Gamma)T_{fA} \tag{5.17}$$

$$T_{cB} = a_1 + a_2\Gamma + (a_3 - a_4\Gamma)T_{fB} \tag{5.18}$$

$$T_{fB} = T_{fA} + \Gamma\ (H_B - H_A) \tag{5.19}$$

In the cases b and c two additional equations were used

$$T_{cC} = a_1 + a_2\Gamma + (a_3 - a_4\Gamma)T_{fC} \tag{5.20}$$

Table 5.9 Predicted and measured values of T_f and Γ

Input data	Calculated data	Field data
a. Deep Mississippi well (Wooley, et. al., 1984)		
H_A=6534 m, H_B=7214 m	T_{fA}=187.2°C	T_{fA}=187.2°C
T_{sA}=171.8°C, T_{cA}=162.8°C	T_{cB}=180.6°C	T_{cB}=177.2°C
r_w=0.0792 m, a=0.0037 m^2/hr	T_{fB}=204.4°C	T_{fB}=204.4°C
t_c @ H_A=50 days, t_S @ H_A=12 hrs	Γ=0.0255 K/m	
b. Well # 16 (Shell and Tragesser, 1972)		
H_A=3177 m,	T_{fA}=134.4°C	T_{fA}=135.0°C
H_B=3747 m	T_{fB}=151.1°C	T_{fB}=162.8°C
H_C=4887 m	T_{fC}=185.6°C	T_{fC}=185.0°C
T_{cA}=104.4°C	T_{cC}=154.4°C	T_{cC}=148.9°C
T_{cB}=121.1°C	Γ=0.0299 K/m	
c. Well # 38 (Venditto and George, 1984)		
H_A=5056 m	T_{fA}=156.7°C	T_{fA}=160.0°C
H_B=5529 m	T_{fB}=165.6°C	T_{fB}=168.3°C
H_C=5898 m	T_{fC}=172.8°C	T_{fC}=184.4°C
T_{cA}=138.3°C	T_{cC}=156.1°C	T_{cC}=165.0°C
T_{cB}=148.3°C	Γ=0.0191 K/m	
d. Deep Mississippi well (Wooley, et. al., 1984)		
H_A=6534 m, H_B=7214 m	T_{fA}=188.9°C	T_{fA}=187.2°C
T_{sA}=171.8°C, T_{sB}=196.7°C	T_{fB}=207.8°C	T_{fB}=206.7°C
r_w=0.0792 m, a=0.0037 m^2/hr	T_{cA}=161.7°C	T_{cA}=163.3°C
t_c @ H_A=50 days, t_c @ H_B=48 hrs	T_{cB}=180.6°C	T_{cB}=172.2°C
t_s @ H_A=12 hrs, t_s @ H_B=12 hrs	Γ=0.0275 K/m	

$$T_{fC} = T_{fA} + \Gamma\ (H_C - H_A) \tag{5.21}$$

From Formulas 5.17-5.21 one obtains the values of T_{fA}, T_{fB}, T_{fC}, T_{cC}, and Γ.

In the last case (Table 5.9d) we assumed that a temperature log was conducted in the well. Like as in the first case, the field data (Wooley, et. al., 1984) were used to calculate values of T_{sA} and T_{sB}. From Formula 5.15 we obtain

$$\gamma_B = \frac{T_{sB} - T_{fB}}{T_{cB} - T_{fB}}, \tag{5.22}$$

The system of equations (5.16-5.19 and 5.22) allows one to calculate values of T_{fA}, T_{fB}, T_{cA}, T_{cB}, and Γ.

5.5.2 Predicting the Geothermal Gradient in Offshore Areas

Let us now assume that well is drilled in a offshore area and the formation temperature (geothermal gradient) cannot be estimated with sufficient accuracy. In this case, we suggest method which utilizes the results of downhole circulating temperatures logs for geothermal gradients predictions.

From Formulas 5.12 and 5.13 one obtains:

$$\Gamma^2 + B_1\Gamma + B_o = 0 \tag{5.23}$$

where

$$B_1 = \frac{a_4T_o - a_2 - a_3H}{a_4H}, \qquad B_o = \frac{T_{mb} - a_1 - a_3T_o}{a_4H}$$

The solution of Eq. (5.23) is:

$$\Gamma = -\frac{B_1}{2} - \sqrt{\frac{B_1^2}{4} - B_o} \tag{5.24}$$

Examples.

Two examples (Table 5.10) show how Eq. 5.24 predicts the geothermal gradient. In the first part of Table 5.10 are the field temperature surveys of T_{mb} and Γ^* for Well No. 16 (Shell and Tragesser, 1972). The comparison shows that the calculated values of the geothermal gradient, Γ, agrees well with the surveyed values of Γ^*.

In the Gulf of Mexico example, only records of the bottomhole circulating temperatures were available for the well (Holmes and Swift, 1970). One should to note that for onshore wells T_o is the undisturbed formation temperature at the depth of 50-60 ft (15-18 m). For offshore wells, T_o can be assumed to be the temperature of sea bottom sediments. The calculations show that geothermal gradient prediction is very dependent on the estimated average surface temperature (Kutasov, 1995a).

5.5.3 Production Liners

The design of cement slurries becomes more critical when a casing liner is used because the performance requirements should be

Table 5.10 Observed and calculated geothermal gradients

	H ft	T_o ^oF	T_{mb} ^oF	Γ $^oF/100ft$	Γ^* $^oF/100ft$	Γ/Γ^*
Well No. 16	5,520	75	146	2.40	2.31	1.04
	10,424	75	220	2.01	1.92	1.05
	11,356	75	235	1.99	1.89	1.05
	12,294	75	250	1.96	2.03	0.97
	16,035	75	285	1.66	1.81	0.92
Gulf of Mexico	7,000	60	163	2.41	-	-
well	10,000	60	180	1.75	-	-
	11,500	60	197	1.65	-	-
	14,000	60	208	1.60	-	-
	12,500	60	232	1.61	-	-
	15,000	60	243	1.56	-	-

simultaneously satisfied at the top and at the bottom of the liner. Formation (undisturbed) temperatures and fluid circulation temperatures at the top of the liner may be much lower than those at the bottom of the liner. Thus, in designing the cement slurry knowledge of the actual temperature to which it is exposed is an important factor. In deep wells the actual downhole temperature during cement setting may significantly differ from the formation temperature. It should be also taken into account that a time lapse exists between the end of mud circulation and placement of the cement. For this reasons it is logical to assume that the bottomhole shut-in temperature should be considered as parameter in the cement slurry design.
Targhi (1987) used actual field data for four deep wells and calculated (after Formula 4.7) shut-in temperatures at the top an at the bottom of four liners.

Below we present the results of calculations for one well drilled in Bee County, Texas (Targhi, 1987). The field data: mud circulation and formation temperatures, depths, and well configuration were taken from the paper by Tragesser and Parker (1972).

A liner was set at a depth of 10,424 to 12,294 feet. A period of 44.5 days was needed to drill this interval. In addition to this, two days were needed to clean up the well and pump the cement slurry; therefore, the duration of the thermal disturbance of the formation at depth of 10,424 ft was 46.5 days and at depth of 12,2949 ft – 2

days. The data for this interval in which the liner was set are: at depth of 10,424 ft; $T_c = 219.6^oF$, $T_f = 275.0^oC$, and at depth of 12,294 ft; $T_c = 254.5^oF$, $T_f = 321.4^oC$. The bit size was 5.0 inches and the geothermal gradient was 0.0248 $^oF/ft$ (0.0452 $^oC/m$). The API correlation cannot be used for estimating the fluid circulation temperature because of the large geothermal gradient. Table 5.11 shows the difference between shut-in and formation temperature at various shut-in times. The temperature variation (Table 5.11) can have a significant effect on the performance of a cement system and has to be taken into account. For example, the temperature at depth of 10,424 ft after 5 hours is not 275^oF (formation temperature), but 236^oF. Also, the temperature at the depth 12,294 ft after 5 hours of shut-in is not 321.4^oF (formation temperature), but 286^oF. The difference of 35^oF (19^oC) can have a substantial impact on the cement slurry design.

Table 5.11 The Difference $T_f - T_s$ for two depths; Bee County, Texas well (Targhi, 1987)

t_s	Depth: 10,424 ft,		12,294 ft	
hrs	^oF	^oC	^oF	^oC
1.0	48.52	26.96	53.54	29.74
2.0	44.53	24.74	45.89	25.49
3.0	41.99	23.33	41.10	22.83
5.0	38.66	21.48	34.96	19.42
10.0	34.02	18.90	26.77	14.87
20.0	29.30	16.28	19.20	10.67
30.0	26.55	14.75	15.27	8.48
40.0	24.60	13.67	12.76	7.09
50.0	23.09	12.83	10.99	6.11

5.6 Cementing of Casing in Permafrost Regions

In Arctic wells the cement is set under unfavorable conditions. On the one hand, drilling operators have to use drilling muds with low inlet temperatures to avoid considerable thermal disturbance of frozen rocks. This circumstance, in addition to current high penetration rates, leads to relatively small thermal disturbance of frozen formations during drilling through permafrost. On the other

hand, it is very difficult to make a good cementing job when the temperature of hole's wall is close to 0°C or even negative. Thus, a contradiction exists between technological requirements during well drilling and completion. In permafrost well sections conventional portland cements may not set.

To find out how to achieve an increase the temperature around the wellbore (prior to cementeng of surface casing), and at the same time allow only a small increase of the thawing radius, hydrodynamical modeling was applied (Li and Kutasov, 1978).

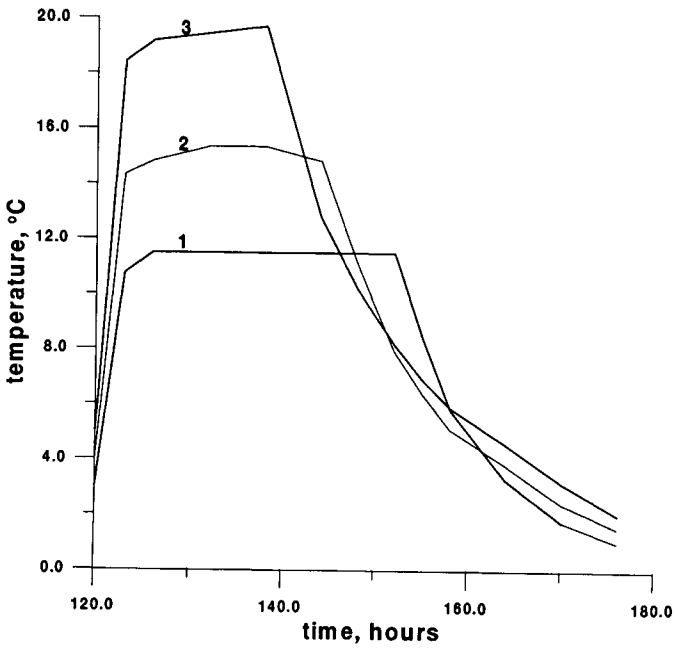


Fig. 5.8. Borehole temperature versus time at $t_{c2} \cdot T_{m2} = 480$ hr·°C. 1 – $t_{c2} = 32.0$ hrs, 2 – $t_{c2} = 24.0$ hrs, 3 – $t_{c2} = 19.2$ hrs.

The cement set time period is relatively short and this means that a small amount of heat is required to increase the temperature around the wellbore. At hydrodynamical modeling the mud circulation time was divided into two periods ($t_c = t_{c1} + t_{c2}$, $t_{c1} >> t_{c2}$). During the main period (t_{c1}) low inlet mud temperature (T_{m1}) is used, and after for a short time (t_{c2}) the mud temperature (T_{m2}) was increased. At modeling the input parameters: mud temperatures,

thermal properties of formations, ice content, and time periods varied in wide ranges. For comparison of the results in all runs the product $t_{c2}T_{m2}$ was constant. It was found that the increase of the mud temperature during the second period is the most effective way to heat formations near the well's wall. Increase of the duration of the second period results only in a small increase of shut-in temperatures. The results of modeling for one run are presented in Fig. 5.8 (Li and Kutasov, 1978). In this run the formation was silt with ice content of 25%, well radius 0.1 m, $T_{m1} = 5^{o}$C, and t_{c1}=120 hrs.

Chapter 6

PRODUCTION AND INJECTION WELLS

6.1 Heat Transfer

6.1.1 Overall Coefficient of Heat Loss

Knowledge of casing temperatures and wellbore heat losses are critical parameters in designing of geothermal, steam injection, and production deep hot wells. Interpretation of temperature logs from production and injection wells very much depends on the heat transmission in the flowing fluid-well completion-formation system (Fig. 6.1). For a steady-state heat flow within the wellbore the rate of heat flow per unit of length is given by

$$q = 2\pi r_{ti} U_{ti} (T_c - T_h) \tag{6.1}$$

where T_h is the temperature at the cement-formation interface, T_c is the temperature of flowing fluid, U_{ti} is the overall heat transfer coefficient between inside of tubing and outside of casing based on r_{ti}, and the subscript ti refers to the inside tubing surface. If the outside tubing area is chosen as the characteristic area, then the overall heat transfer coefficient is

$$U_{to} = U_{ti} \frac{r_{ti}}{r_{to}} \tag{6.2}$$

The value of U_{ti} depends and on well configuration and heat transfer mechanisms (conduction, convection, radiation) between the flowing fluid and wellbore-formation interface. Willhite (1967) suggested

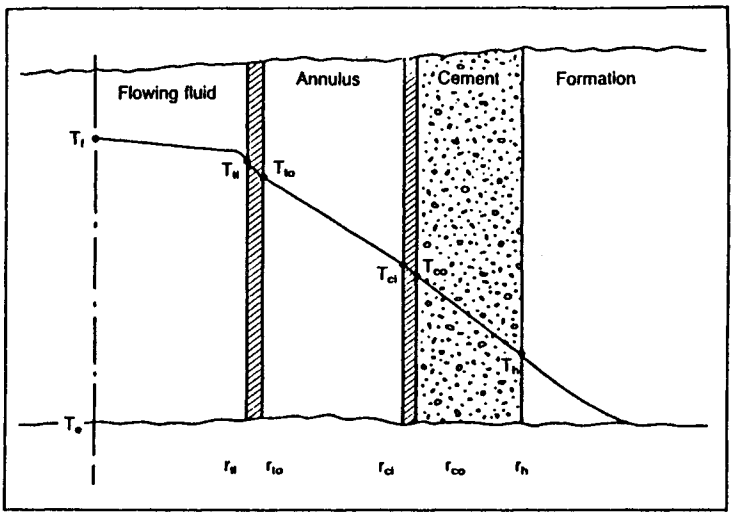


Fig. 6.1. Flowing fluid–well completion–formation system (White and Moss, 1983).

simplified procedures for calculating the overall heat transfer coefficient in steam and hot-water injection wells. In a general form the value of U_{ti} (Fig. 6.1) is given by

$$\frac{1}{U_{ti}} = \frac{1}{h_f} + \frac{r_{ti}\ \ln(r_{to}/r_{ti})}{\lambda_{tub}} + \frac{r_{ti}\ \ln(r_{ci}/r_{to})}{\lambda_{an}} + \frac{r_{ti}\ \ln(r_{co}/r_{ci})}{\lambda_{cas}} + \frac{r_{ti}\ \ln(r_w/r_{co})}{\lambda_{cem}} \tag{6.3}$$

where h_f is the film transfer coefficient of heat transfer between the fluid inside the tubing and the tubing wall, λ_{tub}, λ_{an}, λ_{cas}, and λ_{cem} are the thermal conductivities of the tubing, of the annular material, of the casing, and of the cement respectively. When the annulus is filled with fluid or gas, then

$$\frac{r_{ti}\ \ln(r_{ci}/r_{to})}{\lambda_{an}} = \frac{1}{h_c + h_r} \tag{6.4}$$

where h_c is coefficient of heat transfer due natural convection and h_r is the radiation heat transfer coefficient. Methods of calculations of the radiation and natural convection coefficients are presented in the literature (Willhite, 1967; Prats, 1982; White and Moss, 1983).

Let us now assume that at a given depth the fluid temperature is constant. In this case the rate of heat flow from the wellbore is a

monotonically decreasing function of time. The thermal properties of the surrounding wellbore formation will control the rate of well heat loss.

In his classical paper Ramey (1962) introduced the dimensionless "time function" $f(t_D)$, which accounts for the transient heat conduction in the formation. The $f(t_D)$ function is discussed in the following section. Taking into account that the specific (thermal resistance per unit o length) thermal resistance is time dependent, Prats (1982) introduced the overall specific thermal resistance coefficient (R_h),

$$R_h = \frac{1}{2\pi}\left[\frac{1}{h_f r_{ti}} + \frac{\ln(r_{to}/r_{ti})}{\lambda_{tub}} + \frac{\ln(r_{ci}/r_{to})}{\lambda_{an}} + \right.$$

$$\left. \frac{\ln(r_{co}/r_{ci})}{\lambda_{cas}} + \frac{\ln(r_w/r_{co})}{\lambda_{cem}} + \frac{f(t_D)}{\lambda_f}\right] \tag{6.5}$$

where λ_f is the thermal conductivity of the formation. Now the overall specific thermal resistance coefficient between the producing string and the borehole wall (R_h') is

$$R_h' = R_h - \frac{f(t_D)}{2\pi\lambda_f} \tag{6.6}$$

$$t_D = \frac{a_f t}{r_w^2} \tag{6.7}$$

or if there is an altered zone (skin) around the wellbore with radius of r_{wa}

$$t_D = \frac{a_f t}{r_{wa}^2} \tag{6.8}$$

where a_f is the thermal diffusivity of the formation. It easy to see that

$$R_h' = \frac{1}{2\pi r_{ti} U_{ti}} \tag{6.9}$$

6.1.2 Time Function

As was mentioned by Ramey (1962) the time function $f(t_D)$ may be estimated from solutions for radial heat conduction from an infinitely long cylinder (Carslaw and Jaeger, 1950). Fig. 6.2 presents

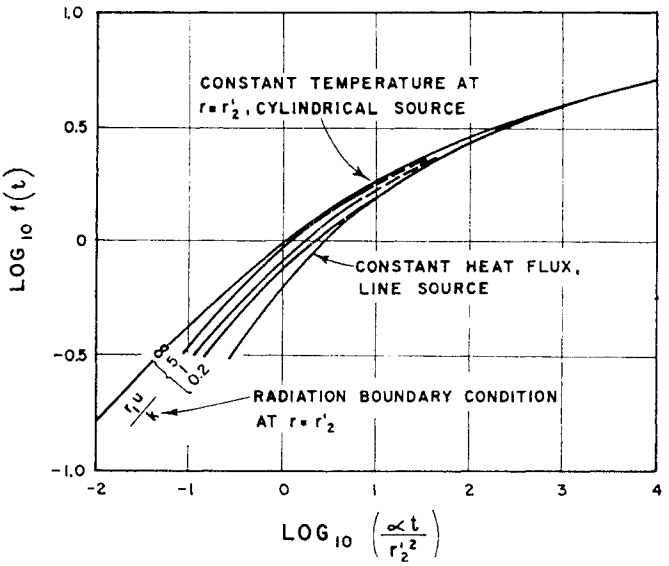


Fig. 6.2. Transient heat conduction in an infinite radial system (Carslaw and Jaeger, 1950).

$f(t) = f(t_D)$ function for three types of boundary conditions. The expression "radiation" boundary condition (Fig. 6.2) is used for shortness instead of linear heat transfer into a medium of constant temperature, or Newton's law of cooling by forced convection. Indeed, this commonly used description is a *little misleading since when heat is transferred by radiation, the heat flow depends on the fourth powers of the absolute temperatures* (Carslaw and Jaeger, 1959, p.19.).

In Fig. 6.2 r_2' is the outside radius of casing (radius of the cylinder), r_1 is the inside radius of tubing, α is the thermal diffusivity of formations, and $U = U_{ti}$. As can be seen from Fig. 6.2 all three solutions converge at large dimensionless times. For large values of t_D the line source solution can be used (Ramey, 1962)

$$f(t_D) \approx 0.5 \ \ln(t_D) + 0.403 \tag{6.10}$$

Willhite (1967) published a table of the $f(t_D)$ function for a range of values of both t_D and $R_h'\lambda_f$ (Table 6.1). When the thermal resistance in the wellbore is negligible, ($R_h' = 0$) the time function is equal to the reciprocal of the dimensionless heat flow rate from a

Table 6.1 Time function $f(t_D)$ for the radiation boundary condition model (Willhite, 1967)

	$2\pi R_h' \lambda_f$										
t_D	100	20	5.0	2.0	1.0	0.5	0.2	0.1	0.05	0.02	0
0.1	0.313	0.314	0.318	0.323	0.330	0.345	0.373	0.396	0.417	0.433	0.445
0.2	0.423	0.424	0.430	0.439	0.452	0.473	0.511	0.538	0.568	0.572	0.588
0.5	0.616	0.619	0.629	0.644	0.666	0.698	0.745	0.772	0.790	0.802	0.811
1.0	0.802	0.806	0.820	0.842	0.872	0.910	0.958	0.984	1.00	1.01	1.02
2.0	1.02	1.03	1.05	1.08	1.11	1.15	1.20	1.22	1.24	1.24	1.25
5.0	1.36	1.37	1.40	1.44	1.48	1.52	1.56	1.57	1.58	1.59	1.59
10.0	1.65	1.66	1.69	1.73	1.77	1.81	1.84	1.86	1.86	1.87	1.88
20.0	1.96	1.97	2.00	2.05	2.09	2.12	2.15	2.16	2.16	2.17	2.17
50.0	2.39	2.40	2.44	2.48	2.51	2.54	2.56	2.57	2.57	2.57	2.58
100.0	2.73	2.74	2.77	2.81	2.84	2.86	2.88	2.89	2.89	2.89	2.90

constant temperature cylindrical source. Then, from Eqs. 3.14 and 3.15 we obtain

$$f(t_D) = \ln(1 + D\sqrt{t_D}), \qquad D = 1.5708 + \frac{1}{\sqrt{t_D} + 4.9589} \tag{6.11}$$

In practice this relationship can be used for any values of t_D at $2\pi R_h' \lambda_f \leq 0.2$ (Table 6.1).

6.1.3 Effective Well Radius

For high flow rate producing wells the film coefficient of heat transfer between the fluid inside the tubing and the tubing's inside wall is very large, and $1/h_f \approx 0$. Then the overall specific thermal resistance coefficient between the producing string and the borehole wall is

$$R_h' = \frac{1}{2\pi}\left[\frac{\ln(r_{to}/r_{ti})}{\lambda_{tub}} + \frac{\ln(r_{ci}/r_{to})}{\lambda_{an}} + \frac{\ln(r_{co}/r_{ci})}{\lambda_{cas}} + \frac{\ln(r_w/r_{co})}{\lambda_{cem}}\right] \tag{6.12}$$

We can consider the layer $r_w - r_{ti}$ as a skin zone with some effective thermal conductivity. Like in the pressure build-up theory we can introduce the effective (apparent) well radius (r_{we}) and assume that the thermal conductivity of the ring $r_w - r_{we}$ is equal to that of the formation. We should only to note that in pressure build-up theory

the skin radius corresponds to the radius of altered zone. In our case the well radius is the radius of the skin zone. Then,

$$R_h = \frac{1}{2\pi}[\frac{\ln(r_w/r_{we})}{\lambda_f}] \tag{6.13}$$

From Eqs. 6.12 and 6.13 we obtain

$$\frac{\ln(r_w/r_{we})}{\lambda_f} = \frac{\ln(r_{to}/r_{ti})}{\lambda_{tub}} + \frac{\ln(r_{ci}/r_{to})}{\lambda_{an}} + \frac{\ln(r_{co}/r_{ci})}{\lambda_{cas}} + \frac{\ln(r_w/r_{co})}{\lambda_{cem}} \tag{6.14}$$

Now a "skin factor" s can be introduced

$$r_{we} = r_w e^{-s} \tag{6.15}$$

6.1.4 Heat Losses From Wells

Estimation of the wellbore heat loss during injection of a hot water or steam is important in the designing of oil recovery projects. It is clear that the these heat losses should be reduced to some practical level. Several important question should be answered. What are the optimal input parameters of steam and water (flow rate, injection pressure and temperature, steam quality)? What is the effect of the size of tubing (or casing) and thermal insulation of tubing on the wellbore heat loss reduction? To explore these questions Ramey (1962) considered three sample cases.

In the first case 500 barrels per day of water at a temperature 397°F is injected down the casing of a well completed with 7 in., 23 lb_m/ft casing. The injection pressure is 1,000 *psig* and water will be in the liquid phase.

In the second case only the injection pressure is reduced from 1,000 *psig* to 223 *psig* (238 *psi*). From the pressure-temperature diagram follows that the water is saturated steam. In the last case the input parameters are identical to those in the first case. Now the hot water is injected down 2 in. tubing centered inside the casing. The annulus is filled with a granular insulating material with an effective thermal conductivity of 0.1 $Btu/ft \cdot day \cdot^o F$.
Figure 6.3 presents the percentage of heat loss versus depth for the preceding cases. Percentage loss is based upon the heat content

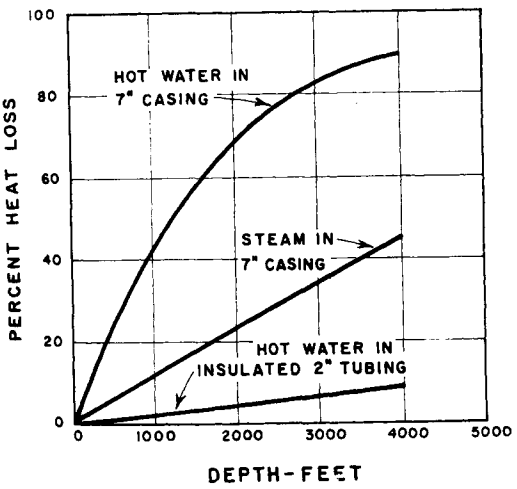


Fig. 6.3. Computed heat loss versus depth for injection of 500 B/D of steam or hot water for one week (Ramey, 1962).

above a formation temperature of 150°F at 4,000 ft (Ramey, 1962).

The equation used to calculate the rate of heat losses per unit of length is

$$q = \frac{T_c - T_f}{R_h} \tag{6.16}$$

However, when water vaporization in formations near the wellbore exists, the determination of the heat losses is more complicated. Based on physical considerations, formation of a dry zone increases the heat losses from a steam injection (or production) wellbore. As the dry zone radius slowly changes with time, the radial temperature gradient at the wellbore-dry formation interface will increase.

If it is assumed that the temperatures in the well will remain practically constant; the temperature change due to heat loss will be compensated for by condensation and reduction of steam quality. Also, there will be a slight change in temperature caused by change in pressure with increased depth (Ramey, 1962).

A computer program obtained a numerical solution of a system of differential equations of heat conductivity (for insulation, dry, and wet zones) and Stefan equation. The results of computer calculations have shown that the rate of heat flow from the wellbore

can be approximated by Eq. 6.17 (Kutasov, 1996)

$$q_{rw} = -\lambda_d \frac{dT_d(r,t)}{dr}|_{r=r_w} = -\frac{\lambda_d T_{st}}{r_w(1+\theta)(J+\ln\ H)} \tag{6.17}$$

$$\theta = \frac{T_{ev}-T_f}{T_{st}-T_{ev}}, \qquad H = \frac{h}{r_w}, \qquad J = \frac{\lambda_d}{\lambda_{ef}}\ \ln\ \frac{r_w}{r_{ti}} \tag{6.18}$$

where h is the radius of drying, λ_d is the thermal conductivity of dry formation, T_d is the temperature in the dry zone, T_{ev} is the vaporization temperature, T_{st} is the temperature of steam, λ_{ef} is the effective thermal conductivity of insulation (the $r_w - r_{ti}$ ring), θ is the dimensionless formation temperature, H is the dimensionless radius of drying, and J the is dimensionless thermal conductivity of insulation. The effective thermal conductivity of insulation is given by

$$\lambda_{ef} = \frac{\ln\ r_w/r_{ti}}{2\pi R_h - f(t_D)/\lambda_d}, \qquad t_D = \frac{a_d t}{r_w^2} \tag{6.19}$$

Here R_h is overall coefficient of heat loss for a well with no altered zone near the wellbore and a_d is the thermal diffusivity of the dry zone. Assuming a steady-state radial temperature distribution in the wellbore and in the dry zone we obtained an equation for the time dependent casing temperature (T_{cas})

$$T_{cas} = \frac{T_{st}\ \ln\ H + T_{ev}J}{\ln\ H + J} \tag{6.20}$$

A Fortran computer program was prepared for calculating values of q_{rw}, H, T_{cas}, and of the total (for a well section) heat loss rate (Kutasov, 1996).

Example.

A field example (Prats, 1982, p. 130) was modified to illustrate the calculations.

Steam at 600°F is injected down 3.5 in. tubing with a packer in 9.625 in., 53.5 lb/ft, N-80 casing. The annulus contains a stagnant gas at zero gauge pressure at the wellhead, and the casing is cemented to surface in a 12 in. hole.

The tubing is insulated with 1 in. of calcium silicate, the insulation being held in place and sealed from accidental entry of liquids in the annulus by a very thin sheath of aluminum. Emissivity at the surface of insulation (ϵ_{ins}) is equal to the emissivity at inner radius

of the casing (ϵ_{ci}).
A temperature survey in the well indicates a mean subsurface temperature of 100°F over the 1,000 ft depth. Therefore we assume that the undisturbed formation temperature is

$$T_f = T_o + \Gamma z, \quad T_o = 70^o F, \quad \Gamma = 0.060^o F/ft$$

To estimate the rate of heat loss 21 days after steam injection started, as well as the casing temperature, one can assume that an altered zone (due to water vaporization) exists. It was also assumed: water content is 20.0 lb_m/ft^3, latent heat of vaporization is is 960 Btu/lb_m, and the vaporization temperature is 212°F. Thus the following data aplly:

$$r_w = 6.00\ in., \quad r_{ti} = 1.75\ in., \quad r_{ins} = 2.75\ in., \quad r_{ci} = 4.27\ in.,$$

$$r_{co} = 4.81\ in., \quad a_d = 0.96\ \frac{ft^2}{day}, \quad \epsilon_{ins} = \epsilon_{ci} = 0.9, \quad \lambda_d = 24 \frac{Btu}{ft \cdot day \cdot^o F},$$

$$R_h = 0.108\ \frac{ft \cdot day \cdot^o F}{Btu}, \quad \epsilon_{ins} = \epsilon_{ci} = 0.9, \quad t = 21\ days, \quad t_D = 80.6$$

$$f(80.6) = 2.60, \quad T_{st} = 600^o F, \quad T_{ev} = 212^o F, \quad W = 20.0\ \frac{lb_m}{ft^3}$$

$$q_v = 960\ \frac{Btu}{lb_m}, \quad \lambda_{cem} = 12\ \frac{Btu}{ft \cdot day \cdot^o F}, \quad \lambda_{ins} = 0.96\ \frac{Btu}{ft \cdot day \cdot^o F}.$$

Eq. 6.19 obtains the effective thermal conductivity of insulation:

$$\lambda_{ef} = \frac{\ln\ 6.00/1.75}{2 \cdot 3.1416 \cdot 0.108 - 2.60/24} = 2.16\ (Btu/ft \cdot day \cdot^o F).$$

Tables 6.2-6.4 present the results of calculations and shows the efficiency of the thermal insulation.

6.2 Temperature Profiles in Wells

Many variables influence the transient temperature profiles in injection and production wells. It is very difficult to apply analytical techniques in predicting the downhole temperatures. Indeed, it is practically impossible to take into account the well configuration, time dependent flow rate, depth dependent formations thermal

Table 6.2 Rate of heat loss rate (in 10^4 $Btu/day \cdot ft$) after 21 days of steam injection

	λ_{ef}, $Btu/ft \cdot day \cdot^o F$							
z, ft	1.50	2.0	2.5	3.0	3.5	4.0	4.5	5.0
100	0.3398	0.4530	0.5643	0.6713	0.7725	0.8679	0.9578	1.0426
200	0.3438	0.4581	0.5701	0.6772	0.7784	0.8738	0.9637	1.0486
300	0.3478	0.4633	0.5757	0.6830	0.7842	0.8796	0.9697	1.0548
400	0.3519	0.4684	0.5814	0.6887	0.7900	0.8855	0.9758	1.0613
500	0.3561	0.4736	0.5869	0.6944	0.7958	0.8915	0.9820	1.0679
600	0.3604	0.4788	0.5924	0.7000	0.8016	0.8976	0.9885	1.0748
700	0.3647	0.4839	0.5978	0.7056	0.8074	0.9038	0.9952	1.0819
800	0.3691	0.4890	0.6032	0.7112	0.8134	0.9102	1.0021	1.0894
900	0.3735	0.4940	0.6085	0.7169	0.8195	0.9168	1.0093	1.0972
1000	0.3779	0.4989	0.6139	0.7226	0.8258	0.9237	1.0168	1.1054
	Total heat loss rate, in 10^6 Btu/day							
	3.585	4.761	5.894	6.971	7.989	8.950	9.861	10.724

Table 6.3 Rate of heat loss rate (in 10^4 $Btu/day \cdot ft$) and total heat loss rate, $\lambda_{ef} = 2.16$ $Btu/ft \cdot day \cdot^o F$

	injection time, days						
z, ft	10	21	50	100	150	200	250
100	0.4892	0.4890	0.4880	0.4865	0.4853	0.4843	0.4834
200	0.4948	0.4943	0.4930	0.4912	0.4897	0.4885	0.4874
300	0.5005	0.4997	0.4980	0.4957	0.4940	0.4926	0.4913
400	0.5061	0.5051	0.5029	0.5002	0.4981	0.4965	0.4951
500	0.5118	0.5104	0.5077	0.5045	0.5022	0.5003	0.4987
600	0.5175	0.5157	0.5124	0.5087	0.5060	0.5040	0.5022
700	0.5232	0.5210	0.5171	0.5128	0.5098	0.5075	0.5056
800	0.5345	0.5262	0.5216	0.5168	0.5135	0.5110	0.5089
900	0.5345	0.5313	0.5260	0.5206	0.5171	0.5143	0.5122
1000	0.5402	0.5364	0.5304	0.5245	0.5206	0.5177	0.5154
	Total heat loss rate, in 10^6 Btu/day						
	5.147	5.129	5.097	5.061	5.036	5.017	5.000

Table 6.4 Dimensionless radius of the dry zone after 250 days of steam injection

	λ_{ef}, $Btu/ft \cdot day \cdot ^{o}F$							
z, ft	1.50	2.0	2.5	3.0	3.5	4.0	4.5	5.0
100	1.004	1.112	1.387	1.778	2.225	2.688	3.144	3.581
200	1.010	1.152	1.470	1.898	2.374	2.857	3.327	3.774
300	1.019	1.293	1.566	2.032	2.536	3.038	3.522	3.977
400	1.035	1.265	1.677	2.181	2.711	3.232	3.728	4.191
500	1.058	1.340	1.803	2.345	2.901	3.439	3.945	4.414
600	1.089	1.431	1.947	2.526	3.107	3.659	4.174	4.647
700	1.133	1.540	2.110	2.725	3.328	3.893	4.414	4.890
800	1.190	1.670	2.293	2.942	3.564	4.140	4.666	5.142
900	1.266	1.822	2.499	3.179	3.817	4.401	4.928	5.404
1000	1.364	2.001	2.728	3.435	4.086	4.674	4.928	5.673

properties and temperatures, vertical heat transfer, the dependence of properties of producing fluids (gases) on temperature and pressure. At the same time the accuracy of downhole temperature predictions by computer models is very much dependent on the availability and quality of input data (Wooley, 1980). However, in many cases simplified analytical solutions with a sufficient accuracy approximate the transient temperature profiles in production and injection wells.

Below we adapt the basic equation obtained by Ramey (1962) and modified by Prats (1982). The main assumptions are: steady-state heat transfer within the borehole, constant formation and fluid (gas) properties, constant geothermal gradient, incompressible liquids or ideal gases, and only radial heat losses to the formation. On the basis of these assumptions the temperature in an injection well is given by

$$T(z,t) = T_f(z) - \Gamma w_i c R_h - b w_i R_h \delta + [T_{inj} - T_o + \Gamma w_i c R_h + b w_i R_h \delta)] exp(-\frac{z}{w_i c R_h}), \quad b = 0.002343\ kcal/m \cdot kg \qquad (6.21)$$

where $\delta = 0$ for liquids and $\delta = 1$ for gases; w_i is the mass rate, T_{inj} is the injection temperature of the fluid (gas), and c is the specific heat capacity of the fluid. The undisturbed formation temperature is a linear function of depth,

$$T_f(z) = T_o + \Gamma z \qquad (6.22)$$

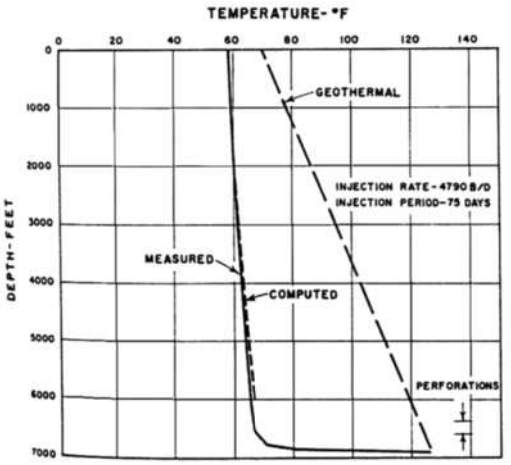


Fig. 6.4. Measured and computed temperatures for a water injection well (Ramey, 1962).

Ramey (1962) conducted comparison of field temperature surveys with computed temperatures (Fig. 6.4 and Fig. 6.5). In Figure 6.4 the computed temperatures were within 1.5°F of the measured temperatures. Figure 6.5 presents a comparison of measured and calculated temperatures for injection of hot natural gas down 3 in. insulating tubing. The test was conducted during 19 months and the gas injection rate varied from 10 to 215 Mcf/D. For production, the mass rate w_p is used instead of w_i and the temperature is given by

$$T(z,t) = T_f(z) + \Gamma w_p c R_h + b w_p R_h \delta + [T_p(t) -$$

$$T_f(z_R) - \Gamma w_p c R_h - b w_p R_h \delta] exp(-\frac{(z_R - z)}{w_p c R_h}) \qquad (6.23)$$

where z_R is the reservoir depth and $T_p(t)$ is the temperature of the producing fluid at z_R.

6.3 Water Formation Volume Factor

In water drive reservoirs large quantities of water production may be required to obtain maximum oil recoveries. To maintain the reservoir pressure a significant amount of water is injected into

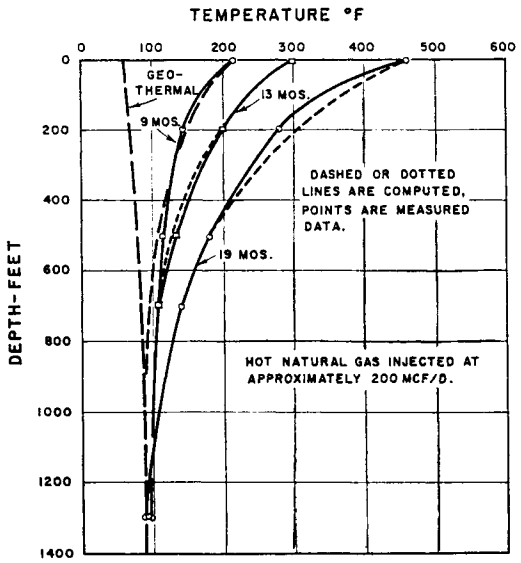


Fig. 6.5. Measured and calculated temperatures for a gas injection well (Ramey, 1962).

producing formation. In many oil fields the number of injection wells can be close to the number of production wells.

Knowledge of the water formation volume factor (B_w) is needed in material balance calculations to predict the change in water volume that occurs between the surface and reservoir. The value of B_w is defined as water volume under reservoir conditions (reservoir barrels) divided by water volume under standard conditions. The volume under standard surface conditions is expressed in stock tank barrels (STB) and under reservoir conditions in reservoir barrels (RB). The B_w is a function of temperature and pressure (p). When the thermal expansion of water is compensated by the compression due to the high reservoir pressure, then $B_w = 1.00$ RB/STB. Dodson and Standing (1944) presented some values of B_w for temperatures up to 250°F and pressures up to 5,000 *psia*.

Below an equation is suggested which will allow one to calculate the values of B_w for temperatures up to 390°F (200°C) and pressures up to 26,000 *psia* (1,800 bar). Our analysis of laboratory density test data (Burnham et al., 1969) shows that for pure water the coefficient of thermal (volumetric) expansion can be

Table 6.5 Coefficients in Equation 6.24

Temperature interval, °C (°F)	Pressure interval, bar (*psig*)	Number of points	ρ_o, *ppg*	α, $1/psig$ 10^{-6}	β, $1/°F$ 10^{-4}	γ, $1/°F \times °F$ 10^{-7}	$\Delta\rho/\rho$ x100 %
20-100 (68-212)	100-1,100 (1,436-15,939)	36	8.3555	2.7384	-1.5353	-7.4690	0.039
100-200 (212-392)	300-1,800 (4,336-26,092)	76	8.4172	3.1403	-2.8348	-3.7549	0.175
20-200 (68-392)	100-1,800 (1,436-26,092)	103	8.3619	3.0997	-2.2139	-5.0123	0.172

expressed as a linear function of temperature, and the coefficient of isothermal compressibility is practically a constant. We have determined that the following empirical formula can be used as an equation of state (pressure-density-temperature dependence) for pure water (Kutasov, 1989c):

$$\rho = \rho_o \exp[\alpha p + \beta(T - T_s) + \gamma(T - T_s)^2] \qquad (6.24)$$

where pressure is in *psig*, temperature is in °F, ρ is water density (in *ppg*), ρ_o, α, β, γ are constants, and $T_s = 59°$F (15°C).
A regression analysis computer program was used to process density-pressure-temperature data (Burnham et al., 1969) and to provide the coefficients of Eq. 6.24 (Table 6.5). The accuracy was estimated from the sum of squared residuals and is presented in Table 6.5. In Table 6.6 the measured (ρ^*) and calculated (ρ) values of water density are compared. These results show a good agreement between the measured and predicted densities.

Results also show that for temperatures up to 100°C Eq. 6.24 is very accurate because, for these temperatures, more precise laboratory test data were available. Taking into account that the specific volume (v) is defined as $v = 1/\rho$, we obtained a relationship for the water formation volume factor

$$B_w = \frac{\rho^*}{\rho} \exp[-\alpha p - \beta(T - T_s) - \gamma(T - T_s)^2] \qquad (6.25)$$

Table 6.6 Measured (ρ^*) and predicted (ρ) water density

p, bar	p, *psig*	T, °C	T, °F	ρ^*, *ppg*	ρ, *ppg*	$\Delta\rho$, *ppg*
100	1436	20	68	8.370	8.376	0.006
400	5787	20	68	8.479	8.477	-0.002
100	1436	40	104	8.317	8.318	0.001
600	8688	40	104	8.488	8.485	-0.003
100	1436	60	140	8.241	8.244	0.003
800	11588	60	140	8.474	8.477	0.003
200	2886	80	176	8.183	8.188	0.005
1000	14489	80	176	8.442	8.452	0.010
300	4336	100	212	8.113	8.116	0.003
1100	15939	100	212	8.372	8.378	0.006
300	4336	120	248	7.991	7.980	-0.011
1400	20291	120	248	8.396	8.390	-0.006
300	4336	140	284	7.856	7.855	-0.001
1400	20291	140	284	8.235	8.258	0.023
300	4336	160	320	7.709	7.724	0.015
1600	23191	160	320	8.173	8.195	0.022
300	4336	180	356	7.551	7.588	0.037
1600	23191	180	356	8.044	8.051	0.007
400	5787	200	392	7.435	7.481	0.046
1800	26092	200	392	7.978	7.974	-0.004

where $\rho^* = 8.3380\ ppg = 0.9991\ g/cm^3$ is the density of water under standard surface conditions (T=59°F, p=0 *psig*).

6.4 Temperature Around the Wellbore

For long production (injection) times the temperature disturbance of formations due to drilling operations can be neglected in comparison with the temperature change caused by production of hot fluids or gases. In this case the Eq. 3.74 can be used to determine the temperatures of formations around the wellbore. The average fluid (gas) temperature (T_p) at a given depth for a production (injection) period (t_p) is calculated from equations (6.21 and 6.23) and the well radius is replaced by the effective well radius. The Eq. 3.74 now

becomes

$$T_D(r_D, t_{Dp}) = \frac{T(r, t_p) - T_f}{T_p - T_f} = \frac{Ei(-r_D^2/4t_D^*)}{Ei(-1/4t_{Dp}^*)} \tag{6.26}$$

$$t_{Dp} = \frac{a_f t_p}{r_{we}^2}; \qquad r_D = \frac{r}{r_{we}}$$

The computer program "TEMVOL" (Appendix C, Table C.3) can be used determine the function $T(r, t_p)$.

Example.
Hot water at 100°C is injected down casing 9.62 in. casing. The casing is cemented in a 12 in. borehole. At some depth the undisturbed formation temperature is 100°C. Find the radial temperature distribution for $100 \leq t_p \leq 10{,}000\ hrs$ and $0.2 \leq r \leq 20\ m$. The following data apply: $r_w = 6.0$ in., $r_{ci} = 4.27$ in., $r_{co} = 4.81$ in.,

$$\lambda_f = 1.9\ \frac{kcal}{hr \cdot m \cdot {}^oC}, \quad \lambda_{cas} = 37\ \frac{kcal}{hr \cdot m \cdot {}^oC},$$

$$\lambda_{cem} = 0.75\ \frac{kcal}{hr \cdot m \cdot {}^oC}, \quad a_f = 0.0034\ \frac{m^2}{hr}$$

From Eq. 6.14 we obtain the effective well radius (r_{we}):

$$\frac{ln\ 6.0/r_{we}}{1.9} = \frac{\ln\ 4.81/4.27}{37} + \frac{\ln\ 6.0/4.81}{0.75} = 0.2975$$

$\frac{6.0}{r_{we}} = 1.760$, $r_{we} = 3.409$ in. $= 0.0866$ m
The results of calculations are presented in Table 6.7. For this example the skin factor (Eq. 6.15) is: $r_{we} = r_w e^{-s}$, $s = 0.565$

Now let us assume that drilling was followed by a short production or injection period. The average circulating fluid temperature (at a given depth) T_c while drilling changed to T_p when production (injection) started at time t_c. Here we will neglect the time gap between cessation of drilling operations and beginning of production. The change in wellbore temperature from T_c to T_p causes an additional change in the distribution of temperature around the wellbore. The function $T(r, t = t_p)$ during the production period can be calculated by adding to the temperature difference caused by T_c, an additional difference caused by $(T_p - T_c)$ beginning at time

Table 6.7 Variation of the formation temperature (^oC) with time and radial distance

	Injection time, hrs						
r, m	100	200	500	1,000	2,000	5,000	10,000
0.20	86.4	88.0	89.6	90.6	91.4	92.3	92.8
0.30	80.0	82.2	84.6	86.0	87.2	88.5	89.4
0.50	72.3	75.2	78.4	80.3	82.0	83.8	85.0
0.70	67.8	70.8	74.4	76.6	78.6	80.8	82.1
1.00	63.9	66.7	70.3	72.8	75.0	77.5	79.1
1.50	61.1	62.9	66.1	68.6	71.0	73.8	75.7
2.00	60.3	61.2	63.6	65.9	68.3	71.3	73.3
2.50	60.1	60.4	62.1	64.1	66.4	69.3	71.4
3.00	60.0	60.2	61.2	62.8	64.9	67.8	69.9
4.00	60.0	60.0	60.3	61.3	62.9	65.5	67.7
5.00	60.0	60.0	60.1	60.5	61.6	64.0	66.0
6.00	60.0	60.0	60.0	60.2	60.9	62.8	64.7
8.00	60.0	60.0	60.0	60.0	60.2	61.4	62.9
10.00	60.0	60.0	60.0	60.0	60.1	60.6	61.8
15.00	60.0	60.0	60.0	60.0	60.0	60.1	60.5
20.00	60.0	60.0	60.0	60.0	60.0	60.0	60.1

$t = t_c$. By applying the principle of the superposition Gogoi (Gogoi and Kutasov, 1986) obtained the following equation

$$T(r, t_c + t_p) = T_p - (T_c - T_f)\frac{\ln\ r_D}{\ln\ R_{int}} - (T_p - T_c)\frac{\ln\ r_D}{\ln\ R_{inp}}, \quad (6.27)$$

$$R_{int} = 1 + 2.184\sqrt{t_{Dt}}, \quad R_{inp} = 1 + 2.184\sqrt{t_{Dp}}, \quad r_D \leq R_{inp} \quad (6.28)$$

$$r_D = \frac{r}{r_{we}}, \quad t_{Dt} = \frac{a_f(t_c + t_p)}{r_{we}^2}, \quad t_{Dp} = \frac{a_f t_p}{r_{we}^2}$$

6.5 Permafrost Thawing and Estimation of Well Thermal Insulation Efficiency

Oil and gas flowing through the wells in permafrost areas can be at a high temperature, such as 190°F (88°C), that makes thawing of permafrost unavoidable during long term production. If the thawed formation cannot withstand the load of the upper soil layers, consolidation will take place, and the corresponding setting can significantly shift the surface.

Estimates show that the magnitude of settlement (the center displacement of the thawed soil ring) and the axial compressive stress are proportional to the squared values of the thawed radius (Palmer, 1978). For injection wells, thawing of the permafrost greatly increases the heat loss from the wellbore. Thus, knowledge of the thawed radius is critical for predicting platform stability and wellbore integrity, as well as for estimating heat loss from wells. In many cases an insulation layer for the producing strings can significantly reduce permafrost thawing.

A computer program was used to obtain a numerical solution for differential equations of heat conductivity (for insulation, frozen and, thawed zones) and Stefan equation. The numerical solutions show that the rate of heat flow from the wellbore into the thawed zone can be approximated by the following equation

$$q_{rw} = -\frac{\lambda_t T_p}{r_w(1+\theta)(J+\ln H)} \tag{6.29}$$

$$\theta = \frac{T_{mel} - T_f}{T_p - T_{mel}}, \quad H = \frac{h}{r_w}, \quad J = \frac{\lambda_t}{\lambda_{ef}} \ln \frac{r_w}{r_{ti}}$$

where q_{rw} is the heat flow rate per unit of length, h is the thawing radius, λ_t is the thermal conductivity of thawed zone, T_{mel} is the temperature of ice melting (0^oC for pure ice), T_f is the undisturbed formation temperature, T_p is the temperature of the producing (injection) fluid, λ_{ef} is the effective thermal conductivity of insulation, θ is the dimensionless formation temperature, H is the dimensionless radius of thawing, and J is dimensionless thermal conductivity of insulation. For high flow rate wells the effective thermal conductivity of insulation is given by

$$\frac{\ln(r_w/r_{ti})}{\lambda_{ef}} = \frac{\ln(r_{to}/r_{ti})}{\lambda_{tub}} + \frac{\ln(r_{12}/r_{to})}{\lambda_1} + \frac{\ln(r_{23}/r_{12})}{\lambda_2} + \ldots \frac{\ln(r_w/r_{(n-1)n})}{\lambda_n} \tag{6.30}$$

where,

r_{ti}, r_{to} are the inside and outside radius of tubing; r_{12}, r_{23}, ... $r_{(n-1)n}$ are the radii of the layers interfaces, and λ_{tub}, λ_1, $\lambda_2 + \ldots \lambda_n$ are the thermal conductivity of tubing and layers within the wellbore.

Usually for producing wells, the value of the dimensionless formation temperature is small, so that to include a safety factor, one can neglect the heat flow to frozen zone. With Eq. 6.29 at $\theta = 0$,

and assuming a steady-state temperature distribution in he thawed zone, one obtains the solution of the Stefan equation

$$\frac{t_D}{I_f} = \frac{H^2}{2} \ln H - \frac{1}{4}(H^2 - 1) + \frac{1}{2}J(H^2 - 1) \tag{6.31}$$

$$t_D = \frac{a_t t}{r_w^2}, \qquad I_f = \frac{a_t q_f}{\lambda_t (T_p - T_{mel})}$$

where a_t is the thermal diffusivity of thawed formation, q_f is latent heat of the formation per unit of volume (amount of heat needed for ice melting), and I_f is the dimensionless latent of the formation. The maximum value of the dimensionless radius of thawing (H_{max}) is when $J = 0$. Then from Eq. 6.31 we obtain

$$\frac{t_D}{I_f} = \frac{H_{max}^2}{2} \ln H_{max} - \frac{1}{4}(H_{max}^2 - 1) \tag{6.32}$$

A good approximation of the last formula is the relationship

$$H_{max} = 1 + A(t_D/I_f)^b \tag{6.33}$$

$$A = 1.2582, \quad b = 0.4376; \quad 3 \le t_D/I_f \le 4,200$$

$$A = 1.1608, \quad b = 0.4477; \quad 4,200 \le t_D/I_f \le 21,000$$

The ratio of thickness of the thawing layers (around the wellbore) with and without insulation can be expressed by the thermal insulation efficiency coefficient ψ,

$$\psi = \frac{H - 1}{H_{max} - 1} \tag{6.34}$$

Combining equations (6.31, 6.32, and 6.34) we obtain

$$\frac{H_{max}^2}{2} \ln H_{max} - \frac{1}{4}(H_{max}^2 - 1) = \frac{1}{2}(1 + \psi H_{max} - \psi)^2 \ln(1 + \psi H_{max} - \psi) -$$

$$\frac{1}{4}[(1 + \psi H_{max} - \psi)^2 - 1] + \frac{1}{2}J[(1 + \psi H_{max} - \psi)^2 - 1] \tag{6.35}$$

To simplify calculations the $\psi = \psi(J, H_{max})$ function was tabulated (Kutasov, 1997) for the following ranges of variables:

$$1 \le J \le 50, \quad 2 \le H_{max} \le 100$$

Example.
An oil company is considering installing insulated 3.5 in. tubing in a 17.5 in. wellbore. The estimated effective thermal conductivity of insulation is $\lambda_{ef} = 0.040\ Btu/hr \cdot ft \cdot {}^{o}F$.
The problem is to obtain the values of the thermal insulation efficiency coefficient ψ after 2-10 years of production.
The following data apply:

$$r_{ti} = 1.496\ in., \quad r_w = 8.75\ in., \quad a_t = 0.030\ ft^2/hr$$

$$\lambda_t = 1.0\ Btu/hr \cdot ft \cdot {}^{o}F, \quad q_f = 3000\ Btu/ft^3, \quad T_p = 180^{o}F$$

$$t_1 = 2\ yrs. = 17,520\ hrs., \quad t_2 = 10\ yrs. = 87,600\ hrs.$$

In Step 1, compute the dimensionless parameters:

$$J = (1/0.04)\ln(8.75/1.496) = 44, \quad I_f = (0.03{\cdot}3000)/(180{\cdot}1) = 0.50,$$

$$t_{D1} = (0.030 \cdot 17,520)/(17.5/24)^2 = 990,$$

$$t_{D2} = (0.030 \cdot 87,600)/(17.5/24)^2 = 4,940,$$

$$t_{D1}/I_f = 990/0.500 = 1,980, \quad t_{D2}/I_f = 4,940/0.500 = 9,940.$$

In Step 2, determine from Eq. (6.33) the values of H_{max} for $t_1 = 2$ years and $t_2 = 10$ years,

$$H_{max,1} = 1 + 1.2582 \cdot 1,980^{0.4376} = 35.86,$$

$$H_{max,2} = 1 + 1.1608 \cdot 9,940^{0.4477} = 72.51$$

Next, in Step 3, find the values of function ψ from Eq. 6.35 or from tables (Kutasov, 1997),

$$\psi_1 = \psi(44., 35.86) = 0.2395, \quad \psi_2 = \psi(44., 72.51) = 0.2754$$

In the last step, Step 4, Eq. 6.34 is used to find H_1 and H_2,

$$H_1 = 1{+}(35.86{-}1){\cdot}0.2395 = 9.35, \quad H_2 = 1{+}(72.51{-}1){\cdot}0.2754 = 20.69$$

Thus, insulation on the producing strings significantly reduces the permafrost thawing around the wellbore. It is interesting to note the drastic reduction of the volume (mass) of the thawed formations. Indeed, introducing the ratio of thawed volumes,

$$M = \frac{(H_{max} - 1)^2}{(H - 1)^2},$$

we estimate that $M_1 = 17.4$ and $M_2 = 13.2$.

6.6 Thermal Stresses

As was shown earlier (Section 3.7) the thermal stresses around the wellbore during drilling are caused by the difference in temperatures at the wellbore (T_m) and the undisturbed formation. For the production period the relationship between the fluid temperatures while drilling, production (T_p), and the formation temperature determines the the type and magnitude of thermal stresses. Let us assume that fluid production begins the moment the drilling operations are stopped. In this case the components of thermal stresses around the wellbore can be determined from the following equations (Gogoi, 1986):

$$\sigma_{r,th} = \frac{\alpha E}{1-\nu}[(T_m - T_f)\{\frac{\ln\ r_D}{2\ \ln\ R_{int}} - \frac{1}{2}(1-\frac{1}{r_D^2})(1+\frac{1}{2\ \ln\ R_{int}})\}+$$

$$(T_p - T_m)\{\frac{\ln\ r_D}{2\ \ln\ R_{inp}} - \frac{1}{2}(1-\frac{1}{r_D^2})(1+\frac{1}{2\ \ln\ R_{inp}})\}] \quad (6.36)$$

$$\sigma_{\theta,th} = \frac{-\alpha E}{1-\nu}[(T_m - T_f)\{1-\frac{\ln\ r_D}{2\ \ln\ R_{int}} - \frac{1}{2}(1-\frac{1}{r_D^2})(1+\frac{1}{2\ \ln\ R_{int}})\}+$$

$$(T_p - T_m)\{1-\frac{1}{2\ \ln\ R_{inp}} - \frac{1}{2}(1-\frac{1}{r_D^2})(1+\frac{1}{2\ \ln\ R_{inp}})\}] \quad (6.37)$$

$$\sigma_{z,th} = \frac{-\alpha E}{1-\nu}[(T_m - T_f)(1-\frac{\ln\ r_D}{\ln\ R_{int}}) + (T_p - T_m)(1-\frac{\ln\ r_D}{\ln\ R_{inp}})] \quad (6.38)$$

where, $\sigma_{r,th}$, $\sigma_{\theta,th}$, $\sigma_{z,th}$ are normal thermal stress components in cylindrical coordinates; $r_D = r/r_w$ is the dimensional radial distance, α is the coefficient of thermal linear expansion, E is the Young's modulus of elasticity, and ν is the Poisson's ratio. The functions R_{int} and R_{inp} were defined by Eqs. 6.28.

To demonstrate the application of the Eqs. 6.36-6.38 we present an example. The input data are: the formation is sandstone (Table 3.18), the depth (z) is 1524 m, well radius r_w is 0.1 m, mud density is 1.1 g/cm^3, oil density 0.8 g/cm^3, the temperature difference $T_m - T_f$ is 25°C, the temperature difference $T_p - T_m$ is 25°C, and time of thermal disturbance at a given depth (mud circulation period) during drilling t_c is 1440 hours.

The total radial stresses and percentage changes in the stresses around the wellbore after 24 hours of production are presented in Tables 6.8 and 6.9.

Table 6.8 Total radial stresses around a wellbore (in MPa) in sandstone formation during the production period (Gogoi, 1986)

	Production time (t_p), hours				
r_D	24	120	240	720	1440
1	-12.192	-12.192	-12.192	-12.192	-12.192
2	-16.791	-16.895	-16.925	-16.967	-16.993
3	-17.117	-17.306	-17.392	-17.481	-17.532
4	-16.955	-17.248	-17.340	-17.465	-17.537
5	-16.708	-17.070	-17.183	-17.336	-17.425
6	-16.460	-16.877	-17.008	-17.185	-17.288
7	-16.225	-16.690	-16.837	-17.034	-17.148
8	-16.009	-16.517	-16.676	-16.891	-17.016
9	-15.254	-16.356	-16.526	-16.757	-16.892
10	-15.196	-16.209	-16.387	-16.635	-16.778

Table 6.9 Percentage changes in the stresses around a wellbore (in MPa) due to thermal stresses after 24 hours of production (Gogoi, 1986)

	Percentage change		
r_D	σ_r	σ_θ	σ_z
1	0	70.76	26.31
2	25.92	33.62	19.92
3	26.35	22.23	16.18
4	24.47	16.61	13.53
5	22.35	12.09	11.47
6	20.37	8.81	9.72
7	18.56	6.57	8.37
8	16.92	4.51	7.14
9	11.37	7.11	6.16
2	10.91	6.56	5.82

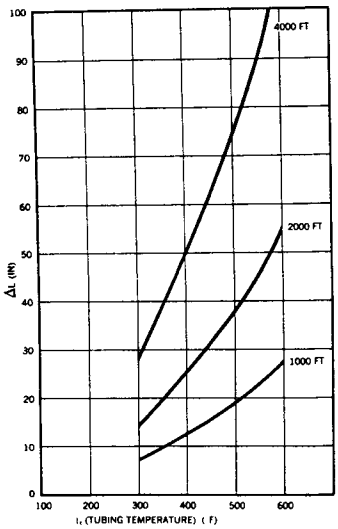


Fig. 6.6. Thermal casing elongation (Leutwyler and Bigelow, 1966).

Because the difference $T_p - T_m$ was positive, the thermal stresses were increased during the production period. In the upper sections of a well the thermal stresses of the drilling period will be increased during production when $T_p > T_f$. For cold water injection well where $T_p < T_f$ over long periods of time the wellbore thermal stresses will be tensile, whether they were compressive or compressive during the drilling period (Gogoi, 1986). The thermal stresses can significantly increase or reduce the total stresses. For the given example (Table 6.9), after 24 hours, of production, the vertical and radial stresses changed as much as by 26% and a change of more than 70% was observed for the circumferential stress. The thermal stresses can be controlled by changing of the wellbore temperature or by using thermal insulation of production strings.

The thermal elongation is used to analyze conditions or elastic and plastic stability of tubing and casing string failures (Leutwyler and Bigelow, 1966). Figure 6.6 illustrates the magnitude of thermal casing elongation as a function of tubing temperature for some selected cases of casing and tubing combinations.

We calculated casing temperatures (Table 6.10) for the field example presented in the Section 6.1.4. From Eqs. 3.88 and 3.89 we

Table 6.10 Casing and formation temperatures (in ^{o}F) after 250 days of steam injection

		λ_{ef}, $Btu/ft \cdot day \cdot^{o} F$							
z, ft	T_f	1.50	2.0	2.5	3.0	3.5	4.0	4.5	5.0
100	76	212	214	222	233	245	257	269	280
200	82	212	215	224	235	248	260	272	283
300	88	212	216	226	238	250	262	274	285
400	94	212	218	228	240	252	265	276	287
500	100	213	219	230	242	255	267	279	289
600	106	213	221	232	245	257	269	281	292
700	112	214	223	235	247	260	272	283	294
800	118	215	225	237	250	262	274	285	296
900	124	216	227	239	252	265	276	287	298
1000	130	218	229	242	255	267	278	289	300

can estimate the change of length (ΔL) due to temperature increase and the change in axial stress (σ_{aT}). From Table 6.10 we find that for $\lambda_{ef} = 1.50\ Btu/ft \cdot day \cdot^{o}$F the average temperature of casing T_{av} is 214^{o}F, and the average temperature of the 1000 ft well section is 100^{o}F. Then,

$$\Delta L \approx 6.9 \cdot 10^{-6} \cdot 1000 \cdot (214 - 100) = 0.79\ (ft),$$

$$\sigma_{aT} = 207 \cdot 114 = 23,600\ (psi)$$

Similarly, for $\lambda_{ef} = 5.00\ Btu/ft \cdot day \cdot^{o}$F

$$\Delta L \approx 6.9 \cdot 10^{-6} \cdot 1000 \cdot (289 - 100) = 1.30\ (ft),$$

$$\sigma_{aT} = 207 \cdot 189 = 39,100\ (psi)$$

Thus this example shows that in steam or hot water injection wells thermal insulation of tubing can significantly reduce the magnitude of thermal stresses and elongation in casing and tubing.

Chapter 7

INTERPRETATION AND UTILIZATION OF TEMPERATURE DATA

7.1 Effect of Free Thermal Convection and Casing

After the complete termination of the recovery process of the temperature field (disturbed by drilling) the temperature in the borehole may still differ from the natural temperature of formations; this is due to the distorting influence of free heat convection and of the casing. Because of this, in the interpretation of thermogram, some investigators assume that small temperature anomalies can be explained by the presence of metallic casing or of convective movements of fluid (gas) in the borehole. At present, no difficulty is anticipated in regard to the establishment of the per se fact of existence of convection in a vertical pipe filled with fluid or gas.

Free heat convection arises when the temperature gradient equals or exceeds the so-called critical gradient A_{cr}. For a vertical pipe Ostroumov (1952) obtained an equation for the determination of A_{cr}. The results of the graphical solution of this equation are presented in Table 7.1. Thus, in order to determine A_{cr}, it is necessary to determine the ratio λ_f/λ, after which the critical Rayleigh number Ra_{cr} (Table 7.1) and A_{cr} are calculated :

$$Ra_{cr} = \frac{g\beta A_{cr} r_o^4}{\nu a}; \qquad A_{cr} = Ra_{cr}\frac{\nu a}{g\beta r_o^4} \tag{7.1}$$

where λ_f, λ are thermal conductivities of formations and of the fluid

Table 7.1 The function $Ra_{cr} = f(\lambda_f/\lambda)$

λ_f/λ	Ra_{cr}	λ_f/λ	Ra_{cr}	λ_f/λ	Ra_{cr}
0	67.4	1.02	104.9	6.27	168.0
0.07	70.7	1.59	118.6	12.5	187.4
0.31	81.0	2.43	133.6	58.4	208.5
0.62	92.4	3.78	150.0	∞	215.8

(gas) in the borehole, respectively, ν is kinematic viscosity, a is the thermal diffusivity of the fluid (gas), β is the coefficient of thermal volumetric expansion, g is the acceleration of gravity, and r_o is the inside radius of the pipe.

Hales (1937) obtained the following equation for the critical temperature gradient:

$$A_{cr} = \frac{g\beta T}{c_p} + C\frac{\nu a}{g\beta r_o^4} \tag{7.2}$$

where T is temperature in K, c_p is specific heat of fluid at constant pressure, and C is a constant, depending on constitution of the convective flow ($C = 216$ or $C = 452$). It is easy to see that Hales does not account the influence of formation thermal properties upon quantity A_{cr}. Formulas (7.1 and 7.2) indicate that the value of A_{cr} strongly depends on the borehole radius.

For shallow boreholes (down to 20 m) we have shown that the convective process plays a substantial role in the thermal regime of boreholes (Kutasov and Devyatkin, 1964). Some results of an annual field experiment are presented below.

For a long time efforts, by direct temperature observations, failed to establish a quantitative estimate of the effect of free thermal convection on temperature regime of deep boreholes.
Several decades ago results of interesting *in situ* and laboratory experiments (Diment, 1967; Gretener, 1967; Sammel, 1968) were published. It was shown that the convective process basically expresses itself in vertical movements of low periodicity (from several minutes to fifteen minutes and above) and that extent of these movements does not exceed several diameters of the borehole. Continuous temperature recording attested to the fact that the temperature in the borehole was subjected to oscillations. For a 360 m borehole (diameter 25 cm) filled with water, the amplitude of temperature

oscillations (ΔT) did not exceed 0.05°C (Diment, 1967). The value of ΔT was approximately proportional to the value of the geothermal gradient (Γ). For this borehole $\Delta T = c\Gamma$; c = 1.25 m. The Gretener's experiments (1967) on two deep wells in Texas lead to analogous results. In Fig. 7.1 are presented results of the study conducted by Sammel (1968).

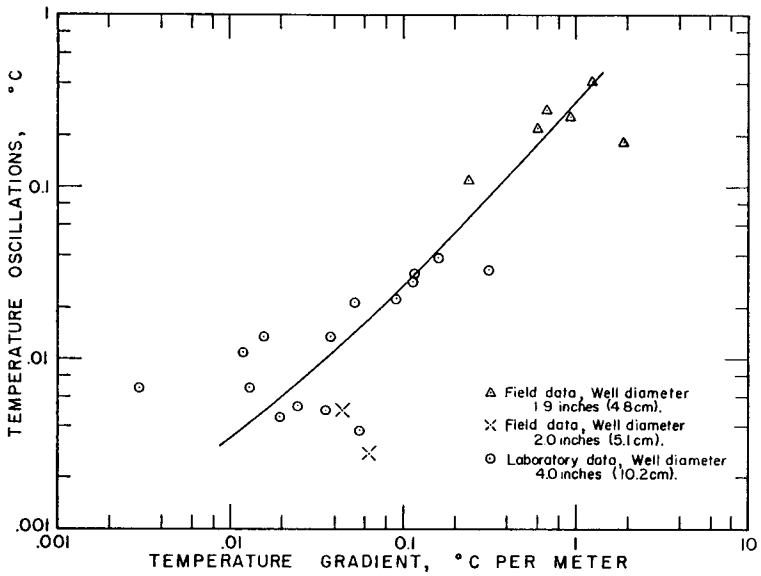


Fig. 7.1. Relationship of temperature gradient at a point to amplitude of temperature oscillations at that point (Sammel, 1968).

For *in situ* investigations in one or in several wells, it is difficult to encompass a wide range parameters entering into the Rayleigh criterion (number). Because of this, Devyatkin (Kutasov and Devyatkin, 1973) chosed the thermal modeling approach. Theory (Ostroymov, 1952) indicates that the Rayleigh criterion is the determining criterion in the free thermal convection modeling. Thus, the following relation should be satisfied:

$$\frac{g\beta A_{cr} r_o^4}{\nu a}\Big|_m = \frac{g\beta A_{cr} r_o^4}{\nu a}\Big|_n$$

where indexes n and m refer to natural (*in situ*) and modeling conditions. Analysis of modeling results indicated that the following

Table 7.2 Values of coefficients D and B

Borehole filler	Ra	D, 1/m	B
Water	1000 - 56300	6.25	0.16
Transformer oil	1400 - 16300	10.53	0.21
	260 - 1400	35.49	0.30
Air	200 - 840	35.49	0.30

Table 7.3 Maximal temperature deviations (°C) at an average temperature 20°C

Substance (filling)	grad T °C/m	well radius, cm			
		4	6	8	10
water	0.03	0.009	0.012	0.015	0.018
	0.05	0.017	0.022	0.028	-
	0.10	0.040	0.050	-	-
	1.00	0.500	-	-	-
Transformer oil	0.03	0.003	0.009	0.013	0.020
	0.05	0.007	0.017	0.026	-
	0.10	0.010	0.040	-	-
	1.00	0.600	-	-	-
Air	2.00	0.0400	-	-	-

function satisfactory describes the maximum value of the temperature disturbance (ΔT_{max}):

$$\Delta T_{max} = \frac{A}{D(1 - B \log Ra)} \tag{7.3}$$

where A is the vertical temperature gradient, D and B are constants (Table 7.2). Table 7.3 represents the maximal temperature deviations calculated after Formula (7.3). Temperature disturbance due to free thermal convection in deep boreholes usually do not exceed 0.03°C (Table 7.3). It is not difficult to see from Formula (7.3) that for a small interval of variation of the Rayleigh number, the quantity of ΔT_{max} is approximately proportional to the vertical temperature gradient (A). Thus, the data of *in situ* observations (Diment, 1967; Gretener, 1967; Sammel, 1968) and those for modeling are in fair agreement.

Let us compare the calculations with field data obtained previously (Kutasov and Devyatkin, 1964) for a borehole filled with transformer oil. The radius of the borehole was 4 cm and the vertical

temperature gradient at depths of 3 to 5 m attained the value of $2.1^oC/m$. For an average filler temperature of -2.0^oC, the Rayleigh number is 5590. From Formula (7.3), one finds $\Delta T_{max} = 0.94^oC$, while for *in situ* observations the temperature deviation due to convection at depth of 3 m is 1.19^oC and at 5 m it is 0.83^oC.

We also present some results of annual observations of the thermal regime of four shallow boreholes drilled in a stratum characterized by annual temperature fluctuations (Kutasov and Devyatkin, 1964). Since this rock stratum is characterized by high temperature gradients values, the convective process should be the most pronounced in such boreholes.

Study of thermal regime of boreholes drilled in a stratum characterized by annual temperature fluctuations is important in itself, since geothermal measurements within limits of this stratum are conducted on a large scale in practice.

Four boreholes up to 20 m were drilled for long term observation of the temperature regime. Boreholes No. 1, No. 2, and No. 3 were situated at a distance of 2.5 m from borehole No. 4. The boreholes were outfitted as follows: No. 1 open and empty, No. 2 covered and empty, No. 3 filled with transformer oil, and No. 4 filled with soil. Borehole No. 3 is cased to the bottom with a 4 cm inside diameter casing. The top of casing is plugged. Boreholes No. 1, No. 2, and No. 4 have metal casings with a 6 cm inside diameter casing to a depth of 2 m. Each borehole was shielded by a wooden duct against entry of rain and snow. Cables with thermistors were installed in the boreholes at various depths. The thermistor resistances were measured (in a lab) with the Wheatston resistant bridge. The total absolute error of the measurements was 0.1^oC and the accuracy of the temperature variations was 0.015^oC. Systematic observation for a period of one year indicated that convective heat exchange plays a significant role in formation of the thermal regime of the test boreholes (Fig. 7.2 and Table 7.4). The effect of convection on the course of the well known in geocriology phenomenon – the time lag of "zero degree" isotherm, is particularly striking. If one assumes that the greater part of the water passes to ice over the $-0.2 \div 0^oC$ temperature interval, the period of transition will vary on basis of the observations of borehole No. 4 (filled with soil) and of borehole No. 2 (covered but not filled). According to the observations in borehole No. 4 (Fig. 7.3) this period amounts to around 50 days,

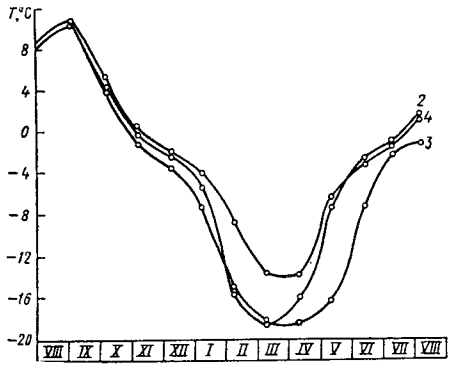


Fig. 7.2. Graphs of variation in temperatures at a depth of 1 m in boreholes No. 2, No. 3, and No. 4.

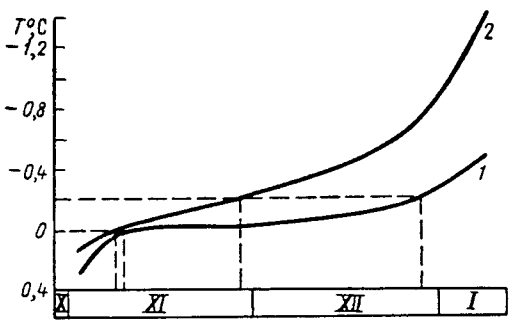


Fig. 7.3. Time lag of "zero degree" isotherm in boreholes No. 1 and no. 2 at a depth 1 m.

Table 7.4 Maximal temperature deviations (^oC) at different depths

H,	well number		
m	1	2	3
1.0	-	6.90	9.80
2.0	0.55	2.35	5.33
3.0	0.65	0.69	1.19
5.0	0.47	0.24	0.83
10.0	0.20	0.42	0.64
15.0	0.15	0.20	0.22

and 20 days in borehole No. 2.

Efforts were made to estimate the effect of casing on the distribution of borehole temperatures. Temperature measurements (Kraskovskiy, 1934) show that the influence of steel casing does not exceed the accuracy of temperature measurements by mercury thermometers ($\pm 0.2^oC$). Guyod (1946) has demonstrated, by means of laboratory modeling, that the presence of a homogeneous steel cylinder having a radius that is identical to the radius of casing does not affect the temperature field of the borehole, except at the end portions of the pipes. In order to quantitatively determine this effect we conducted computer calculations (Kutasov and Devyatkin, 1973).

The statement of problem was as follows: into a homogeneous medium with thermal conductivity λ and temperature $T_f = T_o + \Gamma H$, a steel cylinder with thermal conductivity λ_c is introduced (Fig. 7.4). It is required to determine the disturbance of the temperature field due to the cylinder. Introducing the "disturbance" function $T_B(r, z)$, we assumed that the temperature is a sum:

$$T(r, H) = T_f(H) + T_B(r, H) \tag{7.4}$$

Function $T(r, H)$ is written in the form

$$T(r, H) = T_c(r, H); \quad r \leq r_c; \quad H_1 \leq H \leq H_2; \tag{7.5}$$

$$T(r, H) = T_f(r, H); \quad l \geq r \geq r_c; \quad 0 \leq H \leq H_1; \quad H \geq H_2$$

The values of H_1 and l were selected such that

$$T_B(r, \frac{H_1}{2}) = T_B(r, H_2 + \frac{H_1}{2}) = T_B(l, H) = 0; \quad l \approx 16 r_c$$

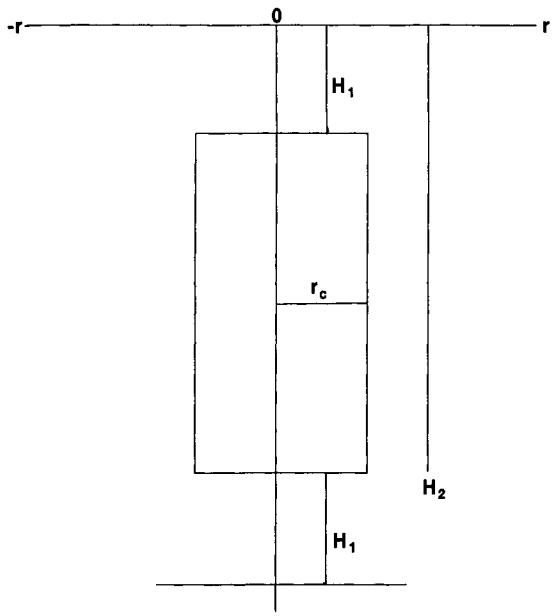


Fig. 7.4. Temperature effect of casing – a schematic model

The determination of $T(r, H)$ amounts to the solution of the system of Laplace equations:

$$\left.\begin{aligned} \frac{\partial^2 T_c}{\partial r^2} + \frac{1}{r}\frac{\partial T_c}{\partial r} + \frac{\partial^2 T_c}{\partial r^2} = 0; \\ \frac{\partial^2 T_f}{\partial r^2} + \frac{1}{r}\frac{\partial T_f}{\partial r} + \frac{\partial^2 T_f}{\partial r^2} = 0 \end{aligned}\right\} \tag{7.6}$$

The following boundary conditions and conditions of coupling, expressed by equality of temperatures and heat flow on the surface of the cylinder (S) should be satisfied:

$$T(r,0) = T_o; \quad T(H_2 + H_1, r) = T_o + \Gamma(H_2 + H_1)$$

$$T(l,H) = T_o + \Gamma H; \quad T_f = T_c|_S; \quad \lambda \frac{\partial T_f}{\partial n} = \lambda_c \frac{\partial T_c}{\partial n}|_S$$

where $\frac{\partial T}{\partial n}$ is the derivative along to the normaly to surface S.
The surface $H = (H_1 + H_2)/2$ is the surface of symmetry and from axial symmetry follows that:

$$\frac{\partial T(r,H)}{\partial r}|_{r=0} = 0$$

The finite-difference method was used to solve the system of equations (7.6).The parameters of the problem were:

$$0.03 \leq \Gamma \leq 0.09\ ^oC/m; \quad 0.05 \leq r_c \leq 0.3\ m; \quad 10 \leq \lambda_c/\lambda \leq 30.$$

The processing of the results of numerical calculations (with the accuracy of 0.0001^oC) showed that the "disturbance" function for the cylinder's axis can be approximated by the following formula:

$$T_B(0,H) = \pm 8.3\ r_c\Gamma(1 - \frac{\lambda}{\lambda_c}) \exp\,(\,-\frac{0.12}{r_c} \mid H_{1,2} - H \mid\,) \qquad (7.7)$$

where the plus sign is attributed to H_1 and the minus sign to H_2. It should be noted that, since the casing pipes are replaced by a solid cylinder (as did Guyod), the influence of the casing on the borehole temperatures will be actually smaller than $T_B(0,H)$. Formula (7.7) shows that the function $T_B(0,H)$ attains a maximum at the ends of the casing pipe. Usually, $\lambda_c >> \lambda$ and for this reason, in practice, the value of the "disturbance" function will practically be determined by the radius of the casing and by geothermal gradient. As an illustration, consider the computer results for one variant of the problem (Fig. 7.5). One can see that the maximum value $T_B(0,H_2) = 0.023^o$C, while at a distance of 1 m from H_2, the quantity T_B is already down to 0.007^oC. Therefore one realizes that the distorting effect due to casing pipes is small and its influence is localized to the ends of the pipes, and is independent of time. However, the value of distortion of the natural temperature field, due to convective movements at a given depth, does vary with time and, during a certain period of time, attains its amplitudinal value ΔT_{max}. Thus the latter quantity, in the final analysis, determines the limiting point in the accuracy that can be reached at temperature surveys in deep boreholes.

7.2 Determination of Formation Temperature

7.2.1 Applicability of the Horner Method

The Horner method (plot) is often used to process the pressure buildup test data for wells produced at a constant flow rate. The

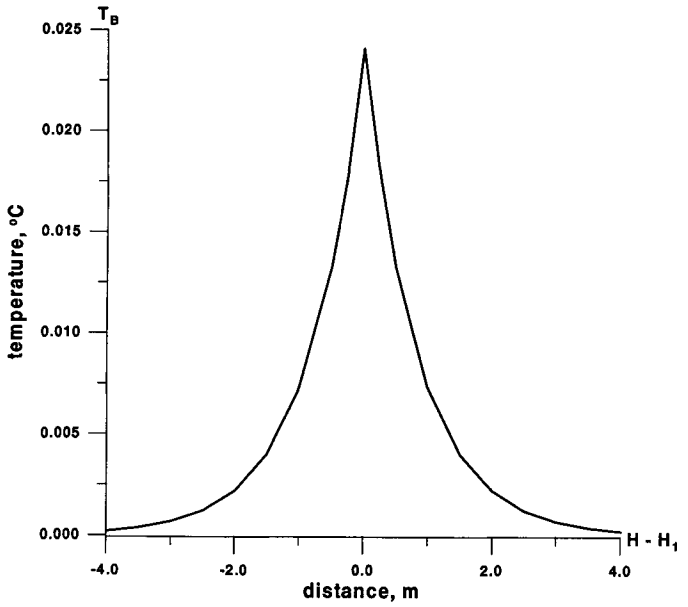


Fig. 7.5. The temperature disturbance along the axis of the cylinder. $r_c = 0.1\ m$, $\lambda_f/\lambda_c = 1/30$, $\Gamma = 0.03^oC/m$.

following formula is utilized to estimate the formation permeability (k) and initial reservoir pressure (p_i)

$$p_{ws} = p_i - \frac{q_p \mu}{4\pi k h} \ln\,(1 + t_p/t_s) \tag{7.8}$$

where p_{ws} is the shut-in bottomhole pressure, p_i is the initial reservoir pressure, q_p is the production rate, μ is the fluid dynamic viscosity, h is the reservoir thickness, t_p is the production time, and t_s is the shut-in time. Note that in reservoir engineering the production rate has a positive sign.

If p_{ws} is plotted versus $\ln\,(1 + t_p/t_s)$, linear regression of the data defines a line with a slope $M = q_p\mu/(4\pi kh)$ that intercepts the axis at $p_{ws} = p_i$. Thus the values of p_i and k can be determined.

In terms of temperature (pressure) and heat flow rate per unit of length ($-q/h$) the Eq. 7.8 becomes

$$T_s(r_w, t_s) = T_f - B\ \ln\,(1 + t_c/t_s), \qquad B = -\frac{q}{4\pi\lambda_f} \tag{7.9}$$

It was suggested to use this relationship for predictions of formation temperature from bottomhole temperature surveys (Timko and

Fertl, 1972; Dowdle and Cobb, 1975; Jorden and Campbell, 1984). However, Eq. 7.9 is valid for large dimensionless fluid production (circulation) times. Indeed, the basic formula which describes the shut-in temperature is

$$T_s = T_f + \frac{q}{4\pi\lambda_f}[-Ei(-\frac{r_w^2}{4a_f(t_c+t_s)}) + Ei(-\frac{r_w^2}{4a_f t_c})] \quad (7.10)$$

This equation represents the cooling of a well in which the drilling process is approximated by a constant (per unit of length) linear heat source. The logarithmic approximation of the Ei-function (with a good accuracy) is valid for small arguments

$$Ei(-x) = \ln x + 0.5772, \quad x = \frac{r_w^2}{4a_f t_c} = \frac{1}{4t_D}; \qquad x < 0.01 \quad (7.11)$$

Now the substitution of Eq. 7.11 into Eq. 7.10 yields the Formula 7.9. However, in many cases, the dimensionless circulation time is small and the Eq. 7.11 cannot be applied.

In addition, as was shown by Lachenbruch and Brewer (1959), the heat source strength (at a given depth) while drilling might more realistically be considered as a decreasing function of time. Hence, the constant wellbore temperature at a given depth during drilling better approximates the thermal effect of drilling operations than a constant linear heat source. It is also known that for large dimensionless fluid circulation times ($\approx 3,000 - 10,000$), the heat conductivity solutions for a cylindrical source with a constant temperature and for a constant linear source will eventually converge (Carslaw and Jaeger, 1959; Ramey, 1962). Therefore theoretically Horner method can be used only for large values of t_D. The circulation fluid period at bottomhole temperature surveys is short (3-6 hours), the coefficients of thermal diffusivity of formations are small, and as a result the calculated values of t_D are small. For this reasons we consider Eq. 7.9 only as an extrapolation formula. As will be shown by the following example, it is difficult to determine the accuracy of the Horner method in predicting undisturbed formation temperatures.

Example.

Data used in the example (Schoeppel and Gilarranz, 1966) are shown in Table 7.5. The example applies to a 7.875 in. borehole to 10,000 ft in a region where the geothermal gradient is

Table 7.5 Shut-in temperatures used in example (Schoeppel and Gilarranz, 1966)

No.	t_s, hr	t_{sD}	T_s °F	$T_f - T_s$ °F	t_s/t_c
1	1.0	0.0431	179.50	34.50	0.333
2	2.0	0.0862	187.80	26.20	0.667
3	3.0	0.1293	191.92	22.08	1.000
4	4.0	0.1724	195.37	18.63	1.333
5	5.0	0.2155	198.13	15.87	1.667
6	6.0	0.2586	200.20	13.80	2.000
7	7.0	0.3017	201.58	12.48	2.333
8	8.0	0.3448	202.27	11.73	2.667
9	9.0	0.3879	202.96	11.04	3.000
10	10.0	0.4310	203.65	10.35	3.333
11	11.0	0.4741	204.34	9.66	3.667
12	12.0	0.5172	205.03	8.97	4.000

1.4°F/100 ft. The bottomhole circulating temperature is determined to be 145°F. The undisturbed formation temperature is is 214°F, the well radius is 0.329 ft, the formation diffusivity is 0.0431 ft^2/hr, and the mud circulation period is 3 hours. The computed temperature-time relation is shown by Fig. 7.6.

We used the Formula 7.9 and a computer linear regression program to process the input data. The predicted values of T_f are presented in Table 7.6. The accuracy of T_f prediction in this example depends on the duration of the shut-in period. For example, if the shut-in period is 3 hours, the $\Delta T_f = 214 - 204.26 \approx 10(°F)$. At the same time the temperature deviations (δT) from the Horner plot are small (Table 7.6).

7.2.2 Analytical Method

The transient shut-in temperatures at the axis of the wellbore are given by Formula 4.7. An assumption was made that the thermal properties are identical within the well and in surrounding formations. From physical considerations follows that, at short circulation times, this assumption may introduce errors in formation temperature predictions.
We also presented an approximate analytical solution (Eq. 4.38)

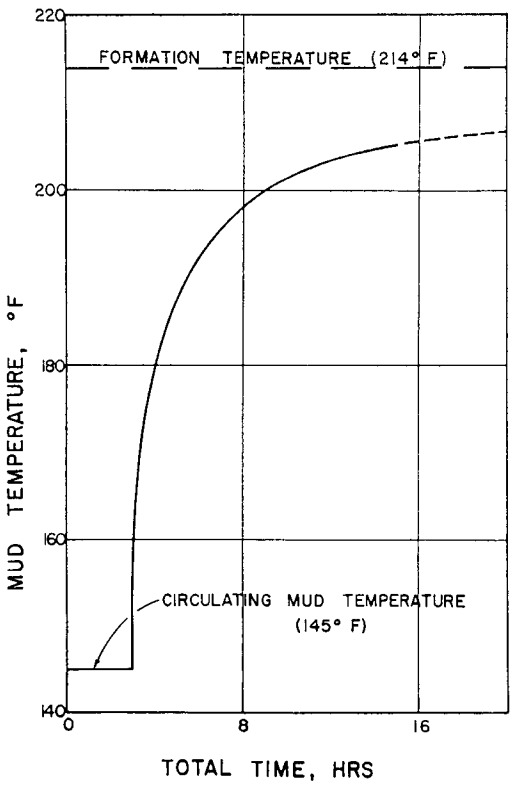


Fig. 7.6. Shut-in temperatures (Schoeppel and Gilarranz, 1966).

Table 7.6 Formation temperature predicted by the Horner plot

Combination	T_f, °F	δT °F	B °F	Combination	T_f, °F	δT °F	B °F
1-2	203.98	-	40.7	3-5	211.03	0.12	63.7
1-3	204.26	0.06	41.2	4-6	212.87	0.02	72.1
1-4	205.36	0.39	43.3	5-12	210.77	0.17	61.1
1-5	206.49	0.65	45.6	9-12	212.09	0.06	73.5
1-8	208.42	0.91	49.9	10-12	212.84	0.03	80.8
2-4	206.84	0.29	48.2				

which describes the temperature distribution in formation surrounding ($r \geq r_w$) the wellbore during the shut-in period. For $r = r_w$ Eq. 4.38 becomes

$$T_{sD} = \frac{T(r_w, t_s) - T_f}{T_c - T_f} = \frac{Ei(-\frac{1}{4(t_D^* + t_{sD})}) - Ei(-\frac{1}{4t_{sD}})}{Ei(-\frac{1}{4t_D^*})} \tag{7.12}$$

At derivation of the Eq. 4.38 the principle of superposition was used and the above mentioned assumption was not made. For this reason we suggest to use Eq. 7.12 for predicting the bottomhole formation temperature, when the mud circulation period is short.
All dimensionless variables in the Formula 7.12 were defined earlier, and one can see that the dimensionless wellbore shut-in temperature is a function of two parameters

$$\frac{T(r_w, t_s) - T_f}{T_c - T_f} = f(t_D, t_{sD}) \tag{7.13}$$

At least two shut-in temperatures are needed to determine the formation temperature. Let us assume that

$$t_s = t_{s1}, \quad T(r_w, t_{s1}) = T_{s1}; \quad t_s = t_{s2}, \quad T(r_w, t_{s2}) = T_{s2}.$$

Then, T_f is determined from Eq. 7.13:

$$\frac{T_{s1} - T_f}{T_{s2} - T_f} = \frac{f(t_D, t_{s1D})}{f(t_D, t_{s2D})} = \gamma, \quad T_f = \frac{\gamma T_{s2} - T_{s1}}{\gamma - 1} \tag{7.14}$$

$$t_{s1D} = \frac{a t_{s1}}{r_w^2}, \quad t_{s2D} = \frac{a t_{s2}}{r_w^2}$$

Only the shut-in temperatures for the first five hours were used to estimate the formation temperature in the previous example (Table 7.7). The calculated average value of $T_f = 213.9^o$F is in a good agreement with the undisturbed bottomhole formation temperature of 214.0^oF (Schoeppel and Gilarranz, 1966). To calculate the geothermal gradient the values of T_f for two depths should be determined. To speed up calculations we prepared a computer program "GRAD" (Appendix C, Table C.7).

7.3 Estimation of the Geothermal Gradient

Very often only one temperature log is conducted in a shut-in borehole. For these cases we present below an approximate method

Table 7.7 Predicted formation temperature for the example

t_{s1}, hr	t_{s2}, hr	T_{s1}, °F	T_{s2}, °F	γ	T_f, °F
1.0	2.0	179.50	187.80	1.2933	216.10
1.0	3.0	179.50	191.92	1.5849	213.15
1.0	4.0	179.50	195.37	1.8729	213.55
1.0	5.0	179.50	198.13	2.1585	214.21
2.0	3.0	187.80	191.92	1.2255	210.19
2.0	4.0	187.80	195.37	1.4482	212.26
2.0	5.0	187.80	198.13	1.6690	213.57
3.0	4.0	191.92	195.37	1.1818	214.35
3.0	5.0	191.92	198.13	1.3619	215.29
4.0	5.0	195.37	198.13	1.1524	216.24
Average value: T_f = **213.9°F**					

for estimation of the geothermal gradient. The utilization of the proposed method will be demonstrated on two field examples.
The dimensionless shut-in wellbore temperature can determined from Eq. 7.12. Let

$$\Phi = T_{sD} = \frac{T(r_w, t_s) - T_f}{T_c - T_f} \tag{7.15}$$

For small sections of deep wells we can assume that $\Phi = T_{sD} = constant$. Let us assume that Γ is the geothermal gradient, T_{f1} is the formation temperature at the vertical depth h_1 and T_{f2} is the formation temperature at the some depth h_2 $(h_1 < h_2)$, then

$$T_{f2} = T_{f1} + \Gamma x; \quad x = h_2 - h_1 \tag{7.16}$$

Combining Formulas 7.12, 7.15, and 7.16 we obtain the following linear equation

$$T_s = \Gamma x(1 - \Phi) + B; \qquad B = T_{f1} + \Phi(T_m - T_{f1}) \tag{7.17}$$

To estimate the value of Φ we suggest the following procedure: calculate the average vertical depth $h_{av} = (h_1 + h_2)/2$ and then estimate the disturbance time (mud circulation time) for this depth

$$t_c \approx t_t - t_{av}$$

where t_t is the total drilling time, t_{av} is the period of time needed to reach the depth h_{av}. The value of t_{av} can be determined

from drilling records. When drilling records are not available the following formula can be used:

$$t_c = t_t(1 - \frac{h_{av}}{H})$$

where H is the total vertical depth of the well.
Theoretically only shut-in temperatures at two depths are needed to estimate the value of the geothermal gradient. However, processing temperature data by a linear regression program will provide more dependable results. Below we present two field examples. In both cases a linear regression program was used to process field data.

Example 1.
Well #272 was drilled for 53 days to the total vertical depth 3305 m, well diameter 17.5 inches (Judge et al., 1979).

Table 7.8 Results of calculations for the 365.8-487.7 m interval. Shut-in time - 82 days

h, m	T, °C	a, m^2/hr	Γ, °C/m
365.8	5.73	0.0030	0.03106
396.2	6.71	0.0040	0.03086
426.7	7.71	0.0050	0.03072
457.2	8.29		
487.7	9.19		

Table 7.9 Estimation of the geothermal gradient from field data (Judge et al., 1979)

Shut-in time 82 days			Shut-in time 29.4 months		
h, m	T, °C	Γ °C/m	h, m	T °C	Γ °C/m
365.8	5.73	0.02789	367.6	2.62	0.03276
426.7	7.71		428.5	4.44	
486.5	9.15		487.7	5.09	
457.2	8.29		459.3	5.85	
487.7	9.19		490.1	6.49	

Example 2.
Well #193 was drilled for 237 days to the total vertical depth 4704 m, well diameter 17.5 inches (Taylor et al., 1982).

Table 7.10 Results of calculations for the 425.5 - 516.9 m interval. Shut-in time – 62 days

h, m	T, °C	a, m^2/hr	Γ, °C/m
425.5	7.89	0.0030	0.03178
456.0	8.09	0.0040	0.03134
486.5	9.15	0.0050	0.03103
516.9	9.98		

Table 7.11 Estimation of the geothermal gradient from field data (Taylor et al., 1982)

Shut-in time 62 days			Shut-in time 55.5 months		
h, m	T, °C	Γ °C/m	h, m	T °C	Γ °C/m
425.5	7.89	0.02417	426.7	3.26	0.03114
456.0	8.09		457.2	4.17	
486.5	9.15		487.7	5.09	
516.9	9.98		517.9	9.98	

In Tables 7.8-7.11 values of Γ are calculated after Formula 7.17 and the results of direct estimations of the geothermal gradients from long term temperature logs are compared. The agreement between the values of Γ by these two methods is seen to be good.

7.4 Mud Density Program

In a tectonically stressed region the pore pressure may drastically be increased over short vertical intervals. In this case the designing of the mud density program becomes a complex task. As an example consider wells drilled in the Central Graben (North Sea). The following data were taken from MacAndrew et al. (1993). The Central Graben contains several jurasic gas condensate prospects at 12,000 to 20,000 ft (3660 to 6100 m), with pressures of 18,000 *psi* or more and temperatures of up to 400°F (205°C). Water depth in the Central Graben varies between 250 to 350 ft (75 to 105 m). In the 10,500-12,500 ft interval an increase in pore pressure (in terms of

equivalent density) from 13.5 to 17.5 *ppg* can occur over an interval of less than 100 ft., yet the fracture gradient of the permeable formations remains below 18.5 *ppg*. In some cases, convergence of pore and fracture pressures means that a small decrease in the mud weight of 0.5 pounds per gallon or less changes the well from losing circulation to taking a kick (MacAndrew et al., 1993). To prevent influxes of reservoir fluid into the well it is suggested to use 14.0 *ppg* density water-based mud while penetrating the 5,000 - 11,500 ft interval. For deeper depths (up to 16,000 ft) the mud density should be increased to 16.5 *ppg* (taken from a plot).

Our objective is to estimate the effect of high temperatures and pressures on the mud density program. In our case this means whether or not suggested values of mud density should be corrected. A number of needed data were not available and some assumptions were made.

We assumed that the average geothermal gradient is $0.02^oF/ft$ and the surface temperature of bottom sea sediments is 40^oF. The assumed values of the outlet mud temperature (T_{ou}) for four depths are presented in Table 7.12. From Eqs. 5.12 and 5.13 we found the values of the bottomhole mud circulating temperature T_{mb}. The conventional constant-surface-mud-density method (Eq. 3.49) was used to calculate the required downhole pressure (p). We should to note that in Eq. 3.49 a more accurate value of the conversion factor B_c (0.051947 instead of 0.052)was used. From Table 3.10 the average coefficients for three water-base muds with ($10.77 \leq \rho_o \leq 18.08\ ppg$) are: $\alpha = 3.2362 \cdot 10^{-6}\ 1/psig$, $\beta = -1.8246 \cdot 10^{-4}\ 1/^oF$, and $\gamma = -4.5312 \cdot 10^{-7}\ (^oF)^{-2}$. These coefficients were used in the computer program "HYDIF" (Appendix C, Table C.2) to calculate the downhole hydrostatic pressure (p_w). The results of calculations are presented in the Table 7.12. In Table 7.12 ρ_o is the mud density at pressure 0 *psig* and temperature 15^oC.

Let us assume that drilling is conducted at overbalance and the differential pressure is +200 *psig*. From Table 7.12 follows that it is safe to drill the 5,000-11,500 ft interval with the surface density mud of 13.648 *ppg*. At the same time for the depth of 16,000 ft the actual differential pressure is:

$$-308 + 200 = -108\ (psig)$$

and drilling is conducted at underbalance instead of overbalance. In this case an influx of formation fluid into the well may occur

Table 7.12 The change of the mud density program and bottomhole pressure

H_t ft	p_w *psig*	ρ_o *ppg*	p *psig*	$p_w - p$ *psig*	T_{ou} °F	T_{mb} °F
5,000	3,647	14.00	3,636	11	60.0	90.5
	3,639	13.97		3		
11,500	8,268	14.0	8,364	-96	125.0	207.0
	8,364	14.16		0		
12,000	10,180	16.50	10,286	-106	130.0	216.0
	10,286	16.67		0		216.0
	10,368	16.80		82		216.0
16,000	13,406	16.50	13,714	-308	170.0	287.7
	13,656	16.80		-58		
	13,714	16.87		0		

resulting in a kick. It is easy to see that for the 12,000 - 16,000 ft section of the well mud density should be increase from 16.5 to 16.8 *ppg*.

7.5 Location of the Cement Column Top

As we mentioned before (Section 5.3) the duration and the magnitude of the temperature anomaly (ΔT_{ch}) associated with the cement hydration depends mainly on the ambient temperature, cement composition, and the thickness of the cement ring. The recovery of the temperature field of formations after completing of drilling operations also affects the value of ΔT_{ch} (Proselkov, 1975). Contamination of the cement slurry by the drilling mud may not only delay (or even prevent) cement setting, but significantly reduce the value of ΔT_{ch}. To interpret the temperature surveys during waiting on cement setting (WOC) a caliper log should be conducted prior to the cement slurry placement. In this case one may expect that the maximum values of ΔT_{ch} should be observed in sections of the wellbore where large washouts were detected by the caliper log. The knowledge of the cement heat generation rate as a function of time, ambient temperature and thermal properties

Table 7.13 Time to run temperature surveys (Halliburton Cementing Tables, 1979)

Cement	Admixture	Time lapse, hrs					
		120° F	140° F	160° F	180° F	220° F	220° F
Portland Cement	0% Gel	8-12	6-9	4-8			
	4% Gel	8-12	6-9	4-8			
	8% Gel	9-12	6-9	6-9			
	12% Gel	9-12	9-12	9-12			
Pozmix Cement	0% Gel	8-12	6-9	4-8			
	2% Gel	8-12	8-12	6-9			
	4% Gel	8-12	8-12	6-9			
Portland Cement	0 ft^3	8-12	6-9	4-8			
with 2 or 4% Gel	1/4 ft^3	8-12	6-9	4-8			
and Perlite	1/2 ft^3	9-12	6-9	6-9			
	1 ft^3	9-12	9-12	9-12			
Portland Cement	10%	8-12	6-9	4-8			
with Diacel D*	20%	8-12	6-9	4-8			
	40%	9-12	6-9	6-9			
Pozmix Cement or							
Portland Cement	0.3%		15-18	12-15	9-12	8-12	6-9
with HR-4 Retarder	0.5%		16-24	16-24	12-18	9-12	8-12
Retarded Cements:							
Texcor			16-24	16-24	12-18	9-12	9-12
Pozmix 140*			16-24	16-20	12-16	8-12	6-9

Note: *has low heat of hydration and may be difficult to pick up on a temperature survey. The time lapse values for the ambient temperature of 100° F are the same as for 120° F.

of formations is needed to estimate the moment of time during the WOC period, when the maximum value of ΔT_{ch} can be observed. The field and laboratory data show that the maximum values of ΔT_{ch} were measured during the first 4 to 24 hours (Table 7.13). Fast setting cement slurries can produce a marked increase in the temperature after several hours of the WOC period (Fig. 7.7).

Comparing the Curves 1 and 3 (Fig. 7.7), one can see that significant temperature changes occur during cementing of casing. In the 2,600-3,500 m section of the well the wellbore temperatures during cement hydration are much higher than the geothermal temperatures (Curves 1 and 2). The top of the cement column in this well can be easily detected at the depth of about 2,670 m.

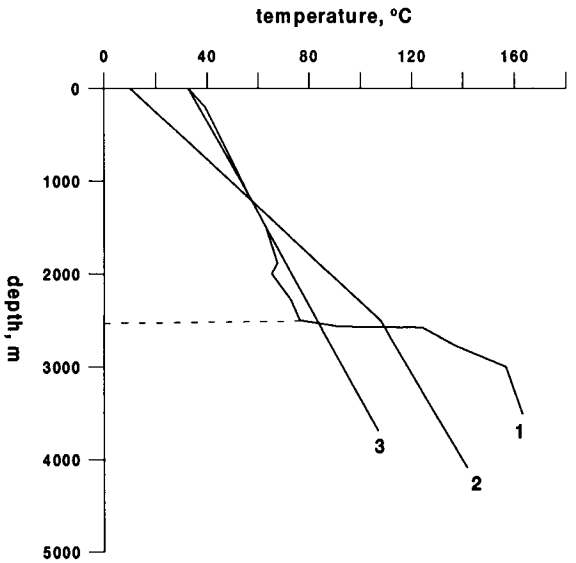


Fig. 7.7. Temperature surveys in the well 6, Russkiy Chutor, Stavropol district, Russia (Proselkov, 1975). 1 – temperature log after 3 hours of waiting on cement setting (WOC); 2 – geothermal curve; 3 – mud circulation temperature.

7.6 The Injectivity Profile

In secondary oil recovery by waterflooding and in maintaining the reservoir pressure significant amount of water is injected into the reservoir. The knowledge of the injectivity profile is needed to predict the water intake distribution over the injection interval. The temperature logs in water injection wells are usually used to locate the injection zone.

In the well's sections above and below the injection zone the rate of heat flow from (or into) the wellbore to the surrounding formations is mainly controlled by thermal conductivity of formations and by the difference between the geothermal (T_f) and wellbore (T_w). temperatures. At the same time in the injection zone not conduction but the forced thermal convection is the main heat transfer mechanism. The intensity of the heat exchange between the flowing radially outward water and formation depends on many factors: porosity, permeability, reservoir pressure, wellbore pressure, temperature difference ($T_f - T_w$), thermal properties of formations

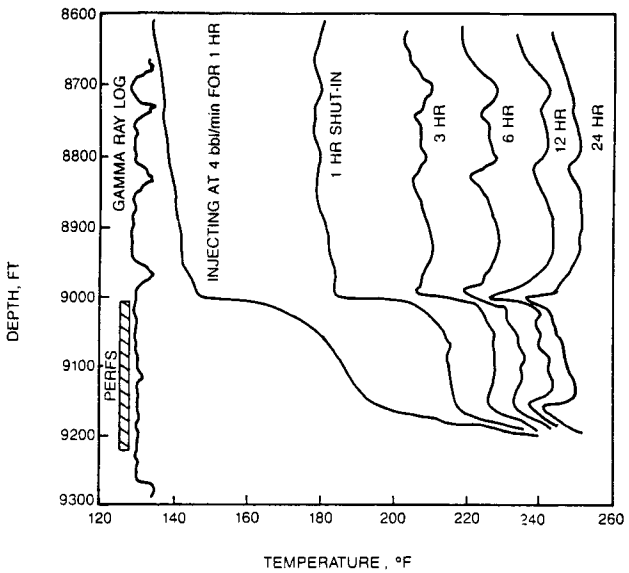


Fig. 7.8. Profiles during temperature recovery (Carlson and Barnette, 1988). Courtesy of Society of Petroleum Engineers.

and water. When the well is shut-in the process of thermal recovery starts. From physical considerations is clear that the thermal disturbance of the injection zone is much greater than in regions above and below the injection zone. Because of this the speed of thermal recovery in the injection zone is low and temperature anomalies can be detected by temperature logs taken at short shut-in times (Fig. 7.8). This production well was fractured, after which the well was shut-in for three weeks. Following the shut-in period, water was injected at 4 bbl/min for 1 hr. Temperature logs were recorded during injection, and at 1, 3, 6, 12, and 24 hrs after shut-in, as shown on Fig. 7.8. The formation temperature at 8780 ft is approximately 255°F (Carlson and Barnette, 1988). As was shown by Smith and Steffensen (1975) washouts (or other hole enlargement) intervals in the open hole below the casing shoe and thief zones can be confused with a major injection zone. A mathematical model was used to demonstrate that such intervals often appears like injection zones on shut-in temperature curves. For example, in a 20-ft thief zone a leakoff at a low rate of 0.5 BWPD/ft creates a temperature anomaly almost of the same size as in the major injection zone. In this case

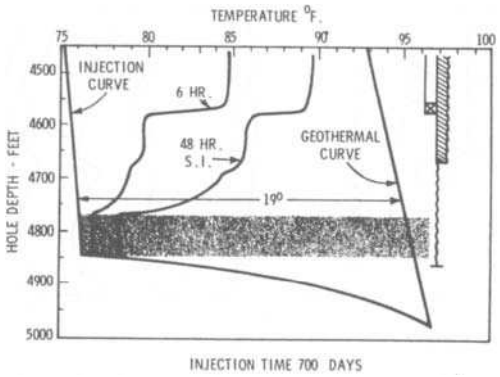


Fig. 7.9. Effect of 19°F temperature difference at injection time of 700 days and injection rate 1,500 BWPD (Smith and Steffensen, 1975).

the injection rate is 20 BWPD/ft over 20-ft interval, injection time is 700 days, and shut-in time is 48 hours (Smith and Steffensen, 1975). From numerical calculations was also concluded that shut-in temperatures curves can define zones of injection if there is at least 10°F (5.5°C) difference between the bottomhole injection-water temperature and the undisturbed formation temperature. As may be seen from Fig. 7.9 a temperature difference of 19°F (10.5°C) creates a sizable temperature anomaly.

An advanced mathematical model and a simulator for temperature logs were suggested by Fagley et al. (1982). The advantage of the mathematical model presented by the Authors is that heat transfer between water in the wellbore and in surrounding rock and rock/liquid matrix is considered both before and after shut-in. The water energy-balance equation in the wellbore is coupled with the diffusivity equation for the surrounding wellbore formation. It is assumed that the wellbore temperature prior to injection is equal to the geothermal temperature. A comparison of field data and simulator results showed a good agreement of temperature logs profiles over the entire well depth. It was shown that hot-water injection, for a short period before shut-in, can be an important tool for defining injection fluid profiles in mature (long-term injection) wells. Figure 7.10 shows a 26-hour shut-in curve following 25 months of 75°F (24°C) water injection at an average rate of 188 ft^3/hr. By

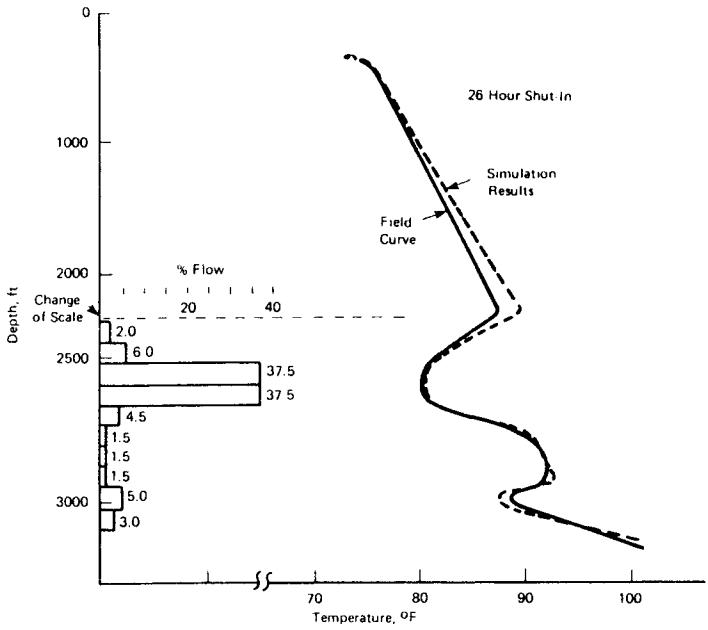


Fig. 7.10. Comparison of simulator and field results in a mature well (Fagley et al., 1982).

the variation of the injection flow profiles a match was obtained between the calculated and field measured temperature logs.

7.7 The Use of Thermistors in Temperature Probes

High temperature-sensitive thermistors are commonly used in geothermal investigations. To protect thermistors from mechanical damages, high pressures, and moisture, thermistors are encased in various fabricated housings. The electrical resistance (R) of a thermistor probe is usually measured by the Wheatstone bridge. A thermistor probe is one leg of a Wheatstone bridge circuit, and three legs of the bridge are low temperature coefficient resistors. For this reason in field conditions the bridge itself may introduce errors in measuring the thermistor's resistance. Osterkamp and Harrison (1982) used the following procedure to minimize these errors. A low temperature coefficient resistor is measured with the bridge before,

during, and after the logging. The same resistance is measured in the laboratory. The change in the resistance measurement between laboratory and field conditions are used to correct the field measured thermistors resistances. Corrected thermistor resistances values are then converted to temperatures.

To process field data it is advantageous to have a general mathematical expression of the temperature-resistance dependence for the thermistor. The following relationship was used by Osterkamp and Harrison (1982) to approximate the calibration data

$$\frac{1}{T} = A + B \ \ln \ R + C \ (\ln \ R)^2 \tag{7.18}$$

where T is in degrees Kelvin, R is the thermistor resistance in ohms, and A, B, and C are constants determined by a least squares fit of equation 7.18 to the calibration data.
Author proposed to approximate the temperature-resistance dependence by the following equation (Bogomolov et al., 1970)

$$R = A \ \exp\left(\frac{B}{T} + \frac{C}{T^2}\right) \tag{7.19}$$

$$T(^oC) = \frac{1}{D_1 - \sqrt{D_2 + \frac{1}{C} \ \ln \ A}} - 273.15 \tag{7.20}$$

$$D_1 = -\frac{B}{2C}, \qquad D_2 = D_1^2 - \frac{1}{C} \ \ln \ A$$

The coefficients A, B, and C are constants within of a 50°C interval. Thus, for a 0-150°C interval at least seven calibrational temperature points are needed. The electrical resistance of a thermistor reduces with the increasing of the temperature and the temperature coefficient is negative. The absolute value of the temperature coefficient can be calculated from Formula 7.21,

$$\alpha = \left|\frac{1}{R} \frac{dR}{dT}\right| = \frac{B}{T^2} + \frac{2C}{T^3} \tag{7.21}$$

and the electrical resistance change per 1K (1°C) is

$$\alpha R = \frac{RB}{T^2} + \frac{2RC}{T^3} \tag{7.22}$$

Calibration data for one thermistor are presented in Table 7.14. For

Table 7.14 Calibrational (R^*) and calculated (R) resistances of the thermistor No. 10185

T, °C	R^*, *Ohms*	R^*, *Ohms*	ΔR, *Ohms*
20.154	7128	7128	0
15.059	8765	8766	-1
10.122	10776	10775	1
5.145	13348	13351	-3
-0.621	17253	17253	0
-5.016	21110	21107	3
-10.066	26794	26793	1
-15.425	34800	34802	-2
-18.184	39958	39958	0

the thermistor No. 10185 the coefficients are:

$$A = 9.6891E - 03\ Ohm, \quad B = 4483.4\ K, \quad C = -1.5289E + 05\ K^2$$

Thermistor No. 10185 (Fenwall type GB35P2) was used in conducting temperature measurements in a deep well (Alaska). The thermistor was calibrated (Dr. A. Jessop) with high precision in the Geothermal laboratory of the Earth Physics Branch (Department of Energy, Mines, and Resources, Canada).
The values of α and αR for thermistor No. 10185 are presented in Fig. 7.11. It is easy to see that the thermistor's sensitivity is more than ten times higher than that of a metallic resistance thermometer ($\alpha \approx 0.4$ percent).

For a wide temperature interval the values of R, α, and αR may vary within wide limits. For one thermistor (KMT type) we found that at 0°C

$$R = 68,170\ \Omega, \quad \alpha = 0.05340\ 1/K, \quad \alpha R = 3,640\ \Omega/K$$

and at 150°C

$$R = 326.5\ \Omega, \quad \alpha = 0.02358\ 1/K, \quad \alpha R = 7.7\ \Omega/K$$

Thermistors have small outer surfaces and for this reason they are very sensitive to the self-heating. The voltage drop across the thermistor (V_h) cannot remain the same when the measured temperatures vary within wide limits. Indeed, for the above mentioned

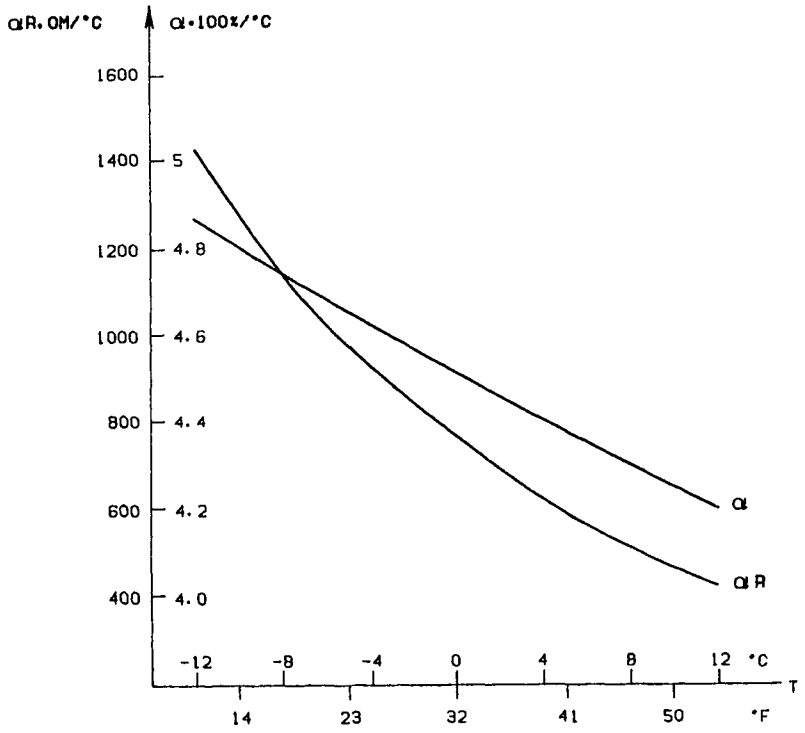


Fig. 7.11. The values of αR and α versus temperature for the thermistor No. 10185.

thermistor the resistance was changed in 187 times in the 0 - 150°C interval. The electric power delivered to the thermistor (P) is

$$P = \frac{V_h^2}{R} \tag{7.23}$$

Let us assume that the temperature of the medium is T_m and the stabilized temperature measured by the thermistor probe is T_h, the temperature difference caused by self-heating is $\Delta T_h = T_h - T_m$. From experimental data we found that for $\Delta T_h \leq 1°C$ the following relationship can be used

$$\Delta T_h = C_d P \tag{7.24}$$

where is C_d is the dissipation constant of the probe. It easy to see that C_d is the power in watts required to raise a thermistor probe

1^oC above the surrounding temperature. To determine this parameter in field conditions we recommend the following procedure. Firstly, insert in the battery circuit a variable resistor for voltage control. Secondly, use two voltage drops across the thermistor V_{h1} and V_{h2} while measuring the constant medium (borehole) temperature. Let the measured temperatures to be T_{h1} and T_{h2}. Then calculate the corresponding values of $P = P_1$ and $P = P_2$ (Formula 7.23). Finally, from following equations determine the value of C_d

$$T_{h1} - T_m = C_d P_1 \tag{7.25}$$

$$T_{h2} - T_m = C_d P_2 \tag{7.26}$$

$$C_d = \frac{T_{h1} - T_{h2}}{P_1 - P_2} \tag{7.27}$$

From Formulas 7.23 and 7.24 we can calculate the allowable voltage drop across the thermistor for a specified value of ΔT_h,

$$V_t = \sqrt{\frac{R \cdot \Delta T_h}{C_d}} \tag{7.28}$$

Example.
A thermistor probe with $C_d = 100$ K/W will be used for downhole temperature measurements in the 50-100°C interval. The corresponding electrical resistance interval is 1224-6903 Ohms and the specified value of ΔT_h is 0.005°C. What are the permissible voltage drops across the thermistor? From Eq. 7.28 we obtain for the temperature of 50^oC

$$V_h = \sqrt{\frac{6903 \cdot 0.005}{100}} \approx 0.60(V),$$

and for 100^oC

$$V_h = \sqrt{\frac{1224 \cdot 0.005}{100}} \approx 0.25(V)$$

Thus during the temperature survey the value of V_h should be gradually reduced from 0.60 to 0.25 Volts, or a constant value of 0.25 Volts can be used.

7.8 Interpretation of Temperature Surveys in Shallow Wells

7.8.1 General Information

Near-surface thermal prospecting is based on temperature measurements in shallow (up to several meters depth) drill holes. Taking into account differentiation of geological objects by their thermal properties, such temperature measurements contain useful information about features of the geological structures in the areas under investigation. It should be underlined that studying of thermal parameters by oil-and-gas exploration often play more important role than gravity, magnetic and sometimes – seismic investigations. At the same time, the noise caused by seasonal temperature variations and terrain relief effects may significantly distort the temperature field observed in the near-surface layer.

The method is used to explore oil and gas pools, pyrite, uranoorganic/uraninite ores, to trace fault or other discontinuities, and to solve other geological and geophysical problems. Despite of measurements in the deep wells where temperature observations are depended on the drilling process, the near-surface measurements are independent investigation, which may be promptly conducted at any area.

In the mid-1930s method of near-surface thermal prospecting was applied for the first time to study a faulted structure near Vintersweek, Netherlands (van den Bouwhuysen, 1934) and to study a salt stock near Hannover (Paul, 1935). These investigations may be considered as the beginning of application of near-surface thermal prospecting in petroleum geology. Results of temperature surveys in shallow wells (oil fields of Azerbaijan) have shown that the geotherms adequately reflect the peculiarities of the geological structures (Gorbenko, 1937). Investigation of thermal field by hydrocarbon prospecting were continued later by many investigators (Selig and Wallick, 1966; Hutchins and Kading, 1969; Poley and Steveninck, 1979; Leschak and Lewis, 1983, etc.). Khesin and Eppelbaum (1994) suggested to use a successive system of near-surface thermal data interpretation developed for complicated environments.

In the period between 1950 and 1970 thermal prospecting was developed mainly for mineral exploration. The postulate that the deep heat flow is redistributed by objects with enhanced thermal conductivity formed the theoretical basis for this technique. Subsequently, shallow thermal prospecting found wide use in solving the problems of petroleum geology as a cost effective and rapid means of singling out and tracing fractures. Thermal logging can be applied to determine quantitatively the characteristics of anomalous bodies. Temperature observations from deep wells and shallow bore- or blast-holes can be used. Observations from deep wells are not subject to seasonal variations, but the limited number of appropriate wells, their irregular spacing, and their possible absence along a selected area under study can reduce their use. At the same time investigation conducted by Mongelli and Morelli (1961) showed the similarity between thermal observations in shallow wells (1.5 m) and those at greater depts.

In majority of cases, however, the application of geothermal data was limited to simple qualitative interpretation, i.e., to the recording and tracing of temperature anomalies. Such simple interpretation may have considerable errors due to the neglect of time variations of the temperature field or the effect of rugged topography. To determine the parameters of disturbing bodies, it is necessary to eliminate noise from the observed temperature field and then to apply quantitative interpretation methods to the corrected field.

7.8.2 Elimination of Temporary Variations

Various methods of geothermal surveying and data processing have been developed for eliminating the temporary variations of temperature. The procedure suggested by Parasnis (1971) speeds up the field works but does not allow to remove seasonal variations. Other method consists of conducting a long-term geothermal investigation of the area under study and selecting a period when seasonal variations are minimal for the field survey (Dobrynina et al., 1985). However this method suffers from such drawbacks as long duration, and hence nonapplicability of the results, since the time of fieldwork is frequently set by organizational factors, etc.

Two other methods are worth mentioning: (1) synchronous

measurement of the temperature variations within the field survey (Khutorsky et al., 1983) similar to the well-known method of eliminating magnetic field variations in magnetic prospecting; (2) measurement of the temperature simultaneously at all points of the profile (Chekalyuk et al., 1974). However, in the first method it is not always possible to avoid the influence of temperature waves delayed in diffusing from the surface. The second method (it should be noted that we do not sure that such a procedure allows to remove all temporary variations) demands simultaneous use of many temperature-measuring devices which impede the surveying.

A method for eliminating temporary variations using repeated observations with subsequent linear filtering of the results was suggested by Eppelbaum and Mishne (1988). It is known that a regional thermal field is stable in time (Lubimova, 1968) and temperature-wave propagation in the medium is linear (Tikhonov and Samarsky, 1963). Taking into consideration these factors, a model of the total temperature field, recorded in the layer with annual temperature oscillations, can be represented in the following form:

$$Q_i(t) = T_i + \sum_{j=t-t'}^{t} \tau(j) f(t-j), \tag{7.29}$$

where $Q_i(t)$ is the observation at the ith point (borehole); T_i is the temperature conditioned by redistributing the deep heat flow caused by the object with contrasting conductivity; $\tau(j)$ is the average temperature at a certain depth Δh at time j along the region including the district under investigation (data from meteorological stations are employed); $f(t-j)$ is the weight step function reflecting the temperature effect at the depth Δh, at time $t-j$ on the temperature measured in the borehole, at depth h at time j; and t' is the delay time of temperature waves diffusing down the surface.

Noises are assumed to be autocorrelative, and the autocorrelation matrix for noises $\mathbf{R}(t-j)$ can be written in the form:

$$\mathbf{R}(t-j) = \begin{matrix} \frac{1}{1+(t-j)^2} & |t-j| \le \psi \\ 0 & |t-j| \ge \psi \end{matrix} \Bigg\}, \tag{7.30}$$

where ψ is some defined parameter.

Measurements at the points of the profile made at different times t enable one to obtain a solvable set of algebraic equations that allow

the desired signal T_i to be extracted with the required accuracy.

7.8.3 Elimination of Terrain Relief Effect

Attempts have been made by many investigators to reduce the terrain relief effects. In particular, we note the investigations conducted by Jaeger and Sass (1963), Lachenbruch (1968), Lee and Henyey (1974), and Brott et al., (1981). Apparently, the most promising of these techniques is the application of 2-D and 3-D modeling of terrain relief using a grid (Henry and Pollack, 1985). However, this approach demands further improvements.

It should be pointed out that the terrain relief effect is generally twofold (Khesin et al., 1996). First, the form and physical properties of topographic masses (e.g., rocks forming the relief) condition the presence of their effects in the anomalous field, which dampens the anomalous effects from the hidden objects to be prospected. Second, uneven observation lines are responsible for variations in the distance from the point of measurements to the source, and these variations manifest themselves differently in the anomalies from different objects. Therefore, in the general case it is necessary to calculate and eliminate the topographic effect from the observed field and to reduce the observation results to a common horizontal level (usually the highest point of the relief). Moreover, to solve a direct geophysical problem one has to know the physical properties of the geological structure, so upward continuation can be used to reduce the anomaly under study.

The problem of topographic effect elimination is described in Khesin (1978). The main forms of the relief may be represented by a combination of inclined slopes. The principle of this technique consists of constructing a correlation between the field values (U) and the heights of observation points (H) in the middle part of the slope, followed by determination of regression coefficients α and β. Thus, we obtain the approximate linear relationship

$$U_{appr} = \alpha + \beta H. \tag{7.31}$$

The value U_{appr} is subtracted from the field value U observed at every point with known height H. Thus, we obtain the corrected field value U_{corr} which reflects the geological inhomogeneity of

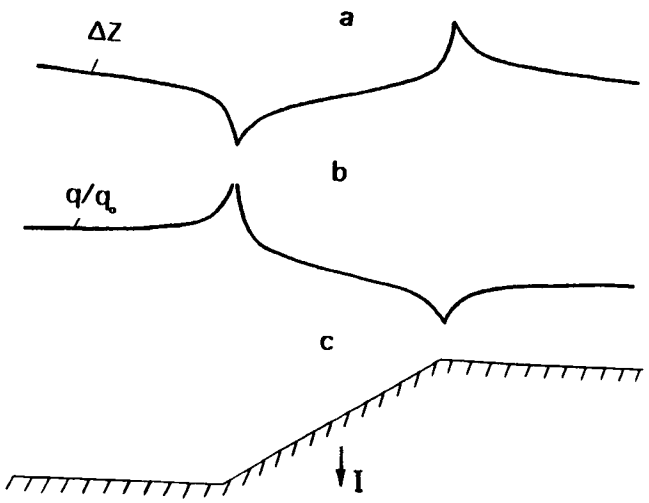


Fig. 7.12. Comparison of plots of (a) the magnetic field vertical component Z, and (b) relative heat flow q/q_o over (c) a slope in terrain. The curve (b) after Lachenbruch (1968).

the section. At the same time, the character of the correlation dependence allows one to form a conclusion concerning the presence and type of the inhomogeneity.

The applicability of the above technique to the results of thermal prospecting can be substantiated with the use of the following data. The inverse dependence of the surface temperature on the height of observations was pointed out by Bullard (1940), and is noted subsequently by many investigators. Lachenbruch (1968) made a calculation of the change in heat flow that governs the temperature variation observed on the inclined slope. A comparison made between the plots of the vertical magnetic field component (at vertical magnetization I) and the relative amount of the heat flow q/q_o is presented in Fig. 7.12. Example of a calculation of relief influence in the near-surface thermal prospecting was presented in Khesin and Eppelbaum (1994).

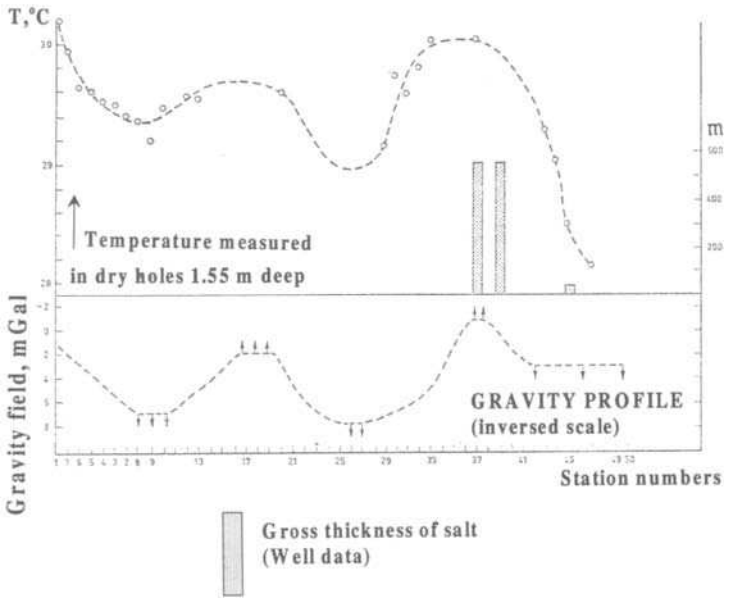


Fig. 7.13. Similarity of thermal and gravity (inversed data) over salt domes (Poley and Steveninck, 1970).

7.8.4 Common Aspects of Graviational, Magnetic and Temperature Anomalies

In this study, we did not consider techniques for the direct solution of thermal conductivity in nonuniform media, for example, by finite difference grid methods or computer-aided selection of temperature fields. Simmons (1967) suggested a method for interpreting of heat flow anomalies analogous to methods in gravity. Similarity between gravimetric and temperature anomalies has also been noted by Poley and Steveninck (1970) and Kappelmayer and Haenel (1974). However, in these studies examples of quantitative interpretation application are not given. Interesting comparison of thermal and gravity data is presented by Poley and Steveninck (1970) (Fig. 7.13). The thermal measurements were conducted in dry holes at a depth of 1.55 m; observation step was 200 m. Zorin and Lysak (1972) made an attempt to use the proportionality of analytical expressions for gravitational and temperature fields of a point source and to apply techniques developed in gravitational prospecting for interpretation

of anomalies in thermal prospecting. The regional anomaly from a deep-seated source in a rift area of Lake Baikal (Russia) was interpreted as an example. The quantitative interpretation was carried out, employing the Smith inequalities developed in gravitational prospecting (Parasnis, 1963). However, the use of these inequalities under complicated conditions (e.g., rugged topography, moderate inhomogeneities, inclined polarization, and unknown level of the normal field) is ineffective.

Carslaw and Jaeger (1959) noted that the problem of the disturbance of steady linear flow of heat in a uniform medium by an object of different conductivity is precisely the same mathematically as that of induced magnetization in a body of the same shape placed in a uniform external field. In connection with this fact, it is expedient to carry the developments from magnetic prospecting over to thermal prospecting.

Conduction is the main process of heat transfer in the upper layers of the earth crust (Cheremensky, 1972; Lakhtionov, 1973). In fractures, where the fluids do not circulate, heat is also transferred by conduction. The differential equation for heat field transfer by conduction in a space containing no heat sources was described in Eg. (2.35). The temperature variation rate in nonstationary thermal processes is evaluated in terms of the $\lambda/C\sigma$ ratio from Eq. (2.35).

Once the seasonal temperature variations, which affect the stationary temperature field, are eliminated, $\partial T/\partial t$ tends to zero. Then Eq. (2.35) takes the standard form of the Laplace equation $\nabla^2 T = 0$, i.e., the temperature field is a potential field. The right side of expression (7.29) is simplified correspondingly, leaving only the value T_i.

Under stationary thermal conditions, heat propagation by conduction in solid bodies follows Fourier's law (see Eq. 2.16).

The magnetic field is also a potential (Tikhonov et al., 1983) when the value of the magnetization is below 0.1 SI units, i.e.,

$$\overrightarrow{U_a} = -grad\ V, \tag{7.32}$$

where $\overrightarrow{U_a}$ is the anomalous magnetic field, and V is the magnetic potential. Expression (7.32) satisfies the Poisson's equation.

It is obvious that expressions (2.16) and (7.32) are proportional. It follows that there is a theoretical basis for extending the well-developed techniques of magnetic anomaly interpretation to the interpretation of near-surface thermal observations.

In magnetic prospecting developed methods for magnetic anomaly quantitative interpretation (improved modifications of the tangent and characteristic point methods) for complicated environments (Khesin et al., 1988; 1996). Unlike some conventional procedures (Grant and West, 1965; Mikov et al., 1966; Naudy, 1970; Rao and Babu, 1984), these methods are applicable in conditions of rugged terrain relief and arbitrary magnetization of the objects where the normal field level is an unknown (Khesin et al., 1996). Later the viability of these methods was established for treating other geophysical fields.

A disturbing object model in the form of a sphere or horizontal circular cylinder (*HCC*) is rather frequently used in thermal prospecting (Carslaw and Jaeger, 1959; Cheremensky, 1972; Lakhtionov, 1973; Kappelmayer and Haenel, 1974). The anomalous effect of a homogeneous sphere does not depend upon its volume; therefore, when volume and thermal conductivity are not of fundamental importance, a material point may be substituted for a model of the sphere. The model of the *HCC* may be used for the approximation of elongated objects having a circular cross-section area.

The analytical expressions for the geothermal field of a sphere and *HCC* were given earlier (see Eqs. 2.83 and 2.86).

The analytical expressions for the vertical magnetic field component Z of a point magnetic source (equivalently a magnetized rod with a distant lower edge) and for a thin bed, respectively, have the following form (Parasnis, 1963; Telford et al., 1976):

$$Z = mz/(x^2 + z^2)^{3/2}; \tag{7.33}$$

$$Z = 2I \cdot 2b \cdot z/(x^2 + z^2), \tag{7.34}$$

where m is the magnetic mass, I is the magnetization, and b is the half-width of the thin bed's upper edge.

The proportionality of the expressions (2.83) and (7.33), (2.86) and (7.34), respectively, is evident.

From this it follows that: (1) the compared fields are physically different but share mathematical expressions in common with potential fields, (2) the fields of compared models are proportional. As follows from the above, rapid interpretation methods, such as modifications of the characteristic points and tangent methods, can be applied to quantitative interpretation of geothermal anomalies (Khesin and Eppelbaum, 1988). This conclusion allows us to test and employ the abovementioned methods of interpretation that are described below.

7.8.5 Description of the Methods Employed by Quantitative Interpretation

Quantitative interpretation of thermal anomalies by hydrocarbon prospecting is based on the differentiation of studied rocks by their thermal conductivity, along with in magnetometric and gravitational methods. Tables in Appendix B show thermal conductivities of some commonly encountered rocks and minerals.

Characteristic Point Method

The following characteristic points are used in the interpretation: abscissas and ordinates (x and y coordinates) of the anomaly maximum (x_{max}, z_{max}) and minimum (x_{min}, z_{min}) [1], x-coordinates of the right and left points of the anomaly semi-amplitude $(x_{0.5Z_A})_r$ and $(x_{0.5Z_A})_l$, respectively; x-coordinates of the right and left inflection points of the anomaly plot x_r and x_l, respectively (Fig. 7.14).

Formulas used for quantitative interpretation are given in Table 7.15. Here x_o and x_c is the horizontal displacement for models of thin bed and horizontal circular cylinder, respectively.

Tangent Method

Unlike the method of the characteristic points, the tangent method employs not only x and y coordinates of maximum and minimum

[1] For an anomaly due to a cylinder, one distinguishes between the right minimum with coordinates $(x_{min,r}, z_{min,r})$ and the left minimum with coordinates $(x_{min,l}, z_{min,l})$.

Table 7.15 Formulas for interpreting anomalies over a thin bed and a horizontal circular cylinder by the method of characteristic points (Khesin et al., 1996)

Parameters to be determined	Parameters employed for anomalies due to models		Formulas to calculate parameters by the anomaly due to models	
	bed	cylinder	bed	cylinder
θ	$d, \Delta h$		$\tan(\theta/2) = d/\Delta h$	$\tan(\theta/3) = d/\Delta h$
	d_1, d_2	d_{1r}, d_{1l}	$\tan\theta = d_2/d_1$	$\cot(\theta/3) = \sqrt{3}\frac{(d_{1l}+d_{1r})}{(d_{1l}-d_{1r})}$
	d_1, d_5	d_{1r}, d_5	$\sin(\theta/3) = d_5/\sqrt{3}\ d_1$	$k'_\theta = \frac{\sqrt{2}\cos(\theta/2)-1}{\sqrt{3}\cos(60°+\theta/3)} = d_5/d_{1r}$
h, h_c	d_1, d_2, θ	d_{1r}, θ	$h = \sqrt{d_1 d_2}/k_{1,2}$, where $k_{1,2} =$	$h_c = d_{1r}/k_{1r}$, where $k_{1r} =$
		θ	$= 2/\sqrt{\sin\theta\cos\theta}$	$= 2\sqrt{3}\frac{\cos(60°+\theta/3)}{\cos\theta}$
		d_{1r},		
	–	$d_{1r}(\Delta h)$		$h_c = \frac{d_{1r}\Delta h}{d_{1r}-d_{1r}(\Delta h)}$
	d_5, θ		$h = d_5/k_5$, where	
			$k_5 = 2\sqrt{3}\frac{\sin(\theta/3)}{\sin\theta}$	$k_5 = 2\sqrt{2}\frac{\cos(\theta/2)-1}{\cos\theta}$
M_e	Z_A, h, h_c		$M_e = 0.5 Z_A h$	$M_e = Z_A h_c/k_m$, where $k_m = (3\sqrt{3}/2)\cos(30° - \theta/3)$
x_o, x_c	$h, \theta, x_{max}, x_{min,r}$		$x_o = 0.5(x_{max} + x_{min,r}) - h\cot\theta$	$x_c = 0.5(x_{max} + x_{min,r}) - h_c\frac{\sin(60°+\theta/3)}{\cos\theta+h_c\tan\theta}$
	$(x_{0.5Z_A})_r$, $(x_{0.5Z_A})_l$	–	$x_o = 0.5[(x_{0.5Z_A})_r - (x_{0.5Z_A})_l] + h\tan\theta$	
	h, θ, x_r, x_l		$x_o = 0.5(x_r - x_l) - h\cot\theta + h\frac{\cos(\theta/3)}{\sin\theta}$	$x_c = 0.5(x_r + x_l) + h_c\tan\theta - \sqrt{2}h_c\frac{\sin(\theta/2)}{\cos\theta}$
ΔZ_{backgr}	Z_{min}, Z_A, θ		$\Delta Z_{backgr} = Z_{min} + Z_A\frac{k_o}{1+k_o}$, where	
			$k_o = \frac{1-\cos\theta}{1+\cos\theta}$	$k_o = \frac{\cos^3(60°+\theta/3)}{\cos^3(\theta/3)}$

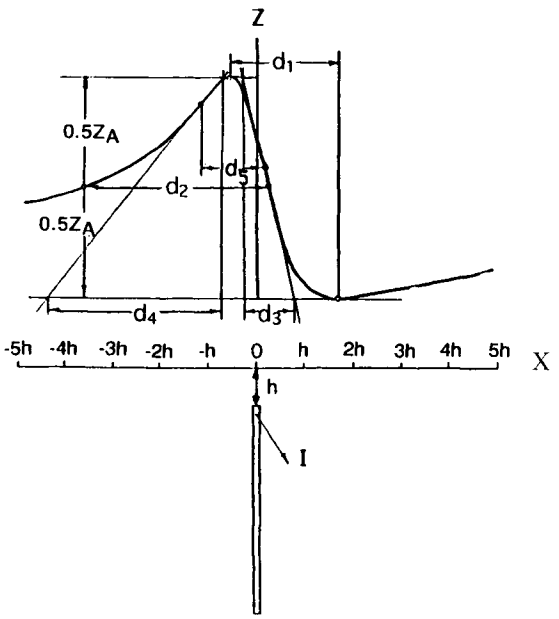


Fig. 7.14. Arrangement of characteristic points and tangents on an anomaly plot for an obliquely magnetized thin bed (I is the magnetization vector) situated in a nonmagnetized medium. Open circles are points of extrema and semiamplitude; closed circles are inflection points of the anomaly plot.

points, inflection points and their differences, but also the first horizontal derivative in inflection points (where the first derivative has its extremums). These values can be readily obtained from the anomaly plot as tangents of the inclination angles of the tangents to the curves at the inflection points. This fact, along with the acceptable accuracy of the method, favors a wide application of the method.

The modification discussed below does not suffer from such a limitation. It is designed specially for the conditions of oblique magnetization and inclined relief. This technique permits us to determine θ and to locate the origin (i.e. position of the body's epicenter) not beforehand, but in the course of the interpretation. Four tangents are used: two inclined ones, passing through the inflection points with the largest in absolute value horizontal gradients of the field, and two horizontal ones, passing through the maximum

and the largest in absolute value minimum of the anomaly. The inflection points at the inclined tangents are the nearest to the largest in absolute values extremums of the anomaly and are found to their left for $\theta = 0 \div 90^o$ and the axis Ox running approximately to the north bearings (to the right in figures).

When interpreting the anomaly Z due to a thin bed or a circular cylinder, the segments d_3 and d_4 are used, taken from the anomaly plot (see Fig. 7.14). Their analytical expressions

$$\left.\begin{aligned} d_3 &= Z_A/|Z_{xr}| \\ d_4 &= Z_A/Z_{xl} \end{aligned}\right\} \tag{7.35}$$

have the following form:

for an anomaly due to a thin bed:

$$\left.\begin{aligned} h &= d_3 \sin^3(60^o + \theta/3) \\ h &= d_4 \sin^3(60^o - \theta/3) \end{aligned}\right\}, \tag{7.36}$$

for an anomaly due to a horizontal circular cylinder:

$$\left.\begin{aligned} h &= d_3 \frac{8}{3\sqrt{3}} \frac{\cos^4[(90^o-\theta)/4]}{\cos[(90^o-\theta)/3]} \\ h &= d_4 \frac{8}{3\sqrt{3}} \frac{\cos^4[(90^o+\theta)/4]}{\cos[(90^o-\theta)/3]} \end{aligned}\right\}. \tag{7.37}$$

In both cases the ratio $k_\theta = d_3/d_4$ is a function of the angle θ only and is used to determine this angle either by the formulas

$$\left.\begin{aligned} \tan(\theta/3) &= \sqrt{3}\,\frac{(1-\sqrt[3]{k_\theta})}{1+\sqrt[3]{k_\theta}} \\ \cot(\theta/2) &= 1 + 2\frac{\sqrt[4]{4k_\theta}}{1-\sqrt{k_\theta}} \end{aligned}\right\}. \tag{7.38}$$

The depth h is obtained by the formula

$$h = d_i/k_i, \tag{7.39}$$

where i is equal to three or four.

The coefficients k_3 and k_4 stand for the values of d_3 and d_4 when $h = 1$. They are functions of θ. Other parameters of a thin bed and a cylinder (magnetic moment M_e, the epicenter location), as well as the normal background level ΔZ_{backgr} correction are determined from the obtained values of θ and h as in the method of

Table 7.16 Formulas for interpreting anomalies over a thin bed and a horizontal circular cylinder by the square method (Khesin et al., 1988;1996)

Disturbing bodies	Analitical expressions	Formulas to calculate parameters
Thin bed	$Q_1 = \int_{-h\tan(\theta/2)}^{h\cot(\theta/2)} (Z - Z_{min})dx =$	$M_e = Q_1/q_M,$
	$= 2M_e\left[\frac{1}{2}\pi\cos\theta + \sin\theta\ln[\tan(\theta/2)] + \right.$	
	$\left. + \tan(\theta/2)\right]$	$h = 2Q_1/(Z_a q_M),$
	$Q_2 = \int_{-h\cot(60°-\theta/3)}^{h\cot(60°+\theta/3)} (Z - Z_{min})dx =$	where $q_M = 2\left[\frac{1}{2}\pi\cos\theta -\right.$
	$= 2M_e\left[\frac{\pi}{3}\cos\theta - \sin\theta\right.$	$\left. - \sin\theta\ln[\tan(\theta/2)] + \tan(\theta/2)\right]$
	$\left.\ln\left[\frac{\sin(60°+\theta/3)}{\sin(60°-\theta/3)}\right] + 4\sqrt{3}\tan(\theta/2)\sin(\theta/3)\right]$	
Horizontal Circular Cylinder	$Q_1 = \int_{-h\tan(60°+\theta/3)}^{h\tan(60°-\theta/3)} (Z - Z_{min})dx =$	$h = (Q_1/Z_a)q_h,$
	$= \frac{3\sqrt{3}}{4}\frac{M_e}{h}\sec(\theta/3)$	$M_e = \frac{Q_1 h}{q_M} = \frac{Q_1^2}{Z_a}\frac{q_h}{q_M},$
	$Q_2 = \int_{-h\tan[90°+\theta/4]}^{h\tan[90°-\theta/4]} (Z - Z_{min})dx =$	where $q_h = 2\cos(\theta/3)\cos(30° - \theta/3),$
	$= \frac{M_e}{h}\left[1 + \frac{3\cos(60°-\theta/3)}{2\cos(\theta/2)+1}\right]$	$q_M = \frac{3\sqrt{3}}{4}\sec(\theta/3)$

characteristic points by the formulas of Table 7.15. A change in θ in the range of $0 \div 90^o$ causes only a slight change in k_3 for an obliquely polarized cylinder, i.e. within the range of 0.77 to 0.65. Therefore, in a simplified way, the occurrence depth can be obtained using only the R.H. branch of the anomaly curve, if the average coefficient is taken to be k_3=0.7 and the following formula is used:

$$h = 1.4d_3. \tag{7.40}$$

Square Method

The developed formulas for interpreting magnetic anomalies by square method are described in Table 7.16. It should be noted that areas Q_1 and Q_2 do not depend on the level of the normal field as well as the beginning of coordinates and may be determined at a rather short intervals of the anomalous graph. For a rough estimation of values h and M_e the averaged parameters (without calculation of parameter Q_2) $q_h = 1.8$, $q_M = 1.4$ may be used. Then

$h = 1.8Q_1/Z_a$ and $M_e = 1.3Q_1^2/Z_a$.

Large-scale testing of the above methods on models and real situations testifies to the fact that their accuracy is 7–15%, and satisfies to the requirements of practical application (Eppelbaum, 1989; Khesin and Eppelbaum, 1994; Eppelbaum et al., 1996).

7.8.6 Calculation of the Inclined Relief Influence

If anomalies are observed on an inclined profile, then the obtained parameters characterize a certain fictitious body. The transition from fictitious body parameters to those of the real body is performed using the following expressions (the subscript "r" stands for a parameter of the real body):

$$h_r = h + x \cdot \tan\omega_o; \tag{7.41}$$

$$x_r = -h \cdot \tan\omega_o + x_o, \tag{7.42}$$

where h is the depth of the upper edge occurrence, x_o is the location of the source's projection to plan relative to the extremum having the greatest magnitude, and ω_o is the angle of the terrain relief inclination ($\omega_o > 0$ when the inclination is toward the positive direction of the x-axis).

Calculation of the Temperature Moment

In order to estimate the intensity of a thermal anomaly, a value equivalent to the magnetic moment M_e can be used (Eppelbaum, 1989; Eppelbaum et al., 1996). This value depends on contrasts in physical parameters between the anomalous body and the host rock, and also on the form and depth of the body. Thus, the value may be use in the interpretation of geothermal data during initial data interpretation. Using the equation for the magnetic moment (see Table 7.16), the value of an analogous "temperature moment", TM $[^oC \cdot m]$, could be determined. A set of this kind data may be used for the classification of the targets analyzed in a particular area.

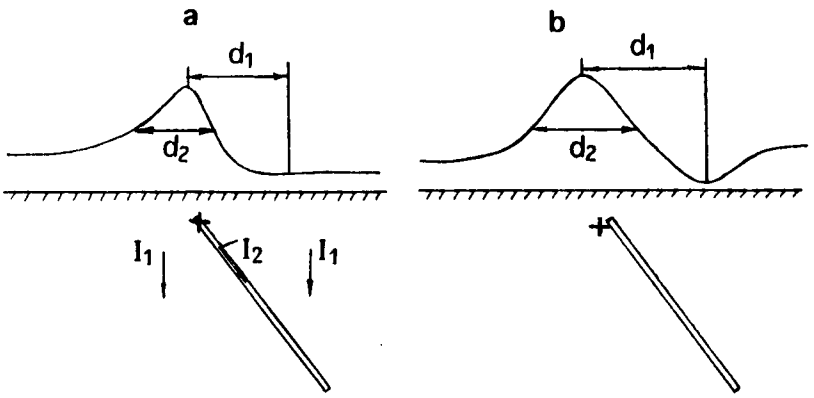


Fig. 7.15 Comparison of magnetic and temperature anomalies over a model of an inclined thin body. The arrow shows the direction of the magnetization vector I. The "+" symbol marks the position of the upper edge of the thin body, as obtained from analysis of the anomaly profiles.

Some Peculiarities of the Discussed Methods

When interpreting plots of the temperature field recorded on an inclined relief, the observation and measurement point heights have an inverse correlation (see Fig. 7.12). This causes reflection of the temperature anomaly plot about the vertical axis as compared with the magnetic Z-anomaly presented in Fig. 7.13. The angle of terrain relief is equivalent to that of the polarization vector on magnetic field (Khesin et al., 1996) and with the sign being inverted for the thermal field (Eppelbaum, 1989). Therefore the parameters d_3 and d_4 on the temperature anomaly plot change places, while the parameter d_1 is measured from the opposite side.

7.8.7 Examples of Quantitative Interpretation

Fig. 7.15 shows the comparison of magnetic (a) and temperature (b) anomalies from an inclined thin bed (rod) and the results of their quantitative interpretation. The ΔZ anomaly has been computed

using 3-D program (Khesin and Eppelbaum, 1994), while the temperature anomaly has been obtained by physical modeling (Ismail-Zade et al., 1980). A rod with raised thermal conductivity can, like a magnetic rod with a distant bottom edge, be approximated by a point source located at the upper end of the rod. As can be seen from Fig. 7.15, the similarity of $\Delta Z(nT)$ and $T(^oC)$ anomalies is consistent with this comparison. The results of quantitative interpretation of these anomalies, which are carried out with the use of the techniques described in the previous paragraph, are also similar.

An interesting thermal anomaly in the northern Dead Sea Basin has been observed by Ben-Avraham and Ballard (1984). The amplitude of the anomaly exceeds 0.2^oC (an accuracy of these observations was about 0.01^oC). Its form suggest that the anomalous body (or its upper surface) has enhanced thermal conductivity, and has the form of a horizontal circular cylinder. Application of the above quantitative methods allowed the position of the cylinder's centre to be determined (Fig. 7.16); it was predicted to be at a depth of about 60 m. Here both characteristic point method (parameters d_1 and d_2) and tangent method (parameters d_3 and d_4) (Khesin and Eppelbaum, 1994) were used. Parameter d_3 is difference in abscissae of the points of intersection of an inclined tangent with horizontal tangents on one branch; parameter d_4 is the same on the other branch (d_3 is selected from the plot branch with conjugated extremums). We suggest that the anomaly was caused by the upper surface of a small salt dome (salt domes are widely presented in this area). Temperature moment here was found to be approximately $9^oC \cdot m$.

The next example illustrates the application of these methods in the Muradkhanly oil deposit in Central Azerbaijan (Fig. 7.17), where the temperature was measured in 3 m deep wells and the data thus obtained were smoothed by the use of a sliding interval average of three points. A fault was revealed here by a field crew from *"YuzhVNIIGeofizika"* (Baku) using gravitational and magnetic methods of prospecting, which were tied in with drilling data. Thermal observations also have been conducted by "YuzhVNIIGeofizuka" (Sudzhadinov and Kosmodemyansky, 1986). The position of the upper edge of the fault was calculated using the methods of tangents and characteristic points; its projection

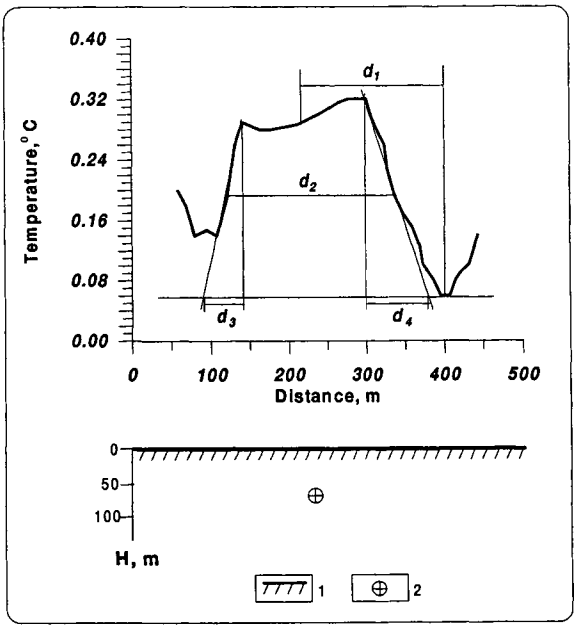


Fig. 7.16 Quantitative interpretation of temperature anomalies in the northern Dead Sea Basin (observed temperature curve after Ben-Avraham and Ballard, 1984): (1) sea bottom; (2) position of centre of a horizontal circular cylinder.

in plan coincided exactly with the fault position obtained from the independent geophysical and geological data. Value of the temperature moment here is sufficiently high – 230 $^oC \cdot m$.

Other example of the inverse method application is presented in Fig. 7.18. Obtained position of the fault upper edge has a good agreement with the available geological data. Interestingly, that the registered temperature curve is very similar to magnetic anomaly from the same inclined thin bed magnetized along its dipping. The TM value was found as $\approx 80^oC \cdot m$.

These interpretation methods can also be used to solve various problems of engineering geophysics. As an example, results of near-surface thermal prospecting over an underground cavity in Cracow, Poland, are interpreted by using the methods described

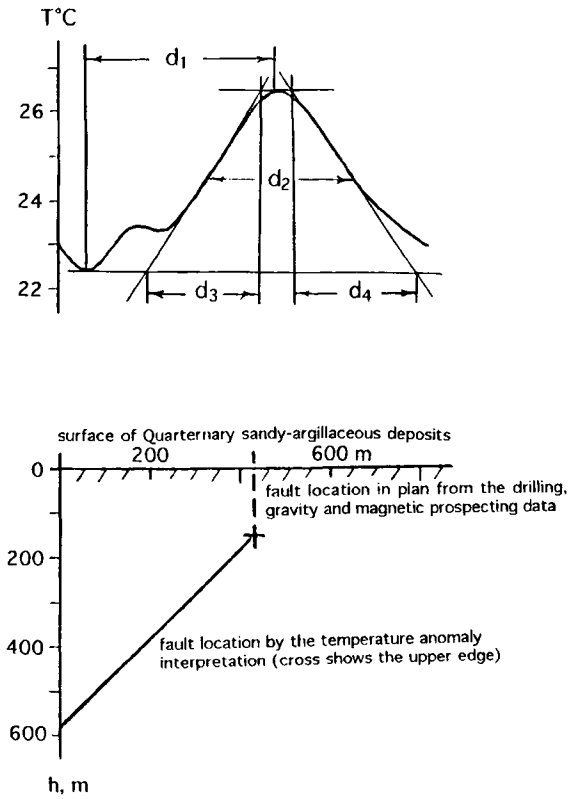


Fig. 7.17. Interpretation of the temperature anomaly in the district of the Muradkhanly oil field in the Middle Kura Depression.

(Fig. 7.19). Measurements were made at a depth of 40 cm and the profile spacing was 1 m (Moscicki, 1987). The underground square cavity is approximated by a horizontal circular cylinder (*HCC*). Application of interpretation methods described above allowed the determination of the center of the *HCC* to satisfactory accuracy. The calculated value of TM was very small: $\approx 0.3°C \cdot m$.

7.8.8 Further Improvement of the Thermal Near-Surface Technique

We consider than the further improvement of the interpreting thermal observations in the near-surface layer can be associated with:
- Development of a reliable and flexible 3-D software for thermal field modeling;
- Application of the accomplished set of different filtering methods for removing noises, recognizing and location of targets;
- Integration with other geophysical as well as geochemical methods;
- Development of an International Data Base.

Thus, we can conclude:
- To reveal a stable geothermal anomaly that can be interpreted quantitatively, effects caused by time variations of temperature and influence of terrain relief must be eliminated from the observed temperature field. Techniques developed for this purpose include repeated geothermal observations at instants of time chosen to eliminate temperature variations. Correlation between observed fields and observation point heights is a technique used for reducing the effect of terrain relief.
- The applicability of methods of magnetic anomaly interpretation, which are thoroughly developed for complicated models including rugged relief, inclined polarization and unknown level of the normal field, to models in thermal prospecting is substantiated on the basis of some common aspects of magnetic and temperature potential fields.
- The use of rapid methods of quantitative interpretation of temperature anomalies, such as characteristic points, tangent and square methods, makes it possible to easily determine the parameters of disturbing thermally conductive bodies. It also makes it possible to use near-surface thermal prospecting to explore for salt bodies to examine faults in oil and gas fields, and to solve some other problems (for instance, mapping).
- Taking into account a contrast thermal conductivities of oil and surrounding rocks (see Appendix B) these quantitative methods may be also applied for a direct searching shallow occurred oil deposits.

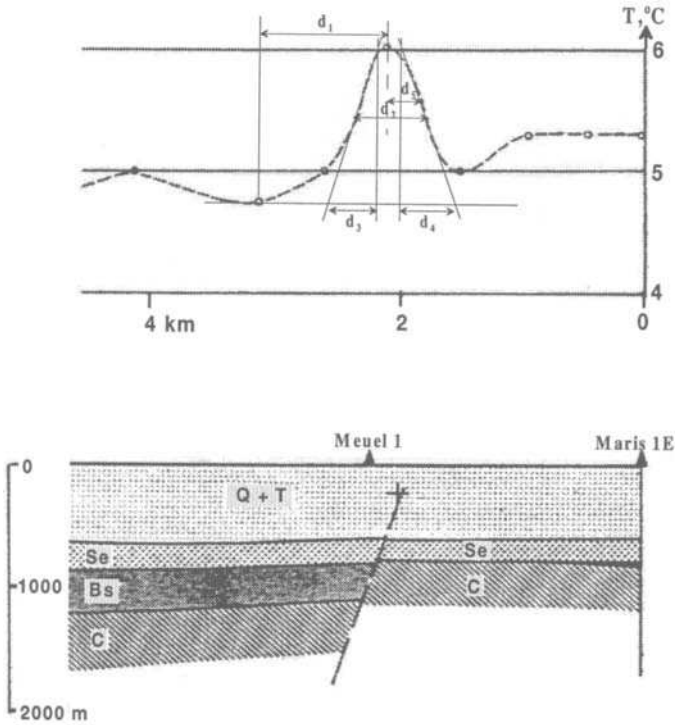


Fig. 7.18. Quantitative interpretation of temperature anomaly over fault in the "Peel" district, southern part of The Netherlands (observed curve and geological section after Poley and Steveninck, 1970). The "+" symbol marks the position of the upper edge of fault.

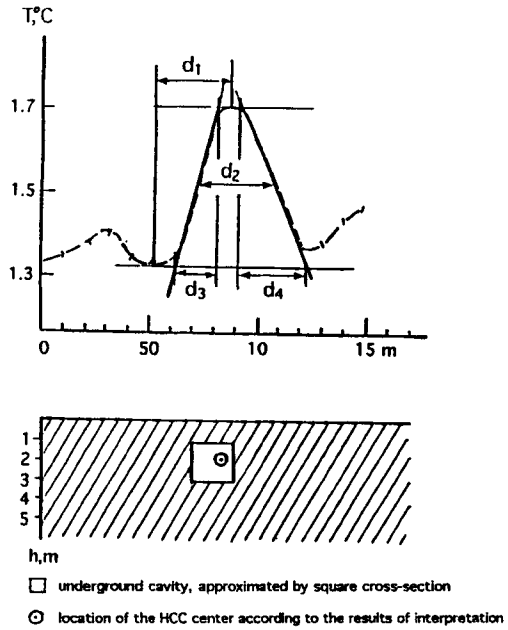


Fig. 7.19. Quantitative interpretation of the temperature anomaly over an underground cavity (Cracow's Planty Park). Observed temperature and geological section is from Moscicki (1987).

Chapter 8

APPENDICES

8.1 APPENDIX A. CONVERSION FACTORS

Table A.1 Conversion Factors. Dimensions: L – length, T – temperature, t – time, m – mass. An asterisk after the third decimal indicates the conversion is exact

To Convert from SI Units and Dimensions	To Customary Units	Multiply by Conversion Factor	Inverse Conversion Factor
LENGTH			
metre (m)	centimetre (cm)	1.000*E+02	1.000*E-02
L	foot (ft)	3.281 E+00	3.048*E-01
	inch (in)	3.937 E+01	2.540*E-02
TIME			
second (s)	day (D)	1.157 E-05	8.640*E+04
t	hour (hr)	2.778 E-04	3.600*E+03
	minute (min)	1.667 E-02	6.000*E+01
TEMPERATURE			
(difference)	°C	1.000*E+00	1.000*E+00
Kelvin degree (K)	°F	1.800*E+00	5.556 E-01
T	°R	1.800*E+00	5.556 E-01
MASS			
kilogram (kg)	gram (g)	1.000*E+03	1.000*E-03
m	pound-mass (lbm)	2.205 E+00	4.536 E-01
	ton (metric)	1.000*E-03	1.000*E+03
AREA			
metre^2 (m^2)	cm^2	1.000*E+04	1.000*E-04
L^2	ft^2	1.076 E+01	9.290 E-02
	in^2	1.550 E+03	6.452 E-04
	darcy	1.013 E+12	9.869 E-13
VOLUME			
metre^3 (m^3)	cm^3	1.000*E+06	1.000*E-06
L^3	litre	1.000*E+03	1.000*E-03
	ft^3	3.532 E+01	2.832 E-02
	gallon	2.642 E+02	3.785 E-03
	barrel (bbl)	6.290 E+00	1.590 E-01
FORCE			
newton (N)	dyne	1.000*E+05	1.000*E-05
mL/t^2	kilogram-force	1.020 E-01	9.807 E+00
	pound-force	2.248 E-01	4.448 E+00

Table A.1 – continued

To Convert from SI Units and Dimensions	To Customary Units	Multiply by Conversion Factor	Inverse Conversion Factor
DENSITY			
kg/m^3	g/cm^3	1.000*E-03	1.000*E+03
m/L^3	lbm/ft^3	6.243 E-02	1.602 E+01
	lbm/gallon (ppg)	8.345 E-03	1.198 E+02
PRESSURE			
Pascal (Pa)	atmosphere (atm)	9.869 E-06	1.013 E+05
m/Lt^2	bar	1.000*E-05	1.000*E+05
	psi	1.450 E-04	6.895 E+03
VOLUMETRIC RATE			
m^3/s	bbl/D	5.434 E+05	1.840 E-06
L^3/t	gallon/min (gpm)	1.585 E+04	6.309 E-05
	ft^3/s	3.532 E+01	2.832 E-02
VISCOSITY			
Pa·s	poise	1.000*E+01	1.000*E-01
m/Lt	centipoise (cp)	1.000*E+03	1.000*E-03
AMOUNT of HEAT			
Joule (J)	Btu	9.478 E-04	1.055 E+04
mL^2/t^2	calorie (cal)	2.388 E-01	4.187 E+00
	Watt·s (W·s)	1.000*E+00	1.000*E+00
HEAT FLOW			
$J/m^2 \cdot s$	W/m^2	1.000*E+00	1.000*E+00
m/t^3	$cal/cm^2 \cdot sec$	2.388 E-05	4.187 E+04
	$kcal/m^2 \cdot hr$	8.598 E-01	1.163 E+00
	$Btu/ft^2 \cdot sec$	8.806 E-05	1.136 E+04
	$Btu/ft^2 \cdot hr$	3.170 E-01	3.154 E+00
SPECIFIC HEAT			
J/kg·K	cal/g°C	2.388 E-04	4.187 E+03
L^2/t^2T	Btu/lbm°F	2.388 E-04	4.187 E+03
	W·hr/g·°C	2.778 E-07	3.600*E+06
THERMAL CONDUCTIVITY	W/cm·K	1.000*E-02	1.000*E+02
J/m·s·K	cal/cm·sec·°C	2.388 E-03	4.187 E+02
mL/t^3T	Btu/ft·hr·°F	5.778 E-01	1.731 E+00
	kcal/m·hr·°C	8.597 E-01	1.163 E+00
THERMAL DIFFUSIVITY	m^2/hr	3.600*E+03	2.778 E-02
m^2/s	ft^2/sec	1.076 E+01	9.290 E-02
L^2/t	ft^2/hr	3.875 E+04	2.581 E-05

8.2 APPENDIX B. THERMAL PROPERTIES OF FORMATIONS

Table B.1 Temperature effect on thermal conductivity (10^{-3}cal/cm s °C) of sedimentary rocks (Kappelmeyer and Haenel, 1974).

Material	ρ, g/cm^3	0	50	100	200	300	400	500°C
Dolomite	2.83	11.90	10.30	9.30	7.95			
Limestone	2.60	7.20	6.14	5.53	4.77			
Limestone, ‖	2.60	8.24	7.55	7.04	6.54			
Limestone, ⊥	2.69	6.09	5.68	5.41				
Quartz-sandstone, ‖	2.64	13.60	11.80	10.60	9.00			
Quartz-sandstone, ⊥	2.65	13.10	11.40	10.30	8.65			
Shale			2.17	2.25	2.38	2.54	2.68	2.83
Slate, ‖	2.70	6.35	6.05	5.85	5.50	5.20	4.95	4.80
Slate, ⊥	2.76	4.83	4.40	4.23	4.08			
Calcite, ‖		27.30	22.40	19.00	15.10	12.30	10.30	
Calcite, ⊥		16.30	13.50	11.80	9.70	8.40	7.40	
Halite	2.16	14.60	12.00	10.05	7.45	5.95	4.98	

Table B.2 Calculated volumetric heat capacities (Btu/cu ft °F) of fluid-saturated rocks (Somerton, 1958)

sample	ϕ	Quartz %	Dry	14.7 *psia*		3000 *psia*	
				methan	water	methan	water
Sandstone	0.196	80	34.0	34.0	34.0	34.6	45.9
Sandstone	0.273	40	32.9	32.9	32.9	33.7	47.6
Silty sand	0.207	20	35.6	35.6	35.6	36.3	49.1
Silty sand	0.225	20	33.5	33.5	33.5	34.3	48.3
Siltstone	0.296	20	32.0	32.0	32.0	32.9	48.7
Siltstone	0.199	25	33.6	33.6	33.6	34.3	47.7
Shale	0.071	40	39.6	39.6	39.6	39.9	40.1
Limestone	0.186	–	35.4	35.4	35.4	36.0	46.8

Table B.3 Coefficient of thermal conductivity (kcal/m ^oC hr) for typical formations in thawed (at $+4^oC$) and frozen (at -10^oC) state (Vyalov, 1974). $W_c = W/\rho_d$; ρ_d is the dry unit weight; W is the total ice-water content of the formation; the unit weight is $\rho = \rho_d(1 + W_c)$

Sands			Clays		Silts		Sands			Clays		Silts	
W_c	K_t	K_f	K_t	K_f	K_t	K_f	W_c	K_t	K_f	K_t	K_f	K_t	K_f
ρ_d = 1200 kg/m^3							ρ_d = 1300 kg/m^3						
0.05	0.51	0.56	0.40	0.46	0.30	0.38	0.05	0.61	0.67	0.50	0.56	0.39	0.49
0.10	0.78	0.92	0.64	0.78	0.46	0.63	0.10	0.90	1.06	0.77	0.89	0.55	0.72
0.15	0.99	1.23	0.83	1.03	0.62	0.84	0.15	1.13	1.37	0.99	1.16	0.73	0.95
0.20	1.15	1.48	1.00	1.26	0.75	1.02	0.20	1.32	1.63	1.18	1.43	0.89	1.16
0.25	1.29	1.70	1.13	1.45	0.89	1.19	0.25	1.48	1.81	1.31	1.64	1.03	1.32
0.30	1.43	1.87	1.22	1.62	1.00	1.33	0.30	1.62	2.00	1.42	1.81	1.15	1.47
0.35	1.55	1.99	1.28	1.75	1.10	1.47	0.35	1.76	2.17	1.50	1.96	1.26	1.64
0.40	1.65	2.08	1.31	1.86	1.20	1.60	0.40	1.86	2.29	1.57	2.11	1.36	1.76
0.45	1.75	-	1.38	-	1.28	1.70							
ρ_d = 1400 kg/m^3							ρ_d = 1500 kg/m^3						
0.05	0.73	0.80	0.62	0.70	0.49	0.63	0.05	0.85	0.94	0.73	0.82	0.60	0.75
0.10	1.03	1.23	0.90	1.05	0.70	0.85	0.10	1.19	1.40	1.03	1.20	0.80	0.99
0.15	1.28	1.56	1.15	1.35	0.85	1.07	0.15	1.45	1.77	1.30	1.53	1.00	1.22
0.20	1.50	1.85	1.35	1.61	1.01	1.27	0.20	1.68	2.11	1.51	1.81	1.16	1.41
0.25	1.68	2.11	1.50	1.84	1.16	1.48	0.25	1.88	2.44	1.69	2.07	1.32	1.59
0.30	1.85	2.30	1.63	2.04	1.29	1.64	0.30	2.05	2.64	1.83	2.27	1.45	1.75
0.35	1.97	-	1.72	-	1.41	-							
ρ_d = 1600 kg/m^3							ρ_d = 1700 kg/m^3						
0.05	0.96	1.06	0.84	0.97	0.70	0.88	0.05	1.09	1.20	0.96	1.07	0.82	1.00
0.10	1.34	1.57	1.18	1.34	0.92	1.12	0.10	1.50	1.71	1.33	1.50	1.06	1.25
0.15	1.63	1.98	1.46	1.71	1.14	1.34	0.15	1.85	1.21	1.66	1.91	1.28	1.50
0.20	1.89	2.33	1.70	2.03	1.32	1.54	0.20	2.15	2.52	1.96	2.23	1.47	1.71
0.25	2.10	2.64	1.88	2.31	1.47	1.71	0.25	2.39	-	2.11	-	1.62	-
ρ_d = 1800 kg/m^3													
0.05	1.22	1.36	1.06	1.22	0.93	1.12	0.20	2.45	2.58	2.20	2.31	1.64	1.86
0.10	1.77	1.93	1.53	1.68	1.21	1.38	0.25	2.47	-	-	-	-	
0.15	2.13	2.23	1.83	2.08	1.42	1.63							

Table B.4 Volumetric thermal capacity (kcal/m^3 °C) of typical formations in thawed (at $+4^oC$) and frozen (at -10^oC) state (Vyalov, 1974)

Sands			Clays		Silts		Sands			Clays		Silts	
W_c	K_t	K_f	K_t	K_f	K_t	K_f	W_c	K_t	K_f	K_t	K_f	K_t	K_f
ρ_d = 1200 kg/m^3							ρ_d = 1300 kg/m^3						
0.05	260	230	270	260	300	300	0.05	280	245	290	280	325	325
0.10	320	260	330	290	360	340	0.10	345	280	360	310	390	370
0.15	380	290	390	320	420	370	0.15	410	315	425	345	455	405
0.20	440	320	450	350	480	400	0.20	475	345	490	380	520	435
0.25	500	350	510	380	540	430	0.25	540	380	555	410	585	470
0.30	560	380	570	410	600	460	0.30	605	410	620	440	600	500
0.35	620	410	630	440	660	480	0.35	670	445	685	475	715	535
0.40	680	440	690	470	720	520	0.40	735	475	750	510	780	565
0.45	740	470	750	500	780	550							
ρ_d = 1400 kg/m^3							ρ_d = 1500 kg/m^3						
0.05	300	265	315	300	350	350	0.05	325	285	335	320	375	375
0.10	370	300	385	335	420	400	0.10	400	325	415	360	450	430
0.15	425	335	455	370	490	435	0.15	475	360	490	400	525	465
0.20	510	370	525	405	560	470	0.20	550	395	560	435	600	505
0.25	580	405	595	440	630	505	0.25	625	435	635	475	675	540
0.30	650	440	665	475	700	540	0.30	700	475	715	510	750	575
0.35	720	475	735	510	770	5755							
ρ_d = 1600 kg/m^3							ρ_d = 1700 kg/m^3						
0.05	345	305	360	345	400	400	0.05	365	325	385	365	425	425
0.10	425	345	440	385	480	455	0.10	450	365	470	410	510	485
0.15	505	385	520	425	560	495	0.15	535	410	545	450	595	525
0.20	585	425	600	465	640	535	0.20	620	450	640	495	680	570
0.25	665	465	680	505	720	575	0.25	705	490	725	535	765	615
ρ_d = 1800 kg/m^3													
0.05	390	345	405	385	450	450	0.20	665	475	675	520	720	605
0.10	475	390	495	430	540	515	0.25	750	520	765	565	810	650
0.15	570	430	585	475	630	560							

Table B.5 Thermal properties of rocks of the Romashkino oil field (Russia), after Proselkov (1975)

Formation	$\rho \times 10^{-3}$ kg/m^3	$a \times 10^7$ m^2/c	λ W/m °C	$c \times 10^{-3}$ J/kg °C
Dolomite	2.75	9.95	2.11	0.802
Limestone	2.70	9.6	2.2	0.851
Clayey limestone	2.65	9.05	1.96	0.844
Argillite	2.3	9.94	2.25	0.838
Siltstone	2.55	10.8	2.22	0.795
Aleurolite, oil-bearing	2.3	12.9	2.8	0.88
Clayey sandstone	2.5	14.3	3.36	0.915
Sandstone, fine-grained	2.4	10.5	1.85	0.845
Sandstone, oil-bearing	2.09	12.54	2.28	0.876
Sandstone, oil saturated	2.2	11.57	1.7	0.737
Sandstone, water saturated	2.3	12.8	2.46	0.84

Table B.6 Thermal properties of rocks (averaged data), after Proselkov (1975)

Formation	$\rho \times 10^{-3}$ kg/m^3	$a \times 10^7$ m^2/c	λ W/m °C	$c \times 10^{-3}$ J/kg °C
Chalk	1.810	4.73	0.82	0.959
Chalk, compacted	1.920	5.80	1.02	0.922
Marl	1.970	4.04	1.38	1.734
Dolomite	2.753	9.95	2.11	0.802
Clayey limestone	2.644	9.05	1.96	0.844
Limestone	2.714	9.60	2.20	0.851
Clay	2.080	3.21	1.42	2.127
Sandy shale	2.057	3.21	1.42	2.151
Argillite	2.555	9.94	2.25	0.838
Sandstone, oil-bearing	2.198	11.57	1.70	0.737
Clayey aleurolite	2.566	10.80	2.22	0.795
Quartzite schist	2.710	18.00	4.19	0.858

Table B.7 Thermal properties of sedimentary rocks at temperature of 50°C (Kappelmeyer and Haenel, 1974)

Material	n	ρ, $\overline{\rho}$ g/cm^3	λ, $\overline{\lambda}$ 10^{-3}cal/cm s °C	n	c, $\overline{c}$ cal/g °C	a, $\overline{a}$ 10^{-3}cm^2/s
Anhydrite	7	2.65–2.91	9.80–14.50	7		17.00–25.7
		2.80	12.61			22.41
Clay	3	2.49–2.54	5.20–5.40	3	0.213–0.240	8.53–10.18
		2.52	5.30		0.223	9.50
Clay marl	7	2.43–2.64	4.14–6.15	7	0.186–0.234	8.01–11.66
		2.54	4.87		0.205	9.34
Claystone	15	2.36–2.83	4.17–8.18	9	0.197–0.223	8.24–15.80
		2.60	5.68		0.211	12.18
Dolomite	6	2.53–2.72	6.01–9.06	6	0.220–0.239	10.75–14.97
		2.63	7.98		0.228	11.17
Schistose clay	3	2.42–2.57	4.60–5.50	3	0.218–0.222	8.10–10.24
		2.49	5.13		0.220	9.37
Limestone	11	2.41–2.67	4.05–6.40	11	0.197–0.227	8.24–12.15
		2.55	5.28		0.204	10.54
Limestone	6	2.58–2.66	5.58–8.38	6	0.197–0.220	10.78–15.21
		2.62	6.75		0.210	12.18
Lime marl	2	2.43–2.62	4.40–5.74	2	0.200–0.227	9.04–9.64
		2.53	5.07		0.214	9.34
Marl	3	2.59–2.67	5.55–7.71	3	0.217–0.221	9.89–13.82
		2.63	6.44		0.219	11.18
Marly clay	2	2.46–2.49	4.21–4.82	3	0.183–0.236	7.17–10.72
		2.47	4.52		0.210	8.94
Clay slate	5	2.62–2.83	3.45–8.79	5	0.205–0.205	6.42–15.15
		2.68	5.13		0.205	9.26
Salt	14	2.08–2.28	10.7–13.7	14		25.20–33.80
		2.16	13.19			30.60
Salt slate	7	2.13–2.57	3.00–10.00	7		6.38–21.70
		2.37	6.59			13.90
Sandstone	54	2.35–2.97	5.20–12.18	31	0.182–0.256	10.94–23.62
		2.65	7.75		0.197	16.45

Table B.8 Effect of pressure on thermal conductivity of sedimentary rocks. Thermal conductivity data after Hurtig and Brugger (1970)

Material	λ at 0.4 kg/cm^2 10^{-3}cal/cm s °C	Pressure kg/cm^2	δ 10^{-3}kg/cm^2
Sandstone			
No 172	6.84	0.4–164	0.434
No 224	5.51	0.4–164	0.612
No 234	6.69	0.4–164	0.626
No 286	7.50	0.4–164	0.931
No 313	9.44	0.4–164	0.905
No 343	8.51	0.4– 41	3.43
Limestone			
No 19	5.06	0.4–164	0.599
No 34	4.22	0.4–164	0.185
No 102	7.67	0.4–164	0.406
No 260	4.33	0.4–123	0.808
No 270	3.53	0.4–164	0.579
Dolomite			
No 103	7.62	0.4–123	1.71
No 365	6.18	0.4–123	0.928

8.3 APPENDIX C. COMPUTER PROGRAMS (FORTRAN)

Table C.1 Computer program "FLOSS"

```
C   Program "FLOSS" (Fortran) determines the rate of fluid losses while
C   drilling. The physical model and working formulas are presented
C   in the SPE paper 13963 "Fluid Losses While Drilling".
C   by I.M. Kutasov and M.S. Bizanti, 1984
C            NOMENCLATURE
C   Flow = Rate of fluid losses, gpm        PE = Permeability, md
C   VE = Penetration rate, ft/hr            PO = Porosity, fraction
C   DB = Bit diameter, inches               CO = Compressibility, 1/psi
C   Ra = Effective well radius, ft          VI = Viscosity, cp
C   H1 = Depth of thief zone bottom, ft     S = Skin factor
C   HO = Depth of thief zone top, ft
C   HB = Position of the bit, ft (HB >HO)
C   DEM =Drilling mud density, ppg
C   DEPO=Pore fluid density, ppg
    Dimension RA(7),HB(90),H1D(7),HOD(7),HBD(90,7),AA(7),AB(7),
   &Q0(7),HDA(90,7),ARG0(90,7),X0(90,7),X03(90,7),X02(90,7),E0(90,7),
   &E03(90,7),E02(90,7),Flow(90,7),ARG1(90,7),X1(90,7),E1(90,7),
   &E13(90,7),X13(90,7),X12(90,7),E12(90,7), X04(90,7),E04(90,7),X14(90,7),
   &E14(90,7),S(7)
    External F
    Data A0,CE,D,AQ /.000263679,.69315,1.5708,50.70/
    Data A3,A2 /1.38629,.405465/
    Open(UNIT=5,FILE='Floss.DA')
    Open(UNIT=6,FILE='Floss.out')
    Read(5,*) NA,(S(N),N=1,NA)
    Read(5,*) JA,(HB(J),J=1,JA)
    Read(5,*) PE,VE,PO,VI,CO
    Read(5,*) DEM,DEPO,DB
    Read(5,*) HO,H1
    Do 220 N=1,NA
    RA(N)=DB/24*exp(-S(N))
    HOD(N)=HO/RA(N)
    H1D(N)=H1/RA(N)
    AA(N)=PE/(VE*PO*VI*CO*RA(N))
    AB(N)=(PE*(DEM-DEPO)*RA(N)*RA(N))/VI
    Q0(N)=(AQ*AB(N))/(AA(N)*AA(N))
    DO 20 J=1,JA
    HBD(J,N)=HB(J)/RA(N)
    HDA(J,N)=HBD(J,N)*D*D*AA(N)*A0
    ARG0(J,N)=SQRT(A0*AA(N)*(HBD(J,N)-HOD(N)))
    X0(J,N)=ALOG(1.+D*ARG0(J,N))
    X03(J,N)=3.*X0(J,N)
    X02(J,N)=2.*X0(J,N)
    X04(J,N)=4.*X0(J,N)
    E0(J,N)=F(X0(J,N))
    E03(J,N)=F(X03(J,N))
    E02(J,N)=F(X02(J,N))
    E04(J,N)=F(X04(J,N))
```

Table C.1 – continued

```
      IF(HBD(J,N).GT.H1D(N)) GO TO 139
      Flow(J,N)=Q0(N)*(HDA(J,N)*(-E0(J,N)+E02(J,N)-CE)-
     &(E04(J,N)-A3-E0(J,N))+3.*(E03(J,N)-E02(J,N)-A2))
      GO TO 20
139   ARG1(J,N)=SQRT(A0*AA(N)*(HBD(J,N)-H1D(N)))
      X1(J,N)=ALOG(1.+D*ARG1(J,N))
      X13(J,N)=3.*X1(J,N)
      X14(J,N)=4.*X1(J,N)
      X12(J,N)=2.*X1(J,N)
      E1(J,N)=F(X1(J,N))
      E13(J,N)=F(X13(J,N))
      E12(J,N)=F(X12(J,N))
      E14(J,N)=F(X14(J,N))
      Flow(J,N)=Q0(N)*(HDA(J,N)*(E02(J,N)-E12(J,N)-
     &E0(J,N)+E1(J,N))+E14(
     &J,N)-E04(J,N)+E0(J,N)-E1(J,N)+3.*(E03(J,N)-E02(J,N)-
     &E13(J,N)+E12(J,N)))
20    Continue
220   Continue
      Write(6,715) PE
      Write(6,615) VE
      Write(6,717) CO
      Write(6,618) DB
      Write(6,719) HO
      Write(6,619) H1
      Write(6,716) PO,VI
      Write(6,718) DEPO,DEM
      Write(6,811)
      Write(6,999)
      Write(6,111)
      Write(6,999)
      Write(6,11) (S(N),N=1,NA)
      Write(6,999)
      DO 550 J=1,JA
550   Write(6,121) HB(J),(Flow(J,N),N=1,NA)
811   Format(//,20X,'Filtration rate , GPM ')
715   Format(5X,'Permeability, md =',F6.1)
615   Format(5X,'Penetration rate, ft/hr =',F6.2)
716   Format(5X,'Porosity = ',F4.3,17x,'Viscosity, cp =',F8.1)
717   Format(5X,'Compressibility, 1/psi =',F12.9)
718   Format(5X,'Pore fluid dens.,ppg =',F8.2,8x,'Mud dens.,ppg =',F8.2)
618   Format(5X,'Bit diameter, inches =',F7.3)
719   Format(5X,'Top of the thief zone, ft, =',1F11.1)
```

Table C.1 – continued

```
619   Format(5X,'Bottom of the thief zone, ft, =',1F11.1)
111   Format(/,2X,'Depth, ft',11X,' Skin factor ')
11    Format(/7X, ' ',7(F7.2,2X))
121   Format(F8.1,2X,7(F7.1,2X))
999   Format('.....')
      STOP
      END
C     Calculates EI(+x)
C     The approximate formulas for the Ei(+x) function were taken from
C     the "Mathematical Handbook for Scientists and Engineers"
C     by G.A. Korn and T.M. Korn, McGraw-Hill Book Company, 1968
      Function F(x)
      IF(x.GT.1.00) GO TO 39
      F=0.5772+ alog(x)+x+0.25*x*x +0.055556*x**3+x**4/96
      GO TO 40
39    IF(x.GT.3.6) GO TO 59
      y1=0.5772+ alog(x)+x+0.25*x*x +0.055556*x**3+x**4/96
      y2=1.0+ 0.015*(x-1.)**2.26
      F=y1*y2
      GO TO 40
59    IF(x.GT.5.0) GO TO 790
      y1=exp(x)/x
      y2=1.+1./x+2./x/x+6./x**3+24./x**4
      y3=0.7153+0.2051*(x-3.)**0.4262
      F=y1*y2*y3
      GO TO 40
79    y1=exp(x)/x
      y2=1.+1./x+2./x/x +6./x**3+24./x**4
      F=y1*y2
40    Continue
      Return
      END
```

Table C.2 Computer program "HYDIF"

```
C   Program "HYDIF" (Fortran) calculates downhole mud density,
C   hydrostatic and differential pressure.
C                NOMENCLATURE
C   FDENS = Downhole mud density, ppg
C   FWS = Mud density at 14.7 psia and 59 degree F, ppg
C   P = Downhole hydrostatic pressure, psig
C   T = Downhole mud temperature, degree F
C   ALFA = Coefficient in equation of state, 1/psig
C   BET1 = Coefficient in equation of state, 1/deg. F
C   BET2 = Coefficient in equation of state 1/deg. F/deg. F
C   N = Index of the Formation fluid: for water (.433 psi/ft) N=1,
C   for salt water(.465 psi/ft) N=2
C   HBOT = Vertical depth of the well, FT
C   OCT = Stabilized outlet (discharge) mud temperature, deg. F
C   BHCT = Stabilized bottomhole circulation mud temperature, deg. F
C   TESC = Standard temperature = 59 deg. F = 15 deg. C
C   HV = Vertical depth of the well
C   WROOT = Normal formation pressure(N=1), psig
C   SROOT = Normal formation pressure(N=2), psig
C   PP = 0.0519475 x (FWS) x (HV), psig
C   (note: a coefficient '0.051947' is used instead of '0.052')
C   DENDIF = FWS-FDENS, ppg
    Double precision B1,B2,B0,A0,X1,X2,ARG
    Double precision ALFA,BET1,BET2,EXX
    Double precision W1,WX1,WX2,WARG
    Double precision S1,SX1,SX2,SARG
    Data W1,W2,W3,W4/2.12492, 0.0000032422,-0.000258363,-4.06131E-07/
    Data S1,S2,S3,S4/2.19304, 0.00000345036,-0.000154207,-3.71040E-07/
    Open(UNIT=5,FILE='Hydif.da')
    Open(UNIT=6,FILE='Hydif.out')
    Read(5,*) N
    Read(5,*) ALFA,BET1,BET2
    Read(5,*) FWS,HBOT,OCT,BHCT,TESC
    IF(N.GT.1) GO TO 109
    Write(6,73)
```

Table C.2 – continued

```
      GO TO 99
109   Write(6,83)
99    Write(6,59)
      Write(6,63)FWS,HBOT
      Write(6,64)OCT,BHCT,TESC
      Write(6,65)ALFA
      Write(6,66)BET1
      Write(6,67)BET2
      Write(6,59)
      Write(6,11)
      Write(6,13)
      Write(6,59)
83    Format(5X,'Formation fluid = salt water with dens. = 9 ppg')
73    Format(5X,'Formation fluid = water ')
63    Format(5X,' Mud dens., ppg =',F6.3,5X,'Total vert. d., ft = ',F7.1)

64    Format(5X,' outlet temp. =',F5.1,5X,'BHCT= ',F5.1,5X,'Stand. temp.
      &=',F4.1)
65    Format(5X,' Isothermal compressibility, 1/psig,=',E15.6)
66    Format(5X,' Temperature coefficient 1, 1/deg. F= ',E15.6)
67    Format(5X,' Temperature coefficient 2, 1/deg. F= ',E15.6)
59    Format(3X,'------------------------------------
      &-------')
11    Format('Depth Well P Form P Dif P Del P Dens Del
      & D Temp')
13    Format(' ft psig psig psig psig ppg
      &ppg deg. F')
      AA1=(BHCT-OCT)/HBOT
      DFW=0.0519475*FWS
      T0=OCT-TESC
      X1=BET1*T0
      Y1=DEXP(X1)
      B0= DFW*Y1/(BET1*AA1)
      WDFW=0.0519475*DEXP(W1)
      WX1=W3*T0
      WY1=DEXP(WX1)
      WB0= WDFW*WY1/(W3*AA1)
      SDFW=0.0519475*DEXP(S1)
      SX1=S3*T0
      SY1=DEXP(SX1)
      SB0= SDFW*SY1/(S3*AA1)
4     Read(5,*,END=1) HV
      CTHV=OCT+AA1*HV
      T=OCT+AA1*HV
      X3=T0+AA1*HV
```

Table C.2 – continued

	X2=BET1*AA1*HV
	B1=DEXP(X2)
	X3=T0+AA1*HV
	A0=1.+BET2*T0*T0-2.*T0*BET2/BET1+2.*BET2/BET1/BET1
	B2=1.+BET2*X3*X3-2.*X3*BET2/BET1+2.*BET2/BET1/BET1
	F=B0*(B1*B2-A0)
	ARG=1./ALFA/ALFA-F*2./ALFA
	ARGSQ=DSQRT(ARG)
	P=1./ALFA-ARGSQ
	PP=DFW*HV
	IPP=PP+0.5
	IP=P+0.5
	IPRDIF=IP-IPP
	EXX=ALFA*P+BET1*(T-TESC)+BET2*(T-TESC)*(T-TESC)
	FDENS=FWS*DEXP(EXX)
	DENDIF=FWS-FDENS
	IHV=HV+0.5
	IF(N.GT.1) GO TO 111
	WX2=W3*AA1*HV
	WB1=DEXP(WX2)
	WA0=1.+W4*T0*T0-2.*T0*W4/W3+2.*W4/W3/W3
	WB2=1.+W4*X3*X3-2.*X3*W4/W3+2.*W4/W3/W3
	WF=WB0*(WB1*WB2-WA0)
	WARG=1./W2/W2-WF*2./W2
	WARGSQ=DSQRT(WARG)
	WROOT=1./W2-WARGSQ
	IWROOT=WROOT+0.5
	IDPRES=IP-IWROOT
	Write(6,46)IHV,IP,IWROOT,IDPRES,IPRDIF,FDENS,DENDIF,T
46	Format(3I9,2I8,F9.2,F8.2,F9.1)
	GO TO 5
111	SX2=S3*AA1*HV
	SB1=DEXP(SX2)
	SA0=1.+S4*T0*T0-2.*T0*S4/S3+2.*S4/S3/S3
	SB2=1.+S4*X3*X3-2.*X3*S4/S3+2.*S4/S3/S3
	SF=SB0*(SB1*SB2-SA0)
	SARG=1./S2/S2-SF*2./S2
	SARGSQ=DSQRT(SARG)
	SROOT=1./S2-SARGSQ
	ISROOT=SROOT+0.5
	IDPRES=IP-ISROOT
	Write(6,76)IHV,IP,ISROOT,IDPRES,IPRDIF,FDENS,DENDIF,T
76	Format(3I9,2I8,F9.2,F8.2,F9.1)
5	Continue
	GO TO 4
1	STOP
	END

Table C.3 Computer program "TEMVOL"

```
C     Program "TEMVOL" (Fortran) calculates the volumetric average
C     temperature of formations for a while drilling for a given radius
C     of investigation. The program also computes the temperature
C     at the radius of investigation.
C                NOMENCLATURE
C     RIN = Radius of investigation, m;   RW = Well radius, m
C     DIF = Formation thermal diffusivity, m^2/hr
C     TEMC = Mud circulating temperature, °C
C     TEMF = Formation static temperature, °C
C     TEMAV = Volumetric average temperature, °C
C     TRF = Formation temperature at the radius of investigation, °C
C     TIC = Duration of the circulation period, hrs;   DEPTH = Depth, m
      External F,FEI
      Open(UNIT=5,FILE='a:temvol.DA')
      Open(UNIT=6,FILE='a:temvol.out')
      Read(5,*) DEPTH,TEMC,TEMF
      Write(6,27) DEPTH
      Write(6,76) TEMC,TEMF
27    Format(' VERTICAL DEPTH , FT. =',F9.1)
76    Format('Circ. temp., = ',F8.1,6X,'Formation temp.=',F8.1)
      Write(6,66)
      Format(10X,'RIN',6X,'DIF',9X,'RW',8X,'TIC',5X,'TRF',5X,'TEMAV')
      Write(6,59)
59    Format(11x,'.....')
      Read(5,*,END=1) DIF,RW,Rin,TIC
      r=rin/rw
      P=R*R
      T=TIC*DIF/RW/RW
      FX= F(T)
      A=-0.25/FX
      AA=-0.25*P/FX
      EIA=-FEI(-A)
      EXA=EXP(A)
      EXAA=EXP(AA)
      EIAA=-FEI(-AA)
      BOT=(P-1.)*EIA
      TOP=P*EIAA-EIA-(EXAA-EXA)/A
      V=TOP/BOT
      TD=EIAA/EIA
```

Table C.3 – continued

```
      TEMAV=(TEMC-TEMF)*V+TEMF
      TRF=(TEMC-TEMF)*TD+TEMF
      Write(6,64) RIN,DIF,RW,TIC,TRF,TEMAV
   64 Format(3X,F9.2,F12.5,F10.3,3F10.1)
      GO TO 4
    1 STOP
      END
C
      FUNCTION F(T)
      IF (T .GT.10.) GO TO 7
      XLN=ALOG(1.+T)
      XLNN=XLN**0.6666667
      F=T*(1.+1./(1.+0.8751733*XLNN))
      GO TO 8
      TX=SQRT(T)
      EXX=EXP(-0.236*TX)
      F=T*(ALOG(T)-EXX)/(ALOG(T)-1.)
    8 RETURN
      END
C
C     Calculates y=-Ei(-x), the exponential integral
C     The equations are taken from the IBM library
      FUNCTION FEI(x)
      IF(x.lT.1.0) GO TO 39
      y1=x**4+8.5733287401*x**3+18.0590169730*x**2
      y2=8.6347608925*x+0.2677737343
      y3=x**4+9.5733223454*x**3+25.6329561486*x**2
      y4=21.0996530827*x+3.9584969228
      z1=y1+y2
      z2=y3+y4
      z=Alog(z1)-alog(z2)
      zz=alog(x)+x
      zy=z-zz
      y=exp(zy)
      GO TO 40
   39 y5=9.999999E-1-2.500001E-1*x
      y6=5.555682E-2*x**2-1.041576E-2*x**3
      y7=1.664156E-3*x**4-2.335379E-4*x**5
      y8=2.928433E-5*x**6-1.766345E-6*x**7+7.122452E-7*x**8
      aux=y5+y6+y7+y8
      auxx=aux*x
      y=auxx-alog(x)-0.57722
   40 continue
      FEI=y
      RETURN
      END
```

Table C.4. Computer program "PERMB"

```
C   Program "PERMB" (Fortran) determines the depth of
C   permafrost base. Two temperature logs are needed.
C   NOMENCLATURE
C   NWELL = Well No.     HTOTm = Total vertical depth,  m
C   TITOTd = Total drilling time, days
C   TIS1d = Shut-in time for the first temperature log, days
C   TIS2d = Shut-in time for the second temperature log, days
C   H1 = Vertical depth 1, ,m     H2 = Vertical depth 2, m
C   TE11,TE12 = Temperature at H1 from first/second log,  °C
C   TE21,TE22 = Temperature at H2 from first/second log, °C
C   TF1,TF2 = Temperature of formations at H1 and H2, °C
C   HPER = Permafrost base depth, m
    Double precision X1,XX1,X2,XX2,AN12,AAN21,AN22,AAAN21
    External EI
    Data D, D1 /1.1925, 0.7532
    Open(UNIT=5,FILE=PERMB.DA')
    Open(UNIT=6,FILE=PERMB.out')
    Read(5,*) HTOTm,TITOTd
    Read(5,*) NWELL
    Write(6,12) NWELL
    Read(5,*) TIS1d,TIS2d
    Write(6,11) HTOTm,TITOTd
    Write(6,13) TIS1d,TIS2d
12  Format(5X,'Well No. =',I7)
11  Format(5X,'Tot. V.D., m =',F9.1,5X,'Tot. Dril. Time, d =',F8.1)
13  Format(5X,'Shutin Time 1, d =',F8.1,5X,'Shutin Time 2, d =',F8.1)
    Write(6,66)
66  Format(3X,'H1,m',3X,'H2,m',4X,'TE11',4X,'TE12',4X,'TE21',
    &4X,'TE22',4X,' TF1',4X,' TF2',3X,'Hper')
    Write(6,59)
59  Format(5x,'————————————————————————————————')
4   Read(5,*,END=1)H1,H2,TE11,TE12,TE21, TE22
    TDR1=TITOTd*(1.-H1/HTOTm)
    TDR2=TITOTd*(1.-H2/HTOTm)
    AN11=TIS1d/TDR1
    AN12=TIS2d/TDR1
    AN21=TIS1d/TDR2
    AN22=TIS2d/TDR2
    X1=D/AN11
    X2=D/AN12
    F1=EI(X1)
    F2=-EI(X2)
    AAN21=AN12/AN11
```

Table C.4 – continued

```
      U1=DLOG(AN12)
      U2=DLOG(AAN21)
      TOP1=F2+U1-D1
      BOT1=F2+F1+U2
      GAM1=TOP1/BOT1
      TF1=TE12+GAM1*(TE11-TE12)
      XX1=D/AN21
      XX2=D/AN22
      FF1=EI(XX1)
      FF2=-EI(XX2)
      AAAN21=AN22/AN21
      UU1=DLOG(AN22)
      UU2=DLOG(AAAN21)
      TTOP1=FF2+UU1-D1
      BBOT1=FF2+FF1+UU2
      GAM2=TTOP1/BBOT1
      TF2=TE22+GAM2*(TE21-TE22)
      GRAD=(TF2-TF1)/(H2-H1)
      HPER=H1-TF1/GRAD
      Write(6,64)H1,H2, TE11,TE21,TE12,TE22,TF1,TF2, HPER
64    Format(2F7.1,6F8.2,F7.1)
      GO TO 4
1     STOP
      END
C     Calculates y=-Ei(-x), the exponential integral
C     The equations are taken from the IBM library
      FUNCTION Ei(x)
      DOUBLE PRECISION x,y1,y2,y3,y4,z1,z2,y,zz,zy
      IF(x.lT.1.0) GO TO 39
      y1=x**4+8.5733287401*x**3+18.0590169730*x**2
      y2=8.6347608925*x+0.2677737343
      y3=x**4+9.5733223454*x**3+25.6329561486*x**2
      y4=21.0996530827*x+3.9584969228
      z1=y1+y2
      z2=y3+y4
      z=dlog(z1)-dlog(z2)
      zz=dlog(x)+x
      zy=z-zz
      y=dexp(zy)
      GO TO 40
39    y5=9.999999E-1-2.500001E-1*x
      y6=5.555682E-2*x**2-1.041576E-2*x**3
      y7=1.664156E-3*x**4-2.335379E-4*x**5
      y8=2.928433E-5*x**6-1.766345E-6*x**7+7.122452E-7*x**8
      auxx=(y5+y6+y7+y8)*x
      y=auxx-Dlog(x)-0.57722
40    Continue
      Ei=y
      RETURN
      END
```

Table C.5 Computer program "SHUTEMP"

```
C   Program "SHUTEMP" (Fortran) calculates the dimensionless
C   shut-in temperature of formations as a function of the radial
C   distance, time of fluid circulation, and shut-in time.
C            NOMENCLATURE
C   RW = Well radius, m     DIF = Thermal Diffusivity, m**2/h**-1
C   R = Radial distance, m     TIC = Fluid Circulation time, hrs
C   TIS = Shut-in time, hrs     FX = Dimensionless shut-in temp.
      Double precision  T,TS,RD
      External  F
      Open(UNIT=5,FILE='Shutemp.da')
      Open(UNIT=6,FILE='Shutemp.out')
      Read(5,*)  RW,DIF
      PAR=DIF/RW/RW
      Write(6,12)  RW,DIF
      Write(6,59)
12    Format(5X,'Well rad., m =',F7.4,5X,'Diffusivity, m**2/h =',F8.5)
      Write(6,66)
66    Format(4X,'Distance, m',5X,'Circ. time, h',2X,'Shut-in time, h',5X
     &,'Tempdless')
      Write(6,59)
59    Format(5x,'-------------------------------------')
4     Read(5,*,END=1)  R,TIC,TIS
      RD=R/RW
      T=TIC*PAR
      TS=TIS*PAR
      FX= F(RD,T,TS)
      Write(6,64)  R,TIC,TIS,FX
64    Format(3F15.2,F16.4)
      GO TO 4
1     STOP
      END
C
      Function F(RD,T,TS)
      Double precision  RD,T,TS,TI,TX,BET,ARG1,ARG2
      External  EI
      IF (T .GT.10.) GO TO 7
      XLN=DLOG(1.+T)
      XLNN=XLN**0.6666667
```

Table C.5 – continued

```
      TI=T*(1.+1./(1.+0.8751733*XLNN))
      GO TO 8
7     TX=DSQRT(T)
      EXX=DEXP(-0.236*TX)
      TI=T*(DLOG(T)-EXX)/(DLOG(T)-1.)
8     BET=0.25/TI
      EIEV=EI(BET)
      ARG1=0.25*RD*RD/(TI+TS)
      ARG2=0.25*RD*RD/TS
      EIRD1=-EI(ARG1)
      EIRD2=-EI(ARG2)
      F=(EIRD2-EIRD1)/EIEV
      Return
      END
C
C     Calculates y= -EI(-x), the exponential integral
C     The equations are taken from the IBM library
      Function EI(x)
      Double precision  x,y1,y2,y3,y4,z1,z2,y,zz,zy
      IF(x.lT.1.0)  GO TO 39
      y1=x**4+8.5733287401*x**3+18.0590169730*x**2
      y2=8.6347608925*x+0.2677737343
      y3=x**4+9.5733223454*x**3+25.6329561486*x**2
      y4=21.0996530827*x+3.9584969228
      z1=y1+y2
      z2=y3+y4
      z=dlog(z1)-dlog(z2)
      zz=dlog(x)+x
      zy=z-zz
      y=dexp(zy)
      GO TO 40
39    y5=9.999999E-1-2.500001E-1*x
      y6=5.555682E-2*x**2-1.041576E-2*x**3
      y7=1.664156E-3*x**4-2.335379E-4*x**5
      y8=2.928433E-5*x**6-1.766345E-6*x**7+7.122452E-7*x**8
      aux=y5+y6+y7+y8
      auxx=aux*x
      y=auxx-dlog(x)-0.57722
40    continue
      EI=y
      Return
      END
```

Table C.6 Computer program "PERMTEMP"

```
C     Program "PERMTEMP" (Fortran) calculates the temperature of
C     permafrost. Three temperature logs taken after a complete
C     freezeback are needed to use this program.
C              NOMENCLATURE
C     HTOT = Total vertical depth, m,    NWELL = Well number
C     TITOTd = Total Drilling Time, days    Z = Depth, m
C     TIS1 = Shut-in time for the first temperature log, days
C     TIS2 = Shut-in time for the second temperature log, days
C     TIS3 = Shut-in time for the third temperature log, days
C     TE1 = Temperature from the first log, °C
C     TE2 = Temperature from the second log, °C
C     TE3 = Temperature from the third log, °C
C     TEF = Temperature of the formation, °C
C     H = 2.0,   EPS = 0.00001,    RSTART = 0.01
      Double precision R,RSTART,H,EPS,FO,RRE,YA,AR1,ARG2,AARG1,PP1
      Double precision XXL ,XXR ,XXM,TE1,TE2,TE3,TI21,TI22,TI23
      Character*72 DSH
      External FF,FG
      Data DSH/'————————————————————————————————————————'/
      Open(UNIT=5,FILE='PERMTEMP.DA')
      Open(UNIT=6,FILE='PERMTEMP.out')
      Read(5,*) H,EPS,RSTART
      Read(5,*) NWELL,HTOT, TITOLd
      Write(6,77)NWELL,HTOT, TITOLd
      Write(6,33)DSH
      Write(6,88)
      Write(6,33)DSH
33    Format(A80)
77    Format('Well No:',I5,3x,'TVD, m =',F7.1,3x,'Dril. time, d =',F8.2)
c 88  Format(8X,'Z, m',5X,' FO',8X,'PAR',10x,'RIN',8X,'TEF')
88    Format(' Z t1',8X,'t2',5x,'t3',8X,'T1',8x,'T2',8x,'T3 Tf')
4     Read(5,*,END=1)Z,TE1,TE2,TE3,TIS1,TIS2,TIS3
      YA=(TE1-TE2)/(TE1-TE3)
      TI21=TIS1+TITOLd*(1.-Z/HTOT)
      TI22=TIS2+TITOLd*(1.-Z/HTOT)
      TI23=TIS3+TITOLd*(1.-Z/HTOT)
      XXL =RSTART
5     XXR =XXL *H
      FFXXL = FF(XXL ,TI21,TI22,TI23,YA)
```

Table C.6 – continued

	FFXXR = FF(XXR ,TI21,TI22,TI23,YA)
	IF (FFXXL *FFXXR .LT. 0.0) GO TO 10
	XXL =XXR
	GO TO 5
10	DO 100 I=1,10000
	XXM =(XXL +XXR)/2
	FFXXL = FF(XXL ,TI21,TI22,TI23,YA)
	FFXXM = FF(XXM ,TI21,TI22,TI23,YA)
	IF (FFXXM * FFXXL) 20,30,40
20	XXR =XXM
	GO TO 50
30	XXR =XXM
40	XXL =XXM
50	IF (ABS(XXL -XXR) .LT. EPS) GO TO 200
100	Continue
200	FO = XXM
	TS1=TI22-TI21
	RRR=DSQRT(FO)
	RRE=1.+2.184*RRR
	AN1=TS1/TI21
	PP1=1./(4.*AN1*FO)
	AARG1=PP1*RRE*RRE
	EEIRD1=fg(AARG1)
	EEIP1=fg(PP1)
	DLR=DLOG(RRE)
	GAM=1.-(EEIRD1-EEIP1)/2./DLR
	TEF=(TE2-GAM*TE1)/(1.-GAM)
	PAR=FO/TI21
	Write(6,96)z,TI21,TI22,TI23,TE1,TE2,TE3,tef
C	Write(6,69)Z,FO,PAR,RRE,TEF
C 69	Format(5x,F9.1,F9.3, F12.5,F10.2,F12.2)
96	Format(F8.1,3F7.1,4F9.2)
	GO TO 4
1	STOP
	END
C	
	Function FF(R,TI21,TI22,TI23,YA)
	Double precision R,TI21,TI22,TI23,YA
	Double precision Rr,re,p1,p2,arg1,arg2
	External FG
	TS1=TI22-TI21
	TS2=TI23-TI21
	RR=DSQRT(R)
	RE=1.+2.184*RR
	AN1=TS1/TI21
	AN2=TS2/TI21
	P1=1./(4.*AN1*R)
	P2=1./(4.*AN2*R)

Table C.6 – continued

```
      ARG1=P1*RE*RE
      ARG2=P2*RE*RE
      EIRD1=FG(ARG1)
      EIRD2=FG(ARG2)
      EIP1=FG(P1)
      EIP2=FG(P2)
      TOP=EIRD1-EIP1
      BOT=EIRD2-EIP2
      FF=TOP/BOT-YA
      Return
      END
C
C     Calculates y=-Ei(-x), the exponential integral
C     The equations are taken from the IBM library
      Function fg(x)
      Double precision x,y1,y2,y3,y4,z1,z2,y,zz,zy
      IF(x.lT.1.0) GO TO 39
      y1=x**4+8.5733287401*x**3+18.0590169730*x**2
      y2=8.6347608925*x+0.2677737343
      y3=x**4+9.5733223454*x**3+25.6329561486*x**2
      y4=21.0996530827*x+3.9584969228
      z1=y1+y2
      z2=y3+y4
      z=dlog(z1)-dlog(z2)
      zz=dlog(x)+x
      zy=z-zz
      y=dexp(zy)
      GO TO 40
39    y5=9.999999E-1-2.500001E-1*x
      y6=5.555682E-2*x**2-1.041576E-2*x**3
      y7=1.664156E-3*x**4-2.335379E-4*x**5
      y8=2.928433E-5*x**6-1.766345E-6*x**7+7.122452E-7*x**8
      aux=y5+y6+y7+y8
      auxx=aux*x
      y=auxx-dlog(x)-0.57722
40    Continue
      fg=-y
      Return
      END
```

Table C.7 Computer program "GRAD"

```
C   Program "GRAD" (Fortran) calculates the geothermal gradient
C   and the temperature of formations.
C   Two temperature logs are needed to use this program.
C   can be used for any values of shut-in or drilling time.
C            NOMENCLATURE
C   HTOTm = Total vertical depth, m,    NWELL = Well number
C   TITOTd = Total Drilling Time, days   DWm = Well Diameter, m
C   TIS1d = Shut-in time for the first temperature log, days
C   TIS2d = Shut-in time for the second temperature log, days
C   H1m = Vertical depth 1, m     H2m = Vertical depth 2, m
C   TEM11 = Temperature at H1m from the first log, °C
C   TEM12 = Temperature at H1m from the second log, °C
C   TEM21 = Temperature at H2m from the first log, °C
C   TEM22 = Temperature at H2m from the second log, °C
C   DIF = Thermal diffusivity of formations, m²h⁻¹
C   TEFOR1= Temperature of formations at H1m, °C
C   TEFOR2= Temperature of formations at H2m, °C
C   GGX = Geothermal gradient (per 100 m), °C/100m
C   GX = Geothermal gradient from the second log, °C/100m
C   GRAT = is the GX and the GGX ratio
    Dimension FX(2), T(2)
    Double precision T,TS1,TS2
    External F
    Open(UNIT=5,FILE='grad.DA')
    Open(UNIT=6,FILE='grad.out')
    Read(5,*) NWELL,DWm
    Read(5,*) HTOTm,TITOTd
    Write(6,12) NWELL,DWm
    Read(5,*) TIS1d,TIS2d
    Write(6,11) HTOTm,TITOTd
    Write(6,13) TIS1d,TIS2d
    Write(6,59)
12  Format(5X,'Well No =',I7,5X,'Well Diameter, m =',F9.3)
11  Format(5X,'Total V.D., ft =',F9.1,5X,'Tot. Dril. time, d =',F8.1)
13  Format(5X,'Shut-in Time 1, d=',F8.1,5X,'Shut-in Time 2, d=',F8.1)
    Write(6,66)
66  Format(//9X,'H1,f',7X,'H2,f',8X,'Dif',4X,'Tef 1',4X,'Tef 2',4X,'Ge
    &ogr',3X,'Gratio')
    Write(6,59)
```

Table C.7 – continued

```
59    Format(5x,'----------')
4     Read(5,*,END=1) H1m,TEM11,TEM12,H2m,TEM21,TEM22,DIF
      TIC1=TITOTd*(1-H1m/HTOTm)*24
      TIC2=TITOTd*(1-H2m/HTOTm)*24
      TIS1=TIS1d*24
      RW=DWm/2
      TIS2=TIS2d*24
      DELH=H2m-H1m
      GX=(TEM22-TEM12)/DELH*100
      TS1=TIS1*DIF/RW/RW
      TS2=TIS2*DIF/RW/RW
      T(1)=TIC1*DIF/RW/RW
      T(2)=TIC2*DIF/RW/RW
      DO 150 N=1,2
      FX(N)= F(T(N),TS1,TS2)
150   Continue
      TEFOR1=(TEM11-FX(1)*TEM12)/(1-FX(1))
      TEFOR2=(TEM21-FX(2)*TEM22)/(1-FX(2))
      GG=(TEFOR2-TEFOR1)/DELH
      GGX=GG*100
      GRAT=GX/GGX
      Write(6,64) H1m,H2m,DIF,TEFOR1,TEFOR2,GGX,GRAT
64    Format(2X,2F11.2,F11.5,4F9.2)
      GO TO 4
1     STOP
      END
C
      Function F(T,TS1,TS2)
      Double precision T,TX,XLN,TI,ARG1,ARG2,BET,TS1,TS2
      External Ei
      IF (T .GT.10.) GO TO 7
      XLN=DLOG(1.+T)
      XLNN=XLN**0.6666667
      TI=T*(1.+1./(1.+0.8751733*XLNN))
      GO TO 8
7     TX=DSQRT(T)
      EXX=DEXP(-0.236*TX)
      TI=T*(DLOG(T)-EXX)/(DLOG(T)-1.)
8     BET=0.25/TI
      EIEV=-Ei(BET)
      ARG1=BET*(1.+TI/TS1)
      ARG2=BET*(1.+TI/TS2)
      EIRD1=-Ei(ARG1)
      EIRD2=-Ei(ARG2)
      F=(EIEV-EIRD1)/(EIEV-EIRD2)
      Return
      END
```

Table C.7 – continued

```
C     Calculates y = -Ei(-x), the exponential integral
C     The equations are taken from the IBM library
      Function Ei(x)
      Double precision x,y1,y2,y3,y4,z1,z2,y,zz,zy
      IF(x.lT.1.0) GO TO 39
      y1=x**4+8.5733287401*x**3+18.0590169730*x**2
      y2=8.6347608925*x+0.2677737343
      y3=x**4+9.5733223454*x**3+25.6329561486*x**2
      y4=21.0996530827*x+3.9584969228
      z1=y1+y2
      z2=y3+y4
      z=dlog(z1)-dlog(z2)
      zz=dlog(x)+x
      zy=z-zz
      y=dexp(zy)
      GO TO 40
39    y5=9.999999E-1-2.500001E-1*x
      y6=5.555682E-2*x**2-1.041576E-2*x**3
      y7=1.664156E-3*x**4-2.335379E-4*x**5
      y8=2.928433E-5*x**6-1.766345E-6*x**7+7.122452E-7*x**8
      aux=y5+y6+y7+y8
      auxx=aux*x
      y=auxx-dlog(x)-0.57722
40    continue
      Ei=y
      Return
      END
```

REFERENCES

Abramowitz, M. and Stegun, I.A. (1972) Handbook of Mathematical Functions with Formulas, Graphs, and Mathematical Tables. National Bureau of Standards, Applied Mathematics Series, **55,** US Government Office.

API Bulletin D10 (1981) Procedure for Selecting Rotary Drilling Equipment. Society of Petroleum Engineers, Richardson, Texas.

API Specifications for Materials and Testing for Well Cements (1982). API Spec. 10, First Edition API, Dallas.

Balobayev, V.T., Devyatkin, V.N., and Kutasov,I.M. (1973) Contemporary Geothermal Conditions of the Existence and Development of Permafrost. Proceedings of the Second International Conference on Permafrost, Yakutsk, Soviet Contribution, 13-28 July, Nat. Acad. Sci., Washington, D.C., 619–624.

Balobayev, V.T., and Shastkevich, Yu.G. (1974) The Estimation of the Talik Zones Configuration and the Steady Temperature Field of Rocks beneath the Lakes of Arbitrary Contour. In: Lakes of the Siberia Cryolithozone (Russian), Novosibirsk, Nauka, 116–127.

Bear, J.(1972) Dynamics of Fluids in Porous Media, American Elsevier Publishing Company, Inc., New York, N.Y.

Bearden, W.G. (1959). Effect of Temperature and Pressure on the Physical Properties of Cement. *Oil-well Cementing Practices in U.S.*, API, 56.

Beck, A.E. and Balling, N. (1988) Determinations of Virgin Rock Temperatures. In: Haenel, R., Rybach, L., and Stegena, L. (Eds.) Handbook of Terrestrial Heat-Flow Density Determination. Kluwer Academic Publishers, Dordrecht/Boston/London, 59–85.

Bejan, A. (1993) Heat Transfer. John Wiley & Sons, Inc. USA.

Beirute, R.M.(1991) A Circulating and Shut-in Well-Temperature- Profile Simulator. *J. Pet. Tech.*, 1140–1146.

Ben-Avraham, Z. and Ballard, D. (1984) Near bottom temperature anomalies in the Dead Sea. *Earth Planet. Sci. Letts.*, **71**, 356–360.

Bia, P. and Combarnous, M. (1975) Transfert de Chaleur et de Masse. Operations. *Revue de l'Institut Francais du Pètrole*, June, 361–376.

Bily, C. and Dick, J.W.L. (1974) Naturally Occurring Gas Hydrates in the Mackenzie Delta, N.W.T. *Bul. Can. Pet. Geol.*, **22**, 340–353.

Birch, R., and Clark, H. (1940) The Thermal Conductivity of Rocks and its Dependence upon Temperature and Composition. *Amer. J. Sci.*, **238**, 529–588.

Blackwell, D.D., and Steele J.L. (1989) Thermal Conductivity of Sedimentary Rocks: Measurement and Significance. In: Naeser N.D. and McCulloh T.H. (Eds.) Thermal History of Sedimentary basins – Methods and Case Histories. Springer, Berlin Heidelberg New York, 14–36.

Blesh, C.J., Kulacki, F.A., and Christensen, R.N. (1983) Application of Integral Methods to Prediction of Heat Transfer from a Nuclear Waste Repository. Open File Report ONWI-495, Battelle Memorial Institute, Columbus, OH, 12–17.

Bodell, J.M. and Chapman, D.S. (1982) Heat Flow in the North-Central Colorado Plateu. *J. Geophys. Res.*, **87**, 2869–2884.

Bogomolov G.V., Lubimova, E.A., Tcibulya, L.A., Kutasov, I.M., and Atroshenko, P.P. (1970) Heat Flow of the Pripyat Through. Reports of Academy of Sciences of the BSSR, Physical-Technical Series, Minsk, No. 2, 97–103.

Bogomolov G.V., Tcibulya, L.A., and Atroshenko, P.P. (1972) Geothermal Zones of the Belarus. Nauka and Technika, Minsk, 216 p.

Bondarev, E.A. and Krasovitskiy, B.A. (1974) Thermal Regime of Oil and Gas Boreholes. Nauka, Novosibirsk, 87p.

Bondarev, E.A., Babe, G.D., Groysman, A.G., and Kanibolotskiy, M.A. (1976) Mechanics of Hydrate Formation in Gas Flows. Nauka, Novosibirsk, 158p.

Borsei, M.A., Sidebottom, O.M., Seely, F.B., and Smith,J.O.(1978) Advanced Mechanics of Materials. Third Edition, John Wiley and Sons, New York.

Bradford, B.B. (1985) Attention to Primary Cementing Practices Leads to Better Jobs. *Oil Gas J.*, 21 October, 59–63.

Bredehoeft, J.D. and Papadopulos, I.S. (1965) Rates of Vertical Groundwater Movements Estimated from the Earth's Thermal Profile. *Water Resources Res.*, **1**, 325–328.

Brott, C.A., Blackwell, D.D., and Morgan, P. (1981) Continuation of Heat Flow Data: a Method to Construct Isotherms in Geothermal Areas. *Geophysics*, **46**, 1732–1744.

Bullard, E.C. (1940) The Disturbance of the Temperature Gradient in the Earth's Crust by Inequalities of Height. *Month. Not. Roy. Astr. Soc., Geophys.*, **4**, 300–362.

Bullard, E.C. (1947) The Time Necessary for a Borehole to Attain Temperature Equilibrium. *Mon. Not. R. Astron. Soc., Geophys. Suppl.*, **5**, 127–130.

Burnham, C.W., Hollaway, J.H., and Davis, N.F. (1969) Thermodynamic Properties of Water to 1,000 °C and 10,000 Bars. *Special Paper*, **132**, Geol. Soc. Amer.

Byrd, P.F. and Friedman, M.D. (1959) Handbook of Elliptic Integrals for Engineers and Physicists. Berlin, Springer, 355 p.

Cao, S., Lerche, I., and Hermanrud, C. (1988) Formation Temperature Estimation by Inversion of Borehole Measurements. *Geophys.*, **53**, 979–988.

Carlson, N.R. and Barnette, J.C. (1988) Determinig a Reliable Estimate of the Geothermal Gradient from Shut-in Temperature Recordings. SPE Paper 18144 Presented at the 63rh Annual Technical Conference and Exhibition, Houston,Texas, 2-5 October.

Carslaw, H.S. and Jaeger J.C. (1950) Conduction of Heat in Solids. Second Edition, Oxford University Press, Amen House, London, 283.

Carslaw, H.S. and Jaeger, J.C. (1959) Conduction of Heat in Solids. Second Edition, Oxford University Press, London.

Čermak, V. and Haenel, R. (1988) Geothermal Maps. In: Haenel, R., Rybach, L., and Stegena, L. (Eds.) Handbook of Terrestrial Heat-Flow Density Determination. Kluwer Academic Publishers, Dordrecht/Boston/London, 261–300.

Chekalyuk, E.B., Fedortzev, I.M., and Osadchy, V.G. (1974) Geothermal Field Survey. Naukova Dumka, Kiev

Cheremenskiy, G.A. (1972) Geothermics. Nedra, Leningrad, 272p.

Cheremenskiy, G.A. (1977) Applied Geothermics. Nedra, Leningrad, 224p.

Clark, S.P., Jr. (1966) Handbook of Physical Constants. *Geol. Soc. Am. Mem.*, **97**, 587.

Craft, B.C., Holden, W.R., and Graves, E.D., Jr. (1962) Well Design: Drilling and Production. Prentice-Hall, Inc., Englewood Cliffs, New Jersey, 48–55.

Davies, G.F. (1980) Review of Oceanic and Global Heat Flow Estimates. *Rev. Geophys. Space, Phys.*, **18**, 718–722.

Davis, S.H. and Faulk, J.H. (1952). Have Waiting - on Cement Practices Kept Pace With Technology? *Drilling and Production Practices*, API, 180

Deykin, V.V., Kogan, E.V., and Proselkov, Yu. M., (1973) Film Heat Transfer Coefficient in Wells During Drilling. In: Mud Circulation and Wells Completion Technology, Nedra, Moscow, 3–7.

Diment, W.H., (1967) Thermal Regime of Large Diameter Borehole: Instability of the Water Column and Comparison of Air-and Water-filled Conditions. *Geophys.*, **32**, 720–726.

Djamalova A.S. (1969) Heat Low of Dagestan. Nauka, Moscow, 128p.

Dobrynina, Z.K., Dmitrieva, T.A., Pletnev, A.A., Semenov, V.G., and Skornyakov, S.M. (1985) Shaping of Seasonal Thermal Anomalies Over Ore Bodies. *Izv. Vysshikh Uchebnykh Zavedeny*, Ser. Geol. i Razv., **8**, 98–101.

Dodson, C.R. and Standing, M.B. (1944) Pressure-Volume-Temperature and Solubility

Relations for Natural-Gas-Water Mixtures. *Drill. and Prod. Prac.*, API, 176.

Dowdle, W.L. and Cobb, W.M. (1975) Static Formation Temperatures from Well Logs-an Empirical Method. *J. Pet. Tech.*, 1326–1330.

Drury, M.L. (1984) On a Possible Source of Error in Extracting Equilibrium Formation Temperatures from Boreholes BHT Data. *Geothermics*, **13**, 175–180.

Dubina, M.M. and Krasovitskiy, B.A. (1983) Heat Exchange and Mechanics of Interaction Pipelines and Boreholes with Soils. Nauka, Novosibirsk, 133p.

Dubina, M.M. (1988) Pressure in Relation to Freezing of Water-Containing Masses in a Confined Space. Proceedings of The Fifth International Conference on Permafrost. **2**, Tapir Publishers, Trondheim, Norway, 1372–1376.

Duchkov, A.D., Sokolova, L.S., Balobaev, V.T., Devyatkin, V.N., Kononov, V.I., and Lysak, S.V. (1997) Heat Flow and Geothermal Field in Siberia. *Geol. and Geophys.*, **38**, Novosibirsk, 1716–1729.

Edwardson, M.L., Girner, H.M., Parkinson, H.R., Williams, C.D., and Matthews, C.S. (1962) Calculation of Formation Temperature Disturbances Caused by Mud Circulation. *J. Pet. Tech.*, 416–426.

Edwards, L.M., Chilingar, G.V., Rieke, H.H., and Fertl, W.H., (1982). Handbook of Geothermal Energy. Gulf Publishing Company, Houston.

Elder, J.W. (1981). Geothermal Systems. Academic Press, London, 508p.

Eppelbaum, L.V. (1989) The Development of Methods for Processing and Interpretation of Natural Geophysical Fields in Prospecting for Pyrite Ores Under Mountainous Conditions. Ph.D. Theses. Tbilisi, Georgia, Institute of Geophysics.

Eppelbaum, L.V. and Mishne, L.R. (1988) Some theoretical aspects of optimum filtration of geophysical signals with depended noises: Deposited by the All-Union Institute of Scientific and Technical Information, USSR Acad. of Sci., No.7842.

Eppelbaum, L.V., Modelevsky, M.M., Jr., and Pilchin, A.N. (1996) Thermal Investigation in Petroleum Geology: the Experience of Implication in the Dead Sea Rift Zone, Israel. *J. Petr. Geol.*, **19**, No. 4, 425–444.

Fagley, J., Fogler, H.S., Davenport, C.B., and Millhone, R.S. (1982) An Improved Simulation for Interpreting Temperature Logs In Water Injection Wells. *J. Pet. Tech.*, 709–718.

Farris, R.F. (1941) A Practical Evaluation of Cements for Oil Wells. *API Dril. and Prod. Prac.*, 283–292.

French, F.R. and McLean, M.R. (1993) Development Drilling Problems in High-Pressure Reservoirs. *J. Pet. Tech.*, 772–777.

Gogoi, R. (1986) Thermal Stresses Around an Uncased Production Well. Dissertation, Louisiana Tech University, 121p.

Gogoi, R. and Kutasov, I.M. (1986) Temperature Distribution Around an Uncased

Well with a History of Variations in Wellbore Temperature. SPE paper 15984, Richardson, Texas, USA.

Gold, L.W. and Lachenbruch, A.H. (1973) Thermal Conditions in Permafrost – A Review of North American Literature. Permafrost (North American Contribution), Second International Conference, 13-28 July, Yakutsk, USSR, Nat. Acad. Sci., Washington, D.C., 10.

Goodman, M.A. (1978) World Oil's Handbook of Arctic Well Completions. Gulf Publishing Company, Houston, 8–10.

Goodman, M.A. and Franklin L.J. (1982) Thermal Model of a New Concept for Hydrate Control During Drilling. Proceedings of the Fourth Canadian Permafrost conference, 2-6 March, Calgary, Alberta, 349–355.

Gorbenko, L.A. (1937) Results of Geothermal Prospecting Application in Azerbaijan. *News of Oil Technique*, Aznefteizdat, Baku, No.1.

Gradshtein, I.S. and Ryzhik, I.M. (1965) Table of Integrals, Series ab Products. Oxford University Press, London, England.

Grant, F.S. and West, G.F. (1965) Interpretation in Theory in Applied Geophysics. McGraw-Hill.

Gretener, P.E. (1967) On the Thermal Instability of Large Diameter Wells – an Observational Report. *Geophys.*, **32**, 727–738.

Gretener, P.E. (1968) Temperature Anomalies in Wells due to Cementing of Casing. *J. Pet. Tech.*, 147–151.

Gretener, P.E. (1981) Geothermics: Using Temperature in Hydrocarbon Exploration. AAPG, Short Course Notes, **17**, 1–156.

Gritsenko, A.I. and Makogon, Yu., F.(1983) Drilling and Operation of Gas Wells in the Presence of Natural Gas Hydrates. Fourth International Permafrost Conference, 17-22 July, 1983, Fairbanks, Alaska. Nat. Acad. Sci., Washington, D.C., 167–172.

Gryaznov, G.S. (1978) Designs of Gas Wells in Permafrost Areas. Nedra, Moscow, 136p.

Guyod, H. (1946) Temperature Well Logging. *Oil Weekly*, **123**, 21 October to 16 December, 7 parts, 42p.

Haenel, R., Rybach, L., and Stegena, L. (1988) Fundamentals of Geothermics. In: Haenel, R., Rybach, L., and Stegena, L. (Eds.) Handbook of Terrestrial Heat-Flow Density Determination. Kluwer Academic Publishers, Dordrecht/Boston/London, 9–57.

Hales, A.L. (1937). Convection Currents in Geysers. *Mon. Not. R. Astron. Soc., Geophys. Suppl.*, **4/1**, 122–132.

Halliburton Cementing Tables (1979) Halliburton Company, Duncan, OK, 24.

Hanni, G. (1973) Drilling the Permafrost. *Baroid News Bull.*, April, 21–23.

Henry, S.G. and Pollack, H.N. (1985) Heat Flow in the Presence of Topography: Numerical Analysis of Data Ensembles. *Geophysics*, **50**, 1335–1341.

Hnatiuk, J. and Randall, A.G. (1977) Determination of Permafrost Thickness in Wells in Northern Canada. *Can. J. Earth Sci.*, **14**, 375–383.

Holmes, C.S. and Swift, S.C. (1970). Calculation of Circulating Mud Temperatures. *J. Pet. Tech.*, 670–674.

Hoberock, L.L., Thomas, D.C., and Nickens, H.V.(1982) Here's How Compressibility and Temperature Affect Bottom-Hole Mud Pressure. *Oil Gas J.*, 159–164.

Hubbard, J.T. (1984) How Temperature and Pressure Affect Clear Brines. *Petrol. Eng. Intern.*, April, 58–64.

Ismail-Zade, T.A., Askerov, R.B., and Aliyev, S.A. (1980) A Method for Determining Crust Fractures. Soviet Inventor Certificate No.792198 MKI GOIV9/00.

Jacob, C.E. and Lohman, S.W. (1952) Non-steady Flow to a Well of Constant Drawdown in an Extensive Aquifer. *Trans. Amer. Geophys. Un.*, 559–564.

Jaeger, J.C. (1956) Numerical Values for the Temperature in Radial Heat Flow, *J. Math. Phys.*, **34**, 316–321.

Jaeger, J.C. (1961) The Effect of the Drilling Fluid on Temperature Measured in Boreholes. *J. Geophys. Res.*, **66**, 563–569.

Jaeger, J.C. and Sass, J.G. (1963) Lee's Topographic Correction in Heat Flow and the Geothermal Flux in Tasmania. *Geofis. Pura. Appl.*, **54**, 63–66.

Jaeger, J.C. (1965) Application of the Theory of Heat Conduction to Geothermal Measurements. In: W.H.K. Lee (Ed.) Terrestrial Heat Flow, Geophysical Monograph Series **8**, American Geophysical Union, Baltimore, Maryland, Port City Press, 7–23.

Jones, R.R. (1986). A Novel Economical Approach for Accurate Real Time Measurement of Wellbore Temperature. SPE Paper 15577, Richardson, Texas, USA.

Jorden, J.R. and Campbell, F.L. (1984) Well Logging I – Rock Properties, Borehole Environment, Mud and Temperature Logging. SPE of AIME, N.Y., Dallas, 131–146.

Judge, A.S., Taylor, A.E., and Burgess, M. (1979) Canadian Geothermal Data Collection Northern Wells 1977 - 78. *Geothermal Series*, **11**, Earth Physics Branch, Energy, Mines and Resources, Ottawa, 187p.

Judge, A.S., Taylor, A.E., Burgess, M., and Allen, V.S. (1981) Canadian Geothermal Data Collection– Northern Wells 1978 - 80. *Geothermal Series*, **12**, Earth Physics Branch, Energy, Mines and Resources, Ottawa, 190p.

Judge, A. (1982) Natural Gas Hydrates in Canada. Proceedings of the Fourth Canadian Permafrost conference, March 2-6, Calgary, Alberta, 320–328.

Kappelmeyer, O. and Haenel, R. (1974) Geothermic with Special Reference to Application. Gebrüder Borntträger, Berlin, 1–240.

Katz, D.L. (1945) Predictions of Conditions for Hydrate Formation In Natural Gases. *Trans., of AIME*, **160**, 141.

Kaye, J. and Elgar, E.C. (1958) Models of Adiabatic and Diabatic Fluid Flow in an Annulus with an Inner Rotating Cylinder. *Trans., of ASME*, **80**, 753–765.

Keller, H.H., Couch, E.J., and Berry, P.M. (1973) Temperature Distribution in Circulating Mud Columns. *Soc. Petr. Eng. J.*, 23–30.

Khesin, B.E. (1978) Estimation of Topographic Effects in Magnetic Prospecting. *Razv. Geofiz.*, **83**, 102–111.

Khesin, B.E., Alexeyev, V.V., and Eppelbaum, L.V. (1988) Optimization of Geophysical Investigations in Mountainous Regions by Increasing the Effectiveness of Interpretation. In: Borisovich, V.T., and Eppelbaum, V.M. (Eds.) Optimization of Prospecting for Useful Ore Minerals in Mountainous Regions. Nedra, Moscow, 79–122.

Khesin, B.E. and Eppelbaum, L.V. (1988) Methods of Quantitative Interpretation of the Data of Near-Surface Thermal Prospecting Under Complicated Physical and Geological Conditions. IL AzNIINTI, No.109, Baku, Azerbaijan.

Khesin, B.E. and Eppelbaum, L.V., (1994) Near-surface Thermal Prospecting: Review of Processing and Interpretation. *Geophys.*, **59**, 744–752.

Khutorsky, M.D., Salnikov, V.E., and Fotogdinov, R.A. (1983) Geothermal Prospecting of Ore Deposits. In: Eds., Kropotkin, B.M. and Smirnov, Ya.B.: Methodical and Experimental Principles of Geothermometry. Nauka, Moscow, 212–229.

Kraskovskiy, S.A. (1934). Geothermal Measurements in Boreholes. Geothermal Measurements in Moscow. Transactions of the TsNIGRI, No. 8, Moscow

Kritikos, W.P. and Kutasov, I.M. (1988) Two-Point Method for Determination of Undisturbed Reservoir Temperature. *Formation Evaluation*, 222–226.

Kuliev, S.M., Esman, B.I., and Gabuzov, G.G. (1968) Temperature Regime of the Drilling Wells. Nedra, Moscow.

Kutas, R.I. and Gordienko, V.V. (1971) The Temperature Field of Ukraina. Naukova Dumka, Kiev, 140p.

Kutasov, I.M. and Devyatkin, V.N. (1964) Experimental Investigation of Temperature Regime of Shallow Convective Holes. In: Thermal Processes in Frozen Rocks. Nauka, Moscow, 143–150.

Kutasov, I.M., Lubimova, E.A., and Firsov, F.V. (1966) Rate of Recovery of the Temperature Field In Wells on Kola Peninsula. In: Problemy glubinnogo teplovogo potoka (Problems of the Heat Flux at Depth), Nauka, Moscow, 74–87.

Kutasov, I.M. (1968) Determination of Time Required for the Attainment of Temperature Equilibrium and Geothermal Gradient in Deep Boreholes. Freiberger Forshungshefte, **C238**, 55–61.

Kutasov, I.M., Atroshenko, P.P., and Tcibulya, L.A. (1971) The Use of Temperature Logs for Predicting the Static Formation Temperature. Reports of Academy of Sciences of the BSSR, Minsk, **15**, No. 3, 266–269.

Kutasov, I.M. and Devyatkin, V.N. (1973) Effect of Free Heat Convection and Casing on the Temperature Field in Boreholes. In: Heat Flows from the Crust and Upper Mantle of the Earth, Mauka, Moscow, 99–106.

Kutasov, I.M. (1976) Thermal Parameters of Wells Drilled in Permafrost Regions. Nedra, Moscow, 119p.

Kutasov, I.M., Balobayev, V.T., and Demchenko, R.Ya. (1977a) Method of "Joining" of Solutions in the Determination of a Plane and a Cylindrical Phase Interface in the Stefan Problem. *Inzhenerno-Fizicheskii Zhurnal*, **33**, 148–152.

Kutasov, I.M., Tarasov, A.A., and Kononov, Yu.I. (1977b) Experimental Study of Washouts in Frozen Rocks Using Models of Drilling Wells. *Neftianoe Khoziaistvo*, June, 21-33.

Kutasov, I.M. (1977) Critical Temperature Governing buckling of Casing in Boreholes. *Kolyma*, No. 4, 23–25.

Kutasov, I.M. and T.R. Bates (1980) Arctic Drilling Technology in the Soviet Union. Paper 80-Pet-73, Presented at the 1980 ASME Energy Technology Conference and Exhibition, New Orleans, 3-7 February.

Kutasov, I.M. and Bizanti M.S. (1984) Fluid Loss While Drilling, SPE paper 17442, Richardson, Texas, USA.

Kutasov, I.M. (1987) Dimensionless Temperature, Cumulative Heat Flow and Heat Flow Rate for a Well With a Constant Bore-face Temperature. *Geothermics*, **16**, No. 2, 467–472.

Kutasov, I.M. and Targhi, A.K. (1987) Better Deep-Hole BHCT Estimations Possible. *Oil Gas J.*, 25 May, 71–73.

Kutasov, I.M. (1988a) Prediction of Permafrost Thickness by the "Two Point" Method. Proceedings of The Fifth International Conference on Permafrost. **2**, Tapir Publishers, Trondheim, Norway, 965–970.

Kutasov, I.M. (1988b) Empirical Correlation Determines Downhole Mud Density. *Oil Gas J.*, 12 December, 61–63.

Kutasov, I.M., Caruthers, R.M., Targhi A.K., and Chaaban, H.M.(1988) Prediction of Downhole Circulating and Shut-in Temperatures. *Geothermics*, **17**, 607–618.

Kutasov, I.M. and Strickland, D.G. (1988) Allowable Shut-in is Estimated for Wells in Permafrost. *Oil Gas J.*, 5 September, 55–60.

Kutasov, I.M. and Caruthers, R.M. (1988) Hole Enlargement Control During Arctic Drilling. SPE Paper 17442 Presented at the SPE California Regional Meeting, Long Beach, California, 23-25 March.

Kutasov, I.M. (1989a) Tables Can be Used to Determine Formation Temperature Away from the Wellbore. *Oil Gas J.*, 16 January, 62–63.

Kutasov, I.M. (1989b) Application of the Horner Method for a Well Produced at a Constant Bottomhole Pressure. *Formation Evaluation*, March, 90–92.

Kutasov, I.M. (1989c) Water FV Factors at Higher Pressures and Temperatures. *Oil Gas J.*, 20 March, 102–104.

Kutasov, I.M. (1991) Correlation Simplifies Obtaining Brine Density. *Oil Gas J.*, 5 August, 48–49.

Kutasov, I.M. (1993a) Arctic Drilling and Completion Problems. Proceedings of the Sixth International Conference on Permafrost. Beijing, China, July 5-9, 362–367.

Kutasov, I.M. (1993b) Tables Simplify Determining Temperature Around a Shut-in Well. *Oil Gas J.*, 26 July, 85–87.

Kutasov, I.M. (1995a) Empirical Correlation Estimates Geothermal Gradients. *Oil Gas J.*, 2 January, 48, 50.

Kutasov, I.M. (1995b) Salted Drilling Mud Helps Prevent Casing Collapse in Permafrost. *Oil Gas J.*, 31 July, 87–88.

Kutasov, I.M. (1995c) Computer Program Predicts Fluid Loss to Thief Zones. *Oil Gas J.*, 14 August, 45–47.

Kutasov, I.M. (1996) Program Predicts Altered Zone Heat Loss in Steam Injector. *Oil Gas J.*, 18 November, 46–48.

Kutasov, I.M. (1997) Method Estimates Arctic Well Thermal Insulation Efficiency. *Oil Gas J.*, 6 October 6, 82–84.

Kvenvolden, K.K. (1988) Methane Hydrate – A Major Reservoir of Carbon in the Shallow Geosphere. *Chemical Geology*, **71**, 41.

Lachenbruch, A.H. and Brewer M.C. (1959) Dissipation of the Temperature Effect of Drilling a Well in Arctic Alaska. *U.S. Geological Survey Bull.*, **1083-C**, 74–109.

Lachenbruch, A.H. (1968) Rapid Estimation of the Topographic Disturbance to Superficial Thermal Gradients. *Rev. Geophys.*, **6**, 365–400.

Lachenbruch, A.H. and Marshall (1977) Subsea Temperatures and a Simple Tentative Model for Offshore Permafrost at Prudhoe Bay, Alaska. Open File Report 77-395, U.S.G.S.

Lachenbruch, A.H., Sass J.H., Marshall, B.V., and Moses, T.H. Jr. (1982) Permafrost, Heat Flow, and the Geothermal Regime at Prudhoe Bay, Alaska. *J. Geophys. Res.*, **87**, No. B11, 9301–9316.

Lachenbruch, A.H., Cladouhos, T.T., and Saltus R.W. (1988) Permafrost Temperature and the Changing Climate. Proceedings of The Fifth International Conference on Permafrost. **3**,. Tapir Publishers, Trondheim,Norway, 9–17.

Lakhtionov, M.O. (1973) Thermal Prospecting. In: Eds., Tarkhov, A.G. and Mu-

dretsova, E.A.: Mining Geophysics, Nedra, Moscow, 145–165.

Leblanc, Y., Pascoe, L.J., and Jones, F.W. (1981) The Formation Stabilization of the Borehole, *Geophys.*, **46**, 1301–1303.

Lee, T.C. and Henyey, T.L. (1974) Heat Flow Refraction Across Dissimilar Media. *Geophys. J. Roy. Astr. Soc.*, **39**, 319–331.

Leutwyler, K. and Bigelow, H.L.(1965) Temperature Effects on Subsurface Equipment in Steam Injection Systems. *J. Pet. Tech.*, 93–101.

Li, G.E. and Kutasov I.M. (1978) Temperature Control at Surface Casing in Permafrost. *Neftianoe Khoziaistvo*, January, 13-16.

Lubimova, E.A., Von Herzen, R.R., and Udintsev, G.B.(1965) On Heat Transfer Through the Ocean Floor. In: W.H.K. Lee (Ed.) Terrestrial Heat Flow, Geophysical Monograph Series **8**, American Geophysical Union, Baltimore, Maryland, Port City Press, 78–86.

Lubimova, E.A. (1968) Thermics of the Earth and Moon. Nedra, Moscow.

Lunardini, V.J. (1988) Heat Conduction with Freezing or Thawing. CRREL Monograph 88-1, Hanover, N.H., USA, 187–214.

MacAndrew, R., Parry, N., Prieur, J-M., Wiggelman, J., Diggins, E., Guicheney, P. and Stewart, A. (1993). Drilling and Testing Hot, High-Pressure Wells. *Oilfield Review*, April/July, 15–23.

McAdams, W.H. (1954) Heat Transmission. Third Edition, McGraw-Hill, New York.

McMordie, W.C., Jr., Bland, R.G., and Hauser, J.M. (1982) Effect of Temperature and Pressure on the Density of Drilling Fluids. SPE Paper 11114, Presented at the 57th Annual Fall Technical Conference and Exhibition of the SPE, New Orleans, LA, 26-29 September.

Medvedskiy, R.I.(1971) The Possibility of Neglecting of the Vertical Heat Transfer in Wellbore Heat Loss Calculations. Proccedings of the Giprotumenneftegas, (Russian), **23**, 88–90.

Melnikov, P.I., Balobayev, V.T., Kutasov, I.M., and Devyatkin, V.N. (1973) Geothermal Studies in Central Yakutia. *Intern. Geol. Rev.*, **16**, 565–568.

Middleton, M.F. (1979) A Model for Bottom-hole Temperature Stabilization. *Geophys.*, **44**, 1458–1462.

Mikov, B.D., Pyatnitsky, V.K., and Rempel, G.G. (19660 The Use of Aeromagnetic Data for Investigation the Basement of Closed Territories. Review of VIEMS.

Milestone, N.B. and Rogers, D.E. (1981). The Use of an Isothermal Calorimeter for Determining Heats o Hydration at Early Ages. *World Cement Technology*, October, 374

Mitchell, R.F. (1981) Downhole Temperature Prediction for Drilling Geothermal Wells. Proceedings of the International Conference on Geothermal Drilling and Comple-

tion Technology, Albuquerque, New Mexico, 21-23 January.

Molochushkin, E.N. (1973) The Effect of Thermal Abrasion on the Temperature of the Permafrost in the Coastal Zone of the Laptev See. Proceedings of the Second International Conference on Permafrost, Yakutsk, Soviet Contribution, 13-28 July, Nat. Acad. Sci., Washington, D.C., 90–93.

Mongelli, F. and Morelli, C. (1961) Contributi alla Prospezione Geotermica. *Boll. Geofis. Teor. Applic.*, **3**, 294–306.

Moscicki, W.J. (1987) Temperature Anomalies Over Underground Cavities. *Geophys. Prosp.*, **35**, 393–423.

Muskat, M. (1946) Flow of Homogeneous Fluids Through Porous Media. J.W. Edwards Inc., Ann Arbor, MI.

Naudy, H. (1970) Une Methode D'analyse Fine des Profiles Aeromagnetiques. *Geophys. Prosp.*, **18**, 56–63.

New Cement Test Schedules Issued (1977) *Oil Gas J.*, July, 25, 179–182.

Ogata, N., Yasuda, M., and Kataoka, T. (1982) Salt Concentration Effects on Strength of Frozen Soils. In: Proceedings of The Third International Symposium on Ground Freezing. 22-24 June, Hanover, New Hampshire, U.S.A. 3–17.

Osterkamp, T.E. and W.D. Harrison (1982) Temperature Measurements in Subsea Permafrost off the Coast of Alaska. Proceedings of the Fourth Canadian Permafrost conference, 2-6 March, Calgary, Alberta, 238–248.

Osterkamp, T.E.(1983) Response of Alaska Permafrost to Climate. Fourth International Permafrost Conference, 17-22 July, 1983, Fairbanks, Alaska, Nat. Acad. of Sci., Washington, D.C., 145–151.

Osterkamp, T.E. and Gosink, J.P., (1984) A Reconnaissance Study of the Hydrothermal Characteristics of Pilgrim Springs, Alaska. *J. Energy Resources Tech.*, **106**, 96–102.

Ostroumov, G.A. (1952) Free Convection Under Internal Problem Conditions. GITTL, Moscow, Russia.

Palmer, A. (1978) Thawing and the Differential Settlement of the Ground Around Oil Wells in Permafrost. The USSR Contribution to the Second International Conference, 13-28 July, Nat. Acad. Sci., Washington, D.C., 619–624.

Parasnis, D.S. (1963) Principles of Applied Geophysics. John Wiley & Sons, Inc.

Parasnis, D.S. (1971) Temperature Extrapolation to Infinite Time in Geothermal Measurements. *Geoph. Prospect.*, **19**, 612–614.

Paul, M. (1935) Uber Messingew der Erdbodentemperatur and Salzodomen. *Z. Geophys.*, **11**, 7/8, 388–392.

Pavlov, A.V. (1974) Seasonal Freezing and Thawing of Rocks. In: Melnikov, P.I. and Tolstikni, N.I. (Eds.) General Geogriology. Nauka, Novosibirsk, 66–68.

Perkins, T.K., J.A. Rochon, and C.R. Knowles (1974) Studies of Pressure Generated Upon Refreezing of Thawed Permafrost Around a Well Bore. *J. Pet. Tech.*, 1159–1166.

Petrazhitskiy, G.B. and Bekneva, E.V. (1973) Experimental and Theoretical Investigations of Free Convection in a Closed Ring System. Proceedings of MVTU, **170**, 98–108.

Pilkington, P.E. (1992) Cement Evaluation - Past, Present, and Future. *J. Pet. Tech.*, 132–140.

Poelchau, H.S., Baker, D.R., Hantschel, Th., Horsfield, B., and Wygrala B. (1997) Basin Simulation and the Design of the Conceptual Basin Model. In: Welte, D.H., Horsfield, and Baker D.R. (Eds.) Petroleum and Basin Evoluation. Springer–Verlag Berlin Heidelburg New York, 36–41.

Poley, J.P. and Steveninck, J.V. (1970) Delineation of Shallow Salt Domes and Surface Faults by Temperature Measurements at a Depth of Approximately 2 Meters. *Geophys. Prosp.*, **18**, 666–700.

Popov, Yu., A., Pevzner, L.A., Romushkevich, R.A., Korostelev, V.M., and Vorob'yev, M.G. (1995). Thermophysical and Geothermal Sections Obtained from Kolvinskaya Well Logging Data. *Phys. Solid Earth*, **30**, 778–789.

Potter, R.W., II and Brown, D.L. (1977) The Volumetric Properties of Aqueous Sodium Chloride Solutions from 0° to 500 °C at Pressures up to 2000 Bars Based on a Regression of Available Data in Literature. In: Pleminary Tables for NaCl Solutions, *Geol. Survey Bull.*, **1421-C**, U.S. Gov't Printing Office, Washington, D.C.

Powell, W.G., Chapman, D.S., Balling, N. and Beck A.E. (1988) Continental Heat-Flow Density. In: Haenel, R., Rybach, L., and Stegena, L. (Eds.) Handbook of Terrestrial Heat-Flow Density Determination. Kluwer Academic Publishers, Dordrecht/Boston/London, 167–222.

Prats, M. (1982) Thermal Recovery. Monograph Series, **7**, Society of Petroleum Engineers, Dallas,

Proselkov, Yu. M. (1975) Heat Transfer in Wells. Nedra, Moscow.

Ramey, H.J., Jr. (1962) Wellbore Heat Transmission. *J. Pet. Tech.*, 427–435.

Rao, D.A. and Babu, H.V. (1984) On the Half-Slope and Straight-Slope Methods of Basement Depth Determination. *Geophysics*, **49**, 1365–1368.

Raymond, L.R. (1969) Temperature Distribution in a Circulating Drilling Fluid. *J. Pet. Tech.*, 333–341.

Robertson, E.C. (1979) Thermal Conductivity of Rocks. U.S. Geol. Survey, Open File Report 79–356, 31p.

Rodionov, P.F. and Sofronov, N.I. (1935) About the Possibility of an Application of Thermal Prospecting to Search of Sulphide Deposits. *Problems of Soviet Geology*,

8, 257–268.

Roger, R. (1990) Selecting a Drilling Fluid. *J. Pet. Tech.*, 832–834.

Roux, B., Sanyal, S.K., and Brown, S.L. (1980) An Improved Approach to Estimating True Reservoir Temperature from Transient Temperature Data. SPE Paper 8888 Presented at the 1980 SPE California Regional Meeting, Los Angeles, 9-11 April.

Rybach, L. (1988) Determination of Heat Production Rate. In: Haenel, R., Rybach, L., and Stegena, L. (Eds.) Handbook of Terrestrial Heat-Flow Density Determination. Kluwer Academic Publishers, Dordrecht/Boston/London, 125–142.

Ruedrich, R.A. and Perkins, T.K. (1974). A Study of Factors Influencing the Mechanical Properties of Deep Permafrost. *J. Pet. Tech.*, 1167–1176.

Rusakov, V.G. and Kononov, Yu. I. (1976) The First Results of Field Thermophysical Investigations in a Drilling Well at Natural Gas Deposit "Medvezhe". In: Problems of Geocryology in Works of Young Scientists and Specialists, (Russian), Yakutsk.

Sammel, E.A., (1968) Convective Flow and its Effect on Temperature Logging in Small-diameter Wells. *Geophys.*, **33**, 1004–1012.

Samuelson, M.L. and Constien, V.G. (1997) Frontier Geothrmal Drilling Operations Succeed at 500 °C Bottomhole Static Temperature. *J. Petrol. Tech.*, 536–537.

Sass, J.H., Lachenbruch, A.H., and Munro, R.J. (1971) Thermal Conductivity of Rocks from Measurements on Fragments and its Application to Heat Flow Determinations. *J. Geophys. Res.*, **76**, 3391–3400.

Sengul, M.M. (1983) Analysis of Step-pressure Tests. SPE Paper 12175 Presented at the 58th Annual Technical Conference and Exhibition, San Francisco, California, 5-8 October.

Schoeppel, R.J. and Gilarranz, S. (1966). Use of Well Log Temperatures to Evaluate Regional Geothermal Gradients. *J. Pet. Tech.*, June, 667–673.

Shell, F. and Tragesser, A.F. (1972). API is Seeking More Accurate Bottom Hole Temperatures.
Oil Gas J., 10 July 10, 72–79.

Sibbitt, W.L., Dodson, J.G., and Tester, J.W. (1979). Thermal Conductivity of Crystalline Rocks Associated With Energy Exrtaction From Hot Dry Rock Geothermal Systems. *J. Geoph. Res.*, **84**, B3, 1117–1124.

Simmons, G. (1967) Interpretation of Heat Flow Anomalies.
Rev. of Geophys., **5**, No.2, 42–52.

Sloan, E.D. (1991) Natural Gas Hydrates. *J. Pet. Tech.*, 1414–1417.

Smith, D.K. (1974). Cementing. Monograph Series, **4**, SPE , Dallas, 24

Smith, R.E. and Clegg, M.W. (1971). Analyses and Design of Production Wells Through Thick Permafrost. Proceedings of the Eighth World Petroleum Congress,

Moscow, June, 379–389.

Smith, R.C. and Steffensen, R.J. (1975). Interpretation of Temperature Profiles in Water-Injection Wells. *J. Pet. Tech.*, 777–784.

Somerton, W.H. (1958) Some Thermal Characteristics of Porous Rocks. *Trans.*, AIME **213**, 375–378.

Somerton, W.H. (1992) Thermal Properties and Temperature Related Behavior of Rock/Fluid Systems. Developments in Petroleum Science, **37**. Elsevier, Amsterdam, 1–260.

Sorelle, R.R., Jardiolin, R.A., and Buckley, P. (1982) Mathematical Field Model Predicts Downhole Density Changes in Static Drilling Fluids. SPE Paper 11118 , Presented at the 57th Annual Fall Technical Conference and Exhibition of the SPE, New Orleans, LA, 26-29 September.

Straus, J.M. and Schubert, G. (1977) Thermal Convection in a Porous Media: Effects of Temperature-and Pressure-Dependent Thermodynamic and Transport Properties. *J. Geophys. Res.*, **82**, 325–333.

Sudzhadinov, R.A. and Kosmodemyansky, V.V. (1986) Mapping for Oil and Gas Structures at Large Depth. In: Ed., Ismail-Zade, T.A.: Complex Interpretation of Geological-Geophysical Materials for Investigating the Structure and Prospecting for Oil and Gas at Large Depth, "YuzhVNIIGeofizika", 94–103.

Sump, G.D. and Williams, B.B. (1973). Prediction of Wellbore Temperatures During Mud Circulation and Cementing Operations. *J. Eng. for Industry*, 1083–1092.

Swayze, M.A. (1954) Effect of High Temperature and Pressure on Cements . *Oil Gas J.*, August 2

Targhi, A.K. (1987) Temperatures Regime of Deep Wells During Cementing (Prediction of Static, Circulating, and Shut-in Temperatures; Evaluation of the Thermal Effects of Cement Hydration). Dissertation, Louisiana Tech University, 210p.

Taylor, A.E. (1978) Temperatures and Heat Flow in a System of Cylindrical Symmetry Including a Phase Boundary. *Geothermal Series*, **7**, Ottawa, Canada, 43.

Taylor, A.E. and Judge, A.S. (1977) Canadian Geothermal Data Collection – Northern Wells 1976-77. *Geothermal Series*, **10**, Earth Physics Branch, Energy, Mines and Resources, Ottawa, 194p.

Taylor, A.E., Burgess, M., Judge, A.S., and Allen, V.S. (1982) Canadian Geothermal Data Collection – Northern Wells 1981. *Geothermal Series*, **13**, Earth Physics Branch, Energy, Mines and Resources, Ottawa, 1982, 153p.

Telford, W.M., Geldart, L.D., Sheriff, R.E., and Keys, D.R. (1986) Applied Geophysics. Cambridge Univ. Press.

Thompson, M. and Burgess, T.M. (1985) The Prediction of Interpretation of Downhole Mud Temperature While Drilling, SPE Paper 14180, Richardson, Texas, USA.

Tikhonov, A.N. and Samarskiy A.A. (1963) Equations of Mathematical Physics. Pergamon Press.

Tikhonov, A.N., Dmitriev, V.I., and Glasko, V.V. (1983) Mathematical Methods in Prospecting for Useful Minerals. Znanie, Moscow.

Timko, D.J. and Fertl W.H. (1972) How Downhole Temperatures and Pressures Affect Drilling. *World Oil*, **175**, 73–78.

Tragesser, A.F., Crawford, P.B., and Crawford, H.R. (1967) A Method for Calculating Circulating Temperatures. *J. Pet. Tech.*, 1507–1512.

Tragesser, A. and Parker, P.N. (1972). Using Improved Technology to Obtain Better Cement Jobs on Deep, Hot Liners.
J. Pet. Tech., November, 1307.

Tsytovich, N.A. (1975) The Mechanics of Frozen Ground. Scripta Book Company, Washington, D.C., 8–250.

Tsytovich, N.A., Kronik, Ya. A., Markin, K.F., Aksenov, V.I., and Samuel'son, M.V. 1973) Physical and Mechanical Properties of Saline Soils. In: Proceedings of the Second International Conference on Permafroist, Yakutsk, Soviet Contribution, 13-28 July, Nat. Acad. Sci., Washington, D.C., 238–247.

Tuman, V.S. (1962) Thermal Stresses Around a Wellbore and Their Small Effect on Velocity Logging. *Soc. Petrol. Eng. J.*, 303–308.

Uraiet, A.A. and Raghavan, R.(1980) Unsteady Flow to a Well Producing at Constant Pressure.*J. Petrol. Tech.*, 1803–1812.

Uyeda, S. (1988) Geodynamics. In: Haenel, R., Rybach, L., and Stegena, L. (Eds.) Handbook of Terrestrial Heat-Flow Density Determination. Kluwer Academic Publishers, Dordrecht/Boston/London, 317–351.

Van den Bouwhuysen, J.N.A. (1934) The Thermocouple Proves Useful on a Geophysical Survey. *Eng. and Min. J.*, **135**, 342–344.

Van Everdingen, A. F. and Hurst, W. (1949) The Application of the Laplace Transformation to Flow Problems in Reservoirs, *Trans., AIME*, **186**, 305–324.

Van Orstrand, C.E. (1941) Temperature of the Earth in Relation to Oil Location . In: Temperature, its Measurement and Control in Science and Industry. American Institute of Physics, Reinhold Publishing Corporation, New York, 1015–1033.

Venditto, J.J. and George, C.R. (1984) Better Wellbore Temperature Data Equals Better Cement Jobs. *World Oil*, February, 47–50.

Vyalov, S.S. (1974) Physical-Mechanical, Thermal, and Electrical Properties of Frozen Rocks. In: Melnikov, P.I. and Tolstikni, N.I. (Eds.) General Geogriology. Nauka, Novosibirsk, 161–191.

Walker, R.E. and Korry, D.E. (1974) Field Method of Evaluating Annular Performance of Drilling Fluids. *J. Pet. Tech.*, 167–173.

White, P.D. and Moss, J.T. (1983) Thermal Recovery Methods. Pennwell Publishing Company, Tulsa, Oklahoma, 92–98.

Wilhelm, H., Baumann, C., and Zoth, G. (1995) Some results of Temperature Measurements in KTB Main Borehole, Germany. *Geothermics*, **24**, No. 1, 101–113.

Willhite, G.P. (1967) Overall Heat Transfer Coefficients in Steam and Hot Water Injection Wells. *J. Pet. Tech.*, 607–615.

Wooley, G.R. (1980) Computing Downhole Temperatures in Circulation, Injection, and Production Wells. *J. Pet. Tech.*, 1509–1522.

Wooley, G.R., Giussani, A.P., Galate, J.W. and Wederlich, H.F., III (1984) Cementing Temperatures for Deep-Well Production Liners. SPE paper 13046 presented at the 59th Annual Technical Conference and Exhibition, Houston,Texas, 16-19 September.

Wu, Y-S. and Pruess, K. (1988) An Analytical Solution for Wellbore Heat Transmission in Layered Formation. SPE Paper 17497 Presented at the SPE California Regional Meeting, Long Beach, California, 23-25 March.

Yefimov, A.V., Kutasov, I.M., and Shipitsyna, L.I. (1975) Zone of Influence of Ground Water Sources on the Temperature Field of Bottom Deposits. Izvestiya of Acad. of Sci. of the SSSR, *Physics of the Earth*, No. 10, 90–95.

Zorin, Yu.A. and Lysak, S.V. (1972) Quantitative Interpretation of Geothermal Anomalies. Izv. Akad. Nauk SSSR, Ser. *Fizika Zemli*, **9**, 68–73.

Index

acceleration constant, 102
active layer, 39
actual well radius, 204
adjusted circulation time, 114
altered zone, 226
ambient temperature, 8, 195
American Petroleum Institute, 82, 208
anisotropic rocks, 12
annual observations, 252
annular flow, 153
annular material, 225
annulus area, 199
annulus size, 204
annulus-formation interface, 66
Arctic drilling, 2, 191
autocorrelation matrix, 278
average density, 6
axial compressive stress, 134
axial convection, 80
axial stress, 124, 247

battery circuit, 275
Beaufort sea, 144
bentonite mud, 149
Bessel function, 181
bit diameter, 151
bit performance, 90
body's epicenter, 286
Boltzmann constant, 5
bottom sediments, 37, 57, 219
bottomhole circulating temperature, 211
bottomhole pressures, 95
bottomhole temperature, 92, 161
bottomhole temperature surveys, 257
bottomhole temperatures, 194
boundary conditions, 14, 227
Bridgman-Tamman equation, 191
buckling of casing, 192
buckling tendency, 124
bulk mud temperature, 71
Bullard method , 12

calcium bromide brine, 96
calcium silicate, 231
Calibration data, 272
caliper log, 266
Caliper logs, 146
casing liner, 219
casing shoe, 125
casing string, 122
casing string failures, 246
casing strings, 66
cement column, 202
cement compounds, 195
cement design, 210
cement hydration, 194, 267
cement setting, 194
cement setting time, 202
cement slurry design, 194, 221
cementing job, 222
cementing jobs, 145
cementing of casing, 194, 267
cementing operation, 200
cementing program, 216
cementing programs, 2
Central Graben (North Sea), 104
characteristic area, 224
chemical composition, 195
chemical interaction, 96
circulating mud temperature, 65
circulating temperatures, 210
Circulation history, 66
circumferential stress, 246
Class H Cement, 199
coastal waters, 34
cohesion of sand, 149

cohesive soils, 37
collapse rating, 193
collapse resistance, 191
Collapsed casing, 132
complete freezeback, 185
completion operations, 158
completion technology, 2
compositional model, 96
compressional seismic waves , 16
compressive strength, 37, 195
compressive stress, 241
computer model, 67
computer program, 32, 177
Consolidated formations, 133
consolidation, 240
constant bore-face temperature, 73
constant heat flow, 114
constant mud densities, 95
contemporary climate change, 30
convective movements, 248
conversion factor, 104
Conversion factors, 3
correlation coefficient, 172
critical Rayleigh number, 248
critical Reynolds number, 152
critical temperature, 191
critical temperature gradient, 249
cross-sectional areas, 80
cryogeneous texture, 35
crystal nucleation, 107
cumulative fluid loss, 75
cumulative heat flow, 113
cumulative time, 66
cuttings, 133
cylinder, 46
cylindrical coordinates, 24, 81
cylindrical source, 24

Darcy equation , 7
Dead Sea Basin, 291
decomposition temperature, 108
deep hot wells, 224
density distribution, 18
density of cement, 197
depositional history, 35
diapiric salt, 45
differential equations, 80
differential pressure, 95
dimensionless circulation time, 118
dimensionless quantities, 26
dimensionless time, 23
discharge pressure, 72
discontinuity of the mud circulation , 66
dissipation constant, 274
disturbance time, 262
Dittus–Boelter formula, 69
downhole conditions, 208
downhole pressure, 265
drill pipe, 70
drill pipe size, 155
drilling at underbalance, 105
drilling bit design, 79
drilling records, 128, 263
drilling site, 34
drilling technology, 72
dry zone, 230
Duhamel's theorem, 119

effect of casing, 254
effective fluid temperature, 112
effective mud temperature, 170
effective thermal conductivity, 19, 228
effective volumetric capacity, 6
Effective Well Radius, 228
effective well radius, 239
efficiency of the thermal insulation, 232
Elastic deformations, 37
electrical integrators, 62
electrical resistivity, 126
elevated temperatures, 2, 96
elliptical integrals, 57
emissivity, 231
empirical equation of state, 95
empirical equations, 16
empirical expression, 211
empirical formula, 86, 144
engineering calculations, 11
equation of state, 4
equivalent circulating fluid density, 101

erosion, 47
error function, 23
error function and , 48
evaporation of water, 22
exothermic reaction, 195
experimental set, 204
exponential integral, 77, 114
external freezeback pressures, 131
external pressures, 190

fictitious body, 289
field experiment, 249
film heat transfer coefficient, 70
film transfer coefficient, 225
finite-difference method, 256
flat relief, 44
flowing fluid, 21
fluid density, 99
fluid flow history, 83
fluid friction, 66
fluid infiltration, 148
fluid velocity, 19, 152
fluid viscosity, 154
fluid-saturated rocks, 5
forced thermal convection, 268
formation permeability, 76
formation pressures, 101
formation temperature profiles, 64
formation temperatures, 258
forward mud circulation, 80
Fourier law, 6
Fourier's law, 282
fracture gradient, 265
free thermal convection, 41
freezeback period, 184
freezing point, 156
freezing process, 24
FTE model, 161

gas hydrate, 2
Gas hydrates, 106
gauge borehole, 152
gauge well, 204
gel strength, 91
geophysical studies, 34
geothermal drilling, 90
geothermal exploration, 91
geothermal field, 27
geothermal gradient, 11, 14, 129, 210
Geothermal investigations, 144
geothermal regions, 44
geothermal reservoir, 44
Geothermal Service of Canada, 180
geothermal wells, 210
gradient distortions, 58

heat conductivity equation, 20
heat convection, 18
heat exchanger, 68
heat flow rate, 73, 140
heat loss reduction, 229
heat production, 14
heat source strength, 159
heat transfer coefficient, 138
heat-flow density , 15
high precision, 273
high-temperature floccation, 91
hole collapse, 101
hole enlargement, 126, 145
Hole enlargement control, 2
hole sizes, 65
homogeneous layer, 12
horizontal circular cylinder, 283, 291
horizontal derivative, 286
horizontal gradients, 286
horizontal layer, 41
horizontal temperature gradient, 53
Horner method, 256
Horner plot, 160
hot fluids, 238
hot wells, 194
hydrate decomposition, 107
hydrate gas influx, 108
hydrate stability, 107
hydrate zones, 107
hydraulic diffusivity, 10
hydraulic diffusivity coefficient, 62
hydraulic power output, 72
hydrodynamical modeling, 137
hydrostatic pressure, 101

hydrothermal circulation, 13

ice concentration, 94
ice content, 223
ice contents, 149
Imperial Valley, California, 84
inclined polarization, 282
inclined slope, 279, 280
incompressible fluid, 62
inflection points, 286
influx of reservoir fluid, 104
Initial conditions, 25
initiation of washouts, 155
injection pressure, 229
injection zone, 268
injectivity profile, 268
input data, 96
inside tubing surface, 224
insulation efficiency coefficient, 242
intensive washouts, 131
intergranular cohesion, 146
intermediate casing, 91
internal freezeback, 142
International standard temperature, 97
Interpretation of electric logs, 112
interval method, 12
inverse correlation, 290
inverse problem, 50
island's surface, 56
isothermal compressibility, 96, 237

Jemez Mountains, 14

Kelvin scale, 5
kinematic viscosity, 19, 152
kinetic energy, 4
Kola peninsula, Russia, 172

lake, 58
laminar flow, 151
Laplace equation, 23
Laplace equations, 255
Laptev sea, 34
latent heat, 6, 24, 151
lateral conductivity contrasts, 10
law of conservation of energy, 20
layered medium, 13
line source, 114
linear filtering, 278
linear heat source, 159
Linear heat transfer, 25
linear regression, 257
Lithologic log, 15
log interpretation, 158
logarithmic approximation, 159, 258
logging tool design, 90
longitudinal movement, 124
Lost of circulation, 74
low inlet temperatures, 221

Mackenzie Delta area, Canada, 107
maps of heat flow, 63
mass rate, 235
material balance, 236
mathematical model, 270
mechanical properties, 35
Medvezhe deposit, 133
melting temperature, 30, 135
metallic casing, 248
meteorological data, 59
meteorological stations, 278
Mississippi well, 83
Moduc County of California, 164
modulus of elasticity, 121, 244
modulus of normal elasticity, 39
moisture content, 35
molal concentration, 96
mud and ice mixtures, 94
mud cake, 75, 149
mud circulation, 64
mud circulation period, 244, 261
mud circulation time, 217
mud column pressure, 75
mud density program, 264
mud program, 74
mud properties, 2
mud temperature, 222
mud weight, 76
multiple regression analysis, 90
Muradkhanly oil deposit, 291
MWD temperature logs, 216

natural convection, 225
Newton equation, 69
Newtonian fluids, 152
normal background, 287
Northern Canada, 129
numerical modeling, 34, 45

Oblate spheroid, 47
offshore area, 219
offshore wells, 219
offshore-to-onshore transition, 35
Ohm's formula, 7
Ohm's law, 61
oil recovery projects, 229
oil-based muds, 98
oilfield units, 3
outer surfaces, 273
outlet mud temperature, 65
overall heat transfer coefficient, 70, 224
overbalance, 265

paleoclimatic history, 50
past climate, 3
penetration rate, 69
periodical function, 17
permafrost base, 27, 127
permafrost degradation, 34
permafrost regions, 11
permafrost response, 30
permafrost thaw, 2
permafrost thickness, 27, 126
permafrost thinning, 127
phase change, 24
phase transitions, 27, 185
physical model, 80
plastic viscosity, 152
platform stability, 134
plugging materials, 74
point of emergence, 53
point source, 291
Poisson equation, 24
Poisson's equation, 282
Poisson's ratio, 121, 244
polarization vector, 290
pore fluid density, 78
pore pressure, 75, 104
porosity, 77
portland cements, 195
Prandtl number, 19
Prescribed heat flow, 25
Prescribed surface temperature, 25
pressure drop, 67
primary cement jobs, 131
principle of superposition, 119, 159, 261
principle of the superposition, 240
production period, 119, 239
production rate, 257
production time, 257
Prolate spheroid, 47
Prudhoe Bay, Alaska, 33
pseudo-state solution, 82
pump input, 67
pump the cement slurry, 220
pumping of cement, 198
pumping time, 194

radial heat flow, 70
radial stresses, 244
radial symmetry, 25
radial temperature, 178, 239
radial temperature gradient, 230
radial temperature profile, 139
radiation heat transfer, 19
radiation heat transfer coefficient, 225
radioactive isotopes, 15
radiogenic heat, 16
radius of drying, 231
radius of investigation, 118
radius of thawing, 134
radius of thermal influence, 112, 139, 181
radius of tubing, 227
rate of fluid loss, 76
rate of heat generation, 196
rate of thawing, 29
Rayleigh number, 19
real body, 289
Rechitskaya oil field, Belarus, 172
reduction of cohesion, 145

reference rate, 197
reference surface, 63
regional heat flow, 3
regression analysis, 211
regression coefficient, 279
relief inclination, 289
reservoir conditions, 236
reservoir depth, 235
reservoir's life, 50
restoration time, 126
resultant of temperature disturbances, 65
retardes, 195
reverse mud circulation, 156
Reynolds number, 149
rheological bodies, 191
rheological processes, 36
rotary horsepower, 72
rotary inputs, 64

safe overbalance, 104
safety shut-in time, 143
salt concentration, 192
salt concentrations, 37
salt content, 29
salt dome, 44
sandstone, 204
saturated steam, 229
sea water, 36
sedimentary formations, 10
sedimentary layer, 48
sedimentation, 47
sedimentation of cuttings, 161
seismic velocity, 126
self-heating, 273
sensitivity study, 91
settlement, 134
shallow boreholes, 249
shallow depths, 50
shear strength, 145
short circulation period, 82
shut-in period, 177
shut-in periods, 64
shut-in temperature, 175
shut-in time, 158
Sieder–Tate correlation, 69
skin factor, 75
Society of Petroleum Engineers, 83
sodium chloride solutions, 96
solid bodies, 282
solid-fluid system, 96
Specific heat, 5
specific surface area, 37
specific volume, 237
speed of rotation, 72, 153
sphere, 46
stabilization time, 88, 217
stagnant gas, 231
standard conditions, 236
state of saturation, 149
Stavropol district, Russia, 86
steady heat flow, 23
steam density, 6
steam injection, 21
steam quality, 230
Stefan equation, 135
Stefan relationship, 24
strength development, 194
stress components, 244
stresses, 36
submergence, 34
subsea permafrost, 34
surface casing, 91
surface casing shoe, 135
surface cooling, 94
surface subsidence, 39
surface temperature, 11
surface temperature variations, 50
surface torque, 72
surrounding formations, 21
synchronous measurement, 278

Taylor number, 152
temperature amplitudes, 17
temperature anomalies, 165, 200, 248
temperature anomaly, 269
temperature charts, 208
temperature difference, 43
temperature distribution, 25, 30, 175
temperature disturbance, 251

temperature equilibrium, 170
temperature gradient, 172
temperature gradients, 54
temperature increase, 197
temperature interval, 273
temperature logs, 130
temperature measurements, 164
temperature moment, 289
temperature observations, 34, 179
temperature of casing, 247
temperature oscillations, 18, 250
temperature predictions, 162
temperature probes, 161
temperature profiles, 234
temperature recovery, 172
temperature scales, 12
temperature stabilization, 85
temperature survey, 201, 275
temperature surveys, 1, 256
temperature variation, 221
temperature wave, 17
temperature–depth curves, 18
temperature-pressure stability diagram, 107
temporary variations, 277
terrain relief effect, 279
terrestrial heat flow, 3
test procedures, 210
thawed formation, 240
thawed radius, 241
thawing radius, 222
thawing regime, 27
thawing soil, 133
theory of elasticity, 121
theory of similarity, 60
thermal abrasion, 34
thermal anisotropy, 9
thermal balance condition, 32
thermal balance method, 112
Thermal conductivity, 6
thermal conductivity, 9
thermal conductivity contrasts, 44
thermal conductivity of insulation, 231
thermal diffusion, 6
Thermal diffusivity, 10
thermal diffusivity, 226
thermal elongation, 246
thermal equilibrium, 4, 127
thermal expansion, 95
thermal history, 11
thermal insulation, 246
thermal insulation of tubing, 229, 247
thermal modeling, 60, 250
thermal recovery, 269
thermal resistance coefficient, 226
thermal resistivity, 9
thermal simulator, 68
thermal stress, 121
thermal stresses, 2, 244
Thermal warming model, 33
thermistor probe, 271
thermistor's resistance, 271
thermistors, 190, 252
thick-walled cylinder, 121
thickening time, 194
thickness of permafrost, 179
thief zone, 75
thief zones, 269
time function, 226
time lag, 252
time lapse, 201, 267
topographic corrections, 60
topographical corrections, 53
total compressibilty, 77
total drilling time, 144
total stresses, 246
transient temperature, 201
transient temperature field, 29
transitional regimes, 149
tricalcium silicate, 196
turbo drilling, 153
turbulent flow, 69
two point method, 127
Two Temperature Logs, 169

underbalance, 265
underground cavity, 292
underground water, 54
unfrozen water, 37, 144
unintentional underbalance, 95

variable resistor, 275
velocity of filtration, 53
vertical depth, 210
vertical heat conduction, 22
vertical heat transfer, 234
viscoelastic liquid flow, 153
viscous-elastic models, 191
voltage drop, 61, 273
volume changes, 39
volumetric average temperature, 116
volumetric flow rate, 152
volumetric heat capacity, 5

waiting on cement, 266
wall stability, 149
warm permafrost, 133
warming effect, 179
washed out formation, 145
washout coefficient, 147
washout diameters, 147
washout formation, 147
water density, 237
water flow, 51
water formation volume factor, 237
water vaporization, 230
water-based muds, 98
water-bearing layer, 55
water-saturated rock, 43
Webb County, Texas, 88
weights of the overburden, 121
well configuration, 220
well depth, 65
well radius, 112
well stability, 35
wellbore geometry, 69
wellbore heat losses, 224
wellbore integrity, 241
WELLTEMP, 67
Wheatston resistant bridge, 252
Wheatstone bridge, 271

zero temperature gradient, 179